

The Journal of the Indian Association of Sedimentologists

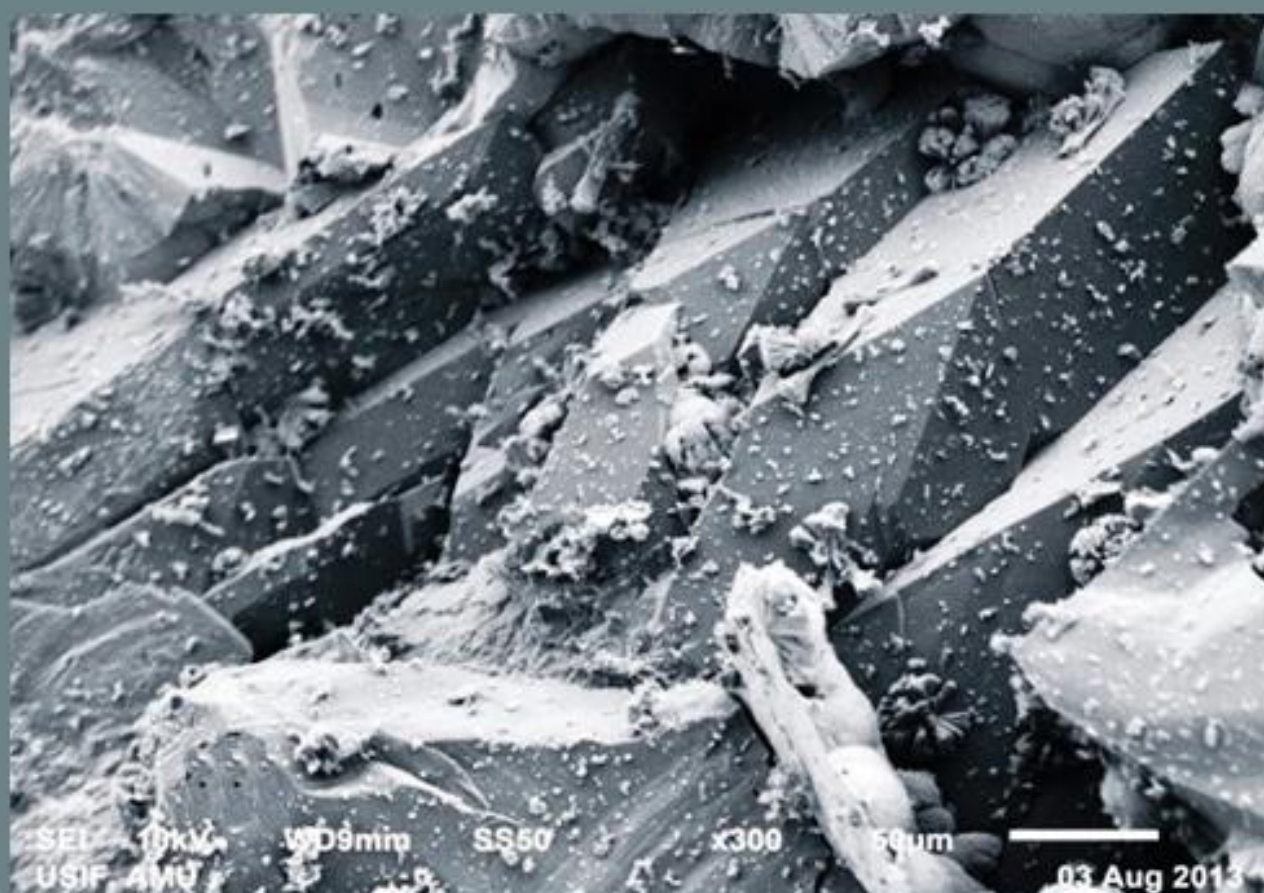


The Indian Association of Sedimentologists

Volume 37

No. 2

July - Dec 2020



SEM Photograph showing quartz overgrowth in Panchmarhi Sandstone

All rights reserved. No part of this publication may be reproduced, distributed, or transmitted in any form or by any means, including photocopying, recording, or other electronic or mechanical methods, without the prior written permission of the publisher, except in the case of brief quotations embodied in critical reviews and certain other non-commercial uses permitted by copyright law. For permission requests, write to the Managing Editor / s.

Editor-in-Chief

Professor Abhijit Basu, Indiana, USA

Associate Editor-in-Chief

Professor D. Rajasekhar Reddy, Vizag

Editorial Board

- 1. Professor G. Shanmugam, Arlington Texas, USA*
- 2. Professor Zhong Qiag-Chen, China University of Geosciences, Wuhan-China*
- 3. Professor M. E. Brookfield, University of Massachusetts at Boston, USA*
- 4. Dr. Aymon Baud, Zurich Switzerland*
- 5. Professor Jon Gluyas, Durham, UK*
- 6. Dr. Jonathan Craig, eni, Milan, Italy*
- 7. Dr. James Riding, British Geological Survey, UK*
- 8. Dr. Ameer Ghori, Geological Survey of Western Australia*
- 9. Dr. Guido Meinhold, Keele University, UK*
- 10. Dr. Daniel Le Heron, Vienna University, Austria*
- 11. Dr. Armstrong Altrin, National Autonomous University of Mexico*
- 12. Professor G.N. Nayak, Goa University, Goa*
- 13. Professor B.P. Singh, Banaras Hindu University, Varanasi*
- 14. Professor Santanu Banerjee, Indian Institute of Technology, Mumbai*
- 15. Professor Subir Sarkar, Jadavpur University, Kolkatta*
- 16. Professor Erfan Mondal, Aligarh Muslim University, Aligah*
- 17. Professor R. Nagendra, Anna University, Chennai*
- 18. Professor S. J. Sangode, Pune University, Pune*
- 19. Professor S.K.Pandita, Jammu University, Jammu*
- 20. Professor Atul V. Joshi M.S. Baroda University, Vadodra*

Managing Editors

- 1. Professor G. M. Bhat, Jammu University*
 - 2. Dr. Bashir Ahmad Lone, Jammu University*
-

The journal of the Indian Association of Sedimentologists

DOI: <http://doi.org/10.51710/jias.v37i2>

Managing Editors:

G. M. Bhat

Bashir Ahmad Lone

The Journal of the Indian Association of Sedimentologists (IAS) is both an international open access online journal and print journal and is leader in its field and publishes ground-breaking research from across the spectrum of sedimentology, sedimentary geology, sedimentary geochemistry, experimental and theoretical sediment transport, mass movement fluxes, modern and ancient sedimentary environments, sequence-, cyclo-, chrono- and chemostratigraphy, sediment-biological interaction, palaeosols, diagenesis, stable isotope geochemistry, environmental sedimentology, neotectonics, geohazards, stratigraphy, palynology, sedimentary mineral resources and hydrocarbons, and allied branches of sedimentary - stratigraphic research. It also publishes review articles, editorials, conference reports, tributes, announcements, advertisements, etc. It is currently distributed to universities and research laboratories in India and abroad. Access to the complete electronic journal archive over the past eight years comes free of cost. Subscribers also have the option to buy the printed journal at subsidized cost.

Indian
Association of
Sedimentologists



TABLE OF CONTENTS

ARTICLES	AUTHOR	PAGE NO
<i>Editorial</i>	G M Bhat	1 – 2
<i>Chemical Weathering, First Cycle Quartz Sand, and its bearing on Quartz Arenite</i>	Abhijit Basu	3 – 14
<i>Petrography, Provenance And Diagenesis Of Murree Group Exposed along Basohli- Bani Road, Kathua District, Jammu and Kashmir</i>	Monika Jamwal, S K Pandita, Meera Sharma, G M Bhat	15 – 26
<i>Assessment of Pre-and Post-Monsoon Groundwater Resource for Irrigation in Bhopalpatnam area, Bijapur District, Chhattisgarh, India</i>	Rajeeva Guhey, Korsa Munna	27 – 36
<i>Diagenesis and Porosity Evolution of the Pachmarhi Sandstones (Early Triassic), Satpura Gondwana Basin, Central India</i>	Dr Anis, Abdullah Khan, Narendra Kumar, Mujeedul Hasan	37 – 48
<i>Spatial and Temporal Variations in the Geochemistry of Cauvery River (Tamil Nadu, India) Sediments and its Implication to Weathering</i>	N. Gobala Krishnan, R. Nagendra, L. Elango, K.N. Prakash Narasimha, K. Vybhav, Pradeep Mujumdar	49 – 60
<i>Gravity flows: Types, definitions, origins, identification markers, and problems</i>	Shanmugam G	61 – 90
<i>Provenance, tectonics and palaeo environment of Mesoproterozoic Saundatti Quartzite Member of Kaladgi Basin, India: A petrographic view.</i>	Purushottam Anil Verlekar, Mahender Kotha	91 – 102
<i>Implications of diverse lithology and tectonics for drainage evolution in basin marginal region: A study from Chandrapur block of Pranhita-Godavari Basin. Central India.</i>	Vijay Sharma, Aditya Kumar Verma	103 – 114
<i>Sedimentological and Geochemical Charectesization of Manaveli and Cuddalore Formations, Puducherry Basin, India</i>	Shyam Narayan Mude, Shyam Yawale, Vishal Choudhari	115 – 130
<i>Potentiality of Uranium Mineralisation in the Environs of Chhattisgarh Basin, India: a new occurrence in Chhibra</i>	Mithilesh Sharma, Ashim Jana, Ajay Kumar, Pramod Kumar, A. K. Rai	131 – 140
<i>Impact of Elevation - Glaciation - Tectonics on landscape characteristics of the watersheds in Bhagirathi valley, Garhwal Himalaya</i>	Sarfaraz Ahmad, Khatib Khan	141 – 147
<i>Obituary : Prof. V. C. Chavadi (1942-2020)</i>	G N Nayak, P T Hanamgond	148
<i>Obituary: Prof. N. P. Bhatt (18.10.1966 – 08.10.2020)</i>	A V Joshi	149
<i>Honours and Awards</i>	Journaladmin IAS	150

Editorial

Sedimentology: Science and Society

DOI : <http://doi.org/10.51710/jias.v37i2.162.g68>

The current world human population is about 7.834 billion as of 25 December 2020 according to the most recent United Nations estimates elaborated by Worldometer. The sustenance and development of civilizations is primarily based on water, mineral and soil resources, and oil and gas hosted in the sediment profile of Earth's crust. The study of natural sediments and sedimentary rocks, and the processes involved in their formation are embedded in the domain of sedimentology. The science of sedimentology is as old as very beginning of the study of geology itself. The term *sedimentology* was first used by A.C. Trowbridge in 1925 (Waddell, 1933), but it was not in common use until the 1950s. The progress of sedimentological studies has passed through various phases during the last about two centuries: 1) development of sedimentary petrology initiated by the Western European School (1849-1950s); 2) granulometry and sedimentation by American School (1920s-1960s); 3) lithology and facies analysis by the Russian School (1870s-1970s).

In the course of development of stratigraphy, sedimentological concepts got new impetus on 1) establishment of the concept of unconformity, 2) geometry of strata based on the geologic maps and stratigraphy, 3) establishment of uniformitarianism and actualism, 4) founding of the facies concept, 5) sedimentary processes and palaeoenvironments, 6) basin analysis, 7) seismic stratigraphy, 8) sequence stratigraphy and 9) chemostratigraphy. With the advancement of modern concepts in sedimentology, the International Association of Sedimentologists (IAS) was founded at the International Geological Congress in Algiers on 11 September 1952, to promote the study of Sedimentology and start of the International Sedimentological Congress (ISC). It was in early 1960s with generous research funding by the industry particularly oil and gas industry sedimentology has come into the new era as an established discipline of earth sciences. This led to organization of educational and research institutes, trinity approach of sedimentary petrology, sedimentation and facies analysis in sedimentology; internationalizing and extension of sedimentology, and planetary sedimentology. It was in 1975 during a symposium at Delhi University the Indian Association of Sedimentologists was established and the first convention was held at Delhi University in 1976.

The contributions of Sedimentologists in the development of the society are of vital importance. May it be the contributions in technical knowhow about discovery and exploitation of earth resources, environment, climate record, atmospheric sciences, natural and anthropogenic hazards, earth surface

processes, etc. The present day challenges in earth resources exploration is increasing gap in energy production and demand. The future sustainable 35% energy demand is expected to be met from tight gas and tight oil in shale resources. The longstanding understanding that mudstones form in standing or slow-moving waters has been facing challenge by the concept that "muds accumulate even when currents move swiftly. The research shows that some mudstones may have formed in fast-moving waters: "Mudstones can be deposited under more energetic conditions than widely assumed, requiring a reappraisal of many geologic records (e. g., Schieber et al., 2007). These results call for critical reappraisal of all mudstones previously interpreted as having been continuously deposited under still waters. Such rocks are widely used to infer past climates, ocean conditions, and orbital variations (Macquaker and Kevin, 2007). Considerable recent research into mudstones has been driven by the recent effort to commercially produce hydrocarbons from them, in both the shale gas and tight oil plays (Loucks, et al., 2009).

Human activities on the earth surface including changing land-use pattern and release of pollutants into the natural environment result in adverse impact on society. We need to raise social awareness of these environmental changes and their future consequences, and predict implications and formulate mitigation strategies. Sedimentologists have critical role to play in characterizing and quantifying the response of nature to the impact of human activities on natural environment vis-à-vis society. There are many opportunities for sedimentologists to contribute in understanding of the human-nature relationship and help to achieve the UN sustainability goals (United Nations Sustainable Development Goals, 2015). Natural hazards like earthquakes, volcanoes, tropical cyclones, dam bursts, landslides, river floods, gulf, soil erosion, etc. which directly or indirectly impact human communities are the areas where sedimentology can play/plays a key role in improving our understanding of sediment mobilization, deposition and processes involved in interplaying with nature and natural resources. For example, how seasonal land-use can dramatically disrupt sediment transport, and alter the potential for erosion. On an average out of 500,000 earthquakes, about 100 great earthquakes occur every year in the world. The instrumental records of these earthquakes are available only for the last c.100 years. We don't know details on location, magnitude and mechanics of the historical records. Subaqueous fossil landslides potentially preserve a valuable record of the historical great earthquakes which provide clues to understand their frequency of occurrence and the pattern. Climatic and land-use changes (natural or man-made) play important role in triggering natural hazards. Climatic changes in combination with tectonic and volcanic activity also impact small islands (viz., small island nations in the Indian Ocean) and coastal regions

around the world. The impact of human activity on natural systems involves complexities in sedimentary routing systems from source to sink. For example, how pollutants and particulates are formed from natural and artificial sources, transported and deposited within the deep seas. Fine-grained sediments impact aquatic ecosystems, water quality, and increase flood risk in large river systems. The implications of future climate change may also affect the rate and nature of such transport. Climate change is the main driving force that shall affect global distribution of water on earth surface in future. It has already effected water variation in some regions in the world including the Himalayan countries which face rapid decline in water reserves. This climate change-driven water variation is likely to affect transboundary water sharing treaties and agreements, and may force the water sharing nations either to conflict or less likely cooperation policies. Great river systems emanating from huge glaciers in the Himalaya; the Brahmaputra, the Indus, the Sutlej, the Salween and the Mekong pass through 11 countries and nourish about 2 billion people in South Asia. Alone, the Indus River system feeds about half a billion people in North India and Pakistan. In the absence of surface water sources, we will have to depend on ground water resources for drinking, agriculture, industry, and other purposes. But we are also polluting the ground water resources by injecting sewerage water into the ground through soakage pits particularly in urban areas. We don't know much about the complex routing system of percolation of particulate and dissolved toxic elements through sediment cover into the water table. The effect of plastic pollution in the natural environment and water bodies is another grave concern. Deep sea is thought to be the ultimate sink for plastics particularly microplastics (Woodall et al., 2014). Less than 1% of the plastic in the oceans floats on the surface (Jambeck et al., 2015; Van Sebille et al., 2015), where does the remaining plastic accumulates or settles down? The research on deep-sea processes involved in transportation of plastic particles in deep seas shall fill the knowledge gaps in this field.

To arrest the atmospheric CO₂ and store it in the earth's sedimentary cover is critical to reduce and mitigate the release of natural carbon. We don't know how subsurface sedimentological variations within the potential CO₂ storage in sandstone reservoirs will impact the subsurface environments. Carbon sequestration is still poorly understood which limits our understanding of the carbon cycle as a whole. Future research should be focused on characterisation of spatio-temporal heterogeneity of the sedimentary deposits which apparently have dominant control on organic carbon hotspots within the earth system (to better constrain the spatial and depth-related variability in natural organic carbon sequestration). Carbon capture and storage can

offer a promising anthropogenic solution in mitigation against the release of CO₂, perhaps utilizing the existing petroleum fields for the purpose.

Coastlines and ocean Islands are often densely populated areas which are vulnerable to sea level rise. Understanding how ecosystems of coastlines and Islands change in response to climate change is the key for sustainable development of these regions. For example about 60% of coastline population of India is affected by the coastal pollution and climate changes. Coastal and shallow marine environments are also potential areas for the growth in renewable wind energy. Understanding of the subsurface geology in the coastal areas particularly in deeper settings is important for foundation of infrastructure development of wind turbines to maximize the wind energy resource. Research on present day coastal sedimentation processes and ancient analogues is critical for providing insights into how systems react to external forcing (processes) and subsurface sedimentary stratal architecture.

References

- Jambeck, J. R., Geyer, R., Wilcox, C., Siegler, T. R., Perryman, M., Andrady, A., et al. (2015), Plastic waste inputs from land into the ocean. *Science* 347, 768–771. doi: 10.1126/science.1260352
- Loucks, R. G., Reed, R. M., Ruppel, S. C., and Jarvie, D. M. (2009), Morphology, Genesis, and Distribution of Nanometer-Scale Pores in Siliceous Mudstones of the Mississippian Barnett Shale, *Journal of Sedimentary Research*, v. 79, p. 848-861
- Macquaker, J. H. S and Bohacs, K. M., (2007), Geology: On the Accumulation of Mud," *Science*, 14: p. 1734-173
- Schieber, J., John Southard, J., and Thaisen, K. (2007), Accretion of Mudstone Beds from Migrating Floccule Ripples, *Science*, p. 1760-1763
- United Nations Sustainable Development Goals (2015), *United Nations Sustainable Development Goals*, Available online at: <http://www.un.org/sustainabledevelopment/sustainable-development-goals/>
- Van Sebille, E., Wilcox, C., Lebreton, L., Maximenko, N., Hardesty, B. D., Van Franeker, J. A., et al. (2015). A global inventory of small floating plastic debris. *Environ. Res. Lett.* 10:124006. doi: 10.1088/1748-9326/10/12/124006
- Waddell, H., 1933. Sedimentation and sedimentology, *Science*, 77: 536–537.
- Woodall, L. C., Sanchez-Vidal, A., Canals, M., Paterson, G. L., Coppock, R., Sleight, V., et al. (2014), The deep sea is a major sink for microplastic debris. *R. Soc. Open Sci.* 1:140317. doi: 10.1098/rsos.140317

G. M. Bhat

Geology Department, University of Jammu
hatgm@jugaa.com

Chemical Weathering, First Cycle Quartz Sand, and its bearing on Quartz Arenite

Abhijit Basu

Department of Earth and Atmospheric Sciences, Indiana University, Bloomington, IN 47408, U.S.A.

basu@indiana.edu

Abstract

A self-consistent set of experimentally determined rates of mineral dissolution (Francke, 2009) has been used to estimate the relative loss of common constituents of plutonic igneous rocks that supply quartz to sands to be lithified as first-cycle quartz arenite. A first-order decay equation is used setting the decay constant of calcite to one, which renders the time-steps of loss dimensionless but keeps the relative loss of each mineral constant. Calculations show that 99.33% of pure calcite would dissolve only after 5 time-steps. On a relative scale, it would take about 1250, 900, and 1040 time-steps respectively to reduce the original compositions of quartz-bearing mafic plutonic, granodioritic, and granitic rocks to leave >95% undissolved quartz as residue that will qualify as quartz-sand, the precursor to first-cycle quartz arenite. These are very large numbers indicating that chemical dissolution alone, as in chemical weathering by itself, is not sufficient to generate first-cycle quartz sand; accompanied mechanical weathering is necessary. Therefore, it is necessary to re-evaluate many explicitly stated inferences of warm, humid climate in provenance studies of first-cycle quartz arenites.

Introduction

In the context of quartz arenite (Pettijohn, 1957; Dott, 1964; Folk, 1980; Garzanti, 2019a), quartz sand is a body of natural material in which 95% or more of the sand-sized fraction (0.0625 mm – 2 mm) consists of clastic quartz. In the context of first cycle quartz arenite, first cycle quartz sand is a product of weathering of plutonic or medium to high grade metamorphic rocks, i.e., *not* derived from pre-existing sedimentary rocks. Prolonged weathering of very low relief granitic terrains under hot, humid, tropical climate and ample vegetation can eventually lead to a product of quartz and clay (Krynine, 1935; Suttner et al. 1981; Johnsson and Stallard, 1988; Soegaard and Eriksson, 1989; Swain and Gorana, 2009; van de Kamp 2010; Garzanti et al., 2013; Lorentzen et al., 2019; Khan et al., 2020 and references therein). Preferential mechanical disintegration of detrital feldspars and lithic fragments, especially through reworking on a sea beach, may generate a quartz-rich sand fraction depending on the composition of the sand reaching a beach (Sedimentation Seminar (Ferree et al.) 1988). However, authentication of any dramatic petrologic change by comparing the composition of a set of “pre-beach and beach sands” are few, if any. Rather, Ruxton (1970) documents a quartz-rich lateritic soil on a sea-cliff and lithic sand on the beach (see also, Basu, 1985).

First cycle quartz sand upon lithification would produce first cycle quartz arenite. First cycle quartzo-feldspathic sand may also produce “first cycle”

quartz arenite if diagenetic processes remove the feldspars (McBride, 1987; Chandler, 1988), replace the feldspars with silica (Wallace, 1976), or alter the feldspars to clay (Sorby, 1859; Brenchley, 1969; Valloni et al., 1991) in which case, however, the arenitic texture moves towards that of wacke (Dott, 1964). Indeed, in its pure form, usually silica cemented and white, first cycle quartz arenite is a fascinating rock that rivals “pure single malt Scotch whiskey” (Dott, 2003). Amajor (1987), however, stresses that “... most ancient quartz arenites are multicycle in origin”. We refer the reader to Garzanti et al. (2019) who has discussed the quartz arenite problem with great erudition followed by Lorentzen et al. (2020) with a dissenting opinion.

The qualitative arguments for the production of quartz sand through weathering are so strong that the inverse, i.e., the occurrence of ancient first cycle quartz arenites has been used to infer the paleoclimate – warm and humid – of source regions (e.g., Dutta and Wheat, 1993; Avigad et al. 2005; Chakraborty and Sensarma, 2008; Quasim et al., 2017). Petrographic evidence of recycling such as presence of mudclasts (Choudhuri, et al., 2020), grain rounding (Suttner and Dutta, 1986; Mehring and McBride, 2007), or abraded quartz overgrowths (Ojkanagas, 1963; Johnsson and Stallard, 1988; Critelli et al., 2013; Garzanti et al., 2013; Basu et al, 2013) are not often discussed in these studies on paleoclimate. Short rivers depositing sand in a basin commonly run through rugged topography and often

change drainage patterns thus preventing long-lived weathering and resulting in deposition of arkosic or lithic sands (Krynine, 1935; Stevens Goddard et al., 2020). Long rivers, such as the Amazon, Congo, Ganges, St. Lawrence, etc., capable of temporarily storing sand on floodplains where further chemical weathering takes place, however, do also drain sedimentary rocks such that the river sands become a mixture of first and recycled detritus. These rivers also flow across different climatic zones. So far, no attempt has been made to quantify the extents of these variables in the context of the origin of first cycle quartz sand.

Sand production is a function of chemical, mechanical, and bio-weathering (Pettijohn et al., 1972; Nesbitt et al., 1997; Napieralski et al., 2019; Caracciolo, 2020). This paper addresses only chemical weathering as a complement to primarily mechanical breakdown of clastic grains during fluvial transport and beach reworking in the production of quartz sand (Blatt, 1967; Sedimentation Seminar (Ferree et al.), 1988; and references therein).

The purpose of this investigation is to assess quantitatively the relative survival of detrital minerals through progressive dissolution, and eventual production of quartz sand and quartz arenite. A theoretical approach is taken to assess the relative efficiencies of producing quartz sand from common plutonic rocks. A simple first order decay equation and experimentally determined relative rates of dissolution of common minerals are used to calculate how many steps of decay – from source to sink – would be necessary to convert a plutonic rock to quartz sand. Mechanical strengths of rocks and minerals are not considered.

Assumptions, Parameters, Proxies and Rationale

It is assumed that the loss of detrital minerals progresses exponentially as a first-order process, which can be monitored using the equation $P_t = P_o e^{-\lambda(m)t}$, where P_o is the original population of mineral “m”, P_t is the population of mineral “m” after time “t” since the beginning of the process of mineral loss, and $\lambda(m)$ is the rate constant of loss of mineral “m”. In reality, the absolute amount of loss of mineral “m”, however, increases at a greater rate as its grain size decreases with concomitant increase in specific surface area. This increase is countered by the precipitation of the alteration product (e.g., clay) that forms a coat on mineral grains and prevents the solvent (~water) from dissolving the mineral efficiently, and, if the solvent reaches saturation before being “washed away”. It is further assumed that the reactive surfaces of all mineral grains are fully available for dissolution throughout the complete process of weathering. In reality, it is not so

Table 1. Mineral Dissolution Rates (~λ values)

Note: Blank in column 3 indicates that the value in column 4 is estimated from other data.

Nomenclature in Francke's Table 2 and Table 3 are not consistent; for example, Ca-Plag (An66) is called anorthite.

Mineral	Composition	Franke Tbl3 mg m ⁻² d ⁻¹	Accept / Est	Factor (cc=1) λ
Muscovite		0.34	0.34	0.0006
Sanidine	Or86	1	1	0.0017
Kyanite		1.5	1.5	0.0025
Biotite		1.6	1.6	0.0027
Alk Feldspar	>Or70	2.1	2.1	0.0035
Na Plag	>Ab50	2.5	2.5	0.0042
Orthoclase			2.5	0.0042
Albite			3	0.0050
Epidote		4	4	0.0067
Med Plag	An50-An65	7	7	0.0117
Augite	Mg83	11	11	0.0183
Leucite	K90	12	12	0.0200
Pyroxene		17	17	0.0283
Bronzite	Mg83	20	20	0.0333
Hornblende		25	25	0.0417
Ca Plag	An66	40	40	0.0667
Chlorite		54	54	0.0900
Nepheline		70	70	0.1167
Anorthite	??An90		100	0.1667
Olivine	Fo90	220	220	0.3667
Magnesite		285	285	0.4750
Calcite		600	600	1.0000
Ilmenite				0.0300
Magnetite				0.0300
Hematite				0.0300
Quartz		0	0	0.0001
Zircon		0	0	0.0001
Apatite		0	0	0.0100

because products of dissolution may coat a mineral grain and the solvent may change its composition. Note that the rate of grain coating and the rate of solvent replenishment cannot be quantified. Further, experiments by Holdren and Speyer (1985, 1987) show that grain surface defects are more important than grain surface area in facilitating dissolution reactions. Hence,

the assumption is a pragmatic compromise for the purpose.

Franke's (2009) experimental data on rates of dissolution of minerals have been used as quantitative guides to estimate λ . Although not as comprehensive as the huge compilation in Palandri and Kharaka (2004), this dataset is internally consistent, i.e., experiments were conducted at the same P, T and pH for all 39 minerals in the same laboratory by the same investigator. The experimentally determined rates of dissolution of common rock forming minerals at 20° C and pH = 5.5 are given in Table 1. To assess quantitatively the relative loss of minerals through progressive dissolution under principally chemical

weathering, λ_m has been normalized to the dissolution rate of calcite (cc) such that $\lambda_{cc} = 1$ (dimensionless). Francke (2009) was not able to determine the rates of dissolution of quartz (qz) and zircon (zr). Palandri and Kharaka's compilation (2004) indicates that the relative rates of dissolution of quartz and zircon under similar conditions would be a few orders of magnitude lower. Values of 0.0001 have been assigned to λ_{qz} and λ_{zr} . Similar reasoning and extrapolations have been used to assign λ_m for minerals for which Francke (2009) did not have direct measurements (Table 1).

Because λ_m is dimensionless, results of calculations represent relative time-steps in the process of chemical dissolution of the minerals but not absolute

Table 2. Modal compositions of parent rocks (from literature)

Sample Ref	Rock	Quartz	K-Felds	Plag	Musc	Biotite	Hbl	Cpx	Opx	Opq	Chlort	Total
Hill R3	Adamellite	34.1	40.9	13.1	1	10.6	0	0	0	0.13	0	99.8
Greenberg SS	Granite	39.2	32.3	25.2	0.4	0.6	0	0	0	2.3	0	100
Hazra AP30	Granite	50.5	21.06	19.88	0	8.29	0	0	0	0.24	0	100
Hazra AP39	Granite	26.05	53.63	12.79	0	4.32	0	0	0	0.37	2.84	100
Hazra AP57	Granite	16.89	55.05	2.32	0	25.26	0	0	0	0.47	0	100
Hazra AP95	Granite	37.42	22.95	27.79	0	10.84	0	0	0	0.58	0	99.6
Hazra P23	Granite	20.5	20.15	26.3	0	31.25	0	0	0	0.2	1.2	99.6
Hazra P7	Granite	18.52	60.9	13.05	0	4.55	0	0	0	0.5	0	97.5
Hill BenNevis*	Granite	27.5	24.2	37.2	0	10.1	0	0	0	1	0	100
Hill R1	Granite	31.3	44.6	19.1	0.14	4.83	0	0	0	0.06	0	100
Lanphere p386-2	Granite	28.1	30.2	21.6	0	16.6	0	0	0	1.2	0	97.7
Bando MBG^	AnOro	35.4	48.3	9.3	0	1.4	2.5	0	0	1.6	0	98.5
Bando SBGII^^	Granite Oro	28.2	15.6	49.2	0.15	1.5	0	0	0	0.5	4.6	99.8
Zanvilevich T1	PerAlk	23	70	0	0	0	2.5	3	0	0.6	0	99.1
D'Amico Gd27	Granodiorite	27.4	15.2	44.3	0	13.1	0	0	0	0	0	100
Erikson 262	Granodiorite	41	6	46	0	6	1	0	0	0	0	100
Hill R2	Granodiorite	25	23.7	41.9	0.18	8.8	0	0	0	0.02	0.2	99.8
Lanphere p386-1	Granodiorite	15	10	40	0	25	7	0	0	3	0	100
Noyes CR29	Granodiorite	26.6	18.7	47	0	5.2	0	0	0	0.3	0.9	98.7
D'Amico T42	Tonalite	24.8	5.6	48.4	0	21.2	0	0	0	0	0	100
Kesler RD72-2	Tonalite	33	6	43	0	6	11	0	0	1	0	100
Kesler RD72-30	Tonalite	13	0	36	0	0	48	0	0	3	0	100
Noyes M10	Diorite	10	0.7	48.3	0	24.6	13.3	0	0	1.6	1.2	99.7
Gandolfi **	Qz Diorite	23	6	49	0	16	0	4	0	0	0	98.0
Olmst W164	Qz Gabbro	3	0.4	52.7	0	3.2	1	25.5	7.6	4.3	0	97.7

time. Each step is an integral of intensity and duration of chemical duration (~ weathering) that is experienced

equally by all minerals in an assemblage of interest. It follows that the amount of absolute dissolution suffered

by each mineral in a time-step is proportionate to their respective values of λm . For example, in five time-steps calcite would be reduced from 100% to 0.67%, plagioclase (~An₆₅) to 71.64%, and K-feldspar to 97.94%.

For assessing the effects of chemical dissolution of source rocks of sediments, modal compositions of a few common plutonic parent rocks were used as starting material, which include 13 granites, 5 granodiorites, 3 tonalites, 2 diorites, one gabbro, and one adamellite (Table 2). The samples were treated in three groups, i.e., granite-adamellite, granodiorite-tonalite, and diorite-gabbro.

Calculations and Results.

Table 3: Normalized compositions of undissolved residuals from three suites of plutonic rocks after stepwise dissolution

Granite											
Time-Steps	Quartz	K-Felds	Plag	Musc	Biot	Hbl	ClinoPx	OrthoPx	Opaque	Chlorite	Total
0	29.92	38.84	19.87	0.12	9.35	0.36	0.22	0.00	0.70	0.62	100
1	30.03	38.82	19.86	0.12	9.36	0.35	0.21	0.00	0.68	0.57	100
5	30.44	38.72	19.81	0.12	9.39	0.30	0.20	0.00	0.61	0.40	100
10	30.94	38.56	19.73	0.12	9.42	0.25	0.19	0.00	0.54	0.26	100
20	31.89	38.15	19.52	0.13	9.46	0.17	0.16	0.00	0.41	0.11	100
30	32.80	37.69	19.28	0.13	9.49	0.11	0.14	0.00	0.31	0.05	100
40	33.71	37.18	19.02	0.13	9.50	0.08	0.12	0.00	0.24	0.02	100
50	34.61	36.65	18.75	0.14	9.51	0.05	0.10	0.00	0.18	0.01	100
60	35.51	36.11	18.47	0.14	9.51	0.04	0.09	0.00	0.14	0.00	100
70	36.41	35.55	18.19	0.14	9.50	0.02	0.07	0.00	0.11	0.00	100
80	37.32	34.99	17.90	0.15	9.49	0.02	0.06	0.00	0.08	0.00	100
90	38.23	34.41	17.60	0.15	9.48	0.01	0.05	0.00	0.06	0.00	100
100	39.15	33.83	17.31	0.15	9.46	0.01	0.05	0.00	0.05	0.00	100
200	48.53	27.93	14.29	0.18	9.07	0.00	0.01	0.00	0.00	0.00	100
300	57.89	22.18	11.35	0.20	8.37	0.00	0.00	0.00	0.00	0.00	100
400	66.63	17.00	8.70	0.22	7.45	0.00	0.00	0.00	0.00	0.00	100
500	74.26	12.62	6.45	0.24	6.43	0.00	0.00	0.00	0.00	0.00	100
600	80.58	9.12	4.66	0.25	5.40	0.00	0.00	0.00	0.00	0.00	100
700	85.57	6.45	3.30	0.25	4.43	0.00	0.00	0.00	0.00	0.00	100
800	89.39	4.48	2.29	0.25	3.58	0.00	0.00	0.00	0.00	0.00	100
900	92.24	3.08	1.58	0.24	2.86	0.00	0.00	0.00	0.00	0.00	100
1000	94.33	2.10	1.07	0.24	2.26	0.00	0.00	0.00	0.00	0.00	100
2000	99.60	0.04	0.02	0.16	0.18	0.00	0.00	0.00	0.00	0.00	100
5000	99.96	0.00	0.00	0.04	0.00	0.00	0.00	0.00	0.00	0.00	100
Granodiorite-Tonalite											
Time-Steps	Quartz	K-Felds	Plag	Musc	Biot	Hbl	ClinoPx	OrthoPx	Opaque	Chlorite	Total
0	25.78	10.69	43.41	0.02	10.67	8.38	0.00	0.00	0.92	0.14	100
1	26.02	10.75	43.33	0.02	10.75	8.11	0.00	0.00	0.90	0.13	100
5	27.00	10.97	42.92	0.02	11.04	7.13	0.00	0.00	0.83	0.09	100
10	28.20	11.23	42.31	0.02	11.38	6.05	0.00	0.00	0.74	0.06	100
20	30.54	11.67	40.81	0.03	12.01	4.32	0.00	0.00	0.60	0.03	100
30	32.79	12.03	39.03	0.03	12.57	3.06	0.00	0.00	0.47	0.01	100
40	34.97	12.32	37.08	0.03	13.07	2.15	0.00	0.00	0.38	0.01	100
50	37.08	12.55	35.03	0.03	13.51	1.51	0.00	0.00	0.30	0.00	100
60	39.14	12.71	32.93	0.03	13.89	1.05	0.00	0.00	0.23	0.00	100
70	41.15	12.83	30.84	0.03	14.24	0.73	0.00	0.00	0.18	0.00	100
80	43.10	12.91	28.78	0.04	14.53	0.50	0.00	0.00	0.14	0.00	100
90	45.01	12.94	26.77	0.04	14.79	0.35	0.00	0.00	0.11	0.00	100
100	46.86	12.94	24.83	0.04	15.01	0.24	0.00	0.00	0.08	0.00	100
200	62.53	11.49	10.42	0.05	15.50	0.00	0.00	0.00	0.01	0.00	100
300	73.14	8.95	3.83	0.06	14.02	0.00	0.00	0.00	0.00	0.00	100
400	80.19	6.54	1.32	0.06	11.89	0.00	0.00	0.00	0.00	0.00	100
500	85.11	4.62	0.44	0.06	9.77	0.00	0.00	0.00	0.00	0.00	100

600	88.72	3.21	0.14	0.06	7.88	0.00	0.00	0.00	0.00	0.00	100
700	91.42	2.20	0.05	0.06	6.28	0.00	0.00	0.00	0.00	0.00	100
800	93.47	1.50	0.02	0.06	4.97	0.00	0.00	0.00	0.00	0.00	100
900	95.02	1.01	0.00	0.05	3.91	0.00	0.00	0.00	0.00	0.00	100
1000	96.20	0.68	0.00	0.05	3.06	0.00	0.00	0.00	0.00	0.00	100
2000	99.71	0.01	0.00	0.03	0.24	0.00	0.00	0.00	0.00	0.00	100
5000	99.99	0.00	0.00	0.01	0.00	0.00	0.00	0.00	0.00	0.00	100

Diorite-Gabbro

Time-Steps	Quartz	K-Felds	Plag	Musc	Biot	Hbl	ClinoPx	OrthoPx	Opaque	Chlorite	Total
0	12.19	2.41	50.80	0.00	14.76	4.79	10.06	2.59	2.00	0.41	100
1	12.68	2.50	49.44	0.00	15.31	4.78	10.28	2.61	2.02	0.39	100
5	14.73	2.85	43.98	0.00	17.60	4.70	11.09	2.65	2.08	0.31	100
10	17.41	3.31	37.26	0.00	20.54	4.51	11.97	2.66	2.12	0.24	100
20	22.82	4.16	25.10	0.00	26.25	3.90	13.08	2.50	2.06	0.13	100
30	27.78	4.86	15.70	0.00	31.14	3.14	13.27	2.18	1.86	0.06	100
40	31.95	5.37	9.27	0.00	34.90	2.38	12.71	1.80	1.59	0.03	100
50	35.29	5.70	5.26	0.00	37.58	1.73	11.70	1.42	1.30	0.01	100
60	37.95	5.88	2.91	0.00	39.39	1.23	10.49	1.10	1.04	0.01	100
70	40.12	5.97	1.58	0.00	40.58	0.86	9.24	0.83	0.81	0.00	100
80	41.93	5.99	0.85	0.00	41.34	0.59	8.05	0.62	0.63	0.00	100
90	43.48	5.97	0.45	0.00	41.79	0.41	6.95	0.46	0.48	0.00	100
100	44.86	5.91	0.24	0.00	42.02	0.28	5.98	0.34	0.37	0.00	100
200	54.51	4.78	0.00	0.00	39.50	0.01	1.17	0.02	0.02	0.00	100
300	61.63	3.60	0.00	0.00	34.55	0.00	0.21	0.00	0.00	0.00	100
400	67.88	2.64	0.00	0.00	29.44	0.00	0.04	0.00	0.00	0.00	100
500	73.45	1.90	0.00	0.00	24.64	0.00	0.01	0.00	0.00	0.00	100
600	78.32	1.35	0.00	0.00	20.33	0.00	0.00	0.00	0.00	0.00	100
700	82.49	0.95	0.00	0.00	16.56	0.00	0.00	0.00	0.00	0.00	100
800	85.99	0.66	0.00	0.00	13.36	0.00	0.00	0.00	0.00	0.00	100
900	88.87	0.45	0.00	0.00	10.68	0.00	0.00	0.00	0.00	0.00	100
1000	91.21	0.31	0.00	0.00	8.48	0.00	0.00	0.00	0.00	0.00	100
2000	99.29	0.01	0.00	0.00	0.71	0.00	0.00	0.00	0.00	0.00	100
5000	100.00	0.00	0.00	0.00	0.00	0.00	0.00	0.00	0.00	0.00	100

Compositions of plagioclase as counted in petrographic modal analyses were respectively assigned as An_{<50}, An₅₀₋₆₅, and An₋₆₅ the rates of dissolution of which are available in Franke (2009). Results of step-wise dissolution of the averages of these three groups are given in Table 3. Proportions of undissolved minerals were recalculated to 100% to obtain mineral percentages of the presumed sand fraction after each time-step. Table 4 lists a few vari-

ables in each sample and the averages, which bear upon the discussion of generating first-cycle quartz sand and quartz arenite.

An example of a complete calculation is given in Appendix Table 1 with a granodiorite (CR29; Noyes et al., 1983) as the parent rock with $\lambda_{PI} = 0.0117$. The corresponding Excel File is archived and can also be obtained directly from the author.

Table 4. Rock compositions and time-steps required for 50% loss and attaining 95% quartz

Sample	Rock	Quartz % Normalized to 100%	Feldspar % Normalized to 100%	Mafic % Normalized to 100%	P/(P+K)	Steps required for ~50% loss of parent rock	Steps required for ~95% quartz in residue	Reference
R3	Adamellite	34.2	54.0	10.7	0.24	360	1100	Hill et al. 1993
G-SS	Granite	39.2	57.5	2.9	0.44	390	860	Greenberg 1981
AP30	Granite	50.5	40.9	8.5	0.49	750	800	Hazra et al. 2010
AP39	Granite	26.1	66.4	7.5	0.19	260	1020	Hazra et al. 2010
AP57	Granite	16.9	57.4	25.7	0.04	750	1400	Hazra et al. 2010
AP95	Granite	37.6	50.7	11.4	0.55	390	950	Hazra et al. 2010
P23	Granite	20.6	46.5	32.7	0.57	285	1400	Hazra et al. 2010
P7	Granite	19.0	74.0	5.1	0.18	230	1150	Hazra et al. 2010
HBN	Granite	27.5	61.4	11.1	0.61	290	700	Hill 1996
R1	Granite	31.3	63.7	4.9	0.30	310	1000	Hill et al. 1993
386-2	Granite	28.8	51.8	17.8	0.42	310	1125	Lanphere 1964
MBG	Granite anorogenic	35.9	57.6	5.5	0.16	350	870	Bandyopadhyay et al. 2001
SBG II	Granite orogenic	27.3	64.8	6.6	0.76	300	975	Bandyopadhyay et al. 2001
T1	Granite PerAlk	23.2	70.0	6.1	0.00	230	1000	Zanvilevich et al. 1995
Average	Granite	29.9	58.7	11.2	0.34	300	1040	
GD27	Granodiorite	27.4	59.5	13.1	0.74	160	950	D'Amico et al. 1971
262	Granodiorite	41.0	52.0	7.0	0.88	210	550	Erikson 1969
R2	Granodiorite	25.1	65.6	9.0	0.64	155	1000	Hill et al. 1993
386-1	Granodiorite	15.0	50.0	35.0	0.80	115	1375	Lanphere 1964
CR29	Granodiorite	27.0	65.7	6.4	0.72	140	800	Noyes et al. 1983
T42	Tonalite	24.8	54.0	21.2	0.90	150	1100	D'Amico et al. 1971
72-2	Tonalite	33.0	49.0	18.0	0.88	130	625	Kesler et al., 1974
72-30	Tonalite	13.0	36.0	51.0	1.00	34	340	Kesler et al., 1974
Average	Granodio- Tonalite	25.8	54.1	20.1	0.80	125	900	
M10	Diorite	10.0	49.0	40.7	0.99	23	1500	Noyes et al. 1983
Gdlf	Diorite	23.5	55.0	20.0	0.89	260	1050	D'Amico et al. 1971
W164	Gabbro	3.1	53.1	41.6	0.99	17	1200	Olmstead 1979
Average	Diorite-Gabbro	12.2	53.2	34.6	0.95	23	1250	

Discussion

Quartz arenite is the extreme and ultimate sand-size product of sedimentary processes (weathering-transport-deposition-diagenesis/ lithification) operating on a planetary body. Intensity and duration of weathering, both physical and chemical, from source to sink may produce sands with >95% detrital quartz dissolving or winnowing out other minerals supplied at source. Most beach sands at the mouths of long rivers are extremely quartz-rich (e.g., Potter, 1978; Johnsson et al., 1991; Mehring and McBride, 2007; Garzanti et al., 2015; and references therein). Long rivers commonly derive their detrital load not only from crystalline igneous and medium to high grade metamorphic rocks, but also from sedimentary and low grade metamorphic rocks, i.e., recycled sands (see definition above; also Suttner et al., 1981). If not, i.e., if the detritals are not recycled, the sand is first cycle. If the sand consists of >95% quartz, it would be lithified into a first cycle quartz arenite. Whereas this is intuitive, one may reasonably inquire if we can quantify time-steps of weathering to produce quartz-sand as undissolved residue through mineral dissolution.

Calculations described above show that relative to calcite that dissolves to <50% in less than one time-step, it takes about 23, 125, and 300 time-steps to dissolve 50% of average quartz-bearing mafic plutonic rocks, granodioritic rocks, and granitic rocks respectively (Table 4). Quartz in the remaining 50% undissolved solid residue amounts to 24%, 51%, and 58% respectively. Assuming that the residue remains in the sand-size fraction, it takes about 1250, 900, and 1040 time-steps respectively for the undissolved residue to become first cycle quartz sand (>95% quartz). At those time-steps, nearly 90%, 75%, and 70% of the original parent rocks would also have dissolved. Under normal surface conditions in the tropics of earth, only “prolonged” weathering of low-relief felsic plutonic terrain can generate first-cycle quartz sand (Krynine, 1935; all textbooks since). To do so, weathering must be prolonged by a factor of 10^3 relative to calcite that reduces by ~65% in *one* time-step. Given how lofty high grounds and mountains of limestone, marble, and other carbonate rocks stand today, expecting such “prolonged” weathering is unrealistic.

During weathering, most of the dissolved components precipitate as alteration products such as clay. If we assume that about 10% of the dissolved component stays in solution in river waters, then the ratio of quartz to clay (*sensu latu*) would be approximately 1:8, 1:7, and 1:6 respectively. If quartz and clay were winnowed from each other and deposited as sand and mud respectively, then upon lithification these would be quartz arenite and mudstone respectively. Under such conditions, the proportion of first cycle quartz arenite and mudstone would vary

between 1:6 and 1:8 in a single stratigraphic unit depending upon the assemblage of parent rocks. Thus, everything else remaining the same, every 1 m thickness of quartz arenite in a single stratigraphic succession should be balanced by 6 to 8 m of mudstone. Quartz-free mafic rocks in source areas, such as basalt or andesite in magmatic arcs, will only add to the mudstone budget.

In the above analysis of mineral dissolution,

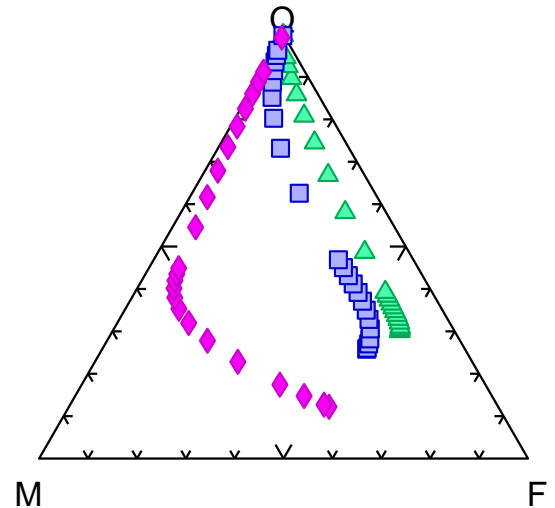


Figure 1. Evolution of quartz-mafic mineral-feldspar compositions of quartzdiorite-gabbro (diamonds), granodioritic (squares), and granitic (triangles) rocks with progressive dissolution

lithic fragments are not treated as a component in the modal composition of a sandstone. Therefore, the results of intermediate products, i.e., the composition of the sand-product on way to becoming quartz-sand, cannot be interpreted by the standard QFL plots (e.g., Dickinson et al., 1983; Marsaglia, 2004; Devi and Mondal, 2008; Sen et al., 2014; Majumder, 2020; and references therein). Those that consist of primarily sand-size quartz and feldspar without or with very little of other minerals, would be counted as either quartz or feldspar in the commonly used GD method. Mafic minerals (e.g., biotite, amphibole, pyroxene, olivine, Fe-oxide phases) in the parent rocks would be present in their weathering products albeit in dwindling proportions. The trajectory of the weathering products can be tracked in a Quartz-Mafic Mineral-Feldspar-(QMF) diagram (Fig. 1). Although mafic minerals are primarily sourced from magmatic arcs, the QMF diagram should not be considered analogous to the standard QFL plot. Rather, this diagram may be considered as a limited quantified version of Figure 1 of Blatt (1967; p. 1036) that tracks the “relative effects of sedimentary processes on sand-sized clastic grains”.

The diagram illustrates the compositional paths of weathering products of the principal plutonic rocks to become quartz sand. If weathering is stopped at any time-step, the product lithified as a sedimentary rock, and subsequently weathered again, the recycled product will still need many time steps to produce quartz sand. For example, if recycling begins after 100 time-steps then it would still be necessary to go through about 800 new time-steps to concentrate quartz to >95%. Under conditions in which only 5 time-steps reduces 100% calcite to <0.7%, 800 is a large number. It is concluded that although possible under extreme conditions, chemical weathering *alone* does not produce first-cycle quartz sand.

Mechanical destruction of feldspars and lithic fragments is necessary to concentrate quartz as residual. In natural stream samples of sand, finer grain size fractions have lesser proportions of feldspars than quartz and very little composite grains, i.e., lithic fragments (e.g., Odom et al., 1976; Basu, 1976; Garzanti, et al., 2009). Transport in a long river and prolonged reworking on a beach can reduce a feldspathic sandy assemblage to quartz sand (Johnsson, 1988; Johnsson et al., 1991). If long rivers from source to sink or if beaches actually remain free of any input of recycled sand from tributaries and aeolian supply in the natural system, will be a matter of discussion in a follow-up note.

There are more than a thousand reports of first-cycle quartz arenites in the literature. All call on primarily chemical and some mechanical weathering for the production of quartz sand. Most explanations include warm and humid climate, low-relief hinterland consisting of felsic plutonic rocks, and long duration weathering. For example, see the discourses by Soegaard and Eriksson (1989) on the Paleoproterozoic Ortega Group in U.S.A.; Chakraborty and Sensarma, (2008) on the Paleoproterozoic Karutola Formation in India; the general discourses by Van de Kamp (2010) and Johnsson et al. (1991); and references therein. If paleotectonic reconstructions indicate rapid erosion and rapid deposition, very toxic atmospheric conditions such as those with high CO₂ capable of rapid chemical weathering have been inferred. For example, Avigad et al. (2005) envisage “An unusually corrosive Cambro-Ordovician atmosphere and humid climate enhanced chemical weathering on the vegetation-free landscape” in all Pan-African terrains; Holland et al. (2020) and Jones et al. (2008) postulate acid weathering in greenhouse atmosphere in combination with mechanical weathering to produce the extensive “quartz arenite successions from Paleoproterozoic and Mesoproterozoic strata throughout North America”, some of which are adjacent to juvenile arcs.

Because chemical weathering by itself does not produce extensive deposits of quartz sand, inferences

about paleoclimate from the presence of first-cycle quartz arenite in a sedimentary basin are not as robust as some publications may lead us to believe.

Examples cited above and numerous others appear to contradict the inference drawn from the theoretical analysis of experimental data on mineral dissolution. Johnsson and Stallard (1988) contended that claims to first cycle origin of detrital quartz can only be tested by the “presence of sedimentary lithic fragments and syntaxial quartz overgrowths” as has been demonstrated in lithified quartz arenites, for example by Ojakangas (1963) but not explicitly followed by others. In view of this study, it is advisable to search for abraded overgrowths on detrital quartz grains in the putative first cycle quartz arenites (e.g., Basu et al., 2013; and references therein).

Conclusion

Theoretical consideration of the relative rates of dissolution of common minerals suggests that production of large volumes of first-cycle quartz sand (quartz >95%) from common plutonic rocks on Earth would require unusually long time and possibly unusually toxic atmospheric conditions. Because supply of first-cycle quartz sand is required to produce first-cycle quartz arenites that have been reported from many parts of the earth throughout geological time, new searches for recycled detrital quartz grains are necessary to verify that indeed such first-cycle quartz arenites are free of recycled detrital quartz. Additionally, inferences about paleoclimate on the basis of the presence of quartz arenite appear to require other independent indicators.

Acknowledgements

Correspondence and discussions with Drs. M. E. Bickford, K. Karlstrom, E. Merino, R. P. Wintsch, and C. Zhu proved enormously helpful. Reviewers and editors of JIAS are thanked for their comments and suggestion that improved an earlier version of the manuscript. This research was supported by Indiana University.

References

- Amajor, L.C. (1987), Paleocurrent, petrography and provenance analyses of the Ajali Sandstone (Upper Cretaceous), southeastern Benue Trough, Nigeria: *Sedimentary Geology*, v. 54, p. 47-60.
- Avigad, D., Sandler, A., Kolodner, K., Stern, R.J., McWilliams, M., Miller, N. and Beyth, M. (2005), Mass-production of Cambro-Ordovician quartz-rich sandstone as a consequence of chemical weathering of Pan-African terranes: environmental implications: *Earth and Planetary Science Letters*, v. 240, p. 818-826.
- Bandyopadhyay, P.K., Chakrabarti, A.K., DeoMurari, M.P. and Misra, S. (2001), 2.8 Ga old anorogenic granite-acid volcanics association from western margin of the Singhbhum-Orissa craton, eastern India: *Gondwana Research*, v. 4, p. 465-475.

- Basu, A. (1976), Petrology of Holocene fluvial sand derived from plutonic source rocks: implications to paleoclimatic interpretation: *Journal of Sedimentary Petrology*, v. 46, p. 694-709.
- Basu, A. (1985), Influence of climate and relief on compositions of sands released at source areas, in Zuffa, G.G., (ed.), *Provenance of Arenites*, NATO-ASI, v. 148, p. 1-18.
- Basu, A., Schieber, J., Patranabis-Deb, S. and Dhang, P.C. (2013), Recycled detrital quartz grains are sedimentary rock fragments indicating unconformities: Examples from the Chhattisgarh Supergroup, Bastar craton, India: *Journal of Sedimentary Research*, v. 83, p. 368-376.
- Blatt, H. (1967), Provenance determinations and recycling of sediments: *Journal of Sedimentary Petrology*, v. 37, p. 1031-1044.
- Brenchley, P.J. (1969), Origin of matrix in Ordovician greywackes, Berwyn Hills, North Wales: *Journal of Sedimentary Petrology*, v. 39, p. 1297-1301.
- Caracciolo, L. (2020), Sediment generation and sediment routing systems from a quantitative provenance analysis perspective Review, application and future development: *Earth-Science Reviews*, v. 209, p. on line S103226
- Chakraborty, T. and Sensarma, S. (2008), Shallow marine and coastal eolian quartz arenites in the Neoproterozoic Palaeoproterozoic Karutola Formation, Dongargarh volcano-sedimentary succession, central India: *Precambrian Research*, v. 162, p. 284-301.
- Chandler, F.W. (1988), Quartz arenites: review and interpretation: *Sedimentary Geology*, v. 58, p. 105-126.
- Choudhuri, A., Schieber, J., Sarkar, S., Bickford, M.E. and Basu, A. (2020), The "Lower Kaimur Porcellanite" (Vindhyan Supergroup) is of sedimentary origin and not tuff: *Journal of the Geological Society of India*, v. 95, p. 17-24.
- Critelli, S., Arribas, J., Le Pera, E., Tortosa, A., Marsaglia, K.M. and Latter, K.K. (2003), The recycled orogenic sand provenance from an uplifted thrust belt, Betic Cordillera, Southern Spain: *Journal of Sedimentary Research*, v. 73, p. 72-81.
- D'Amico, C., Del Monte, M. and Gandolfi, G. (1971), Multiple intrusions in the Cima D'Asta pluton (northern Italy): *Contributions to Mineralogy and Petrology*, v. 13, p. 13-27.
- Devi, S.R. and Mondal, M.E.A. (2008), Provenance and tectonic setting of Barail (Oligocene) and Surma (Miocene) Group of Surma-Barak Basin, Manipur, India: petrographic constraints: *Journal of the Geological Society of India*, v. 71, p. 459-467.
- Dickinson, W.R., Beard, L.S., Brakenridge, G.R., Erjavec, J.L., Ferguson, R.C., Inman, K.F., Knepp, R.A., Lindberg, A.F. and Ryberg, P.T. (1983), Provenance of North American Phanerozoic sandstones in relation to tectonic setting: *Bulletin Geological Society of America*, v. 94, p. 222-235.
- Dott, R.H. (1964), Wacke, greywacke and matrix: What approach to immature sandstone classification? *Journal of Sedimentary Petrology*, v. 34, p. 625-632.
- Dott, R.H. (2003), The importance of eolian abrasion in supermature quartz sandstones and the paradox of weathering on vegetation-free landscapes. *The Journal of Geology*, v. 111, p. 387-405.
- Dutta, P.K. (2007), First-cycle sandstone composition and color of associated fine-grained rocks as an aid to resolve Gondwana stratigraphy in Peninsular India, in Arribas, J., Critelli, S. and Johnsson, M.J., (eds.), *Sedimentary Provenance and Petrogenesis: Perspectives from Petrography and Geochemistry*, Geological Society of America Special Paper, v. 420, p. 241-252.
- Dutta, P.K. and Wheat, R.W. (1993), Climatic and tectonic control on sandstone composition in the Permo-Triassic Sydney foreland basin, eastern Australia, in Johnsson, M.J. and Basu, A. (eds), *Processes Controlling the Composition of Clastic Sediments*, Geological Society of America Special Paper, v. 284, p. 187-202.
- Erikson, E.H. (1969), Petrology of the Composite Snoqualmie Batholith, Central Cascade Mountains, Washington: *Bulletin Geological Society of America*, v. 80, p. 2213-2236.
- Folk, R.L. (1980), *Petrology of Sedimentary Rocks*. Austin, Hemphill's. p. 1-184
- Francke, W.A. (2009), The durability of rocks - developing a test of rock resistance to chemical weathering: *American Journal of Science*, v. 309, p. 711-730.
- Garzanti, E. (2019), Petrographic classification of sand and sandstone: *Earth-Science Reviews*, v. 192, p. 545-562.
- Garzanti, E., Andò, S., Vezzoli, G., Megid, A.A.A. and Kammar, A.E. (2006), Petrology of Nile River sands (Ethiopia and Sudan): Sediment budgets and erosion patterns: *Earth and Planetary Science Letters*, v. 252, p.327-341
- Garzanti, E., Vermeesch, P., Vezzili, G., Andò, S., Bottia, E., Limonta, M., Dini, P., Hahn, A., Baudet, D., De Grave, J. and Yayag, N.K. (2019), Congo River sand and the equatorial quartz factory: *Earth-Science Reviews*, v. 197, p. on line 102918
- Garzanti, E., Andò, S., Limonta, M., Fielding, L. and Najman, Y. (2018), Diagenetic control on mineralogical suites in sand, silt, and mud (Cenozoic Nile Delta): Implications for provenance reconstructions: *Earth-Science Reviews*, v. 185, p. 122-139.
- Garzanti, E., Andò, S., Padoan, M., Vezzoli, G. and El Kammar, A. (2015), The modern Nile sediment system: Processes and products. *Quaternary Science Reviews*, v. 130, p. 9-56.
- Garzanti, E., Andò, S. and Vezzoli, G. (2009), Grain-size dependence of sediment composition and environmental bias in provenance studies: *Earth and Planetary Science Letters*, v. 277, p. 422-432.
- Garzanti, E., Andò, S., Vezzoli, G., Abdel Megid, A.A. and El Kammar, A. (2006), Petrology of Nile River sands (Ethiopia and Sudan): sediment budgets and erosion patterns: *Earth and Planetary Science Letters*, v. 252, p. 327-341.
- Garzanti, E., Padoan, M., Andò, S., Resentini, A., Vezzoli, G. and Lustrino, M. (2013), Weathering and relative durability of detrital minerals in equatorial climate: and petrology and geochemistry in the East African Rift: *Journal of Geology*, v. 121, p. 547-580.
- Garzanti, E., Resentini, A., Andò, S., Vezzoli, G., Pereira, A. and Vermeesch, P. (2015), Physical controls on sand composition and relative durability of detrital minerals during ultra-long distance littoral and aeolian transport

- (Namibia and southern Angola): Sedimentology. Sedimentology, v. 62, p. 971-996.
- Greenberg, J.K. (1981), Characteristics and origin of Egyptian Younger Granites: Bulletin Geological Society of America, v. 92, p. 749-840.
- Hazra, S., Saha, P., Ray, J. and Podder, A. (2010), Simple Statistical and Mineralogical Studies as Petrogenetic Indicator for Neoproterozoic Myllem Porphyritic Granites of East Khasi Hills, Meghalaya, Northeastern India: Journal Geological Society of India, v. 75, p. 760-768.
- Hill, R.J., Tsambourakis, G. and Madsen, I.C. (1993), Improved petrological modal analyses from x-ray powder diffraction data by use of the Rietveld Method I. Selected igneous, volcanic, and metamorphic rocks: Journal of Petrology, v. 34, p. 867-900.
- Hill, S.M. (1996), The differential weathering of granitic rocks in Victoria, Australia: Journal of Australian Geology and Geophysics, v. 16, p. 271-276.
- Holdren, G.R. and Speyer, P.M. (1985), Reaction rate-surface area relationships during the early stages of weathering--I. Initial observations: Geochimica et Cosmochimica Acta, v. 49, p. 675-681.
- Holdren, G.R. and Speyer, P.M. (1987), Reaction rate-surface area relationships during the early stages of weathering. II. Data on eight additional feldspars: Geochimica et Cosmochimica Acta, v. 51, p. 2311-2318.
- Holland, M.E., Grambling, T.A., Karlstrom, K.E., Jones, J.V., Nagotko, K.N. and Daniel, C.G. (2020), Geochronologic and Hf-isotope framework of Proterozoic rocks from central New Mexico, USA: Formation of the Mazatzal crustal province in an extended continental margin arc: Precambrian Research, v. 347, on line 105820
- Johnsson, M.J. (1993), The system controlling the composition of clastic sediments: Geological Society of America Special Papers, v. 284, p. 1-20.
- Johnsson, M.J., Stallard, R.F. and Lundberg, N. (1991), Controls on the composition of fluvial sands from a tropical weathering environment: Sands of the Orinoco River drainage basin, Venezuela and Colombia: Geological Society of America Bulletin, v. 103, p. 1622-1647.
- Johnsson, M.J., Stallard, R.F. and Meade, R.H. (1988), First-cycle quartz arenites in the Orinoco River Basin, Venezuela and Colombia: Journal of Geology, v. 96, p. 263-277.
- Jones, J.V.I., Connelly, J.N., Karlstrom, K.E., Williams, M.L. and Doe, M.F. (2009), Age, provenance, and tectonic setting of Paleoproterozoic quartzite successions in the southwestern United States: Geological Society of America Bulletin, v. 121, p. 247-264.
- Kerrick, R. and Said, N. (2011), Extreme positive Ce-anomalies in a 3.0 Ga submarine volcanic sequence, Murchison Province: Oxygenated marine bottom waters. Chemical Geology, v. 280, p. 232-241.
- Kesler, S.E., Kienle, C.F. and Bateson, J.W. (1974), Tectonic Significance of Intrusive Rocks in the Maya Mountains, British Honduras: Geological Society of America Bulletin, v. 85, p. 549-552.
- Kesler, S.E., Lewis, J.F., Jones, L.M. and Walker, R.L. (1977), Early island-arc intrusive activity, Cordillera Central, Dominican Republic: Contributions to Mineralogy and Petrology, v. 65, p. 91-99.
- Khan, Z., Quasim, M.A., Amir, M. and Ahmad, A.H.M. (2020), Provenance, tectonic setting, and source area weathering of Middle Jurassic siliciclastic rocks of Chari Formation, Jumara Dome, Kachhh Basin, western India: Sedimentological, mineralogical, and geochemical constraints: Geological Journal, v. 55, p. 3537-3558.
- Krynine, P.D. (1935), Arkose deposits in the humid tropics. A study of sedimentation in southern Mexico. American Journal of Science, v. 29 (Series 5), p. 353-363.
- Lanphere, M.A. (1964), Geochronologic Studies in the Eastern Mojave Desert, California: Journal of Geology, v. 72, p. 381-399.
- Lorentzen, S., Augustsson, C., Jahren, J., Nystuen, J.P. and Schovsbo, N.H. (2019), Tectonic, sedimentary and diagenetic controls on sediment maturity of lower Cambrian quartz arenite from southwestern Baltica: Basin Research, v. 31, p. 1098-1120.
- Lorentzen, S., Braut, T., Augustsson, C., Nystuen, J.P., Jahren, J. and Schovsbo, N.H. (2020), Provenance of lower Cambrian quartz arenite on southwestern Baltica: Weathering versus recycling: Journal of Sedimentary Research, v. 90, p. 493-512.
- Majumder, T. and Patranabis-Deb, S. (2020), Classification of the Paleoproterozoic Gulcheru Formation: Implications on Early Paleogeographic and Tectonic Evolution of the Cuddapah Basin, India: Journal of the Geological Society of India, v. 96, p. 151-162.
- Marsaglia, K.M. (2004), Sandstone detrital modes support Magdalena Fan displacement from the mouth of the Gulf of California: Geology, v. 32, p. 45-48.
- McBride, E.F. (1987), Diagenesis of the Maxon sandstone (Early Cretaceous), Marathon Region, Texas: a diagenetic quartzarenite: Journal of Sedimentary Petrology, v. 57, p. 98-107.
- Medaris, L.G., Singer, B.S., Dott, R.H., Naymark, A., Johnson, C.M. and Schott, R.C. (2003), Late Paleoproterozoic climate, tectonics, and metamorphism in the southern Lake Superior region and proto-North America: evidence from Baraboo interval quartzites: Journal of Geology, v. 111, p. 243-257.
- Mehring, J.L. and McBride, E.F. (2007), Origin of modern quartzarenite beach sands in a temperate climate, Florida and Alabama, USA. Sedimentary Geology, v. 201, p. 432-445.
- Napieralski, S.A., Buss, H.L., Brantley, S.L., Lee, S., Xu, H. and Roden, E.E. (2019), Microbial chemolithotrophy mediates oxidative weathering of granitic bedrock: Proc Natl Acad Sci USA, v. 116, 26394
- Nesbitt, H.W., Fedo, C.M. and Young, G.M. (1997), Quartz and feldspar stability, steady and non-steady-state weathering, and petrogenesis of siliciclastic sands and muds. Journal of Geology, v. 105, p. 173-192.
- Noyes, H.J., Wones, D.R. and Frey, F.A. (1983), A tale of two plutons: petrographic and mineralogic constraints on the petrogenesis of the Red Lake and Eagle Peak Plutons, central Sierra Nevada, California. Journal of Geology, v. 91, p. 353-379.
- Odom, I.E., Doe, T.W. and Dott, R.H. (1976), Nature of feldspar-grain size relations in some quartz-rich sandstones: Journal of Sedimentary Research, v. 46, p. 862-870.

- Ojakangas, R.W. (1963), Petrology and sedimentation of the Upper Cambrian Lamotte Sandstone in Missouri: *Journal of Sedimentary Petrology*, v. 33, 860-873.
- Olmsted, J.F. (1979), Crystallization history and textures of the Rearing Pond gabbro, northwestern Wisconsin. *American Mineralogist*, v. 64, p. 844-855.
- Palandri, J.L. and Kharaka, Y.K. (2004), A compilation of rate parameters of water-mineral interaction kinetics for application to geochemical modeling. US Geological Survey Open File Reports 2004-1068, v. 1068, p. 1-64
- Pettijohn, F.J. (1957), *Sedimentary Rocks*. 718p. Calcutta: Oxford.
- Pettijohn, F.J., Potter, P.E. and Siever, R. (1987), *Sand and Sandstone*. New York: Springer-Verlag. p. 1-553
- Potter, P.E. (1978), Petrology and chemistry of modern big river sands: *Journal of Geology*, v. 86, p. 423-449.
- Quasim M.A., Ghosh S.K. and Ahmad A.H.M. (2019), Petrography and diagenetic evolution of the Proterozoic Kaimur Group sandstones, Son Valley, India: Implication towards reservoir quality, in Mondal, M.E.A., (ed.), p. 515-550. Springer.
- Quasim, M.A., Khan, I. and Ahmad, A.H.M. (2017), Integrated petrographic, mineralogical, and geochemical study of the upper Kaimur Group of rocks, Son Valley, India: Implications for provenance, source area weathering and tectonic setting: *Journal of the Geological Society of India*, v. 90, p. 467-484.
- Ruxton, B.P. (1970), Labile quartz-poor sediments from young mountain ranges in northeast Papua: *Journal of Sedimentary Petrology*, v. 40, p. 1262-1270.
- Sedimentation Seminar (Ferree, R.A., Jordan, D.W., Kertes, R.S., Savage, K.M. and Potter, P.E. (1988), Comparative petrographic maturity of river and beach sand, and origin of quartz arenites: *Journal of Geological Education*, v. 36, p. 79-87.
- Sen, S., Mishra, M. and Patranabis-Deb, S. (2014), Petrological study of the Kaimur Group sediments, Vindhyan Supergroup, Central India: implications for provenance and tectonics: *Geosciences Journal*, v. 18, p. 307-324.
- Soegaard, K. and Eriksson, K.A. (1989), Origin of thick, first-cycle quartz arenite successions: Evidence from the 1.7 Ga Ortega Group, northern New Mexico: *Precambrian Research*, v. 43, p. 129-141.
- Sorby, H.C. (1859), On the structure and origin of the Millstone-Grit in South Yorkshire: *Proceedings of the Geological and Polytechnic Society of West Riding of Yorkshire*, v. 3, 669-675.
- Stevens Goddard, A., Carrapa, B. and Aciar, R.H. (2020), Recognizing drainage reorganization in the stratigraphic record of the Neogene foreland basin of the Central Andes. *Sedimentary Geology*, v. 405, p. on line 105704
- Suttner, L.J. and Dutta, P.K. (1986), Alluvial sandstone composition and paleoclimate; I. Framework mineralogy: *Journal of Sedimentary Petrology*, v. 56, p. 329-345.
- Suttner, L.J., Basu, A. and Mack, G.H. (1981), Climate and the origin of quartz arenites: *Journal of Sedimentary Petrology*, v. 51, p. 1235-1246.
- Swain, S. and Gorana, S. (2009), Provenance history of Kolhan Sediments from Chaibasa-Noamundi Basin: *Journal Indian Association of Sedimentologists*, v. 18, p. 87-99.
- Valloni, R., Lazzari, D. and Calozari, M.A. (1991), Selective alteration of arkose framework in Oligo-Miocene turbidites of the Northern Apennines foreland: impact on sedimentary provenance analysis, in Morton, A.C., Todd, S.P. and Haughton, P.D.W., (eds.), *Geological Society Special Publication*, v.57. p. 125-136.
- van de Kamp, P.C. (2010), Arkose, subarkose, quartz sand, and associated muds derived from felsic plutonic rocks in glacial to tropical humid climates: *Journal of Sedimentary Research*, v. 80, p. 895-918.
- Wallace, C.A. (1976), Diagenetic replacement of feldspar by quartz in the Uinta Mountain Group, Utah and its geochemical implications: *Journal of Sedimentary Petrology*, v. 46, p. 847-861.
- Zanvilevich, A.N., Litvinovsky, B.A., Wickham, S.M. and Bea, F. (1995), Genesis of alkaline and peralkaline Syenite-Granite Series: The Kharitonovo Pluton (Transbaikalia, Russia): *Journal of Geology*, v. 103, p. 127-145.

Appendices

Construction of Appendix Table 1

For tracking the progressive relative dissolution of minerals in principal parent rocks through time steps, an Excel Worksheet was set up (for example, see Table 3). Principal minerals that survive as detritals are listed in Column A (Rows 4-14). Appropriate λ values relative to calcite (i.e., $\lambda_{cc} = 1$), for each mineral are entered in Column B. Finally, the modal composition (in mineral %) of a parent rock is input in Column C, which is normalized to 100% and appears in Column D. The amount remaining of each mineral after loss in time-steps of 0 to 5000 according to the equation $P_t = P_0 e^{-\lambda(m)t}$ (where P_0 is the original population of mineral "m", P_t is the population of mineral "m" after time-step "t" since the beginning of the process of mineral loss, and λm is the rate constant of loss of mineral "m") are in Columns F-AC. These compositions are normalized to 100% and listed in Columns F-AC, Rows 23-33.

Row 18 shows the amount of loss ($P_0 - P_t$) of the parent rock to dissolution. Row 20 is a nominal check for 100% calcite treated as a parent rock that decreases to ~37% in just one time-step.

In the example (Granodiorite Noyes CR29), 30% of the parent rock is lost after 60 time-steps during which plagioclase (Row 6) decreases from 47.6% (Column D, F) to 23.7% (Column N). And, it would take 800 time-steps to produce quartz-sand (Qz >95%; Column Y, Row 23).

It should be easy for any user of the spreadsheet to input the composition of a suspected parent rock, say R, in Column C to assess possible contribution to a siliciclastic rock from R.

EXAMPLE	λ	G'diorite		0	1	5	10	20	30	40	50	60	70	80	90	100	200	300	400	500	600	700	800	900	1000	2000	5000	Mineral	
Mineral	CC=1	Noyes CR29		Remaining after step "x" ...																									
		Mode %	Recalc 100%																										
Quartz	0.0001	26.6	26.95	26.95	26.95	26.94	26.92	26.90	26.87	26.84	26.82	26.79	26.76	26.74	26.71	26.68	26.42	26.15	25.89	25.64	25.38	25.13	24.88	24.63	24.39	22.07	16.35	Quartz	
K-Feldspar	0.0042	18.7	18.95	18.95	18.87	18.56	18.17	17.43	16.72	16.04	15.38	14.76	14.15	13.58	13.02	12.49	8.23	5.43	3.58	2.36	1.56	1.03	0.68	0.45	0.29	0.00	0.00	K-Feldspar	
Plagioclase An 50-65	0.0117	47	47.62	47.62	47.07	44.92	42.38	37.71	33.56	29.86	26.57	23.65	21.04	18.73	16.66	14.83	4.62	1.44	0.45	0.14	0.04	0.01	0.00	0.00	0.00	0.00	0.00	Plagioclase	
Muscovite	0.0006		0.00	0.00	0.00	0.00	0.00	0.00	0.00	0.00	0.00	0.00	0.00	0.00	0.00	0.00	0.00	0.00	0.00	0.00	0.00	0.00	0.00	0.00	0.00	0.00	0.00	Muscovite	
Biotite	0.0027	5.2	5.27	5.27	5.25	5.20	5.13	4.99	4.86	4.74	4.61	4.49	4.37	4.26	4.14	4.04	3.09	2.37	1.81	1.39	1.06	0.81	0.62	0.48	0.37	0.03	0.00	Biotite	
Hornblende	0.0417		0.00	0.00	0.00	0.00	0.00	0.00	0.00	0.00	0.00	0.00	0.00	0.00	0.00	0.00	0.00	0.00	0.00	0.00	0.00	0.00	0.00	0.00	0.00	0.00	0.00	Hornblende	
Clinopyroxene	0.0183		0.00	0.00	0.00	0.00	0.00	0.00	0.00	0.00	0.00	0.00	0.00	0.00	0.00	0.00	0.00	0.00	0.00	0.00	0.00	0.00	0.00	0.00	0.00	0.00	0.00	Clinopyroxene	
Orthopyroxene	0.0333		0.00	0.00	0.00	0.00	0.00	0.00	0.00	0.00	0.00	0.00	0.00	0.00	0.00	0.00	0.00	0.00	0.00	0.00	0.00	0.00	0.00	0.00	0.00	0.00	0.00	Orthopyroxene	
Olivine	0.3667		0.00	0.00	0.00	0.00	0.00	0.00	0.00	0.00	0.00	0.00	0.00	0.00	0.00	0.00	0.00	0.00	0.00	0.00	0.00	0.00	0.00	0.00	0.00	0.00	0.00	Olivine	
Opakes	0.0300	0.3	0.30	0.30	0.29	0.26	0.23	0.17	0.12	0.09	0.07	0.05	0.04	0.03	0.02	0.02	0.00	0.00	0.00	0.00	0.00	0.00	0.00	0.00	0.00	0.00	0.00	Opakes	
Chlorite	0.0900	0.9	0.91	0.91	0.83	0.58	0.37	0.15	0.06	0.02	0.01	0.00	0.00	0.00	0.00	0.00	0.00	0.00	0.00	0.00	0.00	0.00	0.00	0.00	0.00	0.00	0.00	Chlorite	
Steps				0	1	5	10	20	30	40	50	60	70	80	90	100	200	300	400	500	600	700	800	900	1000	2000	5000		
Total%		98.7	100	100	99	96	93	87	82	78	73	70	66	63	61	58	42	35	32	30	28	27	26	26	25	22	16	Total	
Loss%				0	1	4	7	13	18	22	27	30	34	37	39	42	58	65	68	70	72	73	74	74	75	78	84	Loss	
Check CC	1		100	100.00	36.79	0.67	0.00	0.00	0.00	0.00	0.00	0.00	0.00	0.00	0.00	0.00	0.00	0.00	0.00	0.00	0.00	0.00	0.00	0.00	0.00	0.00	0.00		
				Normalized%	0	1	5	10	20	30	40	50	60	70	80	90	100	200	300	400	500	600	700	800	900	1000	2000	5000	
				Quartz	26.95	27.15	27.93	28.89	30.79	32.69	34.59	36.50	38.42	40.32	42.22	44.10	45.96	62.36	73.91	81.60	86.83	90.51	93.13	95.02	96.38	97.36	99.86	100.00	
				K-Feldspar	18.95	19.01	19.24	19.50	19.96	20.34	20.67	20.94	21.16	21.33	21.44	21.50	21.52	19.44	15.34	11.28	7.99	5.55	3.80	2.58	1.74	1.17	0.02	0.00	
				Plagioclase	47.62	47.42	46.57	45.47	43.17	40.83	38.48	36.17	33.91	31.71	29.57	27.52	25.54	10.90	4.06	1.41	0.47	0.15	0.05	0.02	0.01	0.00	0.00	0.00	
				Muscovite	0	0	0	0	0	0	0	0	0	0	0	0	0	0	0	0	0	0	0	0	0	0	0	0	
				Biotite	5.27	5.29	5.39	5.50	5.72	5.92	6.10	6.28	6.44	6.59	6.72	6.84	6.95	7.30	6.69	5.71	4.70	3.79	3.02	2.38	1.87	1.46	0.12	0.00	
				Hornblende	0	0	0	0	0	0	0	0	0	0	0	0	0	0	0	0	0	0	0	0	0	0	0	0	
				Clinopyroxene	0	0	0	0	0	0	0	0	0	0	0	0	0	0	0	0	0	0	0	0	0	0	0	0	
				Orthopyroxene	0	0	0	0	0	0	0	0	0	0	0	0	0	0	0	0	0	0	0	0	0	0	0	0	
				Olivine	0	0	0	0	0	0	0	0	0	0	0	0	0	0	0	0	0	0	0	0	0	0	0	0	
				Opakes	0.30	0.30	0.27	0.24	0.19	0.15	0.12	0.09	0.07	0.06	0.04	0.03	0.03	0.00	0.00	0.00	0.00	0.00	0.00	0.00	0.00	0.00	0.00	0.00	
				Chlorite	0.91	0.84	0.60	0.40	0.17	0.07	0.03	0.01	0.01	0.00	0.00	0.00	0.00	0.00	0.00	0.00	0.00	0.00	0.00	0.00	0.00	0.00	0.00	0.00	
				Total	100	100	100	100	100	100	100	100	100	100	100	100	100	100	100	100	100	100	100	100	100	100	100	100	

Petrography, provenance and diagenesis of Murree Group of rocks exposed along Basohli- Bani Road, Kathua, Jammu

Monika Jamwal, S. K. Pandita, Meera Sharma and G. M. Bhat

Department of Geology, University of Jammu, Jammu- 180006 (India)

Abstract

Sandstones of Murree Group of rocks exposed along Bani- Basohli road, Kathua District in Jammu were analyzed for petrography, petrofacies and provenance. These sandstones are classified as sublithic arenites and have been derived from mixed provenance including plutonic basement, sedimentary and metasedimentary rocks. Different types of quartz grains and other constituent minerals suggest the source from lower and middle and upper rank metamorphic terrains of the continental block-recycled orogen and subduction zone complex. The imprints of shallow burial diagenesis suggest low mechanical compaction probably just before cementation leading to moderate packing and reduction of porosity.

Introduction

Murree Group of rocks is a widespread succession of red and maroon shales, siltstones, sandstones and pseudo-conglomerates exposed along the Himalayan foothills of Kohat–Potwar (Pakistan) and Jammu (India) regions. In India, it overlies the Palaeocene - early Middle Eocene Subathu Group with an apparent conformable contact, as there is no field evidence to suggest a break between the two successions (Kumar and Sashi, 2002). However, most researchers, both in India and Pakistan, have suggested a gap of sedimentation spread over the whole Oligocene between Subathu and Murree successions (Ranga Rao, 1986; Ibrahim Shah, S. M., 1977). In Jammu province these rocks are exposed from Poonch in the west upto Basohli in the east and lie south of the Main Boundary Thrust (MBT). In Himachal Pradesh the equivalents of Murree Group are named as Dharamshalla Group (at Dalhousie) whilst at Solan these are referred to as Dagshai and overlying Kasauli formations (Karunakaran and Ranga Rao, 1979). In Jammu region Murree Group has very good exposures along the road cut sections of Jammu-Srinagar National Highway and on the Basohli - Bani road. The area under investigation lies near Mandrera on Bani-Basohli road and is covered in Toposheets 43P/13 NE and 43 P/14 NW of Survey of India and lies at longitude 75°52' 00E and latitude 32°37' 29'N.

A brief account of Murree Group of rocks has been reported by Medlicot (1876), Simpson (1904) and Middlemiss (1929). Lydekker (1876 and 1883) mapped the Murree Group of rocks in Jammu region. Wadia (1928) has given a detailed account of these rocks and suggested a southerly source (Indian Craton) for the Murree Group and considered these rocks as brackish water deposits. A detailed account of the stratigraphic and structural setting of the Murree Group of rocks has been given by Karunakaran and Ranga Rao (1979). They are of the opinion that the Upper Murree beds north of Udhampur should be of lower Miocene or younger age. Singh *et al.* (1990) on the basis of petrochemical data suggested that these sediments were deposited in a near shore environment. Singh *et al.* (1995) have postulated tidal influence during the sedimentation of

Murree Group on the basis of facies assemblages and sedimentary structures present in the Udhampur district. Singh (1994) worked on the diagenetic influence and porosity pattern of these sandstones. Singh (1996, 1999, 2000) concluded a northerly source for the Murree sediments on the basis of sandstone mineralogy, nature of rock fragments and palaeocurrent pattern. Textural analyses of the sandstones of Murree Group has been carried out by Sharda and Verma (1977), who suggested quite water, lagoonal environment for the Lower Murree and a fluvio-deltaic environment for the Upper Murree sediments. In the western part of the Jammu region, Murree Group of rocks has received significant attention in terms of stratigraphy, structure, sedimentology, soil dynamics, geotechnical investigations, microfossils, reservoir potential and petrography (Bhatia *et al.*, 2001; Bhat *et al.*, 2008; Singh *et al.*, 2012; Craig *et al.*, 2018, and references therein), but no such study has been carried out in the eastern part of the region especially in Bani-Basohli area. The present work is the first account of petrographic study of sandstones of Murree Group of rocks in this area. The main objective of this study is to understand the source rock characters, tectonic setting and the diagenetic history and porosity evolution of these deposits.

Geological setup

Geologically the study area is bound by Murree Thrust (MT, a subsidiary of MBT) in the south and Panjal Thrust (PT) in the north and displays younging of its constituent formations due north (Fig. 1). At places it rests directly on Sirban Limestones (Hakhoo *et al.* 2011). There is another thrust running in between these two thrusts and is named as Shali Thrust. The MT separates the Proterozoic Souni Volcanics and Tertiary Murree Group of rocks and is characterized by a thick zone of crushed and shattered rocks whose width is about 80m in the vicinity of the Sewa hydroelectric project in the study area. MBT is lying between Murree Group and the Upper Siwalik sub-Group in the region. The regional tectonostratigraphic setup (after Choudhary, 2006) of the study area is given in Table 1.

Table 1 :Tectonostratigraphic setup (north- south) of the study area (after Choudhary, 2006)

Subgroup/Formation	Lithology	Age
Bhadarwah	Phyllites, schists and slate	Precambrian
Dalhousie	Augen gneisses and granites (granodiorite to quartz diorites)	
----- Panjal Thrust (= Jutogh Thrust)-----		
Sincha	Sandy dolomites occasionally phosphatic, pinkish, grey limestone having zebra type banding	Precambrian
Ramban	Grey to dark grey shales/slates with bands of grey quartzites, bluish grey phyllitic slates	Precambrian
Baila	Calcareous shale, nodular and lenticles of limestone, black to carbonaceous slates	?Neoproterozoic
-----Shali Thrust (=Sudh Mahadev Thrust)-----		
Gamir	Quartzite, bands of conglomerate and cherty shales and bands of limestone and purple shale	Mesoproterozoic
Souni Volcanics	Basaltic lava, greenish and greyish green in colour	Palaeoproterozoic
-----Murree Thrust-----		
Murree	Sandstones, mudstones and shales	Miocene
-----Main Boundary Thrust-----		
Upper Siwalik	Sandstone and conglomerate	M. Pleistocene

Methodology

The results of the current study are based on both the field and laboratory investigations. In the field a 86.1m lithosection was systematically measured and a litholog was prepared to document the variations in lithology, nature of bedding and bed contacts. Representative fresh rock samples were collected from different lithounits. Thin sections of sandstone samples were prepared to work out petrography and petrofacies. Point-counting was carried out to identify quantity of the individual minerals using the Dickinson method (Dickinson, 1970). Compositional fields are shown as triangular QtFL (quartz-feldspar-lithic fragments) and QmFLt (monocrystalline quartz-feldspar-total lithic fragments) diagrams to differentiate maturity and source rocks (Dickinson and Suczek, 1979; Dickinson *et al.*, 1983; Dickinson, 1985). In order to reconstruct the original detrital composition of the sandstones, the effects of diagenesis were taken into consideration as much as possible during counting. The nature of detrital grain contacts were studied and classified after Taylor (1950).

Field Observations

The measured lithosection displays very good exposure of the Murree rocks consisting of sandstone, mudstone and splintery shale (Fig. 3a).

The sandstone beds are medium to coarse grained, friable, buff and grey coloured, massive with thickness ranging from 0.5 to 6m. The contact between the sandstone beds and the Mudstone beds is mostly erosional, however, the contacts with overlying splintery shales are gradational to sharp. At places the sandstone bodies are 1 to 6m thick showing multistoried nature (Fig.3b) and the individual stories range between 0.30 to 1.5m. The individual storeys are bound by erosion surfaces that contain intraformational mud clasts. Occasionally, sandstone lenses upto 45 cm thick are observed. Some sandstone beds display intraformational mud clasts which are evenly distributed along the beds. Quartz veins upto 5mm in thickness are observed in some sandstone beds (Fig.3c).

The mudstones are grey, brown to reddish brown in colour and range in thickness from 0.50 to 4.3m in the measured section (Fig.3d). These mudstones are massive to nodular and show erosion and sharp contacts with the overlying sandstones. The shales are friable and splintery in nature and reddish brown in colour. The sandstone beds are often interbedded with mudstone or splintery shale beds. The mudstone beds are water sensitive and flow under soaking conditions.

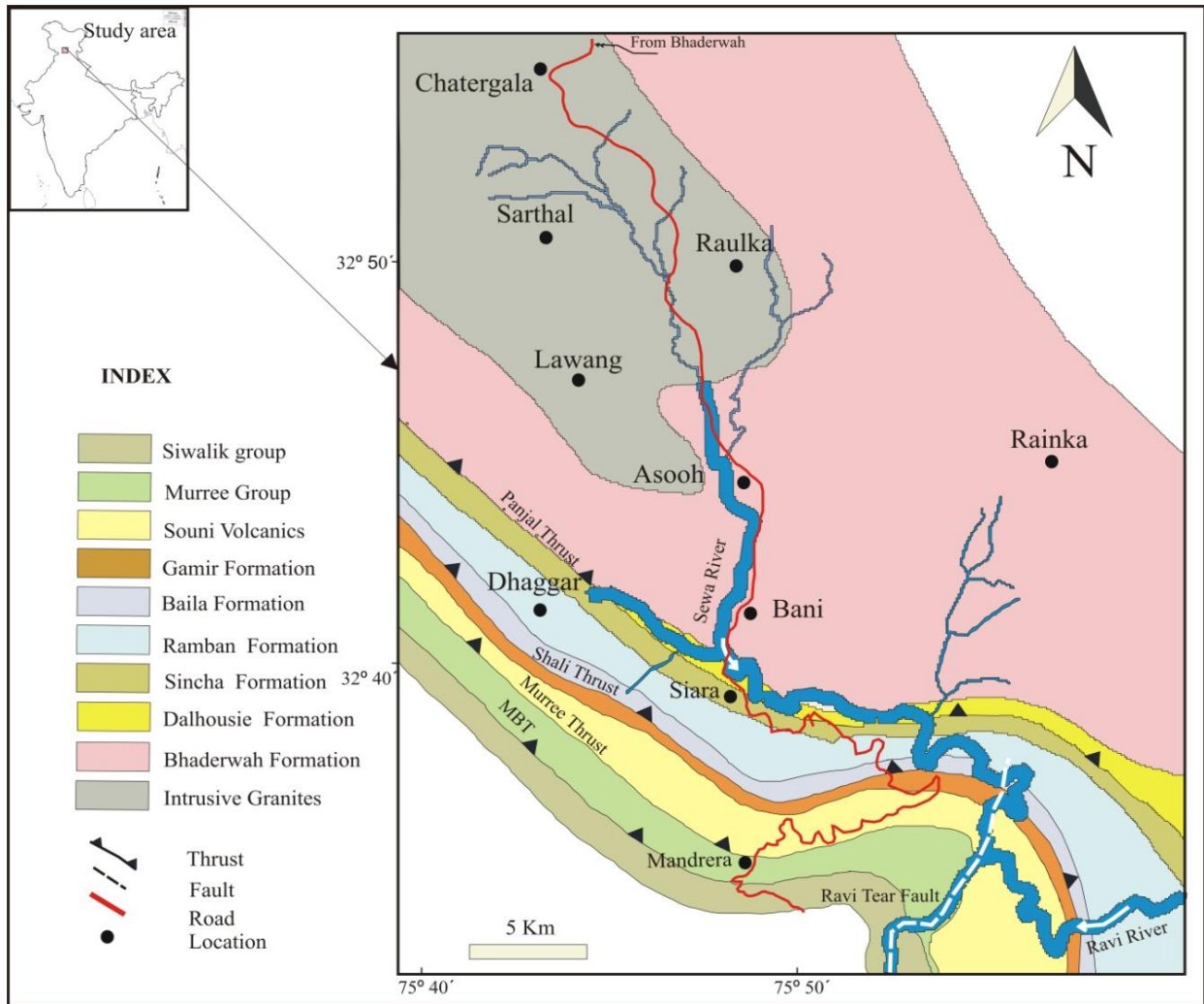


Fig.1: Geological map of the study area (Choudhary, 2006)

Laboratory Observations

Petrography

The sandstone samples were collected around Mandrera along the Bani – Basohli road. Twenty three thin sections were studied for the qualitative and quantitative analysis for mineralogy, cement and diagenetic signatures. Petrographically, these sandstones are sublithic arenite in nature comprising of quartz (73 to 85%), feldspar (2 to 7%) and rock fragments (9 to 19%) (Fig.4). Quartz grains are generally subangular to subrounded (Fig.5a), elongate quartz grains are rarely observed. Quartz grains show floating, point, line and concavo-convex contacts. These grains are represented by monocrystalline and polycrystalline quartz (Fig.5b,c). Monocrystalline quartz (Qm) grains are dominant over polycrystalline quartz (Qp). Nearly 80% of the total detrital quartz belong to common (plutonic) quartz variety. The remaining detrital grains of quartz belong to recrystallized and stretched metamorphic quartz. Monocrystalline quartz grains show slightly undulatory ex-

inction, whereas, polycrystalline quartz grains show straight to highly undulatory extinction and also contain elongated individuals with sutured and crenulated boundaries. Two varieties of feldspar have been recognized which include microcline and plagioclase in order of abundance which are subangular to subrounded in nature. Alteration and leaching of feldspars is observed along the cleavage plains and grain boundaries (Fig.5d). Both muscovite and biotite occur as tiny to large elongated flakes. Biotite grains are brown coloured. Some muscovite flakes show bending in thin sections (Fig.5e). Detrital micas were recognized both by their relatively large size and definite detrital boundaries. Such grains are seen to curve around the adjacent quartz grains. Rock fragments comprise 9 to 19 percent of detrital fraction and averages 12 percent. Both sedimentary and metamorphic rock fragments occur in the studied sandstones. The sedimentary rock fragments include siltstone and chert (Fig.5f).

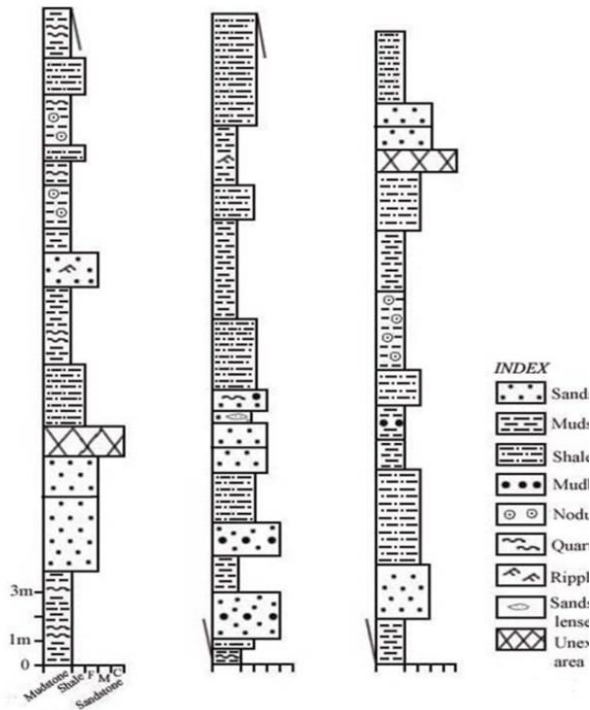


Fig.2 : Litholog of the studied section of Murree Group

Provenance and Tectonic Settings

To discriminate the provenance of quartz, percentages of monocrystalline and polycrystalline quartz

were plotted in diamond diagram (after Basu *et al.*, 1975). From the plot it is observed that most of the data fall in the middle and upper rank metamorphic fields (Fig.6). However, the presence of strain free quartz grains suggests their source in plutonic rocks (e.g. Basu, 1985). Most of the monocrystalline quartz shows undulose extinction which is indicative of low rank metamorphic source (Basu *et al.*, 1975). This interpretation is also supported by the presence of opaque minerals which were derived from the metamorphic and igneous rocks.

Detrital framework modes of sandstone suites provide information about the tectonic setting of basins of deposition and associated provenances (Dickinson *et al.*, 1983). The petrofacies data of the present study were plotted in standard triangular diagrams Qt-F-L, Qm-F-Lt, Qp-Lv-Ls and Qm-P-K (after Dickinson, 1985). The Qt-F-L diagram emphasizing factors that were controlled by provenance, relief, weathering and transport mechanism is based on total quartzose, feldspar and lithic modes. In this diagram, the current sample data fall in the continental block orogen and recycled orogen provenance (Fig.7a) with a source primarily in the quartzose recycled orogen provenance field. The Qm-F-Lt data plot of the study area shows that these sandstones were derived from recycled quartzose provenance (Fig.7b). The Qp-Lv-Ls plot, which is based on rock fragment population from a polygenetic source, gives a more resolved picture about the tectonic elements and the current sample data fall in subduction complex sources (Fig.8a).



Fig3: Field photographs a) alternation of sandstone-mudstone beds, b) multistoried sandstone, c) quartz veins, d) grey and brownish mudstone

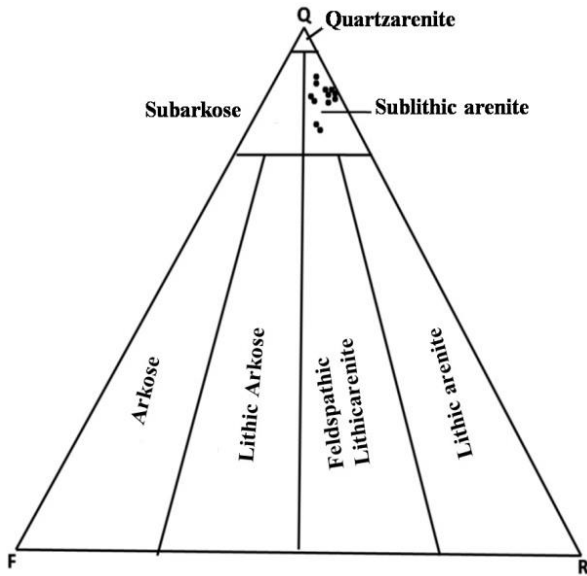


Fig.4 : Classification of sandstone of Murree Group in the study area

Provenance and Tectonic Settings

To discriminate the provenance of quartz, the percentages of monocrystalline and polycrystalline quartz were plotted in diamond diagram (after Basu *et al.*, 1975). From the plot it is observed that most of the data fall in the middle and upper rank metamorphic fields (Fig.6). However, the presence of strain free quartz grains suggests their source in plutonic rocks (e.g. Basu, 1985). The most of the monocrystalline quartz show undulose extinction which is indicative of plutonic and low rank metamorphic source (Basu *et al.*, 1975). This interpretation is also supported by the presence of opaque mineral grains, which reflect derivation from metamorphic and igneous rocks.

Detrital framework modes of sandstone suites provide information about the tectonic setting of basins of deposition and associated provenances (Dickinson *et al.*, 1983). The petrofacies data of the present study were plotted in standard triangular diagrams Qt-F-L, Qm-F-Lt, Qp-Lv-Ls and Qm-P-K (after Dickinson, 1985).

Table 2: Detrital framework grains (count percentage) of the sandstone samples of Murree Group in study area

Sample	Q (%)	F(%)	L(%)	RF(%)	Qm(%)	NUM	UM	Lt(%)	P2-3	P>3	P(%)	Ls(%)	Lv(%)
MR-2	76	6	1	5	71	16	55	30	5	24	5	1	3
MR-4	80	5	15	5	70	21	50	28	8	21	5	2	3
MR-5	79	5	16	4	76	29	51	35	9	15	4	3	2
MR-6	76	6	18	5	67	16	52	29	9	23	5	1	4
MR-7	80	4	16	5	77	10	67	25	9	15	5	5	3
MR-8	78	6	16	3	67	17	50	33	8	23	3	1	3
MR-10	80	6	14	5	77	12	65	26	14	17	5	2	2
MR-13	73	9	18	2	68	19	51	30	6	15	2	5	2
MR-15	76	5	19	2	77	20	57	34	10	10	2	4	4
MR-16	82	3	15	5	72	9	63	32	8	21	5	1	3
MR-18	77	7	16	5	68	10	58	30	7	7	5	1	3
MR-21	84	6	10	5	72	10	62	16	7	6	5	2	2
AVG	78	7	16	4	57	15	62	29	8	16	4	2.3	3

(Qt=Total quartz, Qm= Monocrystalline quartz, Qp=Polycrystalline quartz, F=Total feldspar, L=Lithic fragments, NUM=Non undulatory monocrystalline quartz, UM=Undulatory monocrystalline quartz, Lt=Total lithic fragments, Ls=Metasedimentary rock fragments, Lv=Volcanic lithics, P=Plagioclase feldspar, P2-3 crystal units/ grain = or > 75% of total polycrystalline quartz, P>3 crystal units / grain < 25% of polycrystalline quartz).

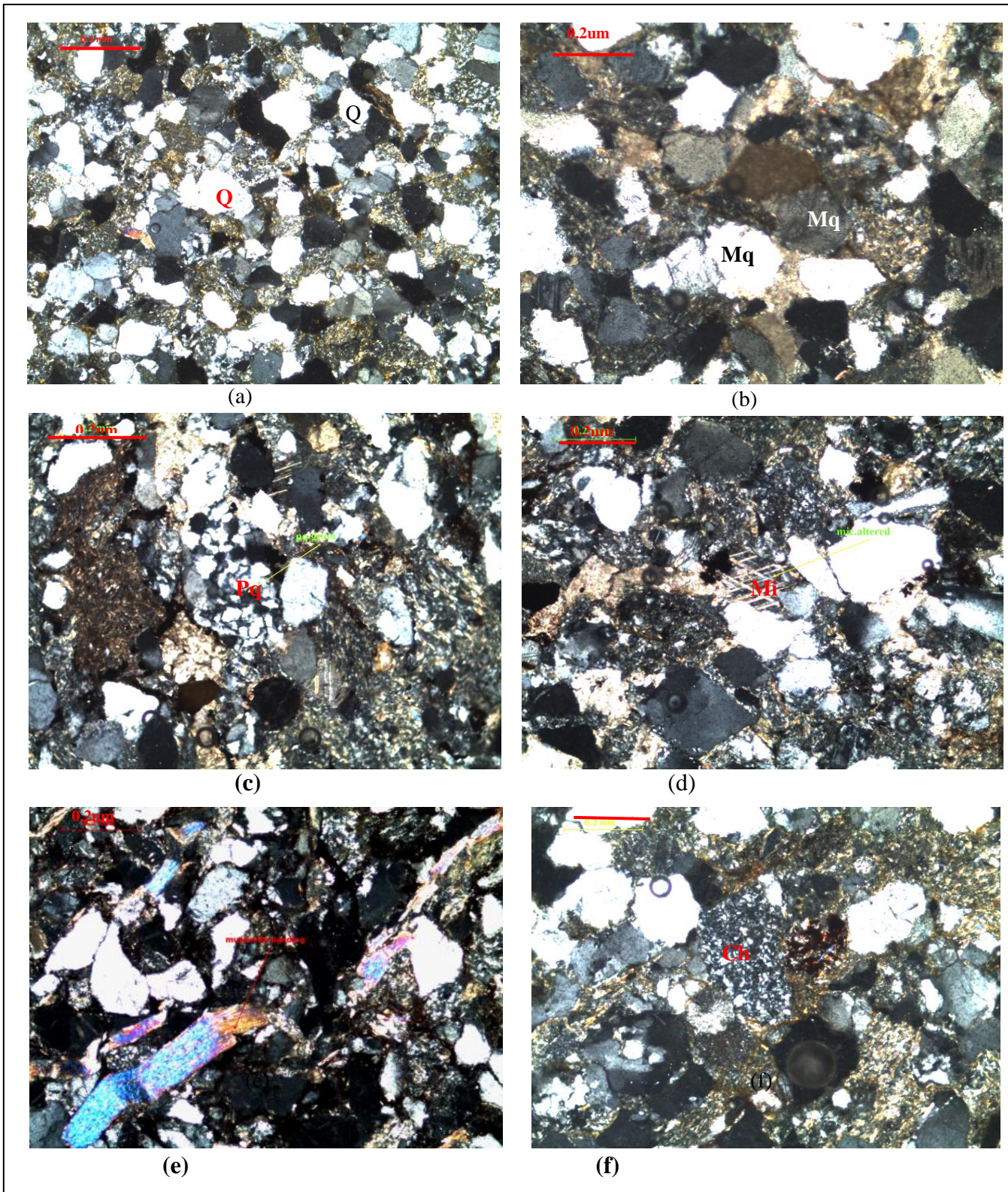


Fig. 5: Photomicrographs showing: a) subangular to subrounded quartz grains; b) monocrystalline quartz (Mq); c) polycrystalline quartz (Pq); d) alteration of microcline (Mi); e) bending of muscovite grain; f) chert grain (Ch)

The Qt-F-L diagram emphasizing factors that were controlled by provenance, relief, weathering and transport mechanism is based on total quartzose, feldspar and lithic modes. In this diagram, the sample data fall in the continental block orogen and recycled orogen provenance (Fig.7a) with a source primarily in the quartzose recycled orogen provenance field. The Qm-F-Lt data plot of the

study area shows that these sandstones are derived from recycled quartzose provenance (Fig.7b). The Qp-Lv-Ls plot, which is based on rock fragment population from a polygenetic source, gives a more resolved picture about the tectonic elements and the sample data fall in subduction complex sources (Fig.8a). The Qm-P-K plot shows that the sediment contribution is from continental block provenances

(Fig.8b) and represents the increasing trend of maturity and stability of the sediments because of the low percentage of

plagioclase (P) and high amount of quartz grains (Qm)

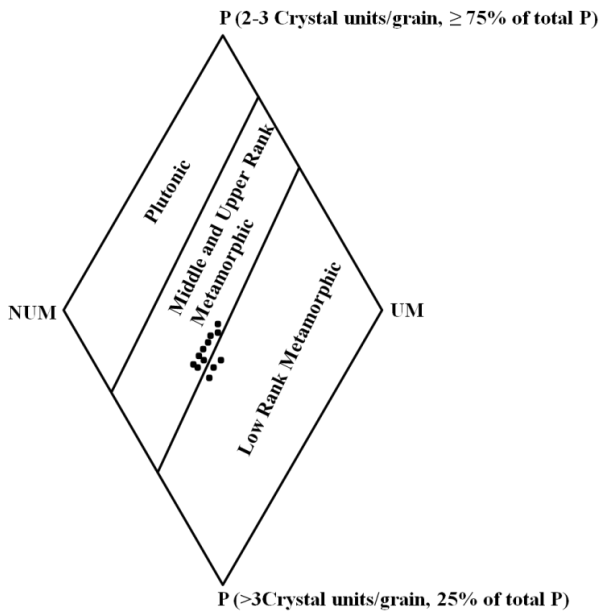


Fig. 6: Diamond diagram showing provenance of different quartz type of the study area (after Basu et al., 1975)

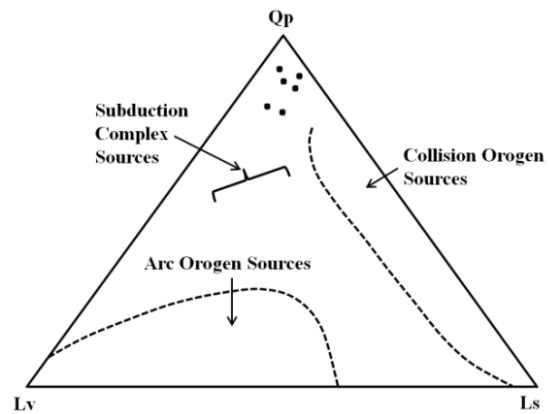


Fig. 8a and 8b: QmPK and QpLvLs plot of framework grains of sandstone samples of Murree Group

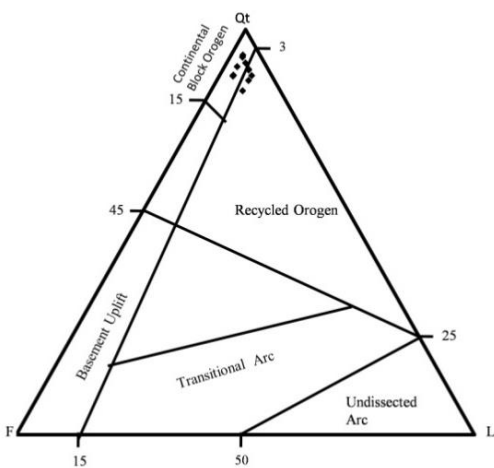
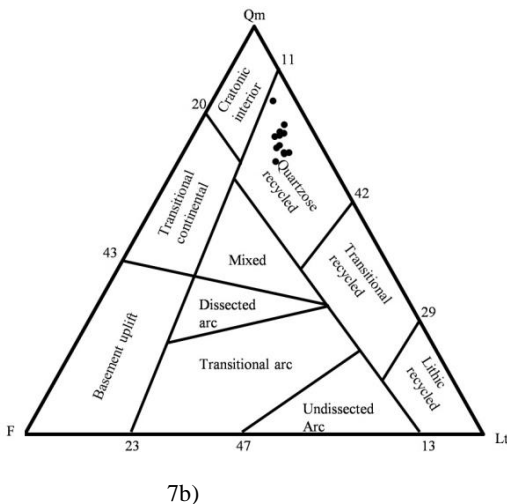
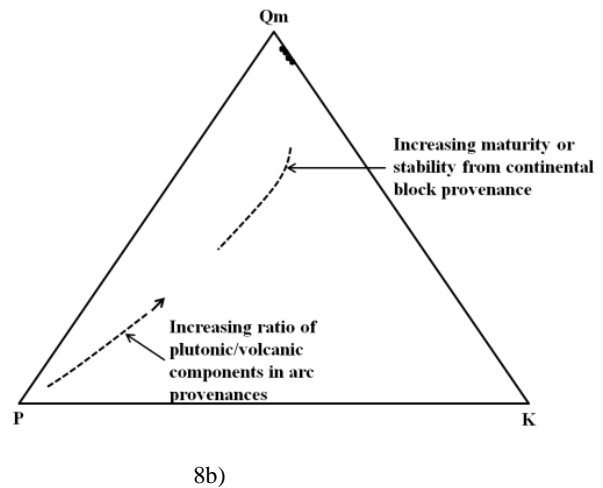


Fig. 7a and 7b: QtFL and QmFLt plot of framework grains of studied sandstone of Murree Group



7b)

Diagenesis

In the present study, an attempt was made to find out the changes that represent a series of diagenetic events controlled by the depositional environment through which these sandstones have evolved. The diagenetic changes observed in the present study are described below:

Compaction and porosity

The studied sandstones exhibit four types of grain contacts, which include floating, point, line and concavo-convex contacts (Fig.9a,b,c,d). The point and long contacts average 13.83% and 27.4% and concavo-convex contacts average 12.16% (Table-3) are suggestive of limited pressure solution activity in these sandstones. The contact index (CI) also gives an indication about the degree of compaction of the sediments (Pettijohn *et al.*, 1987). The average contact

index value for these sandstones is very low (1.3%). In this study on an average 60.1% grains do not show grain

to grain contact, which accounts for the overall low contact index for these sandstones.

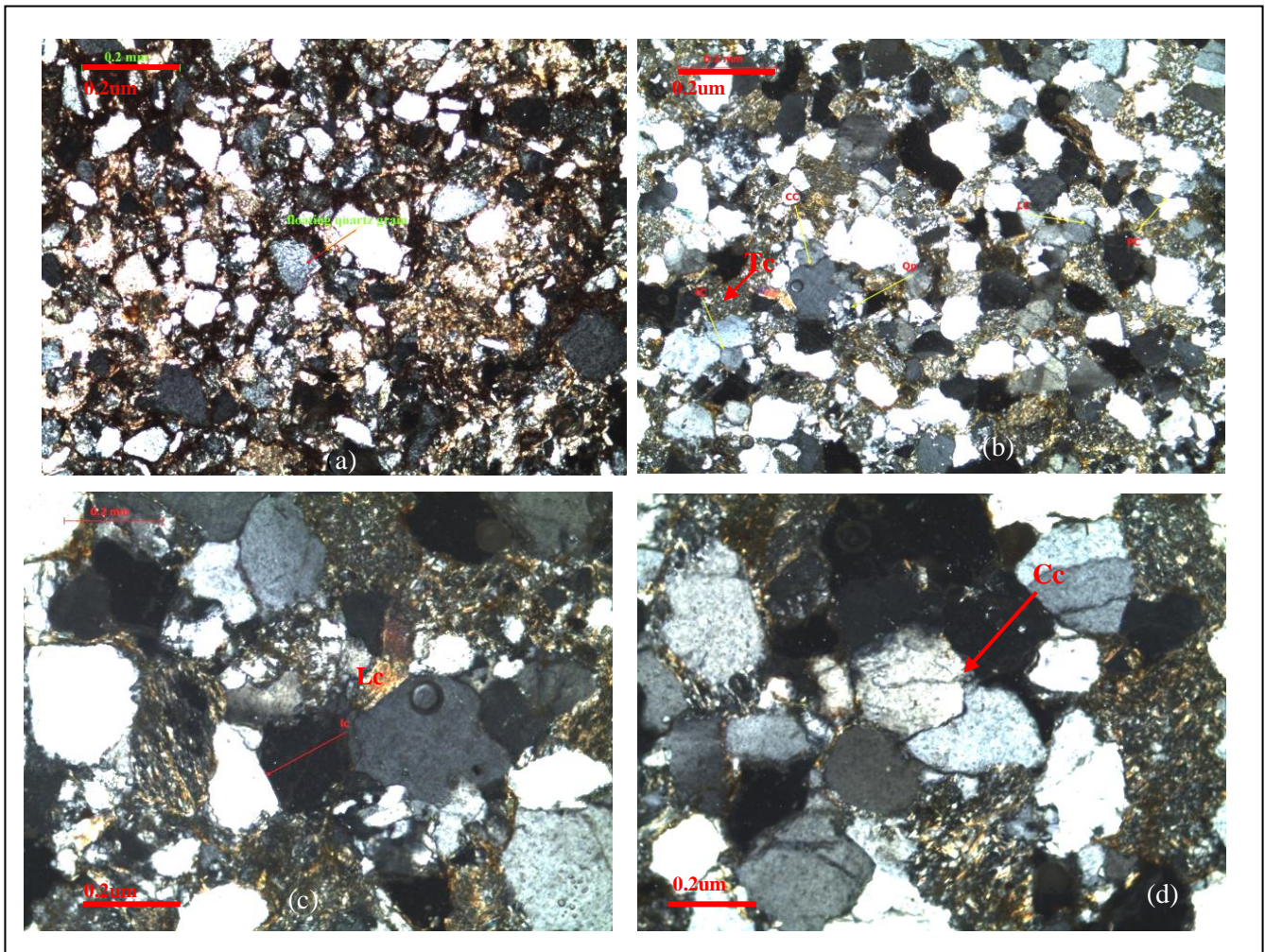


Fig. 9: Photomicrographs showing a) floating grain; b) point contact (Pc); triple contact (Tc); c) line contact (Lc); d) concave contact (Cc).

It is well known that the original porosity of sandstones generally vary between 30 and 35%, which can be reduced by 10-17% by mechanical compaction (Pryor, 1973; Beard and Weyl, 1973). The initial high porosity is attributed to loose packing of sediments at the onset of deposition. The intergranular quartzose cement (minus cement porosity) in these cases averages 32.6% porosity (Table-3), which may be due to less mechanical compaction during the early stages of diagenesis. The iron oxide cement forming 9-22% of the cement and up to 16.3% volume of the rock (Table-3) also occurs as coating around the detrital grains. Silica cement occurs in small amounts (averages 0.3%) as overgrowth around detrital grain boundaries. In some thin sections, silty to clayey matrix is present in varying amounts. The matrix also influenced diagenetic process by supplying Fe and reducing porosity and permeability by pore filling.

Depth of burial and Porosity

The petrographic studies have been widely used to predict the depth and temperature of burial of the sediments (Smosna, 1989). The current study reveals that the existing optical porosity (EOP) ranges from 6 to 13% with an average

of 9.6%, while minus cement porosity (MCP) ranges from 25 to 40% (average 32.6%) (Table 3). The average minus cement porosity of these sandstones is plotted on different graphs of porosity versus depth after McCulloh (1967), Lapinskaya and Preshpyakove (1971), Selley (1978) and Atwater and Miller (1965) (Fig. 12). These plots were employed for estimation of depth of burial of sandstone of the Murree Group. The data plotted on these graphs suggests the depth of burial of these sandstones is 792m to 1600m (Table-4). In general the depositional porosity for the sandstones ranges from 40 to 50% with the initial contact values ranging from 0.5 to 1.5 (Atkins and McBride, 1992). In the present study the empirical porosity value has been taken as 45% to model the porosity evolution and relative role of compaction and cementation. This has been quantitatively worked out by using the following formula and variation diagram of Lundegard (1992).

- (i) $COPL = Pi - (100 - Pi) \times MCP / (100 - MCP)$
- (ii) $CEPL = Pi - COPL \times (Tc / MCP)$

where, COPL is porosity loss due to compaction, Pi is the initial porosity (= 45%), MCP is minus cement porosity, Tc is the total cement and CEPL is the loss due to cementation.

The plot COPL versus CEPL (Fig.12d) shows a clear, decreasing trend of CEPL with increase in COPL. However, most of the data fall in the COPL quadrant suggesting that compaction was the major cause of porosity reduction. High minus cement porosity values also suggest low mechanical compaction probably just before cementation leading to moderate packing. The early cementation may have reduced porosity and established the constituent framework, which appears to have restricted late stage chemical compaction during burial (e.g. Houseknecht, 1987). This conclusion is supported by the study of grain to grain relationships that also suggest that the studied sandstones were cemented early and were subjected to little compaction effects.

Table 4: Calculated depth of burial of Murree Group in the study area

Depth of Burial vs Minus cement porosity	Meter
Mc Culloh (1967)	1280
Lapinskaya and Preshpyakove (1971)	792
Selley (1978)	1050
Atwater and Miller (1965)	1600

Discussion

Petrographic study of the Murree Group sandstones reveals that the sandstones are fine to medium grained which are composed of quartz, feldspar, and lithic fragments. Quartz, feldspar and lithic fragments play an important role in the determination of the provenance of the clastic rocks. The compositional results of the sandstones of the study area show abundant quartz with small amount of feldspar, lithic fragments, micas and other accessory minerals and thus, are classified as sublitharenites (Folk 1980). Basu et al. (1975) suggests that the dominance of quartz and undulose extinction indicate plutonic and low rank metamorphic source respectively. The presence of polycrystalline quartz suggests low grade metamorphic source (Blatt and Christie, 1963; Blatt, 1967). In our study area, the presence of common quartz, polycrystalline quartz, feldspar, rock fragment including igneous and metamorphic minerals suggests that the sediments were derived from the igneous as well as metamorphic terrain. Diamond diagram plot suggests that the sediments were derived from mixed provenance including plutonic basement, sedimentary and metamorphic rocks. Pandita (1996), Pandita and Bhat (1995) and Pandita et al. (2014) have come to similar conclusion of mixed

provenance for Siwalik Group of rocks. Bhat (2008) while working in Ramnagar area of Udhampur concluded that the sediments of Lower Siwalik Subgroup were derived from low rank metamorphic source terrains.

The QtFL and QmFLt plots are suggestive of the sediments under present study are the product of continental, recycled and quartzose recycled orogen indicating that the provenance was rich in sedimentary and metamorphic rocks. As defined by Dickenson et al. (1983) mostly the sedimentary, partly metamorphic and subordinate volcanic rocks of the orogenic belt constitute the recycled orogen. Singh (1996) also is of the opinion that the Murree sandstones are the product of recycled orogen provenance rich in sedimentary and metamorphic rocks. Mughal et al. (2018) suggested that Murree Formation of Muzzafrabad Pakistan are derived from the recycled orogen and transitional recycled orogen and are rich in quartz, feldspar and lithic fragments. The product of recycled orogen are commonly feldspar poor and lithic rich (Fig 7a and b) and are often deposited in closing ocean basins, diverse successor basins and foreland basins (Dickinson & Suczek, 1979). In our case Ternary plot clearly indicates that the recycled provenance. Under moderate to low relief condition, the sediments have experienced the transportation and depositional process resulting in their compositional maturity.

The Qp-Lv-Ls plot, which is based on rock fragment from a polygenetic source, gives a more resolved picture about the tectonic elements. The plot shows that these sediments were derived from subduction complex sources. The Qm-P-K plot represents the increasing trend of maturity and stability of the sediments. Sands derived from fold–thrust systems of indurate sedimentary and low–grade metamorphic rocks show consistently low contents of feldspar and volcanic rock fragments (Dickinson & Suczek, 1979)

Diagenetic signatures observed in the sandstones of the study area include different stages of compaction, cementation and nature of development of grain contacts. In our study dissolution of feldspar develops long and concavo-convex grain contacts. The concavo-convex and sutured grain boundaries have been interpreted as a result of pressure solution (Dapples, 1972). The long grain contacts and bending of detrital muscovite reveals mechanical compaction of the sediments (Ahmed and Bhat, 2006; Ahmad et al., 2006). This is indicative of compaction and pressure solution due to shallow burial or early cementation. The high percentage of floating grains and point contacts with low contact index values are mainly found in these sandstones with pervasive development of calcite, Fe-cement and silica cement which probably precipitate at later stage (Bhat et al., 2006). Plagioclase and microcline feldspars show alteration and leaching of grain boundaries indicating effect of pressure solution during diagenesis.

Table 3: Types of Cement, porosity and packing data of Murree Group in the study area

S.No	Cements (%)					Porosity (%)		Types of contacts (%)				No. of contacts/grain (%)							(CI)	COPL	CEPL
	Fe	C	S	M	Tc	EOP	MCP	F	L	P	Cc	0	1	2	3	4	>4				
MR-2	16	1	0	2	19	6	25	46	27	15	12	60	27	11	2	0	0	0.8	26.4	24.9	
MR-4	20	5	0	2	27	8	35	26	38	24	12	70	20	4	2	3	1	0.9	15.4	33.1	
MR-5	17	1	0	1	19	11	30	45	28	13	14	60	24	11	5	0	0	1.3	21.4	31.4	
MR-6	18	0	0	1	19	9	28	51	22	14	11	66	20	10	3	1	0	1	23.6	29.1	
MR-7	9	4	1	4	18	12	30	51	23	13	13	50	35	10	4	1	0	1.6	21.4	32.2	
MR-8	20	5	0	2	27	8	35	54	22	13	11	73	15	7	3	2	0	1.3	15.4	33.1	
MR-10	22	0	0	2	24	11	35	60	18	12	10	55	21	15	5	2	2	0.8	15.4	34.4	
MR-13	14	5	2	10	31	9	40	47	25	15	13	43	24	20	10	2	1	1.5	8.3	38.6	
MR-15	12	4	0	6	22	10	32	52	25	9	14	61	24	9	4	2	0	1.3	19.1	31.9	
MR-16	18	4	0	6	28	7	36	48	30	8	14	60	20	10	6	3	1	1.3	14.1	34	
MR-18	9	5	1	4	19	11	30	79	32	5	5	52	25	12	8	0	3	1.5	21.4	31.4	
MR-21	20	3	0	3	26	13	35	64	35	14	7	71	27	1	1	0	0	1.5	20.2	30.1	
Avg.	16.3	3	0.3	3.6	23.6	9.6	32.6	51.92	27.4	13.83	12.16	60.1	23.5	10	4.4	1.3	0.7	1.2	18.51	32.6	

(Fe=Iron cement, C=Calcite, S-Silica, M=matrix, Tc=Total cement, EOP=Existing optical porosity, MCP=Minus cement porosity, F=Floating grain, P=Point contact, L=Long/line contact, Cc=Concave-convex contact, CI=Contact index, CEPL=Porosity loss due to cementation, COPL=Porosity loss due to compaction)

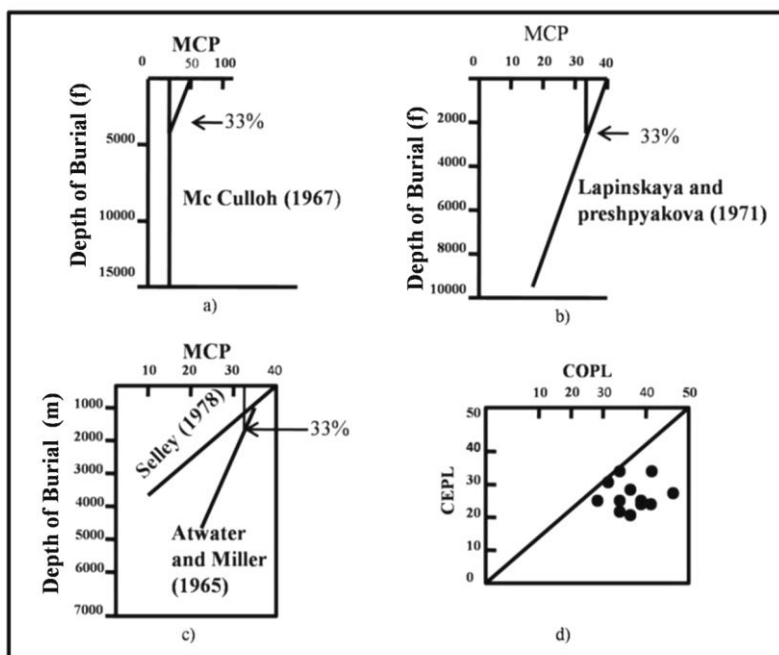


Fig. 10: The relationship between minus cement porosity (MCP) and depth of burial on three bivariate diagrams (a, b, c). The plot (d) shows porosity loss due to cementation (CEPL) v/s porosity loss due to compaction (COPL)

The average intergranular quartzose cement (minus cement porosity) is 33% which may be due to less mechanical compaction during the early stages of diagenesis. Bhat (2008) suggested that the less mechanical compaction and high content of intergranular cement may be related to high grain strength, good sorting and early cementation.

Bhat (2008) have worked on Lower Siwalik Subgroup of Ramnagar area of Jammu region and suggested the depth of burial in the range of 364 to 1141m for the sandstones. Whereas the present study is the first attempt to know the burial depth of the sandstone of Murree Formation in this region. The existing optical porosity (EOP) of sandstone is 9.6%, while minus cement porosity (MCP) is 33% which suggest that the depth of burial is in the range of 792 to 1600m. High minus cement porosity values at Mandrera section suggest that the low mechanical compaction just

before cementation leads to moderate packing and grain to grain relationship indicates that the sandstones were cemented early and were subjected to little compaction effects.

Conclusions

The petrography of the sandstones of Murree Group in Basohli - Bani area reveals that these rocks are sublitharenites in nature and are derived from a variety of source rocks including metamorphic, plutonic and recycled sediments contributed from uplifted margins of continental block and recycled orogen provenances and have undergone diagenetic changes at shallow depth of burial between 792 to 1600m.

Acknowledgement

The authors are grateful to the department of Geology; University of Jammu for providing necessary facilities to carry out laboratory work.

References

- Ahmad, A. H. M., Bhat, G. M. (2006). Petrofacies, provenance and diagenesis of Dhosa Sandstone member (Chari Formation) at Ler, Kachchh sub-basin, Western India, *Jour. of Asian Earth Sciences*, 27, 857-872.
- Ahmad, A. H. M., Bhat, G. M., Khan, A. F., Saikia, C. (2006), Petrography, Diagenesis, Provenance and Tectonic Setting of the Sandstones of Upper Katrol Formation (Kimmeridgian), Nakhtarana Area, Kachchh, Gujarat, *Jour. Geol. Soc., India*, V. 67 (2), P, 243
- Atkins, J. E. and McBride, E. F. (1992). Petrology and packing for Holocene river, dune and beach sands. *Jour. Bull. Amer. Assoc. of Petrol. Geol.*, 76, 329-335.
- Atwar, G. I. and Miller, E. G. (1965). The effects of decrease in porosity with depth on future development of oil and gas reserves in South Louisiana. *Jour. Bull. Amer. Assoc. of Petrol. Geol.*, 49, 622-626.
- Basu, A. (1985). Reading provenance from detrital quartz. *In: Zuffa, G. G. (Ed.), Provenance of Arenites. NATO-ASI. V. C. 148. Reidel, Holland, 231-247p.*
- Basu, A., Young, S. W., Suttner, L. J., James, W. C. and Mack, G. H. (1975) Re-evaluation of the use of undulatory extinction and polycrystallinity in detrital quartz for provenance interpretation. *Journal of Sediment. Petrol.*, 45, 873-882.
- Beard, D. C. and Weyl, P. K. (1973). Influence of texture on porosity and permeability of unconsolidated sand. *Jour. Bull. of the Amer. Assoc. of Petro. Geol.*, 57, 349-369.
- Bhat, S .K. (2008). Fluvial architecture of lower Siwalik subgroup of Ramnagar area, Udhampur, North West Himalaya. unpubl., Ph.D. Thesis, Jammu University.

- Bhat, G.M., Kundal, S. N., Pandita, S. K. and Prasad, G.V. R. (2008); Depositional origin of tuffaceous units in the Pliocene upper Siwalik Subgroup, Jammu (India), NW Himalaya, Geological Magazine 145 (2), 279-294
- Bhatia, S. B., Bhat, G. M., Pandita S. K. (2001), Microfossils from the Nagrota Formation, Upper Siwalik Subgroup, Jammu Hills, Journal of the Geological Society of India 58 (6), 509-518
- Bhattacharjee, J., Ghosh, K. K., Bhattacharya, B. (2017). Petrography and geochemistry of sandstone-mudstone from Barakar formation (early Permian), Raniganj basin, India: implications for provenance, weathering and marine depositional conditions during Lower Gondwana sedimentation. Geological Journal, 53, 1102-1122.
- Blatt, H., (1967). Provenance determinations and recycling of sediments. Jour. Sediment Petrol., 37, 1031-1044.
- Blatt, W. and Christie, J. M. (1963). Undulatory extinction in quartz of igneous and metamorphic rocks and its significance in provenance studies of sedimentary rocks. Jour. Sediment Pet., 33, 559-579.
- Choudhary, J. B (2006). Geotechnical and Structural evaluation of Tectonostratigraphic units along head Race Tunnel , Sewa Hydroproject. Stage-II, kathua District. Unpublished Ph.D Thesis. University of Jammu.
- Craig, J., Hakhoo, N., Bhat, G. M., Hafiz, M., Khan, M. R., Misra, R., and Pandita, S. K. (2018). Petroleum systems and hydrocarbon potential of the North-West Himalaya of India and Pakistan, Earth-Science Reviews 187, 109-185
- Dapples, E. C. (1972). Some concepts of cementation and lithification of sandstone. Jour. Bull. Amer. Assoc. Petrol. Geol., 56(1), 3-25.
- Dickinson, W. R. (1970). Interpreting detrital modes of greywacke and arkose. Jour. of Sediment. Petrol., 40, 695-707.
- Dickinson, W. R. (1985). Interpreting provenance relation from detrital modes of sandstones. In: Zuffa, G. G. (Eds.), Provenance of Arenites Reidel, Dordrecht, 333-363.
- Dickinson, W. R. and Suzek, C. A. (1979). Plate tectonics and sandstone compositions. Jour. Bull. of the Amer. Assoc. Petro. Geol. 63, 2164-2181.
- Dickinson, W. R., Beard L. S., Brakenridge, G. R., Erjavec, J. L., Ferguson, R. C., Inman, K. F., Knepp, R. A., Linberg, F. A. And Ryberg, P. T., (1983). Provenance of North America Phanerozoic sandstone in relation to tectonic setting. Bull. Geol. Soc. Amer., 94, 122-135.
- Folk, R. L. (1980). Petrology of Sedimentary Rocks. Hamphill, Austin, texas, p182
- Hakhoo, N., Bhat, G. M., Koul, S., Craig, J., Thusu, B. (2011); Potential Proterozoic Petroleum System, Northwest Himalayan Thrust Belt, Jammu (India) Abstract presented at the American Association of Petroleum Geologists, Italy
- Houseknecht, D. W. (1987). Assessing the relative importance of compaction processes and cementation to reduction of porosity in sandstones. Jour. Bull. of the Amer. Assoc. Petro. Geol., 71, 633-642.
- Ibrahim Shah, S. M., Mem. Geol. Surv. Pak., (1977), 12, 1-138.
- Ingersoll, R.V., Bullard, T.F., Ford, R.L., Grimm, J.P., Pickle, J.D. and Sares, S.W. (1984). The effect of grain size on detrital modes: a test of the Gazzi-Dickinson point-counting method. Jour. Sediment. Petrol., 54, 103-106.
- Karunakaran, C. and Ranga Rao, A. (1979). Status of exploration for hydrocarbon in the Himalayan Region. Himalayan Geol.Seminar. New Delhi 1976, Jour. Geol. Surv. India, Misc. Publ., 41, 1-66.
- Kumar, K., and Kad, S. (2002). Early Miocene cricetid rodents (Mammalia) from the Murree Group of Kalakot, Rajauri District, Jammu and Kashmir, India. Current Sciences, vol. 82, No. 6.
- Lapinskaya, T. A. and Preshpyakove, B. K. (1971). Problem of reservoir rocks during exploration for oil and gas at depths. In: Sideranko, A. V. (Eds.), Status and Problems, 115-121.
- Lundegard, F. D. (1992). Sandstone porosity loss 'a big picture' view of the importance of compaction. Jour. Of Sediment. Petrol., 62: 250-260.
- Lydekker, R. (1883). Synopsis on the fossil vertebrate of India. Rec. Geol. Surv. India, 16, 61-93.
- McCulloh, T. H. (1967). Mass properties of sedimentary rock and gravimetric effects of petroleum and natural gas reservoirs, US Geological Survey Professional Paper, 528A, 1-50p.
- Medlicott, H. B. (1876). Note upon the Sub-Himalayan Series in the Jammu (Jummoo) Hills. Rec. Geol. Surv. India, 9, 49-57.
- Middlemiss, C.S., (1929), Kalakot, Metka, Mahgola and other coal fields of Jammu peovince. Mineral survey report, Jammu and Kashmir Government, 116p.
- Pandita S. K. and Bhat G. M., (1995), Petrographic and facies evaluation of Middle Siwalik Subgroup of Jammu Himalaya. Journal Geol. Soc. of India, V. 46(4), 369-375
- Pandita S. K., Sunil K. Bhat, Sham S. Kotwal, Yudhbir Singh and Kuldeep K Thakur (2014) Provenance and Tectonic Settings of the Lower Siwalik Subgroup, Jammu, Northwest Himalaya. The Palaeobotanist, 63, 17-23; .
- Pettijohn, F. J., Potter, P. E. and Siever, R. (1987); Sand and Sandstone New York: Springer Verlag. 547p.
- Pryor, W. A. (1973). Permeability-porosity patterns and variations in some Holocene sand bodies. Jour. Bull. of the Amer. Assoc. Petrol. Geol., 57, 162-189.
- Ranga Rao, A., Bull. Oil Nat. Gas Comm., (1986), 23, 109-128.
- Selley, R. C. (1978). Porosity gradients in North Sea oil-bearing sandstones. Jour. of Geol. Soc. of London 135, 119-132.
- Sharda, V. P. and Verma, V.K., (1977) Palaeo environments during Murree and Siwalik Sedimentation around Udhampur, Jammu Himalaya. Proc. Cent. Adv. Study Geol., Chandigarh, 23-35.
- Simpson, R.R., (1904). Report on the Jammu coal fields. Memoirs Geological Survey of India, vol. 32, p. 189- 225.
- Singh, B.P., and Singh, H., (1995), Evidences of Tidal influence in the Murree Group of rocks of the Jammu Himalaya, India. Special Publication International Association of Sedimentologist, 24. 343-351.
- Singh, B.P., (1994). Diagenetic influence and porosity percentage in the sandstone of Murree Group, Jammu Himalaya, India. Him. Geol. 15, 202-217.
- Singh, B.P., (1996) Murree sedimentation in the Northwestern Himalaya. Geol. Surv. India Misc. Publ., 21, 157-164.
- Singh, B.P., Andotra, D. S., and Kumar, R. (2000). Provenance of lower tertiary mudrock in the Jammu Sub-Himalayan Zone, Jammu and Kashmir State (India), NW Himalaya and its tectonic implications. Geo Sciences Jour. Vol. 4, 1-9.
- Singh, B. P., Fotedar, B.K., and Rao, A.S. (1990). Petrography and Geochemistry of Sandstone of Murree Group around Laren, Udhampur, Jammu Himalaya. Jour Geological Society of India, Vol. 36, 502-511.
- Singh, B.P. (1999). Sediment Dispersal Pattern in the Murree Group of Jammu area, NW Himalaya, India. Himalayan Geology, Vol. 21(1&2), 189- 200.
- Smosna, R. (1989). Compaction law for cretaceous sandstone of Alaska's North Slope. Jour. Sed. Petrol., 51, 1235-1246.
- Singh, Y., Bhat, G. M., Sharma, V., Pandita, S. K., Thakur, K. K. (2012). Reservoir induced landslide at Assar, Jammu and Kashmir: a case study, Journal of the Geological Society of India 80 (3), 435-439
- Taylor, J. M. (1950). Pore-space reduction in sandstones. Jour. Bull. of the Amer. Assoc. Petrol. Geol., 34, 701-716.
- Wadia, D.N., (1928). The Geology of the Poonch state (Kashmir) and adjacent portions of the Panjab. Mem. Geol. Surv. India, 51, 331-362.

Assessment of Pre-and Post-Monsoon Groundwater Resource for Irrigation in Bhopalpatnam area, Bijapur District, Chhattisgarh, India

Korsa Munna and Rajeeva Guhey*

Department of Geology, Government N.P.G. College of Science, Raipur
GE Road, Raipur-492010, Chhattisgarh, India.

*Email: guheygeol@gmail.com, korsamunna@gmail.com

Abstract

The current study was conducted to determine the suitability of groundwater used for irrigation in and around the Bhopalpatnam area of Bijapur District, Chhattisgarh, during pre-and post-monsoon seasons of 2016. In this study, sixty two groundwater samples were collected from different villages and analyzed for various hydrochemical parameters like pH, EC, alkalinity, hardness, TDS, Ca, Mg, Na, K, CO₃, HCO₃, Cl, SO₄, NO₃, PO₄, Fe and F. Physico-chemical characterization of the samples revealed that groundwater from most of the sources is not fit for drinking owing to a high concentration of EC, HCO₃, NO₃, Fe and F. Irrigation indices such as sodium adsorption ratio (SAR), sodium percentage (Na %), residual sodium carbonate (RSC), permeability index (PI), Kelly's ratio (KR), magnesium hazard (MH) and EC were also calculated. The SAR values obtained for all the samples were plotted against EC values in the US salinity laboratory diagram and it was revealed that most of the samples fall under water type C3-S1 indicating high salinity and low SAR. The analysis of the various parameters indicated moderate suitability of groundwater for irrigation purpose.

Keywords: Groundwater, Irrigation, SAR, %Na, KR, PI and MH

Introduction

The present study has been carried out in Bhopalpatnam area, situated about 54 km west from Bijapur, Chhattisgarh. The study area is confined between latitudes 18°47'30" to 18°55'28" N and longitudes 80°20'00" to 80°31'43" E under survey of India Toposheet No. 65 B/5 and covers an area of 165.71 km² (Fig. 1). The people of the study area are economically backward, main occupation of villagers is agriculture. Physiographically, the major part of the district exhibits pediment/pediplain landforms. Most of the district area falls in Godavari, Indravati and Sabari catchments. Indravati, Godavari, Sabari rivers and their tributaries constitute the surface drainage network of the district. The area experiences a semi-arid climate with an annual mean temperature of 30° C. The mean annual rainfall is recorded at 745 mm, occurring generally during the southwest monsoon period (June – September). The drainage is pattern in the study area is dendritic to sub-dendritic. Groundwater occurs under phreatic conditions in the weathered and fractured zones. The depth to water table ranges from 5.6 to 12.1 m below the ground surface. The depth of dug wells ranges from 8 to 13 m and the diameter of the dug wells ranges from 2 to 7 m. The maximum depth of the hand pump for drinking water use is 40 m below ground level. The current study focuses on the assessment of

pre- and post monsoon suitability of ground water for irrigation purposes to sustain agricultural practice in the region.

Geology of the Study Area

The study area comprises of rock formations belonging to Archaean, Neo Proterozoic and Quaternary age are exposed in the study area. The oldest rocks in the area comprises of Eastern Ghat Supergroup and Bengapal Group of Archaean age. Rock of Bengapal Group are exposed in the major part of the study area and comprises various types of gneisses and schists, amphibolites, meta-basics, metaultramafics, migmatites and different varieties of quartzites. The rocks of the area are mainly pyroxene gneisses, amphibole gneisses, mica gneisses, garnetiferous gneisses, white quartzites, magnetite quartzites, micaceous quartzites, amphibolites etc. of the Dharwarian period. The gneisses are the most prevalent rocks while amphibolites and pyroxenites occur in the form of dykes and are widely distributed in the area. The major litho-units of the study area comprise of granitic gneiss and phyllites rocks, which are overlain by red, sandy soil cover. Secondary intrusives such as dykes, pegmatite and quartz veins, which occur to a limited extent, are present in the rocks.

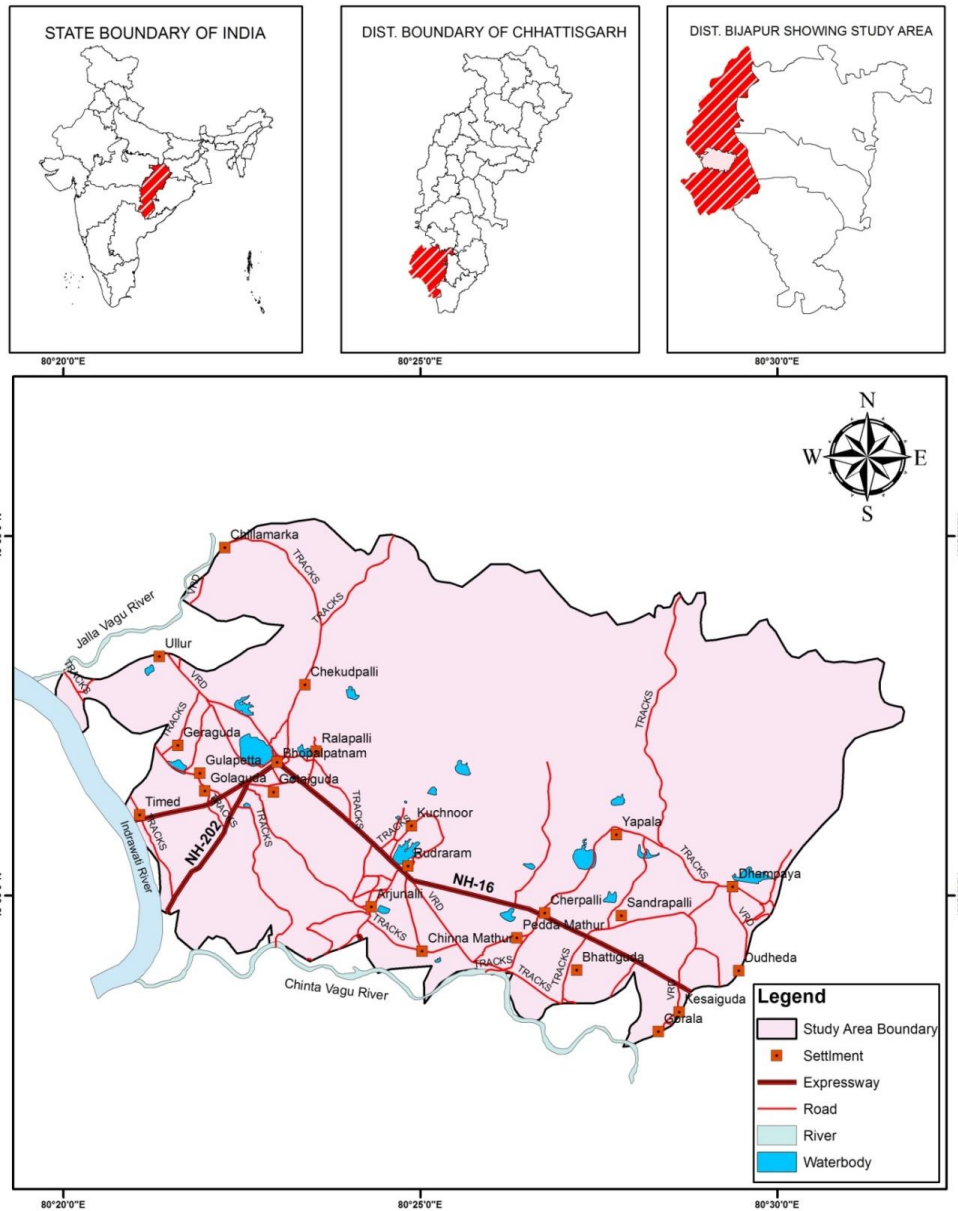


Fig.1. Location map of the study area Bhopalpatnam, district-Bijapur

Materials and Methods

In order to assess water quality of the study area, 62 groundwater samples were collected to cover the entire study area in the pre-and post-monsoon period during May and November 2016. The groundwater samples were collected in pre-washed polythene, narrow mouth bottles from study area and the bottles were rinsed twice before sampling. Based on this study, representative wells were selected. The

location map is presented as Figure 1. The water samples from the bore wells were collected after pumping out water for about 10 minutes remove stagnant water from the well. Samples were immediately transferred to pre-cleaned polythene bottles with 500 ml. capacity. Collected samples were taken to the laboratory for analysis. Analysis of groundwater samples for evaluation of chemical parameters were done as per Standard Methods (APHA,

1995) procedure, from CGCOST central laboratory Raipur (CG).

The Chemical parameters calculated were pH (hydrogen ion concentration), EC (electrical conductivity), TDS (total dissolved solid), TH (total hardness) and concentrations of all major cations like Ca (calcium), Mg (magnesium), Na (sodium) and K (potassium) and anions like Cl₂ (chloride), HCO₃ (bicarbonate), F (fluoride), SO₄ (sulfate) and NO₃ (nitrate N). The pH and electrical conductivity respectively were measured by using pH meter and conductivity meter. CO₃ and HCO₃ concentrations were determined using acid titration method; Alkalinity and Phosphate were determined by titration method, Cl concentration by the AgNO₃ titration method, SO₄ concentration by the BaCl₂ method using spectrophotometer and NO₃ concentration by the titration method. Na and K were analyzed using Micro Processor Flame Photometer, Ca and F were analyzed by Cary,100 Bio, UV-visible spectrophotometer, Mg and Fe were analyzed by using Atomic Absorption Spectrometer (AAS) and TDS of the groundwater was determined by the following equation:

$$\text{TDS in mg/l} = \text{EC} * 0.64.$$

Table 1. Statistical analyses results of the major ions concentration in groundwater samples.

S.No.	Parameters	Pre-monsoon					Post-monsoon				
		Minimum	Maximum	Mean	Median	SD	Minimum	Maximum	Mean	Median	SD
1	pH	6.40	7.83	7.11	7.18	0.29	6.50	7.30	7.10	7.10	0.13
2	EC (µS/cm)	233.00	2920.00	1019.82	962.00	431.38	215.00	3580.00	1029.10	985.00	455.63
3	Alka (mg/l)	120.00	560.00	362.58	365.00	96.07	150.00	600.00	374.50	366.00	85.54
4	Hard (mg/l)	110.00	800.00	357.58	340.00	131.93	88.00	1640.00	374.19	330.00	207.77
5	TDS (mg/l)	149.12	1868.80	651.80	615.68	275.76	137.60	2291.20	658.01	625.40	291.57
6	Ca (mg/l)	29.06	347.21	89.85	79.41	43.65	25.04	305.05	91.25	89.29	38.02
7	Mg (mg/l)	1.02	159.23	45.15	35.72	33.61	11.20	89.21	52.78	53.11	19.51
8	Na (mg/l)	0.02	189.23	59.47	59.22	34.45	1.09	110.08	54.29	48.65	29.20
9	K (mg/l)	0.34	46.40	3.10	2.40	5.76	0.52	30.12	3.07	2.64	3.72
10	CO ₃ (mg/l)	18.00	48.00	32.82	33.90	7.87	20.08	59.50	36.25	35.78	8.09
11	HCO ₃ (mg/l)	14.89	450.18	255.57	252.54	81.31	12.55	415.50	252.24	257.25	76.10
12	Cl (mg/l)	60.00	370.00	123.87	100.00	55.85	80.00	380.00	134.03	120.00	51.61
13	SO ₄ (mg/l)	1.20	765.92	53.74	22.28	103.02	0.09	788.61	57.55	35.56	104.52
14	NO ₃ (mg/l)	30.00	65.00	50.24	50.00	7.43	0.27	87.02	38.85	32.70	25.57
15	PO ₄ (mg/l)	0.00	1.00	0.15	0.00	0.27	0.00	0.90	0.08	0.00	0.19
16	Fe (mg/l)	0.00	5.13	0.50	0.08	0.98	0.00	3.99	0.43	0.22	0.58
17	F (mg/l)	0.00	2.56	1.06	0.90	0.68	0.19	3.99	1.96	2.01	0.88

The groundwater of the study area is used also for the agricultural purpose. The suitability of groundwater for irrigation purpose depends upon the mineral constituents present in the water. Irrigation water of good quality is essential to maintain the soil crop productivity at a higher level. Water used for irrigation

Results and Discussion

The statistical analyses of the parameters concentration are shown in Table 1. There is a significant variation in the concentration of most of the parameters from well to well as reflected in the high median and standard deviation values (Table 1). The pH value mean for pre-and post-monsoon seasons was slightly higher than 7.0 which indicate alkaline conditions. Bicarbonate (HCO₃) prevails and carbonate (CO₃) concentration becomes negligible under these pH conditions (Table 1). For example, TDS, which is an important water quality parameter that reflects the concentration of all dissolved ions, ranged from 149.12 to 1868.80 mg/l and 137.60 to 2291.20 mg/l pre-and post-monsoon seasons respectively. These results indicate that groundwater suitability for irrigation may vary from well to well. SAR, % Na, RSC, KR, PI and MH as calculated from Equations 1–6 (given in the following sections) and salinity (EC) are used for assessment of water for irrigation suitability due to the significant effect of these parameters on crop and soil physical properties.

causes an increase in soil solution osmotic pressure (Throne and Peterson 1954), which makes difficult for the plant root to extract water for osmosis. The various salts present in the irrigation water not only affect the plant growth directly, but also affect the soil structure, permeability and aeration which indirectly affect the plant growth (Mohan and others 2000). Hence the groundwater in the study area needs

to be analyzed for its suitability for irrigation purpose. The chemical parameters which are used for assessing the suitability of water for irrigation are sodium content which are expressed by using EC, Sodium Absorption ratio (SAR), Percentage of Sodium (%Na), Residual Sodium Carbonate (RSC), Kelly's ratio (KR), Permeability Index (PI) and Magnesium hazard (Table 2).

Table 2. Calculation of SAR, %Na, RSC, KR, PI and MH for groundwater in pre-and post-monsoon seasons.

Sample ID	Pre-monsoon, 2016						Post-monsoon, 2016					
	SAR meq/l	%Na meq/l	RSC meq/l	KR meq/l	PI meq/l	MH meq/l	SAR meq/l	%Na meq/l	RSC meq/l	KR meq/l	PI meq/l	MH meq/l
TIM-1-1	0.88	21.05	-0.25	0.26	49.12	36.95	0.91	21.29	-1.07	0.26	47.15	36.73
TIM-1-3	0.64	12.95	-3.69	0.15	31.75	65.06	1.03	22.28	-2.76	0.28	42.68	61.81
GOL-2-5	0.87	15.32	-6.80	0.18	29.39	33.84	1.51	25.42	-5.93	0.33	38.32	56.50
GOL-2-6	0.00	6.86	-9.23	0.00	20.25	58.52	0.02	6.41	-5.95	0.00	23.79	61.51
GUL-3-7	0.00	1.01	-1.59	0.00	29.44	51.07	0.03	1.75	-3.58	0.01	23.99	47.58
GUL-3-9	0.10	3.20	-0.74	0.03	35.92	51.30	0.27	7.35	-2.42	0.08	33.13	49.85
GER-4-10	0.01	0.51	-22.35	0.00	5.45	29.96	0.12	2.15	-18.59	0.02	6.98	29.92
GER-4-11	2.26	35.13	-0.54	0.53	54.47	53.57	1.89	30.05	-2.43	0.42	46.84	56.13
GER-4-12	1.86	28.26	-4.65	0.39	42.73	71.61	1.78	28.40	-4.41	0.39	42.89	50.41
GER-4-13	1.65	29.31	-0.80	0.41	50.85	63.53	1.28	21.58	-4.62	0.27	38.31	49.46
ULL-5-15	1.52	23.48	-8.03	0.30	34.98	61.17	1.40	25.18	-4.23	0.33	40.87	51.70
ULL-5-16	2.34	36.08	-1.26	0.56	54.26	63.00	1.67	26.74	-4.41	0.36	41.56	56.54
CHI-6-17	0.96	19.10	-1.82	0.23	41.73	57.01	0.83	15.33	-4.12	0.18	33.32	48.97
CHI-6-19	0.66	17.33	-2.42	0.19	38.21	46.95	0.63	15.24	-2.94	0.17	35.17	35.01
CHE-7-20	0.21	6.84	-4.15	0.07	15.44	72.87	0.26	12.65	-0.78	0.12	30.90	42.44
CHE-7-21	0.98	18.88	-3.86	0.22	36.15	58.54	0.95	18.99	-3.34	0.22	36.97	31.81
BHO-8-24	2.43	37.14	0.25	0.59	57.22	64.85	1.75	27.29	-3.85	0.37	42.96	44.90
BHO-8-26	1.45	29.83	-0.60	0.41	52.43	50.02	1.14	20.19	-5.87	0.25	34.30	48.07
BHO-8-28	4.63	56.75	-0.42	1.30	71.67	40.26	2.00	29.79	-4.92	0.42	43.85	51.16
BHO-8-29	2.33	38.42	-2.57	0.62	54.39	21.39	1.78	31.54	-3.43	0.45	46.73	21.99
BHO-8-32	1.67	31.85	-1.74	0.46	51.31	58.50	1.13	21.36	-3.76	0.27	38.77	50.93
GOT-9-33	1.05	21.38	-3.71	0.26	39.08	48.54	0.94	19.55	-3.99	0.24	37.23	43.29
GOT-9-35	0.55	12.02	-3.47	0.13	33.59	40.17	0.58	11.90	-5.11	0.13	29.16	40.76
BHO-8-36	1.70	24.96	-8.11	0.33	36.39	51.31	1.66	25.44	-6.57	0.34	38.41	49.27
BHO-8-37	1.74	28.38	-3.93	0.39	43.98	59.96	1.54	24.02	-6.72	0.31	37.19	46.43
RAL-10-38	1.57	29.28	-1.21	0.41	50.36	55.90	1.19	23.47	-2.88	0.30	42.09	55.70
RAL-10-39	1.23	23.35	-4.00	0.29	39.93	33.12	1.08	18.97	-5.79	0.23	33.90	47.59
KUC-11-43	2.04	35.40	0.67	0.54	58.67	60.20	1.90	31.75	-2.22	0.46	49.67	67.04
KUC-11-44	1.50	27.97	-1.92	0.38	47.51	57.55	1.62	27.19	-4.36	0.37	42.38	62.95
RUD-12-45	1.03	25.22	1.25	0.32	57.35	45.52	2.22	38.77	-1.27	0.62	57.32	45.56
RUD-12-46	2.40	36.15	-2.49	0.56	52.71	76.43	1.84	29.48	-2.20	0.40	47.04	63.99

RUD-12-49	1.85	33.21	-0.83	0.48	54.17	34.31	1.51	25.05	-5.42	0.32	39.50	44.59
RUD-12-50	0.90	14.57	-9.28	0.17	26.69	47.22	0.88	15.95	-5.32	0.18	31.88	45.55
RUD-12-51	0.77	18.56	-2.40	0.22	39.53	34.38	0.75	17.86	-2.72	0.21	38.05	47.98
RUD-12-52	1.91	36.13	-0.70	0.55	58.46	34.72	1.59	28.29	-4.14	0.39	42.95	59.03
RUD-12-53	1.56	30.45	-1.66	0.43	51.01	33.48	1.63	33.49	-0.66	0.49	56.61	40.23
RUD-12-54	1.95	34.41	-0.91	0.52	54.97	33.37	1.90	32.27	-3.63	0.47	47.56	40.68
ARJ-13-55	1.55	31.71	-1.76	0.46	52.76	21.93	0.29	7.33	-4.67	0.07	24.25	81.94
ARJ-13-57	1.48	25.99	-3.68	0.35	43.25	34.98	1.69	30.58	-1.09	0.44	50.23	20.18
CHI-14-59	0.94	20.71	-1.27	0.26	45.46	12.47	0.83	17.15	-1.58	0.20	39.85	39.86
CHI-14-60	0.62	14.08	-2.20	0.16	37.69	27.37	0.81	16.81	-2.49	0.20	38.65	40.16
PED-15-61	1.68	33.61	-1.22	0.50	55.97	4.26	1.43	26.81	-2.88	0.36	45.18	48.04
PED-15-63	2.63	45.24	1.14	0.81	69.51	23.36	2.59	43.35	1.48	0.75	67.35	49.80
PED-15-64	1.64	37.99	0.35	0.59	66.30	8.59	1.22	28.00	-0.43	0.37	54.92	35.10
CHE-16-66	0.54	13.61	-3.06	0.16	34.55	50.30	0.44	9.38	-6.29	0.10	24.81	71.57
CHE-16-67	1.54	31.95	-0.84	0.46	56.95	27.32	1.07	22.26	-1.77	0.28	45.51	49.63
CHE-16-69	0.77	18.55	-1.35	0.22	45.09	34.85	0.57	11.82	-4.49	0.13	31.15	61.86
YAP-17-71	0.34	6.37	-8.16	0.06	21.24	69.79	0.72	13.53	-4.85	0.15	30.79	46.25
YAP-17-72	1.90	37.97	-0.15	0.60	62.57	30.75	0.71	15.16	-4.10	0.17	33.93	75.98
SAN-18-73	1.54	41.74	2.69	0.69	85.70	4.72	2.49	43.27	0.67	0.75	66.45	63.59
SAN-18-75	0.61	15.50	-1.73	0.17	42.05	39.11	0.94	20.26	-1.79	0.24	42.98	50.65
BHA-19-77	1.09	27.07	-0.05	0.36	58.16	17.26	1.29	29.84	1.28	0.41	62.93	56.90
BHA-19-79	0.87	20.51	-1.29	0.26	46.11	11.52	0.72	15.52	-1.99	0.18	38.82	36.54
GOR-20-81	1.53	33.49	-1.04	0.50	57.71	1.77	1.04	20.88	-3.69	0.25	38.50	39.26
GOR-20-83	1.85	38.77	0.49	0.62	67.37	26.26	1.05	20.96	-3.11	0.26	39.50	53.29
DHA-21-84	1.37	18.79	-11.21	0.22	30.00	70.68	1.53	25.07	-3.93	0.32	41.72	54.00
DHA-21-86	1.01	15.10	-10.87	0.17	26.62	58.62	0.83	15.00	-4.59	0.17	32.87	55.42
DHA-21-87	0.99	21.28	-3.31	0.26	40.30	11.03	0.24	6.73	-2.82	0.06	29.78	27.47
DUD-22-89	1.61	32.57	-1.55	0.47	54.08	42.42	0.66	17.32	0.14	0.19	48.75	39.40
DUD-22-92	1.94	38.49	-0.22	0.61	61.72	24.54	0.42	10.04	-2.16	0.10	33.65	57.65
KES-23-93	1.04	25.83	-1.83	0.34	48.02	24.03	0.42	11.79	-2.81	0.13	32.03	31.59
KES-23-95	1.24	21.66	-8.66	0.26	31.42	34.23	1.13	21.22	-5.92	0.25	35.51	42.18
Mini	0.00	0.51	-22.35	0.00	5.45	1.77	0.02	1.75	-18.59	0.00	6.98	20.18
Max	4.63	56.75	2.69	1.30	85.70	76.43	2.59	43.36	1.48	0.75	67.35	81.94
Average	1.35	25.31	-2.91	0.36	45.84	41.42	1.13	21.20	-3.55	0.28	39.85	48.59
SD	0.77	11.38	3.94	0.22	14.48	19.12	0.60	9.09	2.72	0.16	10.31	11.98

Salinity Hazard (EC)

The most influencing water quality for crop production is salinity hazard which is expressed as electrical conductivity (EC), reflected by an increase in TDS value of groundwater. Electrical Conductivity is a measure of the degree of the mineralization of the water, which is dependent on rock water interaction and thereby the residence time of

the water in the rock (Eaton, 1950). EC of the irrigation water becomes one of the important parameters to evaluate the overall chemical quality of groundwater. Based on the classification of EC (Wilcox 1955), waters are classified as Excellent, Good, Permissible, Doubtful and unsuitable. The standard classification of water quality is given in (Table 3).

Table 3. Irrigation water quality based on Electrical Conductivity (Wilcox 1955)

Classification of Water	Range of EC in $\mu\text{S}/\text{cm}$	No. of samples		Percentage of Samples	
		Pre-monsoon	Post-monsoon	Pre-monsoon	Post-monsoon
Excellent (C1)	<250	1	1	1.61%	1.61%
Good (C2)	250-750	15	16	24.19%	25.80%
Permissible (C3)	750-2000	45	44	72.58%	70.96%
Doubtful (C4)	2000-3000	1	Nil	1.61%	Nil
Unsuitable (C5)	>3000	Nil	1	Nil	1.61%

As groundwater moves and stays for a longer time along its flow path the increase in total dissolved concentration and major ions normally occurs. It has been noticed in many groundwater investigations that the groundwater in recharge area is characterized by a relatively low EC than the groundwater in the discharge area it is higher (Freeze and Cheery, 1979). Hence, irrigation water with high EC will affect the root zone and water flow, due to high osmotic pressure. From the classification of EC most of the water falls under permissible category to be used for irrigation purpose in pre-monsoon and post-monsoon seasons 2016.

medium which influences the properties of the soil and the growth of the plant is sodium absorption ratio (SAR). Sodium ions have a tendency to get adsorbed on the soil colloids. Excess sodium in water produces the undesirable effects of changing soil properties and reducing soil permeability and soil structure (Kelly, 1957). SAR is an important parameter for the determination of the suitability of irrigation water because it is responsible for the sodium hazard (Todd, 1980). Hence, the assessment of sodium concentration is necessary while considering the suitability for irrigation. The SAR can be found out by the relation given by Karnath (1987) as follows:

Sodium Absorption Ratio (SAR)

The measurement of the sodium content relative to the calcium and magnesium in soil and water

$$\text{SAR} = \frac{\text{Na}^+}{\sqrt{(\text{Ca}^{2+} + \text{Mg}^{2+})/2}} \dots\dots\dots (1)$$

Table 4. Alkalinity Hazard Classification of Groundwater (Richards 1954)

SAR	Alkalinity Hazard	Water Class	Samples number		Percent of samples	
			Pre-monsoon	Post-monsoon	Pre-monsoon	Post-monsoon
<10	S1	Excellent	62	62	100%	100%
10-18	S2	Good	Nil	Nil	Nil	Nil
18-26	S3	Doubtful	Nil	Nil	Nil	Nil
>26	S4	Unsuitable	Nil	Nil	Nil	Nil

All the values are expressed in meq/litre. According to Richards (1954), water with SAR values less than 10 is excellent, 10-18 is good, 18-26 is doubtful and greater than 26 is unsuitable is given in the (Table 4).According to the above classification, the SAR values in the study area range from 0.00 to 4.63 meq/l pre-monsoon and 0.02 to 2.59 meq/l post-monsoon (Table 2), and the samples of the study area have been classified as there is no danger of sodium consideration in soil as per SAR. From this classification around 100% of water is under the excellent category of water (S1) of both the pre and post monsoon seasons.

Sodium percentage (%Na)

Sodium concentration is important in classifying the irrigation water because sodium reacts with the soil to reduce its permeability content (Kaur & Singh 2011). Percent sodium in water is a parameter computed to evaluate the suitability of water quality for irrigation (Wilcox 1948). The %Na is computed with respect to relative proportions of cations present in water, where the concentrations are expressed in meq/l using the formula:

$$(\%) \text{Na}^+ = \frac{(\text{Na}^+ + \text{K}^+)}{(\text{Ca}^{2+} + \text{Mg}^{2+} + \text{Na}^+ + \text{K}^+)} \times 100 \dots\dots\dots (2)$$

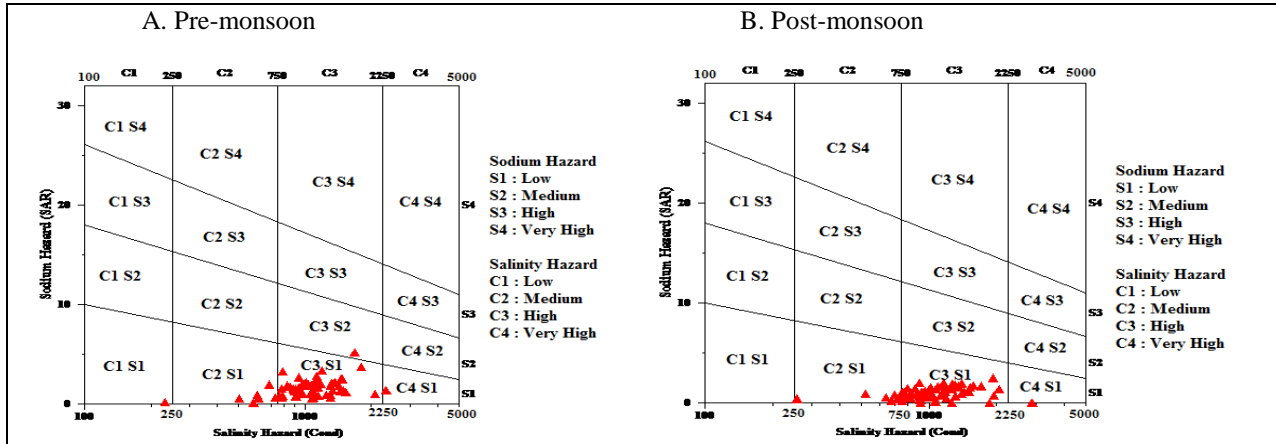


Fig. 2. Salinity and sodium hazard of irrigation water in US salinity diagram (after Wilcox 1955) for A. (pre-monsoon) and B. (post-monsoon) seasons, 2016.

Table 5. Classification of groundwater based on % Na (Wilcox 1955).

%Na	Quality of water	Samples number		Percentage of samples	
		Pre-monsoon	Post-monsoon	Pre-monsoon	Post-monsoon
<20	Excellent	20	26	32.25%	41.93%
20-40	Good	39	34	62.90%	54.83%
40-60	Permissible	03	02	4.83%	3.22%
60-80	Doubtful	Nil	Nil	Nil	Nil
>80	Unsuitable	Nil	Nil	Nil	Nil

All the values are expressed in terms of meq/litre. Wilcox (1955) classified the irrigation water based on percentage of Na as excellent (<20), good (20-40), permissible (40-60), doubtful (60-80) and unsuitable (>80). The classification of groundwater based on Wilcox 1955 is given in (Table 5). Table 5 shows most of the analysed groundwater samples collected during the pre-monsoon and post-monsoon periods fall under the category of excellent to good quality. A few samples fall under permissible category. The results of the analysis are plotted in the Wilcox’s diagram (Wilcox 1955) for the classification of groundwater for irrigation (Figure 2).

Residual sodium carbonate (RSC)

The quantity of bicarbonate and carbonate in excess of alkaline earth metal cations, (Ca²⁺ +

Mg²⁺) also influences the suitability of water for irrigation purposes (Karanth 1989). The bicarbonate and carbonate in the irrigation water tend to precipitate calcium and magnesium ions in the soil resulting in an increase in the proportion of the sodium ions. For this reason, RSC was considered as an indicative of the sodicity hazard of water. The RSC values were computed, where ions are expressed in meq/l using the following formula.

$$RSC = (CO_3^{2-} + HCO_3^-) - (Ca^{2+} + Mg^{2+}) \dots\dots\dots (3)$$

All the values are expressed in terms of meq/liter. A high value of RSC in water leads to an increase in the adsorption of sodium on soil (Eaton 1950).

Table 6. Suitability of irrigation water based on residual sodium carbonate

RSC (meq/l)	Suitability for irrigation	Samples number		Percentage of samples	
		Pre-monsoon	Post-monsoon	Pre-monsoon	Post-monsoon
<1.25	Safe	61	60	98.38%	96.77%
1.25-2.5	Moderate	Nil	2	Nil	3.22%
>2.5	Unsuitable	Nil	Nil	Nil	Nil

Irrigation waters having RSC values greater than 5 meq/l have been considered harmful to the growth of plants, while waters with RSC values above 2.5 meq/l are unsuitable for irrigation. An RSC value between 1.25 and 2.5 meq/l is considered as the marginal quality and value < 1.25 meq/l as the safe limit for irrigation. The variation in RSC values of the study area during pre- and post-monsoon seasons is given in Table 6. However, with respect to RSC all samples fall within the safe quality category for irrigation. From the Table 6, it is found that well nos 43 and 52 are moderate for post-monsoon seasons. The calculated RSC values are 98.38% for pre-and 96.77 for post-monsoon seasons of the analyzed groundwater samples which are below 2.5 meq/l, indicating that in general groundwater is suitable to marginally suitable for irrigation purposes.

Kelly’s ratio

Based on Kelly’s ratio waters are also classified for irrigation. Sodium measured against calcium and magnesium was considered by Kelly (1957) to calculate this parameter. The concentration of Na⁺ in irrigation water is considered to be one of the prime factors in making the water unsuitable, if Kelly’s ratio is >1.

$$\{KR = \frac{Na^+}{Ca^{2+} + Mg^{2+}} meq/l\} \dots (4)$$

Where, the groundwater is categorized into suitable, if KR is <1, marginal, when KR is 1-2 and unsuitable if KR is >2 (Table 7).

Table 7. Classification of groundwater (Kelly 1951)

Range of Kelly’sratio	Category	Number of samples		Percentage of samples	
		Pre-monsoon	Post-monsoon	Pre-monsoon	Post-monsoon
<1	Suitable	61	62	98.38%	100%
1-2	Marginal	1	Nil	Nil	Nil
>2	Unsuitable	Nil	Nil	Nil	Nil

A Kelly’s ratio of more than one indicates an excess level of sodium in waters. Therefore, water with the Kelly’s ratio less than one is suitable for irrigation, while those with a ratio more than two are unsuitable for irrigation. Kelly’ ratio of groundwater of the study area varies from 0.00 to 1.30 meq/l with an average 0.36meq/l during the pre-monsoon while in the post-monsoon it varies from 0.00 to 0.75 meq/l with an average of 0.28 meq/l (Table 2). Therefore, according to the Kelly’s ratio, all the water samples are in the category of suitable for irrigation except only one sample in pre-monsoon season. The majority of groundwater samples of the current study are suitable

98.38% in pre-monsoon and 100% in post-monsoon seasons for irrigation.

Permeability index (PI)

The soil permeability is affected by long term use of irrigation water as it is influenced by sodium, calcium, magnesium and bicarbonate content of the soil. Doneen (1964), WHO (1989) gave a criterion for assessing the suitability of groundwater for irrigation based on the permeability index (PI). The PI is formulated is as:

$$PI = \frac{(Na+K) + \sqrt{HCO_3}}{Ca+Mg+Na+K} \times 100, \dots (5)$$

Table 8. Classification of Permeability Index.

Class	Order %	Samples numbers		Percentage of Samples	
		Pre-monsoon	Post-monsoon	Pre-monsoon	Post-monsoon
I	>75%	01	Nil	1.61%	Nil
II	25-75%	57	57	91.93%	91.93%
III	<75%	61	62	98.38%	100%

where all the ions concentrations are in meq/l.

Accordingly, the permeability index is classified under class 1 (>75%), class II(25-75%) and class III(<75%) orders. Class I and class II waters are categorised as good quality for irrigation with 75% or more of maximum permeability (Table

8). Class III waters are unsuitable with 25% of maximum permeability. In the study area, the PI during the pre-monsoon varies from 5.45 to 85.70 with an average of 45.84, while PI values vary from 6.98 to 67.35 with an average value 39.85 during the post-

monsoon seasons (Table 2). According to Doneen classification, 1.61% of the samples are acceptable for irrigation purpose of pre-monsoon and none for post-monsoon (Table 8).

Magnesium hazard MH)

Generally calcium and magnesium maintain a state of equilibrium in groundwater. Excess magnesium in water affects the soil quality converting it to alkaline and decreases crop yield. Szabolcs and Darab (1964) proposed magnesium hazard (MH) value for irrigation water as given below.

$$MH = Mg / (Ca + Mg) \times 100 \quad \dots\dots (6)$$

where all ionic concentrations are expressed in milliequivalent/litre. The magnesium hazard (MH) value in the groundwater samples varies between 1.77 to 76.43% with the average value 41.42% during pre-monsoon and varies between 20.18 to 81.94% with average value 48.59% during post-monsoon period (Table 2).

Table 9. Magnesium Hazard Ratio (MH) of GW samples in the study area.

Range	Class	No. of samples		Percentage of no. of samples	
		Pre-monsoon	Post-monsoon	Pre-monsoon	Post-monsoon
<50	Suitable	37	37	59.67%	59.67%
>50	Unsuitable	25	25	40.32%	40.32%

MH > 50 is considered harmful and unsuitable for irrigation purpose. In the analyzed waters, 40.32% and 40.32% of the groundwater samples having magnesium hazard (MH) > 50% during pre-and post-monsoon seasons respectively (Table 9).

Conclusion

Evaluation of groundwater quality for irrigation purposes is of paramount importance in semi-arid and arid regions of the world, particularly in the developing countries like India owing to burgeoning population, expansion of irrigated farming and mushroom growth of industrial clusters. Results of the current study revealed that water samples from two wells are not suitable for irrigation based on SAR and %Na, and all other groundwater samples are suitable for irrigation based on RSC. US salinity laboratory diagram, however, showed that the majority of the groundwater samples fall in the high or very high salinity zone which indicates that special requirements

should be met before the water from these wells can safely be used for irrigation. This includes cultivation of salt-tolerant crops or fruits, good drainage soil, application of leaching requirements, and using improved irrigation systems. Since groundwater is a precious resource, therefore, there is a need to preserve and protect this valuable resource by following preventive measures to control the contamination.

Acknowledgements

The authors wish to express special thanks to Chhattisgarh Council of Science & Technology (CGCOST) for providing laboratory facilities for chemical analysis of groundwater samples. Authors are also thankful to the Principle, Govt. N. P. G. College of Science, Raipur (CG) and Head, Department of Applied Geology, National institute of Technology Raipur,(CG) for providing necessary permission and facilities to complete the task.

References

- APHA (1995). Standard methods for the examination of water and waste water, 19th ed., American Public Association, Washington D. C., p.1467.
- Babiker, I. S., Mohamed, A. M. and Hiyama, T. (2007). Assessing groundwater quality using GIS. *Water Resour. Manage.* v. 21 (4), p.699-715.
- Dhiman, S. D. (2005). Factoring groundwater quality. *Geospatial Today*, v.4 (1), p.50-54.
- Doneen, L. D. (1964). Notes on water quality in agriculture. *Water Science and Engineering Paper 4001*, California, Department of Water Sciences and Engineering, University of California.
- Eaton, F. M. (1950). Significance of carbonates in irrigation waters. *Soil science*, v.39, p.123- 133.
- Freeze RA, Cherry JA (1979). *Groundwater*. Prentice, Hall Engle wood Cliffs, p 604.

- Karant, K. R. (1987). *Groundwater assessment, development and management*. Tata McGraw Hill publishing Company Limited, New Delhi.
- Karnath K.R. (1989). 'Hydrogeology', McGraw-Hill, New Delhi.
- Krishna Kumar, S., Rammohan, V., Dajkumar Sahayam, J. and Jeevanandam, M. (2011). Assessment of groundwater quality and hydrogeochemistry of Manimuktha river basin, Tamil Nadu. *J Environ Monit Assess*, v.159 (1-4), p.341-351.
- Kelley, W.P. (1951). *Alkali soils-their formation properties and reclamation*. Reinhold Publ. Corp., New York.
- Kelly W.P. (1957). 'Adsorbed sodium cation exchange capacity and percentage sodium sorption in alkali soils', *Science*, v.84, p.473-477.
- Magesh, N.S., Chandrasekar, N. (2011). Evaluation of spatial variations in groundwater quality by WQI and GIS

- technique: A case study of Virudunagar District, Tamil Nadu, India. Arab J. Geosci. Doi: 10.1007/s12517-011-0496-z.
- Mohan, R. Singh, A.K., Tripathi, J.K. and Choudhary (2000). G.C Jour. Geol. Soc. India., v.55, p.77-89.
- Richards, L. A. (1954). Diagnosis and improvement of saline and alkali soils. Hand Book, No. 60. U.S. Department of Agriculture, Washington, D.C.
- Sujatha, D. and Reddy, R. B. (2003). Quality characterization of groundwater in the south eastern parts of the Ranga Reddy district, Andhra Pradesh, India. Environ Geol., 44(5), p.579-586.
- Subramani, T., Elango, L. and Damodarasamy, S. R. (2005). Groundwater quality and its suitability for drinking and agricultural use in Chithar River Basin, Tamil Nadu, India. Environ. Geol., v.47, p.1099-1110.
- Schiavo, M. A., Havser, S., Gusimano, G. and Gatto, L. (2006). Geochemical characterization of groundwater and submarine discharge in the south-eastern Sicily. Cont Shelf Res., v.26 (7), p.826-834.
- Szabolcs, I. & Darab, C.(1964). "The influence of irrigation water of high sodium carbonate content of soils", Proceedings of 8th International Congress of Isss, 2, p.803-812.
- Todd, D. K. (1980). Groundwater hydrology, 2nd Edn. Wiley, New York, p.535.
- Throne D.W. and Peterson H.B. (1954). 'Irrigated soils', Constable and Company Ltd., London Vol. 113. p.715-719.
- Walton, W. C. (1970). Groundwater resources evaluation. Mc Graw Hill Book Co, New York.
- Wilcox, L. V. (1955). Classification and use of irrigation waters. USD Circular No.969, p.19.
- Wilcox, L.V. (1948). The quality of water for irrigation. U.S. Department of Agriculture Technical Bulletin No. 962, p.1-40.
- WHO. (1989). Health Guidelines for the Use of Wastewater in Agriculture and Aquaculture. Report of a WHO Scientific Group-Technical Report Series 778, WHO Geneva, p.74.
-

Diagenesis and Porosity Evolution of Pachmarhi Sandstones (Early Triassic), Satpura Gondwana Basin, Central India

Anis^{1,*}, Abdullah Khan², Narendra Kumar³, Mujeebul Hasan²

¹Department of Geology, School for Earth and Environmental Sciences, Babasaheb Bhimrao Ambedkar University, Lucknow-226025

²Department of Geology, Aligarh Muslim University, Aligarh-202002

³Department of Environmental Sciences, School for Earth and Environmental Sciences, Babasaheb Bhimrao Ambedkar University, Lucknow-226025

*Email: anisgeology74@gmail.com

Abstract: This study deals with the diagenetic history of the Pachmarhi Sandstones of Satpura Gondwana Basin, Central India. The sandstones are classified as quartz-arenite and sub-arkose type. Monocrystalline quartz grains dominate the detrital mineralogy followed by polycrystalline quartz grains, feldspars (more alkali-feldspar than plagioclase), rock fragments, detrital mica and heavy minerals. The diagenetic signatures observed in the Pachmarhi Sandstones include mechanical compaction, cementation (Fe-oxide, quartz overgrowths, calcite, matrix and clay minerals), replacement and dissolution of feldspar and calcite cement. The most commonly observed type of secondary porosity is dissolution of feldspars. The porosity loss is mainly due to cementation by pore occlusion and by early stage of mechanical compaction. In addition, several clay minerals occurred as pore-filling and pore-lining cements. The nature of various types of grain- to grain contacts suggests early cementation and consequent minor compaction. Among the various cements, calcite is the earliest followed by iron oxide while silica cementation occurred probably at a late stage. The carbonate cement formed during burial by dissolution and re-precipitation represents redistributed calcite which was buried with the sandstone. The iron cement was perhaps derived from weathering and leaching of ferromagnesian minerals of overlying Deccan traps. Silica cement was derived from the corrosion of quartz and feldspar grains. Types of grain contacts, minus-cement porosity and porosity reduction indicate a shallow depth of burial conditions for these sandstones.

Keywords: Satpura Gondwana basin, Pachmarhi Sandstones, Mechanical compaction, Cementation, Dissolution, Porosity modification.

Introduction

The relationship between diagenesis and reservoir quality is well documented in geological literature and detailed information of diagenesis comes from studies involving sandstone reservoir properties evaluation and quality prediction (Wilson, 1994; Primmer et al., 1997; Jeans, 2000, Ahmed and Bhat, 2006, Ahmed et al., 2006). Assessment of reservoir quality is based on understanding of potential controls of diagenesis, framework grains and provenance composition (De Ros et al., 1994; Bloch, 1994; De Souza et al., 1995; Nentwich and Yole, 1997; Ramm, 2000, Jamwal et al., 2020, this volume)), palaeoclimate (Worden et al., 2000) and depositional environment (Fuchtbauer, 1983; Lowry and Jacobsen, 1993; Bloch and McGowen, 1994; McKay et al., 1995; Hamlin et al., 1996; Bailey et al., 1998; Dos Anjos et al., 2000; Rossi et al., 2001; Hiatt et al., 2003). The Gondwana deposits of Peninsular India record resumption of sedimentation during the Carboniferous period after a prolonged depositional gap since the Proterozoic. In Peninsular India, the Gondwana sedimentary successions (~1-4 km thick) accumulated in

a number of discrete, intracratonic basins which record depositional history up to the Cretaceous period. The Gondwana Basins of the Peninsular India are intracratonic rift basins within Proterozoic terrains. The basins occurring along three distinct linear belts are defined by the present-day ENE-WSW trending Narmada-Son-Damodar valley, NNW-SSE trending Pranhita-Godavari valley and NW-SE trending Mahanadi valley (Fig. 1). It is widely believed that these basins originated under extensional tectonic regime due to failure of attenuated crust along the pre-existing zones of weakness imparted by Precambrian structural grains (Chatterjee and Ghosh, 1970; Naqvi et al., 1974; Mitra, 1994; Biswas, 1999; Acharyya, 2000; Chakraborty and Ghosh, 2005). However, disposition of the basins and their structural architecture indicate that the kinematics of all the basins cannot be extensional (Chakraborty and Ghosh, 2005). The current study focuses on diagenetic signatures in the Pachmarhi Sandstones of Satpura basin vis-à-vis compaction, cementation and porosity evolution in these rocks.

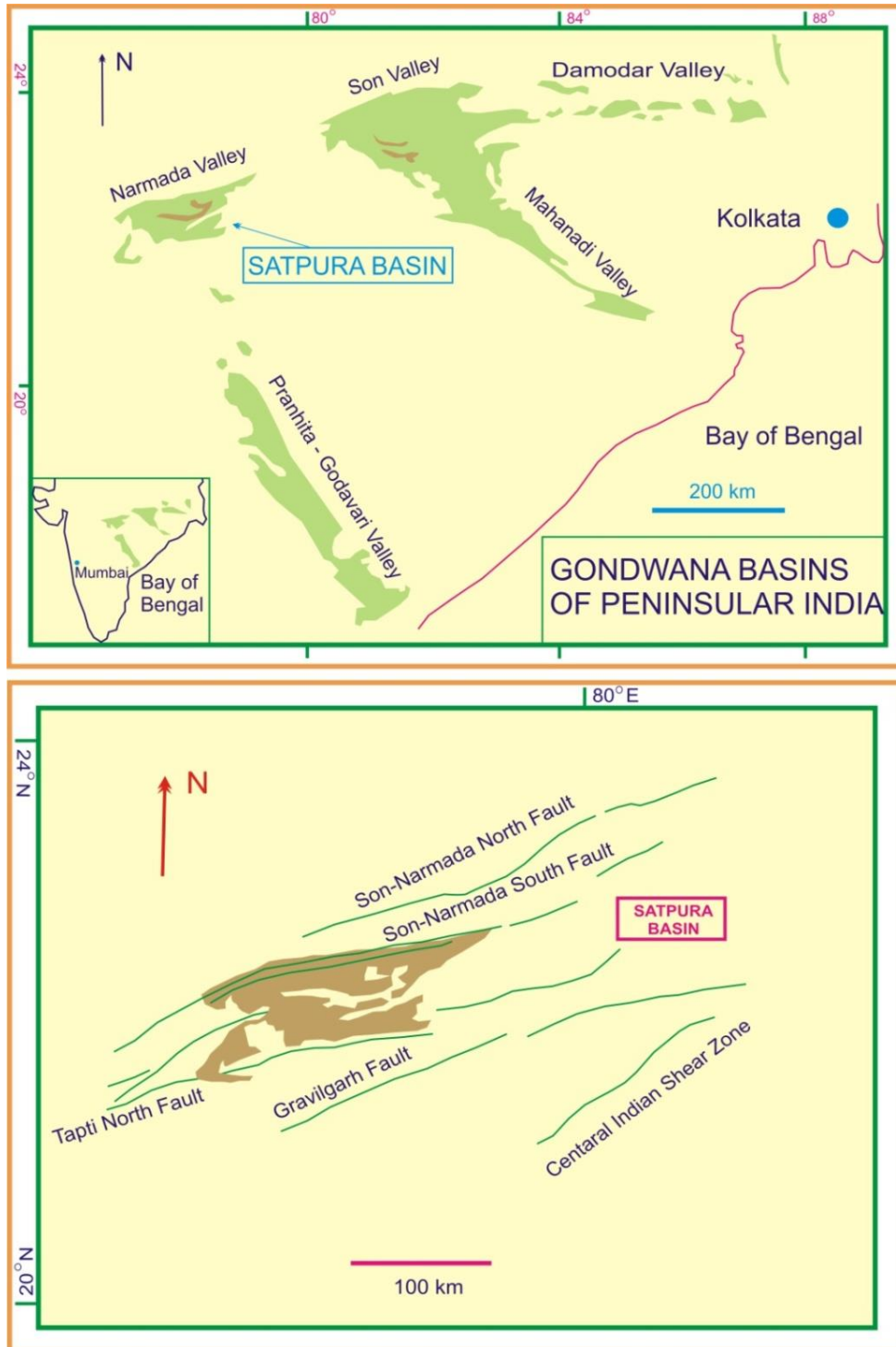


Fig. 1. (a) Outcrops of the Gondwana basins in the Peninsular India. Note that the Satpura basin is the westernmost Gondwana basin cropping out along the present-day ENE– WSW trending Narmada–Son–Damodar valley. (b) Major boundary faults of the Satpura Gondwana basin (based on Narula et al., 2000). Shaded area represents the outcrop of the Satpura basin.

Geological Setting

The Satpura Basin of Central India is the westernmost of the series of discrete Indian Gondwana Basin occurring along the ENE-WSW trending Narmada-Son- Damodar valley and preserves stratigraphic record of Permian to Cretaceous (Robinson, 1967; Crookshank, 1936). This basin is located between latitude 22° 06' N and 22° 28' N and longitude 77° 48' E

and 78° 53' E. The basin (~200 km long, ~60 km wide) is rhomb-shaped, elongate along the ENE-WSW direction and is filled with approximately 5-km-thick pile of siliciclastic sediments which unconformably lies over the Precambrian basement. The regional strike of the basin-fill strata is NE–SW, and the regional dip (~5°) is northerly. Based on the shape of the basin, its

disposition, and structural architecture, Chakraborty and Ghosh (2005) considered it to be of pull-apart origin. The Gondwana succession of Satpura Basin has been classified into seven major lithostratigraphic units which

include the Talchir, Barakar, Motur, Bijori, Pachmarhi, Denwa and Bagra formations, from old bottom to top in chronological order (Fig. 2).

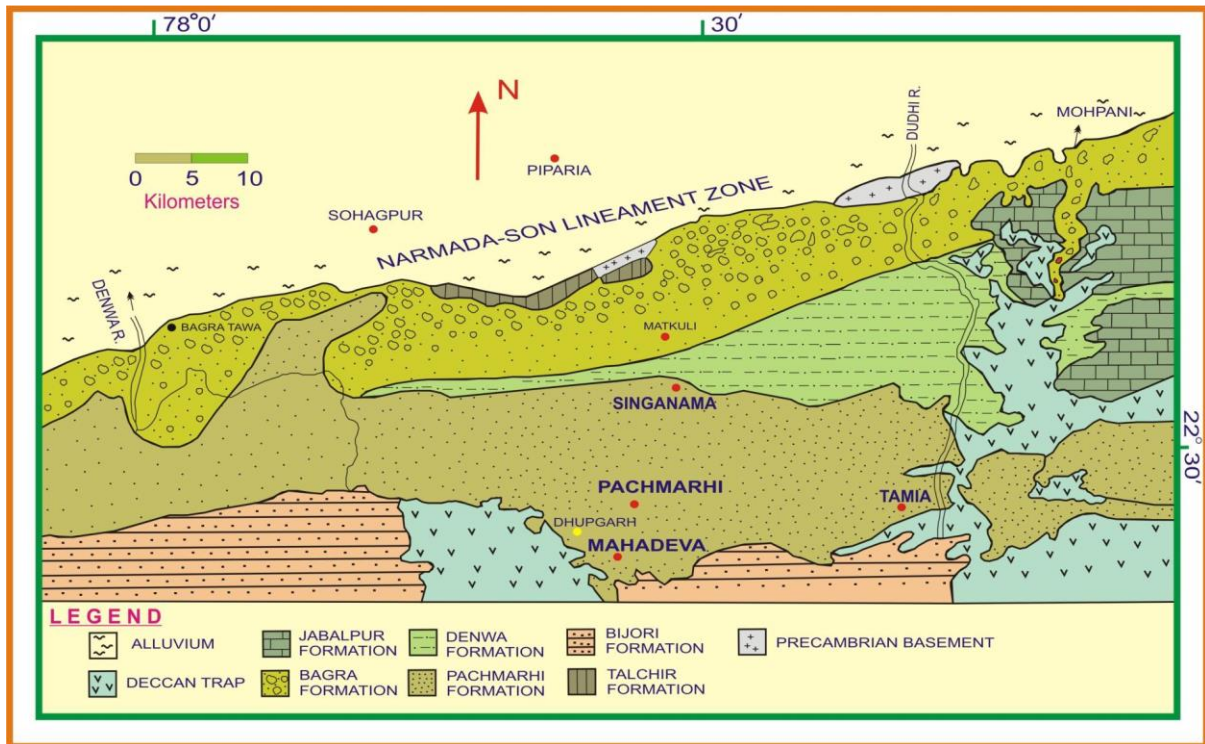


Fig. 2. Geological map of the Satpura Gondwana succession, Central India (modified after Raja Rao, 1983).

Methodology

The present study is based on 50 representative sandstone samples which were cut into standard petrographic thin sections. Some thin sections were etched and stained for identification of carbonate cement and potassium feldspars. The sampling of sandstone units was carried out at regular intervals of the measured section keeping in view the physical variation between different units (Fig. 3). About 300 to 350 grains were counted per thin section. The traditional method (Ingersoll et al., 1984) was used for classification and tabulation of grain types. Standard petrological techniques using a polarizing microscope were employed to describe the thin sections. Authigenic components (cement and matrix) were counted separately and the amount of matrix, cement and porosity were measured by a single operator. In order to reconstruct the original detrital composition of the sandstones, the effect of diagenesis was taken into consideration as far as possible during the counting. Taylor’s (1950) method was applied for the study of the nature of detrital grain contacts where as computation of contact index was made as per Pettijohn et al. (1987). Scanning electron microscopy (SEM) was applied to study clay minerals, and diagenetic features. The samples were coated with a gold palladium alloy and were examined under a (JSM-6510LV model; Jeol, Japan) scanning electron microscopy (SEM).

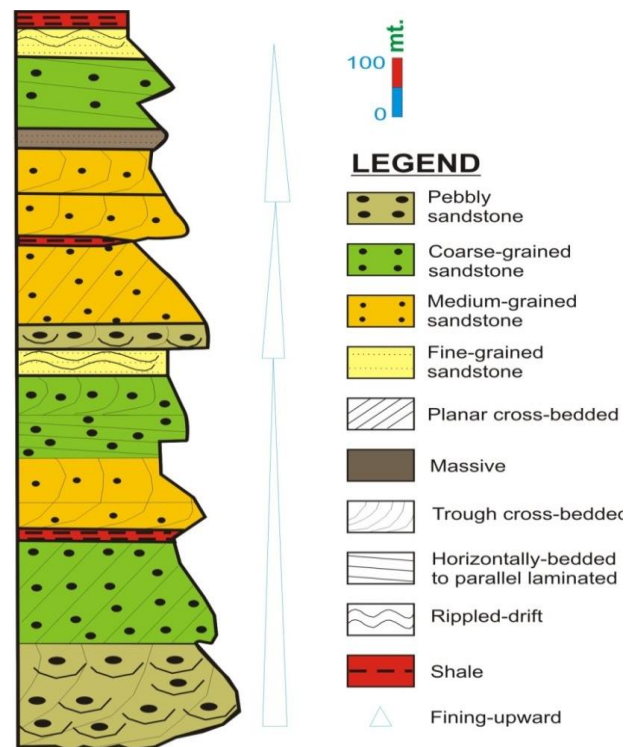


Fig. 3. A generalized lithology of the Pachmarhi Formation, Satpura Gondwana Basin.

Detrital Mineralogy

The Pachmarhi sandstones are composed of various types of quartz, feldspars, rock fragments, detrital mica and heavies which are medium- to coarse-grained, moderately to moderately well sorted, and with generally loose packing. These sandstones are in general

texturally sub-mature to mature. The overall average composition of these sandstones is $Q_{95.55} F_{2.70} R_{1.75}$. As per Folk's scheme (Table 1, Fig. 4; Folk, 1980) these sandstones are mostly quartz-arenite and minor amounts of sub-arkose.

Table 1. Grain size, sorting and detrital mode of the Pachmarhi Sandstone

Sample No.	Texture		Framework		
	Mean size (Mz Φ)	Sorting ($\sigma 1 \Phi$)	Quartz (Q)	Feldspars (F)	Rock fragments (R)
Range	0.26-3.5	0.66-0.93	91-98	1-5	0-4
Avg.	1.86	0.78	95.55	2.70	1.75

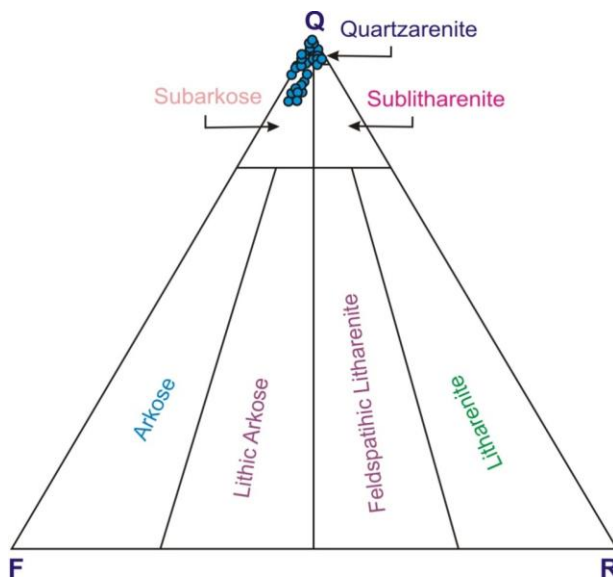


Fig. 4. Detrital composition of Pachmarhi Sandstones samples plotted on Folk (1980) classification diagrams.

Diagenesis

The Pachmarhi Sandstones in the Satpura Gondwana Basin has undergone through compaction, cementation, replacement, and dissolution of feldspars and carbonate cements resulting in the secondary porosity development.

Compaction and Porosity

The process of compaction results in the expulsion of pore fluids and reduction of pore volume due to the load of overburden (Fuchtbauer, 1967; Rittenhouse, 1971; Chilingar, 1983, Ahmed and Bhat, 2006). Compaction occurs in response to four types of processes grain rearrangements, plastic deformation, dissolution and brittle deformation (Wilson and Stanton, 1994, Ahmed and Bhat, 2006). In sandstones,

compaction is in fact controlled by various factors, which includes inherent grain properties, mass properties, fluid and basal dynamics, tectonics, rate of sedimentation and burial time. Mechanical compaction and cementation of sediments plays a vital role in reducing porosity (Fisher et al., 1999, Ahmed and Bhat, 2006). A grain to grain contact of sediments gives an idea about pore space reduction and compaction history of the sediments. Both, the nature of contacts and contact index are helpful in understanding the aggregate packing of the rocks. Grain contacts of the Pachmarhi Sandstones were studied in thin sections with a view to interpret their compaction history. In the present study the closely packed sandstones exhibit four types of grain contacts (after Taylor, 1950; Ahmed and Bhat, 2006), which include point, long (line contact), concavo-convex and sutured contacts (Plate 1A).

The observed number of various types of grain contacts in different samples is given in Table 2 and bar diagram constructed on the basis of grain contact data is shown in Fig. 5. In loosely packed sandstones some grains may not make any contact with other grains, such grains are referred to as floating grains (F). The average percentage of different types of contacts in the studied sandstones is 1) floating grains (8.85%), 2) point contact (13%), 3) long contact (57.7%), 4) concavo-convex contact (10.9 %), and 5) sutured contact (9.65 %) (Table 2). The dominance of point and long contacts, together averaging at 70.70% in the Pachmarhi Sandstones, indicates that the detrital grains did not suffer much pressure solution, as a result of either shallow burial or early cementation. Long contacts might have developed in the early stages of compaction as a result of rotation and adjustment of grains to the adjacent grain boundaries. The pressure effects are absent or at minimum in sandstones which have undergone early cementation (Taylor, 1950).

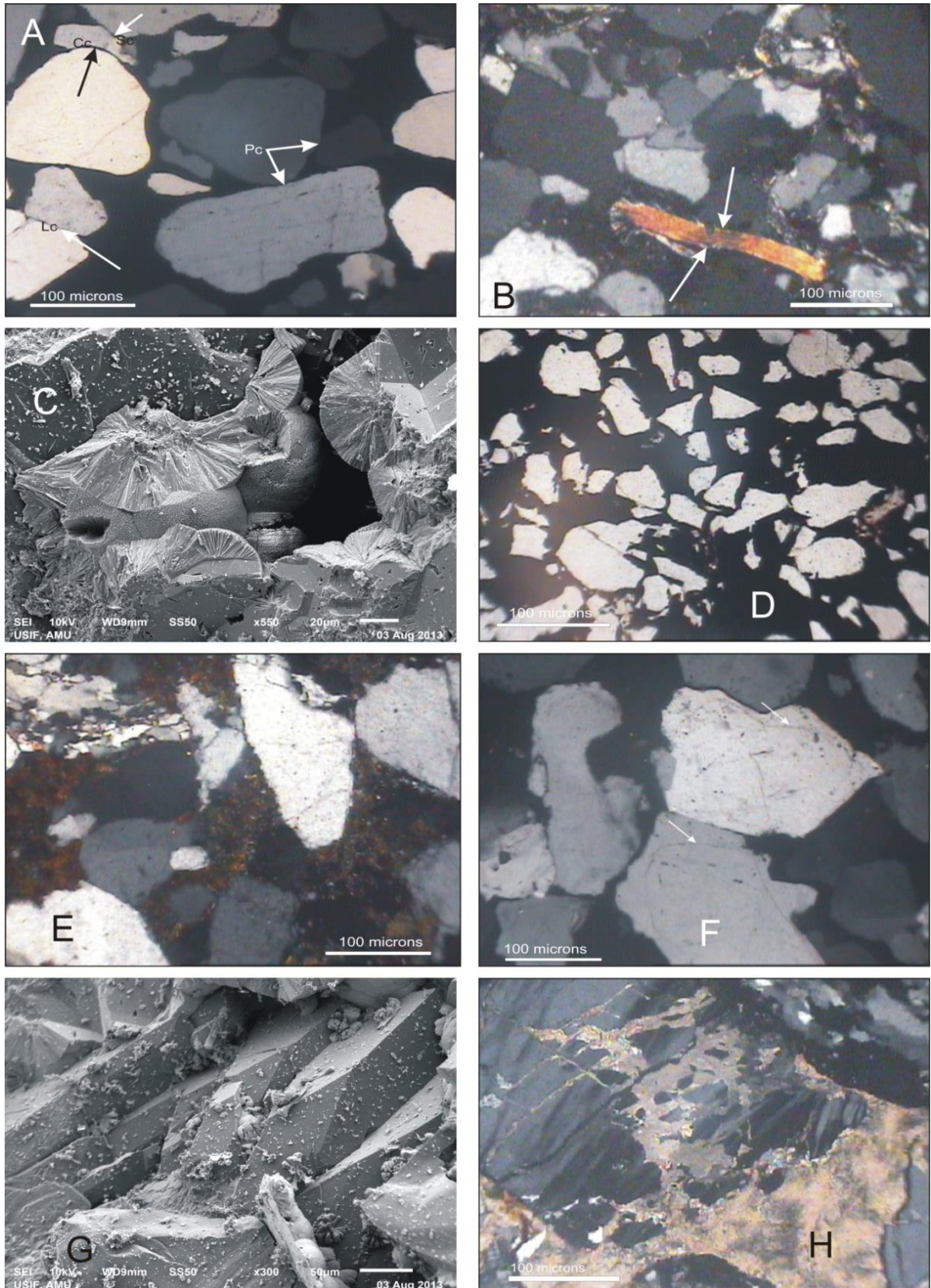


Plate 1. (A) Photomicrograph showing different types of grain contacts (Pc = point contact, Lc = long contact, Cc = concavo-convex and Sc = suture contacts), (B) Muscovite flake in contact with quartz grains showing effect of compaction, (C) SEM Photograph showing pore occluding iron-oxide cement, (D) Pervasive iron oxide cement extensively corroding and digesting framework grains, (E) Pervasive pore filling iron oxide cement replacing calcite cement, (F) Quartz overgrowth partially fill the intergranular spaces. The grain contacts are generally long; (G) SEM Photograph showing quartz overgrowth, (H) Photomicrograph of calcite replaced the framework grains.

Table 2. Percentage of various types of grain to grain contacts for the Pachmarhi Sandstones, Satpura Gondwana basin, central India.

	Types of grain contacts					No. of contacts per grains						Contact index (CI)
	Floating	Point	Long	Concavo-Convex	Sutured	0	1	2	3	4	>4	
Range	4-25	3-23	38-78	1-29	3-21	1-27	15-59	20-53	3-32	1-9	1-2	1.55-2.72
Avg.	8.85	13.0	57.7	10.9	9.65	9.25	32.4	38.35	16.9	2.95	0.15	2.20

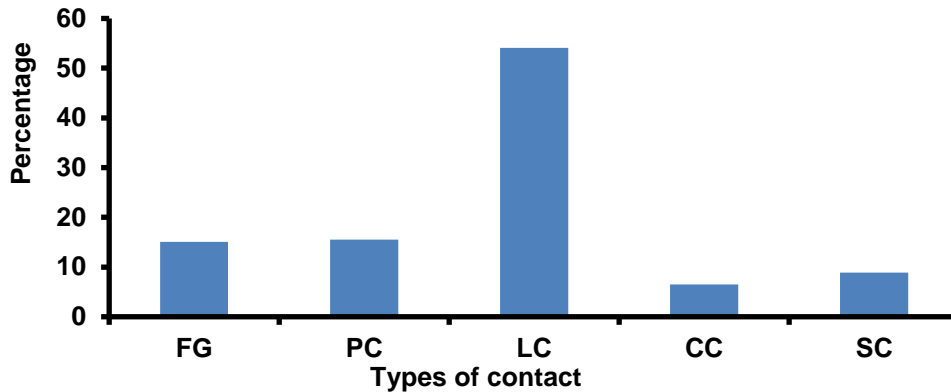


Fig. 5. Bar diagram showing types of grain contacts for sandstones of the Pachmarhi Formation, Satpura Gondwana Basin. (FG = Floating grains, PC = Point contact, LC = Long contact, CC = Concavo-convex contact, SC = Sutured contact).

It is well known that the original porosity of sandstones generally vary between 30 and 50%, which can reduce by 10-17% by mechanical compaction (Pryor, 1973, Beard and Weyl, 1973). The intergranular quartzose cement (minus-cement porosity) averages 32% porosity, which may be due to less mechanical compaction during the early stages of diagenesis. Less mechanical compaction and high content of intergranular cement may be related to high grain strength, good sorting and early cementation. Mechanical compaction and physical readjustment to the overburden load in the sandstones are evidenced by deformed mica grains (Plate 1B). The compaction effect is also evidenced by straight, concavo-convex and sutured contacts of neighbouring framework grains. During compaction framework grains are sliding past each other and packed into a tighter configuration. The presence of sutured boundaries of quartz overgrowth indicates the post cement compaction. Therefore, it may be concluded that some compaction of the Pachmarhi Sandstones took place in the early stages, when grains rotated and adjusted themselves to the boundaries of adjacent grains, and later compaction took place after cementation.

The contact index (C.I.), is the average number of grain contacts a grain has with its neighbouring grains (Pettijohn et al., 1987), infers the degree of compaction of the sediments. The grains are in contact with two grains followed by three grains. The overall average contact index value of the Pachmarhi Sandstones is 2.20 (Table 2). This is due to the dominance of long and point contacts and also attributed to mechanical compaction, which increases the value of contact index and packing density. Presence of significant numbers of sutured as well as concavo-convex contacts indicates that chemical compaction also played a role, which resulted in pressure

dissolution in point and long contacts which converted them to concavo-convex and sutured contacts.

Cements

The cementation is normally considered to reduce the porosity but dissolution improves porosity and permeability of the reservoir. Most of the secondary porosity resulted from the partial or complete dissolution of feldspar and calcite cement. Three types of cementing materials occur in the sandstones of the Pachmarhi Formation 1) iron oxide, 2) calcite and 3) silica overgrowths while clay occurs as matrix.

Iron cement

The iron-oxide cement in the Pachmarhi Sandstones is distinguished into three different forms such as thin coatings around the detrital grain boundary, isolated patches, and pervasive pore fillings (Plate 1C). The iron-oxide cement in the Pachmarhi sandstones ranges from 2% to 40% with an average of 17% (Table 3 and Fig. 6). In some thin sections characterized by Fe-calcite cement, the corroded quartz grains exhibit calcite cement infilling. This evidence suggests the presence of syndepositional calcite cement, which was later replaced by Fe-calcite cement. The oversized pore spaces might have been resulted from destruction and leaching of labile framework grains, possibly feldspars. This cement has corroded the detrital grains extensively (Plate 1D). The clastic grains have lost their grain morphology and are present now in the form of protrusions, embayments and notches. The iron oxide cement also has replaced calcite cement (Plate 1E). Coating of iron cement on detrital grains may be extra-basinal and weathering rinds generated during burial (Walker, 1974). The iron-oxide cement most probably was derived from weathering and leaching of ferromagnesian silicates of overlying Deccan traps by meteoric water which percolated during the upliftment.

Table 3. Percentage of detrital framework grains, cements and porosity of the Pachmarhi Sandstones, Satpra Gondwana basin, central India.

	Detrital grains	Cement					Porosity		Porosity loss	
		Iron	Calcite	Silica	Matrix Clay	Total Cement	Existing Optical Porosity (EOP)	Minus cement porosity (MCP)	Compactional porosity loss (COPL)	Cementational porosity loss (CEPL)
Range	58 - 76	2 - 40	0 - 12	0 - 9	0- 10	17 - 40	1 - 11	24 - 42	5.24 - 27.63	21.97 - 40.01
Avg.	68	17	4	3	4	27	5	32	18.99	29.07

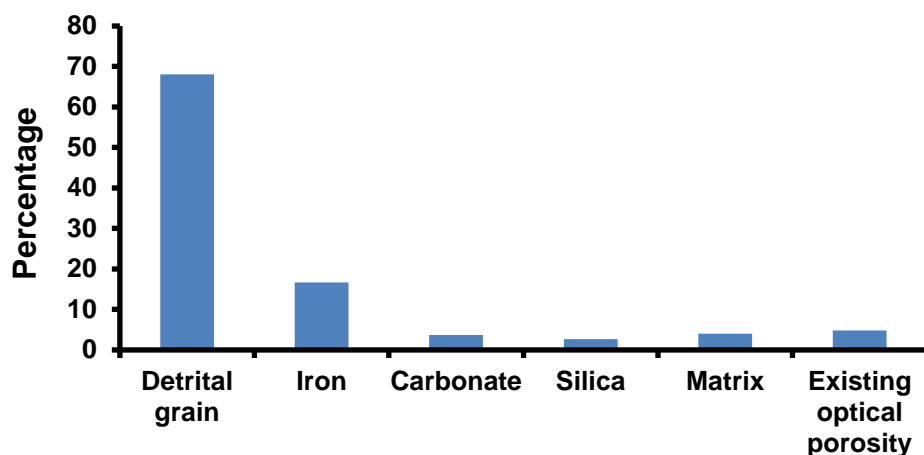


Fig. 6. Bar diagram showing percentage of detrital grains, cement and porosity for sandstones of the Pachmarhi Formation, Satpura Gondwana Basin.

Silica overgrowth

The silica cement occurs in the form of quartz overgrowth (Plate 1F, G) which shows the optical continuity with detrital quartz grains forming secondary enlargement. The amount of silica cement varies from sample to sample depending upon degree of condensation and pressure solution undergone by the rocks. The percentage of silica cement in the sandstones ranges from 0% to 9%, average 3% (Table 3 and Fig. 6). Authigenic quartz overgrowths on detrital grains of quartz are observed to fill up the intergranular spaces partly. In the studied sandstones quartz overgrowths are dominantly developed on monocrystalline quartz compared to polycrystalline quartz grains. The quartz overgrowths partially fill the intergranular space but where well developed, overgrowths from adjacent grains meet along sharp and planar crystal faces. The source of silica cement may be the descending meteoric water saturated with silica or pressure solution of detrital quartz and other silicates at grain contacts (Dutton, 1993; Walderhaug, 1994). The conversion of clay minerals during diagenesis and decomposition or feldspar alteration may release silica solutions (Hower et al., 1976; Bole and Franks, 1979).

Carbonate cement

Calcite cementation plays a key role in the porosity evolution of sandstones (Alaa et al., 2000).

Calcite cement shows patchy distribution and forms 0% to 12% and averages at 4% (Table 3 and Fig. 6). Two different kinds of calcite cement are present, 1) poikiliotopic calcite which has large crystal size with well developed cleavage planes and show pin point birefringence, 2) neomorphic xenotopic sparry calcite present in grain supported sandstones. The poikiliotopic calcite cement is in oversized pores and has floating grains than the sparry calcite-cemented sandstone suggesting its early stage precipitation. The calcite-cemented sandstones are high minus-cement porosity and corrosion of detrital grains. Apart from quartz, the feldspars are subjected to corrosion along grain boundary and cleavage planes (Plate 1H). The oversized pore filling poikiliotopic calcite cementation process may have taken place at the sediment-water interface. The xenotopic calcite cemented sandstones show close framework and have corroded to a lesser extent than the poikiliotopic calcite cement. Xenotopic cementation may have taken place after considerable burial under groundwater saturated with calcium carbonate flow through pores (Tandon and Friend, 1989).

The source of carbonate may be biogenic or early marine carbonate precipitated during the period of slow sedimentation. Thus, carbonate cement may have extrabasinal source into the sandstones. Very little carbonate may have precipitate from pore water without the dissolution of other carbonate minerals. The calcite

cement formed during deep burial by dissolution and reprecipitation represents redistributed carbonate which was buried with the sandstones. In some thin sections characterized by iron oxide cement, the corroded quartz grains exhibit calcite cement inclusions. This evidence suggests the presence of syndepositional calcite cement, which was later replaced by iron oxide. It is well known that the early precipitation of carbonate cement takes place a few centimetres below the sediment-water interface (Bjørlykke, 1983). This type of cementation occurs by exchange of interstitial marine pore water either by meteoric or pore water expelled from the underlying sediments.

Matrix and clay minerals

In most of the samples, clayey to silty matrix is present in varying amounts (Plate 2A). Matrix constitutes 0 to 10% (average 4%) of the total rock components (Table 3 and Fig. 6). The matrix is represented by silt-size quartz grains, chert and chalcedony mixed with fine grained muscovite and clay. Most of the matrix material is syndepositional, and hence pore-filling. The matrix also influenced diagenetic process by supplying Fe and reducing porosity and permeability by pore occlusion. Very low amount of matrix present in a few sandstone samples is probably decanted from infiltrating muddy pore water. SEM study also corroborate that Kaolinite is the dominant clay mineral, with illite, smectite and chlorite. Mixed layers of illite smectite also occur in varying amounts and in several forms. Kaolinite is authogenic and includes both cements and replacement of silicate framework grains. Scanning electron micrographs (SEM) of Kaolinite shows good crystals of pseudo-hexagonal plates, commonly with face-to-face stacking (Plate 2B). Pore-filling Kaolinite is a common feature in which pore spaces are usually plugged with authogenic Kaolinite with no apparent preferred orientation (Plate 2C, D). Authogenic smectite clay as pore-filling cement is also present in these sandstones (Plate 2E). However, in some sandstones honeycomb nature of smectite clay indicate the conversion stage to illite, which may act as bridges in the pore spaces and results in decreases of porosity.

The weathering of acidic plutonic rocks was likely responsible for generating the Kaolinite-rich clay in the Pachmarhi Sandstones. This weathering likely involved very intense kaolinization under the influence of a climate characterised by high temperatures and heavy rainfall (Nakagawa et al., 2006; van de Kamp, 2010) and it is therefore suggested that the Kaolinite present in the Pachmarhi Sandstones was derived through the intense chemical weathering of crystalline source rocks containing abundant of feldspar in the

presence of meteoric water (Bjørlykke, 1998; Bertier et al., 2008; Islam et al., 2002; van de Kamp, 2010).

Porosity Reduction

Intergranular porosity is primary porosity or has resulted from the dissolution of pore-filling cement (Plate 2F) (Felixa, *et al.*, 2005). Essentially all intergranular pores are thought to be primary porosity in the Pachmarhi sandstones. Primary pores were mainly those formed during the connate deposition of rocks and have been preserved till now. The primary pores can be subdivided into the primary intergranular ones remained by compaction, the intergranular ones remained by cementation and the micropores in the matrix. The secondary pores were formed during the burial stage arising from dissolution and other geological factors, such as tectonic movement and syneresis. The dissolved pores (such as intragranular dissolved pores, intergranular pores, mould pores and super pores/oversized pore) are the main type of secondary pores. Intragranular porosity was generally formed by the dissolution of detrital grains. Mould pores were predominantly generated by the dissolution of detrital feldspar, and sponge spicules. Oversized pores are intergranular pores and intragranular pores large enough to be identified; it is interpreted as the product of complete detrital grain dissolution (Plate 2G). Microporosity generally forms within altered feldspar grains, ductile grains and authogenic clay aggregates (Plate 2H). Microporosity is not only dependent on the amount of rock components but also on the growth habit of the clays. Intergranular void spaces constitute the primary porosity. Estimation, prediction and understanding the evolution of depositional porosity are essential for pre-drill prediction of porosity, permeability and reservoir modelling to enhance hydrocarbon exploitation. The parameters which control the porosity are detrital composition, grain size, sorting; basin temperature and pressure history.

The sandstones, which are mainly coarse to medium grained, moderately to moderately well sorted and have dominance of quartz (average 95.6%) in framework composition, qualify to have an initial depositional porosity (P_i) of 45 % (Atkins and McBride, 1992), which we have used here as an assumed initial porosity and with this value have tried to model the porosity evolution and relative role of cementation and compaction. This has been quantitatively worked out by using the following formula and variation diagram of Lundegard (1992).

$$\text{Compaction porosity loss (COPL)} = P_i - ((100 - P_i) \times \text{MCP}) / (100 - \text{MCP})$$

$$\text{Cementation porosity loss (CEPL)} = P_i - \text{COPL} \times (\text{Tc} / \text{MCP})$$

Where P_i = the initial porosity (45%), MCP = the minus-cement porosity, and Tc = the total cement.

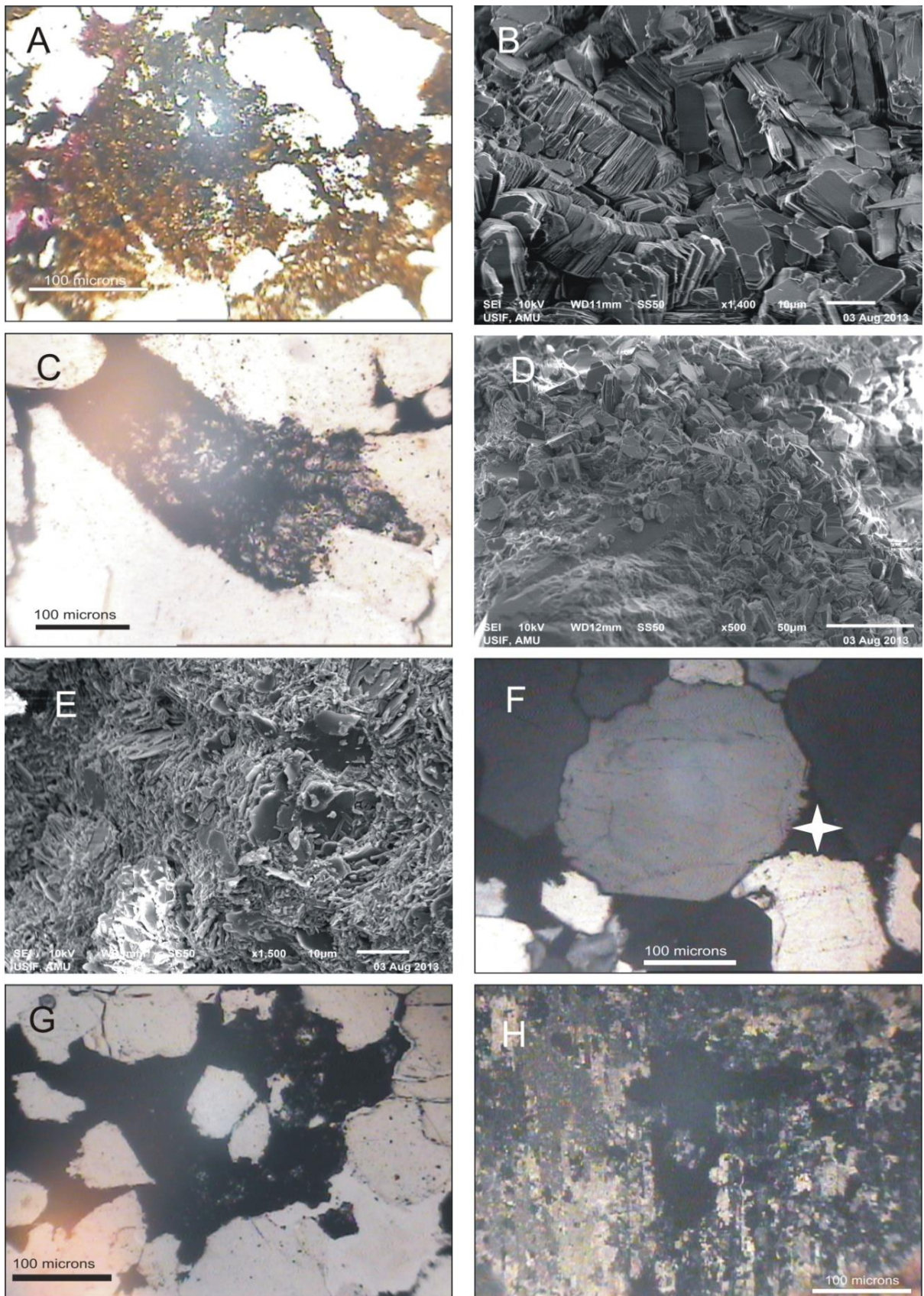


Plate 2. (A) Detrital grains corroded by clayey to silty matrix, (B) SEM Photograph of well crystallized authigenic Kaolinite booklets occurring as grain-replacement cement, (C) Pore-filling clay cement, (D) SEM Photograph of stacks of pseudo-hexagonal plates or books of grain-replacement Kaolinite cement, (E) Pore-filling mechanically infiltrated smectite, (F) Intergranular pores, (G) Oversized pores, (H) Micropores.

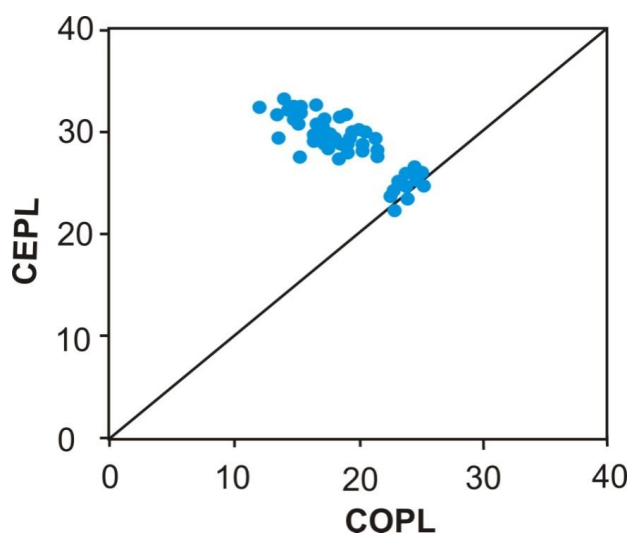


Fig.7. The plot of porosity loss due to compaction (COPL) v/s porosity loss due to cementation (CEPL) reflecting the evolution and relative importance of compaction and cementation in porosity loss.

The plot COPL versus CEPL (Fig. 7) shows a clear, decreasing trend of CEPL with increase in COPL suggesting that cementation was the major cause of the porosity reduction and hence compaction is secondary in porosity reduction. Porosity loss due to compaction averages 18.99% and due to cementation averages 29.07%

References

- Acharyya, S. K. (2000). Tectonic setting and nature of the Gondwanic Indian crust. In: Proceedings volume, International Seminar, Precambrian Crust in Eastern and central India. Geological Survey of India, Special Publications, v. 57, p. 1–8.
- Ahmad, A. H. M., Bhat, G. M. (2006). Petrofacies, provenance and diagenesis of Dhosa Sandstone member (Chari Formation) at Ler, Kachchh sub-basin, Western India, *Jour. of Asian Earth Sciences*, 27, 857–872.
- Ahmad, A. H. M., Bhat, G. M., Khan, A. F., Saikia, C. (2006), Petrography, Diagenesis, Provenance and Tectonic Setting of the Sandstones of Upper Katrol Formation (Kimmeridgian), Nakhtarana Area, Kachchh, Gujarat, *Jour. Geol. Soc., India*, V. 67 (2), P, 243
- Atkins, J. E., McBride, E. F. (1992). Porosity and packing of Holocene river, dune, and beach sands. *American Association of Petroleum Geologists Bulletin*, v. 76, p. 339–355.
- Bailey, A. M., Roberts, H. H., Blackson, J.H. (1998). Early Diagenetic minerals and variables influencing their distributions in two long cores (> 40 m), Mississippi River delta Plain. *Jour. Sed. Research*; 68: 185–197.
- Beard, D. C. and Weyl, P. K. (1973). Influence of texture on porosity and permeability of unconsolidated sand. *American Association of Petroleum Geologists Bulletin*, v. 57, p. 349–369.
- Bertier, P., Swennen, R., Largrou, D., Laenen, B. and Kemps, R. (2008). Palaeo-climate controlled diagenesis of the Westphalian C & D fluvial sandstones in the Campine Basin (north–west Belgium). *Sedimentology*, v. 55, p. 1375–1417.
- Biswas, S. K. (1999). A review on the evolution of rift basins in India during Gondwana with special reference to western Indian basins and their hydrocarbon prospects. In: Sahni, A. and Loyal, R.S. (Eds.) *Gondwana Assembly: New Issues and Perspectives*. Proceeding Indian National Science Academy, Special Issues, v. 65, p. 261–283.
- Bjorlykke, K. (1983). Diagenetic reactions in sandstones. In: Parker, A. and Sellwood B.W. (Eds.), *Sediment diagenesis*, Reidel publishing, Holland, p. 169–213
- Bjorlykke, K. (1998). Clay mineral diagenesis in sedimentary basin. A key to the predication of rock properties. Examples from the North Sea Basin. *Clay Minerals*, v. 33, p. 15–34.
- Bloch, S. and McGowen, J. H. (1994). Influence of depositional environment on reservoir quality prediction. *Reservoir quality assessment and prediction in clastic rocks*. SEPM Short Course, v. 30, p. 41–57.
- Boles, J. R. and Franks, S. G. (1979). Clay diagenesis in Wilcox sandstones of southwest Texas: implications of smectite diagenesis on sandstone cementation. *Journal of Sedimentary Research*, v. 49, p. 55–70.
- Chakraborty, C., Ghosh, S. K. (2005). Pull-apart origin of the Satpura Gondwana basin, central India. *Journal of Earth System Science*, v.114, p. 259–273.
- Chatterjee, G. C., Ghosh, P. K. (1970). Tectonic framework of peninsular Gondwanas of India. *Records Geological Survey of India*, v. 98, p. 1–15.

(Table 3). High minus cement porosity values also suggest low mechanical compaction probably just before cementation, leading to grain dissolution.

Conclusion

Monocrystalline quartz is predominant followed by polycrystalline (recrystallized and stretched metamorphic) quartz. The sandstones are classified as quartz-arenite and sub-arkose. The diagenetic signatures observed in the Pachmarhi Sandstones include compaction, cementation, replacement and dissolution. The porosity loss is mainly due to cementation by pore occlusion and little by mechanical compaction. The nature of various types of grain contacts suggests early cementation and consequent minor compaction. Most of the porosity in the Pachmarhi Sandstones is primary inter-granular and little porosity is secondary inter-granular and intra-granular. The development of secondary porosity is mainly due to dissolution pores in iron oxide and calcite cement and intra-grain dissolution micro-pores in feldspars.

Acknowledgement

The authors are grateful to the Chairperson, Department of Geology, AMU, Aligarh for providing the necessary facilities in the Department. The authors express sincere gratitude to the USIF for providing SEM facility.

- Chilingar, G. V. (1983). Compositional diagenesis. In: Parker, A. and Sellwood, B.W. (Eds.), *Sediment Diagenesis*, D. Reidel, Dordrecht, p. 57- 167.
- Crookshank, H., 1936. Geology of the northern slopes of the Satpura between the Morand and Sher rivers. *Memoir Geological Survey of India*, v. 66, p. 173-381.
- De Ros, L. F., Morad, S., Paim, P. S. (1994). The role of detrital composition and climate on the diagenetic evolution of continental molasses: evidence from the Cambro-Ordovician guaritas sequence, southern Brazil. *Sedimentary Geology*, v. 92, p. 197-228.
- De Souza, R. S., De Ros, L. F., Morad, S. (1995). Dolomitic diagenesis and porosity preservation in lithic reservoirs: Carmopolis Member Sergipe-Alagoes Basin, northeastern Brazil. *American Association of Petroleum Geologists Bulletin*, v. 79, p. 725-748.
- Dos Anjos, S. M. C., De Ros, L.F., De Souza, R.S., De Assis Silva, C. M., Sombra, C. L. (2000). Depositional and diagenetic controls on the reservoir quality of lower Cretaceous Penencia rift- Basin, Brazil. *American Association of Petroleum Geologists Bulletin*, v. 84, p. 1719-1742.
- Dutton, S. P. (1993). Influence of provenance and burial history on diagenesis of Lower Cretaceous Frontier Formation sandstones, Green River Basin, Wyoming. *Journal of Sedimentary Petrology*, v. 63, p. 665-667.
- Felixa L. C., Luis A., Munoz B. (2005). Representing a relation between porosity and permeability based on inductive rules. *Journal of Petroleum Science and Engineering*, v. 47, p. 23-34.
- Fisher, Q. J., Casey, M., Clennell, M. B. (1999). Mechanical compaction of deeply buried sandstones of the North Sea. *Marine and Petroleum Geology*, v. 16, p. 605-618.
- Fuchtbauer, H. (1967). Influence of different types of diagenesis on sandstone porosity. In 7th World Petroleum Congress, p. 353-369.
- Fuchtbauer, H. (1983). Facies controls on sandstone diagenesis. In: Parker, A. and Sellwood, B.W. (Eds.), *Sediment Diagenesis*, p. 269-288.
- Hamlin, H. S., Dutton, S. P., Seggie, R. J., Tyler, N. (1996). Depositional controls on reservoir properties in a braid-delta sandstone, Tirrawarra oil field, South Australia. *American Association of Petroleum Geologists Bulletin*, v. 80, p. 139-156.
- Hiatt, E. E., Kyserb, K., Dalrymple, R. W. (2003). Relationships among sedimentology, stratigraphy, and diagenesis in the Proterozoic Thelon Basin, Nunavut, Canada: implications for paleo-aquifers and sedimentary-hosted mineral deposits. *Journal of Geochemical Exploration*, v. 80, p. 221-240
- Hower, J., Eslinger, E. V., Hower, M. E., Perry, E. A. (1976). Mechanism of burial metamorphism of argillaceous sediment: I. mineralogical and chemical evidence. *Geological Society of America Bulletin*, v. 87, p. 725-737.
- Ingersoll, R. V., Bullard, T. F., Ford, R. L., Grimm, J. P., Pickle, J. D., Sares, S.W. (1984). The effect of grain size on detrital modes: a test of the Gazzi-Dickinson point-counting method. *Journal of Sedimentary Research*, v. 54, p. 103-116.
- Islam, M. R., Stuart, R., Risto, A., Vesa, P. (2002). Mineralogical changes during intense chemical weathering of sedimentary rocks in Bangladesh. *Journal of Asian Earth Sciences*, v. 20, p. 889-901.
- Jamwal, M., Pandita, S. K., Sharma, M and Bhat, G. M. (2020), Petrography, provenance and diagenesis of Murree Group of rocks exposed along Basohli- Bani Road, Kathua, Jammu, *Journal Indian association of Sedimentologists*, Vol. 37 (2), p. 15-26
- Jeans, C.V. (2000). Mineral diagenesis and reservoir quality—the way forward: an introduction. *Clay Minerals*, p. 35: 3-4.
- Lowry, P., Jacobsen, T. (1993). Sedimentological and reservoir characteristics of a fluvial-dominated delta-front sequence: Ferron Sandstone Member (Turonian) east-central Utah, U.S.A. In: Ashton, M. (Ed.) *Advances in reservoir geology*. Geological Society, London, Special Publications, v. 69, p. 81-103.
- Lundegard, P. D. (1992). Sandstone porosity loss; a "big picture" view of the importance of compaction. *Journal of Sedimentary Research*, v. 62, p. 250-260.
- McKay, J. L., Longstaffe, F. J., Plint, A. G. (1995). Early diagenesis and its relationship to depositional environment and relative sea-level fluctuations (Upper Cretaceous Marshybank Formation, Alberta and British Columbia). *Sedimentology*, v. 42, p. 161-190.
- Mitra, N.D. (1994). Tensile resurgence along fossil sutures: a hypothesis on the evolution of Gondwana basins of peninsular India. In: *Abstracts of Proceedings of 2nd Symposium on Petroliferous Basins of India*. KDMIPE, Dehradun, p. 55-62.
- Nakagawa, M., Santoish, M., Yoshikura, S., Miura, M., Fukuda, T. and Harada, A. (2006). Kaolin deposits at Melthonnakkal and Pallipuram within Trivandrum block, southern India. *Gondwana Research*, v. 9, p. 530-538.
- Naqvi, S. M., Rao, D., Narain, H. (1974). The protocontinental growth of the Indian shield and the antiquity of its rift valleys. *Precambrian Research*, v. 1, p. 345-398.
- Nentwich, F. W., Yole, R. W. (1997). Petrology and diagenetic history of deltaic litharenites, Oligocene Kugmallit Sequence, Beaufort-Mackenzie Basin, Arctic Canada. *Bulletin of Canadian Petroleum Geology*, v. 45, p. 339-355.
- Pettijohn, F. J., Potter, P. E., Siever, R. (1987). *Sand and Sandstone*. Springer-Verlag, New York. 553p.
- Primmer, T. J., Cade, C. A., Evans, J., Gluyas, J. G., Hopkins, M. S., Oxtoby, N. H. and Worden, R. H. (1997). Global patterns in sandstone diagenesis: their application to reservoir quality prediction for petroleum exploration. In: Kupecz, J. A., Gluyas, J. G. and Bloch, S. (Eds.), *Reservoir quality prediction in sandstones and carbonates*. AAPG Memoir, v. 69, p. 61-77.
- Pryor, W. A. (1973). Permeability-porosity patterns and variations in some Holocene sand bodies. *American Association of Petroleum Geologists Bulletin*, v. 57, p. 162-189.
- Ramm, M. (2000). Reservoir quality and its relationship to facies and provenance in Middle to Upper Jurassic sequences, northeastern North Sea. *Clay Mineral*, v. 35, p. 77-94.
- Rittenhouse, G. (1971). Pore-space reduction by solution and cementation. *Am. Assoc. Petrol. Geol. Bulletin*; 55: 80-91.
- Robinson, P. L. (1967). The Indian Gondwana Formations – a review. In: 1st IUGS International Symposium on Gondwana Stratigraphy UNESCO, Buenos Aires, p. 201-268.
- Rossi, C., Marfil, R., Ramseyer, K., Permanyer, A. (2001). Facies-related diagenesis and multiphase siderite cementation and dissolution in the reservoir sandstones of the Khatatba Formation, Egypt's Western Desert. *Journal of Sedimentary Research*, v. 71, p. 459-472.

- Taylor, J. M. (1950). Pore space reduction in sandstone. American Association of Petroleum Geologists Bulletin, v. 34, p. 710-716.
- van de Kamp, P. C., Leake, B. E. (1995). Petrology and geochemistry of siliciclastic rocks of mixed feldspathic and ophiolite provenance in the Northern Apennines, Italy. Chemical Geology, v. 122, p. 1-20.
- Walderhaug, O. (1994). Temperatures of quartz cementation in Jurassic sandstones from the Norwegian continental shelf – evidence from fluid inclusions. Journal of Sedimentary Research, v. A64, p. 311–323.
- Walker, T. R. (1974). Formation of red beds in moist tropical climate: A hypothesis. Geological Society of America Bulletin, v84, p. 633-638.
- Wilson, M. D. (1994). Introduction, In: Wilson, M.D. (Ed.), Reservoir quality assessment and prediction in clastic rocks. SEPM Short Course, v. 30, p. 1–4.
- Worden, R. H., Ruffell, A. H., Cornford, C. (2000). Palaeoclimate sequence stratigraphy and diagenesis. Journal of Geochemical Exploration, v. 69, p. 453-457.
-

Spatial and Temporal Variations in Geochemistry of Cauvery River Sediments (Tamilnadu, India): Indicators of Provenance and Weathering

N. Gobala Krishnan¹, R. Nagendra*², L. Elango², K.N. Prakash Narasimha³, K. Vybhav³ and Pradeep Mujumdar³

¹Malankara Catholic College, Kaliakkavilai-629153

²Department of Geology, Anna University, Chennai-600025

³Department of Earth Science, University of Mysore, Mysuru-570006

*geonag@gmail.com/044-22358452

Abstract

South-West, North-East and Post-monsoon Cauvery River sediment geochemistry characterizes the intensity of chemical weathering ascribing to the relative mobility of elements during weathering. The negative correlation between Al₂O₃% and SiO₂% signifies that the sediments are enriched with quartz. The Al₂O₃% vs. TiO₂% relationship deduces the granite and granodiorite as the major source rocks of Cauvery River sediments. The weathering trend of sediments is accounted by the incidence of illite clay minerals. The weathering intensity of SW monsoon sediments (57.73%), NE monsoon sediments (64.17%) and post-monsoon sediments (64.79%) specifies the weak to intermediate intensity of weathering, which is controlled by precipitation. The higher concentration of Ba (459.45-856.95ppm) reflects presence of K-feldspar in the source rocks.

Keywords: Geochemistry, Cauvery River, Weathering, South India.

Introduction

Studies on weathering of rocks deduce the continental erosion and consumption of CO₂. The processes of weathering of rocks modify the earth surface and factors in the geochemical cycle. The bedrock is transformed into sediments and to the soil by the combined effects of physical, chemical, and biological weathering. Hence the unique signature of the source rock remains in the sediments (Singh, 2010). The study attributes of the chemical composition of clastic sediments which is controlled by the composition of source rocks, atmospheric chemistry, temperature, precipitation and topography, duration weathering, transportation mechanism, depositional environment and post-depositional processes (Hayashi et al., 1997). The trace elements; Sc, Th, Zr, Cr, Ni, Co and REEs in the sediments are immobile during the weathering processes and are indicators of source rock composition and environment. This paper appraises the spatio-temporal variations of geochemical elements of Cauvery River sediments in middle and lower regions (Tamilnadu region) and their provenance, paleo-weathering, intensity of weathering and maturity.

Geological Setting

The Cauvery River is an easterly flowing river of the Peninsular India which flows across three states of southern India. The river originates at Tala Kaveri, Western Ghats, and traverses through the Mysore plateau, forming a delta on the eastern coastline of southern India, before it debouches into

the Bay of Bengal (Fig.1). The upper part of the river basin comprises of granitoid-gneisses, granulite, charnockites, meta-igneous, meta-sedimentary and carbonates rocks (Ramakrishna and Swaminath, 1981; Narasimha et al., 2009; Radhakrishna, 1992; Mahabaleswar et al., 1995; Valdiya, 1998). The middle part of the river basin comprises of granulites, migmatite gneissic, granite, small patches of carbonate rocks (John et al., 2005), calcareous sandstone, limestone, marl, fossiliferous limestone, and shale. The river flows through the alluvium sediments in its lower region. The tributaries of the Cauvery River are Bhavani and Amaravathy which receive water during the NE monsoon and join the river in the middle region (Fig. 1).

Materials and Methods

The middle and lower regions of the Cauvery River flows 400km in Tamilnadu. The sediment sampled at 25km interval from the middle region (Pannavadi (L-1) to Mutharasanur (L-9)) to lower region (Appakudathan kovil (L-10) to Pommbugar (L-15)) of the river basin. The conning and quarter method was followed for surface sediment sampling during South-West (SW), North-East (NE) and Post monsoon. The powdered samples were treated for removal of moisture, organic matter and CaCO₃. The dried (50°C) sediment powdered in agate mortar and sieved to 230 ASTM mesh. The powder samples dried at 110°C for removing the moisture content. After LOI pressed pellets were prepared using aluminium cups (Govil, 1985) which

are filled with boric acid as binder. 1gm of the fine powdered sample placed on the top of the boric acid and pressed with a hydraulic press at 20 tons pressure to obtain a 40mm diameter pellet. Bruker model S4 Pioneer sequential wavelength dispersive X-ray spectrometer equipped with a goniometer with 4kW Rh X-ray tube with 60 samples loading system was used at NCESS, Thiruvananthapuram. Calibrated the major and trace elements were completed by taking care of dead time correction, background, line overlap correction and matrix effects. The results are in weight % and in ppm.

Results and Discussion

Major oxides and trace element concentration of SW monsoon sediments

The distribution of major and trace elements of the sediments reflects the composition of the source rocks and sorting of sediments (He et al., 2015). The concentration of SiO₂ in analysed sediments ranges from 65.51% to 85.1% (avg. of 75.81%), whereas the TiO₂ ranges from 0.21% to 3.08% with an average of 0.90% (Table. 1). The Al₂O₃ varies from 6.71% to 15.14% with an average of 10.2% and the MnO varies from 0.03%-0.17% (avg. of 0.07%). Besides, Fe₂O₃ concentration varies from 1.62% to 8.49%. These variations of major oxides indicate the presence of garnet, ilmenite, and rutile heavy minerals in the Cauvery River sediments. Similarly, the CaO content is ranging from 1.52% to 4.72% with an average of 2.89%, MgO varies from 0.54%–2.66% with an average of 1.33%. The Ca and

Mg characterizes for the higher mobility of the geochemical elements during the chemical weathering of rocks. Successively, the concentration of Na₂O concentration of 1.6 to 3.43%, and K₂O from 1.43 to 3.63% (Fig. 2) and P₂O₅ of 0.06% to 0.26% (avg. of 1.33%; Table. 2). These variations in major oxides in the downstream of the river appraise the nature of sorting processes (He et al., 2015). The increasing trend of major oxides is SiO₂>Al₂O₃>Fe₂O₃>CaO>Na₂O>MgO >K₂O>TiO₂> P₂O₅ (Fig.2) in the studied samples of middle and lower regions of the river basin. The chemical alteration index (CIA) of SW monsoon sediments varies from 55.59% to 61.61% with an average of 57.73% reflecting weak to moderate rate of weathering. The plagioclase index alteration varies from 57.42% to 64.8% indicating weak to moderate maturity of sediments. The concentration of Ba ranges from 236.84ppm to 1269.74ppm with an average of 630.09ppm. This comparatively higher concentration of Ba in the sediments represents the presence of K-feldspar (Nemee, 1975). The Cr and Ni are enriched in sediments due to the adsorption of clay minerals (Table.3) (Young et al., 2013). The concentration of Cu (56 ppm to 96ppm) and Sr (190.01 ppm to 603.16ppm) indicates that the source of these elements is weathering of plagioclase feldspar in the Cauvery River sediments (Rahman & Suzuki, 2007). The concentration of Zn (90.30ppm to 162.72ppm) is relatively higher in the sample no.15 (162.72ppm) (Table.3) which is attributed to the influence of seawater with river water and local fishing harbour interface (Shilpa et al., 2015).

Table. 1 Sediment sample locations

L.No	Sample locations	Stage wise	Latitude	Longitude	Elevation. (m)
1	Pannavadi	Middle regions of the river	11°54'28.7" N	77°46'19.2" E	236.2
2	Kudakal		11°40'14.1" N	77°46'08.7" E	190.5
3	Konavaikal		11°25'22.0" N	77°40'48.1" E	159.1
4	Sitharkovil		11°18'44.7" N	77°46'34.9" E	155.1
5	Karuvelampalayam		11°09'10.1" N	77°53'07.3" E	135.3
6	Killakkuthavitupalayam		11°03'48.0" N	78°07'28.2" E	123.7
7	Sriramasamuthiram		10°57'46.1" N	78°12'41.8" E	110.6
8	Kulithalai		10°56'21.0" N	78°25'51.7" E	88.4
9	Mutharasanur		10°51'59.1" N	78°39'05.6" E	72.8
10	Appakudathan kovil	Lower regions of the river	10°50'07.5" N	78°51'45.0" E	56.9
11	Kandiur bridge		10°51'54.2" N	79°05'22.7" E	44.2
12	Thiruvanchuli		10°56'56.1" N	79°19'38.8" E	33.2
13	Suriyanarkovil		11°01'34.9" N	79°28'59.2" E	21.64
14	Paniur		11°08'12.9" N	79°35'29.4" E	13.4
15	Poombugar		11°08'12.2" N	79°51'24.1" E	2

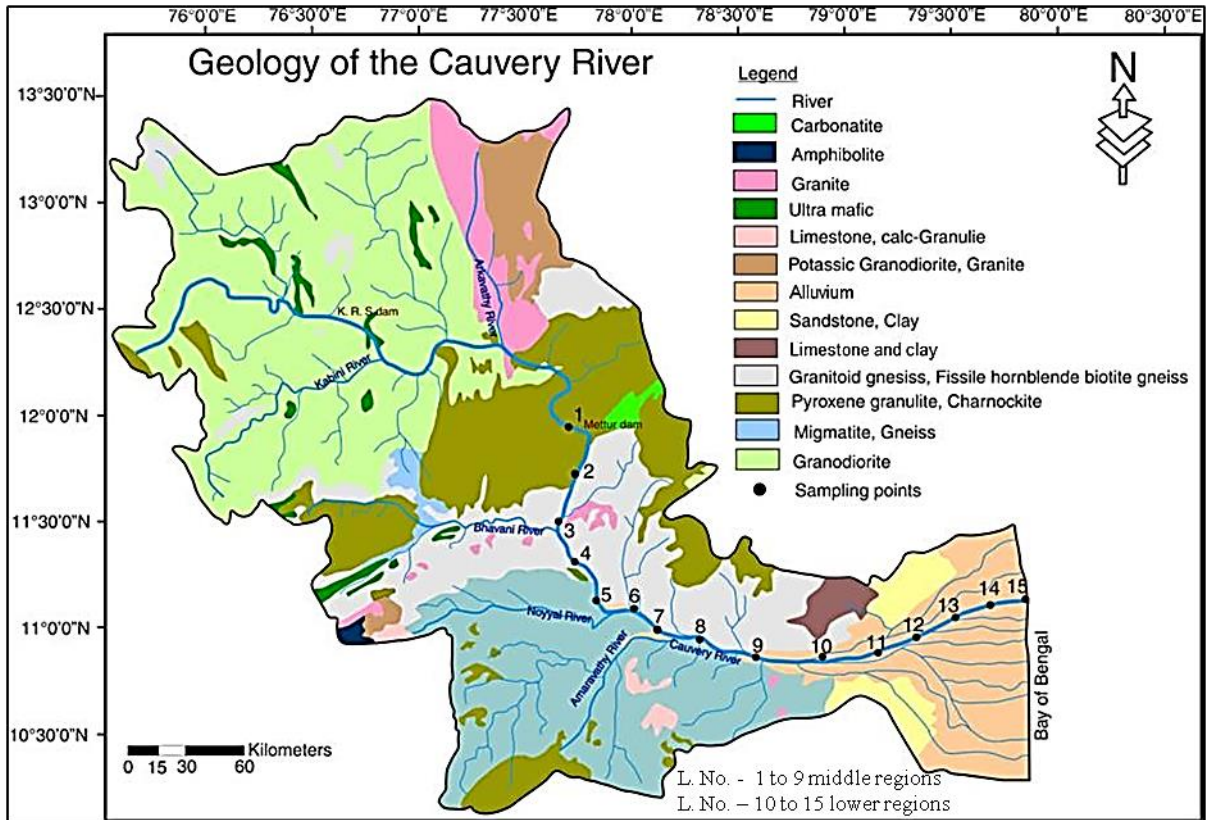


Fig. 1 Cauvery River Basin with sediment sample locations (1-15)

Table. 2 Distribution of major oxides in the sediments of SW monsoon

Loc. Nos.	SiO ₂	TiO ₂	Al ₂ O ₃	MnO	Fe ₂ O ₃	CaO	MgO	Na ₂ O	K ₂ O	P ₂ O ₅	CIA	PIA
1	67.68	1.04	15.14	0.08	4.52	3.75	1.43	3.6	2.2	0.16	61.32	63.78
2	65.51	0.94	14.43	0.08	4.39	4.72	2.13	3.18	3.63	0.23	55.59	57.75
3	67.93	1.48	12.61	0.09	6.41	4.14	2.14	3.01	1.43	0.21	59.51	60.99
4	66.32	0.79	14.64	0.07	4.8	4.67	2.31	3.43	2.15	0.26	58.82	60.66
5	83.35	0.28	7.33	0.03	2.22	1.96	0.87	2.04	1.56	0.07	56.87	59.06
6	84.47	0.22	7.04	0.04	1.9	1.82	0.7	1.98	1.57	0.07	56.73	59.01
7	76.47	0.56	10.2	0.06	3.31	2.81	1.45	2.77	1.92	0.11	57.63	59.74
8	81.49	0.41	8.27	0.04	2.28	2.11	0.89	2.23	1.88	0.12	57.07	59.55
9	81.58	0.21	8.75	0.04	1.71	2.04	0.7	2.44	2.2	0.07	56.71	59.38
10	77.24	1.47	8.38	0.07	4.7	2.34	1.09	2.31	1.86	0.1	56.28	58.37
11	85.1	0.22	6.88	0.03	1.62	1.52	0.54	1.89	1.89	0.06	56.49	59.4
12	78.84	0.39	9.87	0.05	2.53	2.44	0.94	2.5	2.18	0.08	58.09	60.89
13	75.31	0.67	11.97	0.05	3.08	2.76	1.06	2.59	2.11	0.14	61.61	64.83
14	65.57	3.08	10.78	0.17	8.49	4.43	2.66	2.46	1.49	0.23	56.26	57.42
15	80.37	1.69	6.71	0.09	4.82	1.84	0.97	1.6	1.63	0.08	56.96	59.62

Major and trace element concentration of NE monsoon sediments

The concentration of major and trace elements in the NE monsoon sediments is presented in Tables 4 & 5. The SiO₂ concentration varies from 60.87% to 84.65% in the studied sediments. The other dominant major oxides include Al₂O₃ (8.3% to 15.63%), Fe₂O₃ (1.78% to 7.69%) and CaO (1.27 to 6.42%) representing the variation in the degree of weathering of the source rocks. The MgO is relatively uniform (0.44% to 3.03%), the lesser concentration of Ca and Mg signify

higher mobility of elements during chemical weathering. Similarly, the concentration of TiO₂ (0.25% to 2.38%), K₂O (0.3% to 2.18 %), and MnO (0.02% to 0.15%) content is relatively uniform. The CIA of NE monsoon sediments ranges from 54.71% to 72.59% (average of 64.17%) which indicates weak to intermediate weathering intensity, whereas the PIA varies from 54.69% to 73.5% with an average 66.94%. The relative abundance of major oxides is SiO₂>Al₂O₃>Fe₂O₃>CaO>MgO>Na₂ O>K₂O>TiO₂>MnO>P₂O₅ (Fig. 3).

Table 3. Distribution of trace elements in the sediments of SW monsoon

Loc. No.	V	Cr	Co	Ni	Cu	Zn	Ga	Rb	Sr	Zr	Nb	Cs	Ba
	Concentration (ppm)												
1	54.79	94.19	10.06	33.54	42.99	95.37	12.24	31.91	338.16	66.46	7.38	0.26	669.28
2	42.84	65.26	10.71	38.17	54.58	125.25	11.01	34.52	281.46	53.73	2.75	0.37	630.53
3	50.81	67.28	7.87	28.02	47.46	117.04	7.61	28.13	190.01	77.59	2.37	0.28	511.93
5	39.06	62.26	7.82	32.46	55.05	92.04	8.61	29.15	234.20	57.28	2.94	0.28	560.60
7	39.88	72.19	8.58	28.44	39.61	90.30	8.16	25.63	220.53	70.74	2.44	0.21	531.67
14	116.95	76.66	15.66	36.31	48.13	112.80	15.00	22.99	603.16	146.20	5.26	0.28	1269.74
15	471.20	258.28	27.49	51.54	46.80	162.72	17.02	5.09	238.32	87.35	12.23	0.17	236.84

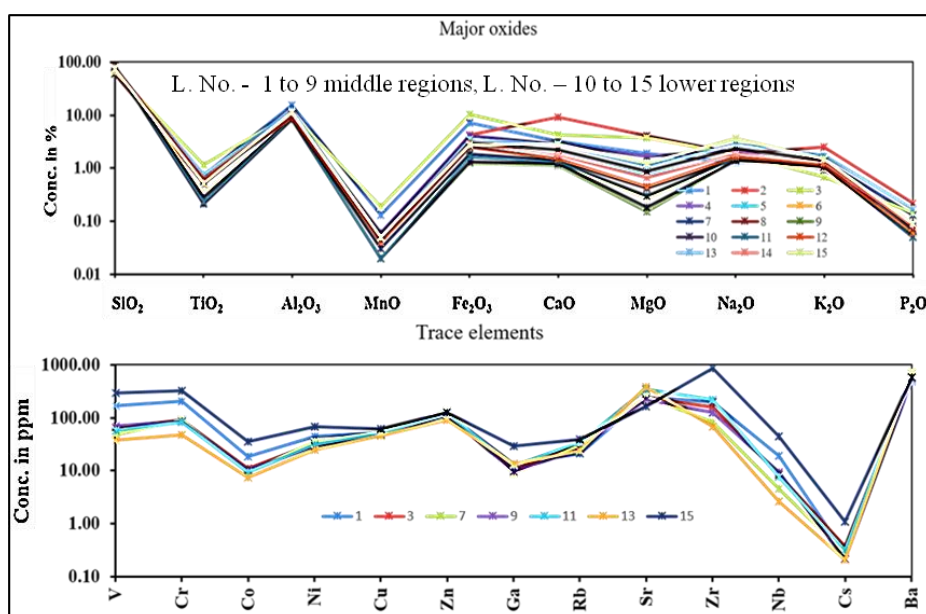


Fig. 2 Distribution of major oxides and trace elements in sediments of SW monsoon

The Ba is the principal element in the Cauvery River sediments whose concentration varies from 459.45 ppm to 856.95ppm. This variation is influenced by the K-feldspar (Neme, 1975). The other trace elements are Zn (74.81ppm-155.58ppm), V(25.25ppm-121.61ppm),Cr (33.72ppm-153.36ppm), Co (5.71ppm-16.06ppm), Ni (26.01ppm-38.18ppm), Cu (41.88 ppm-55.12ppm), Ga (6.78 ppm-14.22ppm), Rb (24.08 ppm-31.67ppm), Sr (197.51 ppm-376.13ppm), Zr (36.80 ppm-194.03ppm), Nb (1.74 ppm-11.98ppm) and Cs (0.18 ppm-0.32ppm) (Fig.3). The variation of Zn concentration 155.58ppm in the sediments at Poombugar (L-15) is attributed for the river water, and sea water and local fishing harbor interface.

The distribution of major oxides in the post-monsoon sediments is presented in Tables 6 & 7. The SiO₂ (58.09% to 85.35%) concentration is higher as

compared to the other oxides. The Al₂O₃ (8.28% to 15.63%), Fe₂O₃ (1.22% to 10.32%), and CaO (1.22% to 9.02%) are relatively uniform. The K₂O (0.68%-2.52 wt. %), MgO (0.26%- 4.04 wt. %), Na₂O (1.4-3.57 wt. %), TiO₂ (0.21-1.16 wt. %), P₂O₅ (0.05-0.22 wt. %) and MnO (0.02-0.19 wt. %) are of low concentration in these sediments. The relative abundance of major oxides is in the order of SiO₂>Al₂O₃>Fe₂O₃>CaO>Na₂O >K₂O>MgO> TiO₂> P₂O₅>MnO (Fig. 4). The concentration of trace elements in the post-monsoon sediments reflects the directive pathway to understand the provenance and its environments (Table. 7). The trace elements Co, Sc, and Cr having low concentrations specify the felsic source (Bhuiyan et al., 2011). The trace element concentrations tend to decrease towards the downstream due to the variation of sorting of sediments.

Table 4 Distribution of major oxides in the NE monsoon sediments

Loc. Nos.	SiO ₂	TiO ₂	Al ₂ O ₃	MnO	Fe ₂ O ₃	CaO	MgO	Na ₂ O	K ₂ O	P ₂ O ₅	CIA	PIA
	Concentration in %											
1	75.13	0.89	11.2	0.08	6.08	2.48	1.4	1.45	0.3	0.07	72.59	73.5
2	62.44	0.81	13.13	0.07	4.36	5.99	2.79	2.7	2.18	0.27	54.71	55.75
3	60.87	1.08	11.86	0.13	7.41	6.42	3.03	2.32	1.31	0.19	54.13	54.69
4	74.32	0.5	10.65	0.07	4.45	3.15	1.76	2.4	1.13	0.11	61.45	63.17
5	82.29	0.42	8.72	0.04	2.77	1.56	0.68	1.6	1.15	0.06	66.92	70.55
6	83.7	0.23	8.54	0.02	1.92	1.39	0.56	1.57	1.15	0.06	67.51	71.4
7	82.65	0.25	9.02	0.03	2.18	1.62	0.69	1.79	1.21	0.05	66.13	69.61
8	84.65	0.25	8.45	0.02	1.78	1.27	0.44	1.49	1.25	0.05	67.82	72.29
9	83.98	0.34	8.22	0.03	2.15	1.27	0.48	1.38	1.22	0.05	67.99	72.54
10	70.03	0.77	12.98	0.06	4.29	3.08	1.38	2.78	1.8	0.13	62.89	65.61
11	78.64	0.72	10.13	0.05	3.28	2.05	0.83	2.17	1.46	0.07	64.07	67.26
12	71.31	0.77	13.21	0.06	3.74	3.05	1.22	3.21	1.9	0.13	61.82	64.37
13	71.82	0.54	13	0.06	3.81	2.47	1.13	2.36	1.71	0.14	66.53	70.04
14	67.1	0.7	14.8	0.09	4.96	2.82	1.51	2.48	1.83	0.12	67.49	70.99
15	69.84	2.38	10.25	0.15	7.69	3.42	2.13	2.05	1.21	0.16	60.54	62.3

Table 5. Distribution of trace elements in NE monsoon sediments

Loc. Nos.	V	Cr	Co	Ni	Cu	Zn	Ga	Rb	Sr	Zr	Nb	Cs	Ba
	Concentration in ppm												
1	71.56	113.29	11.30	36.50	55.12	81.41	13.00	30.54	344.05	136.18	11.00	0.28	662.34
3	82.39	105.09	11.78	32.36	43.00	79.25	12.74	31.67	283.26	194.03	11.98	0.32	636.52
5	42.04	71.92	7.71	26.89	42.28	74.81	9.31	30.12	259.91	64.00	3.83	0.24	606.21
7	25.25	33.72	5.86	26.01	45.60	87.33	6.78	28.80	197.51	45.12	1.74	0.20	459.45
9	121.61	153.36	16.06	38.18	42.47	114.01	14.22	37.13	310.84	127.76	11.88	0.30	611.64
11	70.89	96.33	10.78	30.96	41.88	82.59	9.93	24.08	264.63	93.95	6.84	0.19	573.36
15	26.86	36.68	5.71	23.30	45.14	155.58	11.80	29.06	376.13	36.80	2.21	0.18	856.95

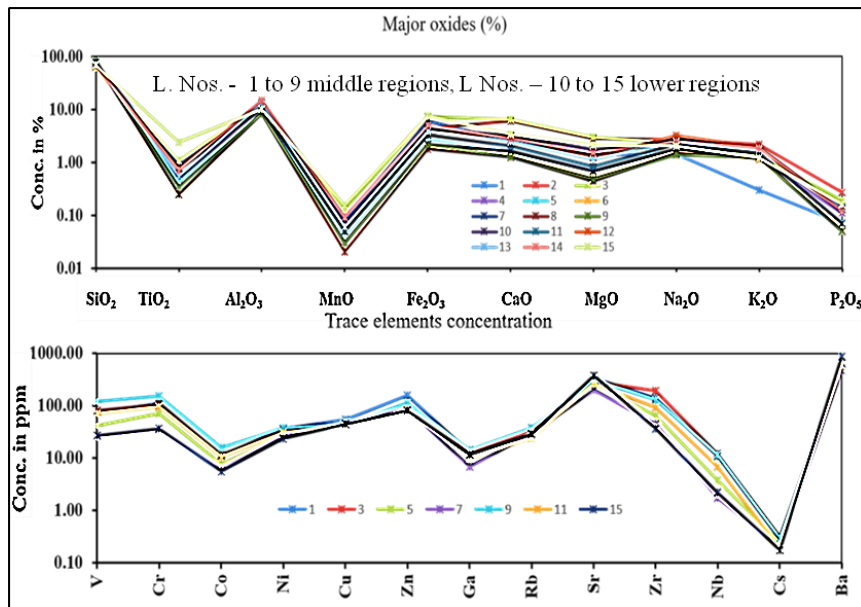


Fig. 3. Distribution of major oxides in NE monsoon sediments

Major and trace elements concentration of Post-monsoon sediments

The sample (L-15) at Poombugar shows higher concentration of trace elements linking to the influence of Bay of Bengal. Concentration of Ba ranges from 477.61ppm to 731.39ppm pointing towards the presence of K-feldspar, similarly, the concentration of Zn (90.43 ppm to 140.05ppm) is representing intermixing of river and sea waters and local fishing harbor interface. The Sr (165.32 ppm to

374.85ppm) variation is due to the weathering of plagioclase feldspar. The other trace element concentration in the sediments are V (37.15 ppm - 297.88ppm), Cr (47.09 ppm -328.22ppm), Co (7.31 ppm -35.20ppm), Ni (24.79 ppm -66.76ppm), Cu (45.85 ppm -61.94ppm), Ga (8.82-29.20ppm), Rb (20.82 ppm-39.12ppm), Zr (66.73 ppm-847.75ppm), Nb (2.58 ppm -43.83ppm) and Cs (0.20 ppm-1.09ppm) (Fig. 4).

Table 6. Distribution of major oxides in Post-monsoon sediments

Loc. Nos.	SiO ₂	TiO ₂	Al ₂ O ₃	MnO	Fe ₂ O ₃	CaO	MgO	Na ₂ O	K ₂ O	P ₂ O ₅	CIA	PIA
Concentration in %												
1	58.09	0.73	15.63	0.13	7.04	3.2	1.9	1.26	1.4	0.13	72.73	76.14
2	61.53	0.51	10.75	0.05	4.17	9.02	4.04	1.88	2.52	0.22	44.48	43.02
3	66.19	1.16	10.6	0.19	10.32	4.24	3.71	1.82	0.68	0.14	61.13	62.08
4	76.55	0.53	10.23	0.06	4.14	2.81	1.69	2.22	0.94	0.09	63.15	64.87
5	81.79	0.34	9.1	0.04	2.59	1.79	0.76	1.75	0.98	0.06	66.81	69.64
6	84.43	0.34	8.28	0.02	1.85	1.22	0.26	1.4	1	0.05	69.58	73.54
7	84.33	0.28	8.5	0.03	1.85	1.38	0.42	1.49	1.05	0.05	68.44	72.19
8	78.39	0.58	10.32	0.04	3.04	2.22	0.89	2.37	1.41	0.07	63.24	66
9	84.62	0.21	8.45	0.02	1.22	1.13	0.15	1.45	1.19	0.05	69.15	73.78
10	85.35	0.21	8.3	0.02	1.31	1.23	0.18	1.4	1.15	0.05	68.71	73.11
11	84.7	0.23	8.49	0.02	1.61	1.31	0.3	1.53	1.14	0.05	68.08	72.13
12	82.27	0.59	8.75	0.04	2.49	1.48	0.45	1.63	1.13	0.06	67.36	71.02
13	72.78	0.75	12.28	0.05	3.56	2.87	1.1	2.84	1.71	0.17	62.34	64.93
14	78.46	0.62	10.22	0.05	2.96	1.76	0.66	1.83	1.25	0.08	67.86	71.42
15	73.73	0.52	11.22	0.05	2.78	2.8	1.23	3.57	1.48	0.09	58.84	60.46

Table. 7 Distribution of trace elements in post-monsoon sediments

Loc. Nos.	V	Cr	Co	Ni	Cu	Zn	Ga	Rb	Sr	Zr	Nb	Cs	Ba
Concentration in ppm													
1	169.0	202.1	18.2	43.9	52.3	123.1	13.2	20.8	244.9	195.8	9.21	0.2	477.6
3	66.28	90.38	10.8	33.0	52.5	111.3	10.4	30.9	242.2	157.0	8.50	0.3	556.6
7	46.65	89.96	9.43	35.0	52.1	127.0	8.82	29.8	246.7	81.66	4.57	0.2	611.6
9	70.60	84.21	10.4	28.9	46.6	110.8	9.50	25.2	220.1	125.9	9.33	0.2	519.8
11	58.44	81.41	9.30	31.2	50.2	118.0	12.5	33.6	341.5	218.4	7.61	0.3	714.3
13	37.15	47.09	7.31	24.7	45.5	90.43	13.1	24.3	374.8	66.73	2.58	0.2	731.3
15	297.8	328.2	35.2	66.7	61.9	140.0	29.2	39.1	165.3	847.7	43.8	1.0	581.9

Mineral Composition

The major and trace element concentration in sediments reflects the mineralogy of Cauvery River sediments. The average concentration of SiO₂ is 75.82% (SW monsoon), 74.58% (NE monsoon), and 76.88% (Post-monsoon). The Al measures 10.2%, 10.9% and 10.1% for SW, NE and Post-monsoon samples with the average concentration of alkalis;

CaO is 2.89% (SW monsoon), 2.80% (NE monsoon) and 2.56% (Post-monsoon), followed by Fe₂O₃ average concentration is 3.79% (SW monsoon), 4.06% (NE monsoon) and 3.39% (Post-monsoon). Comparatively, the higher concentration of Fe₂O₃ (Avg.3.9%), denotes that the source rocks were involved in oxidation, leaching, and hydration processes during weathering (Mikkil and Henderson, 1983).

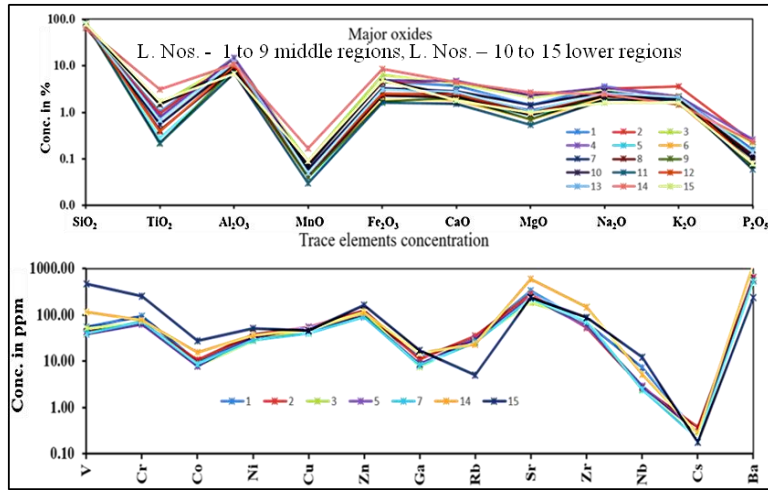


Fig. 4 Distribution of major oxides in Post-monsoon

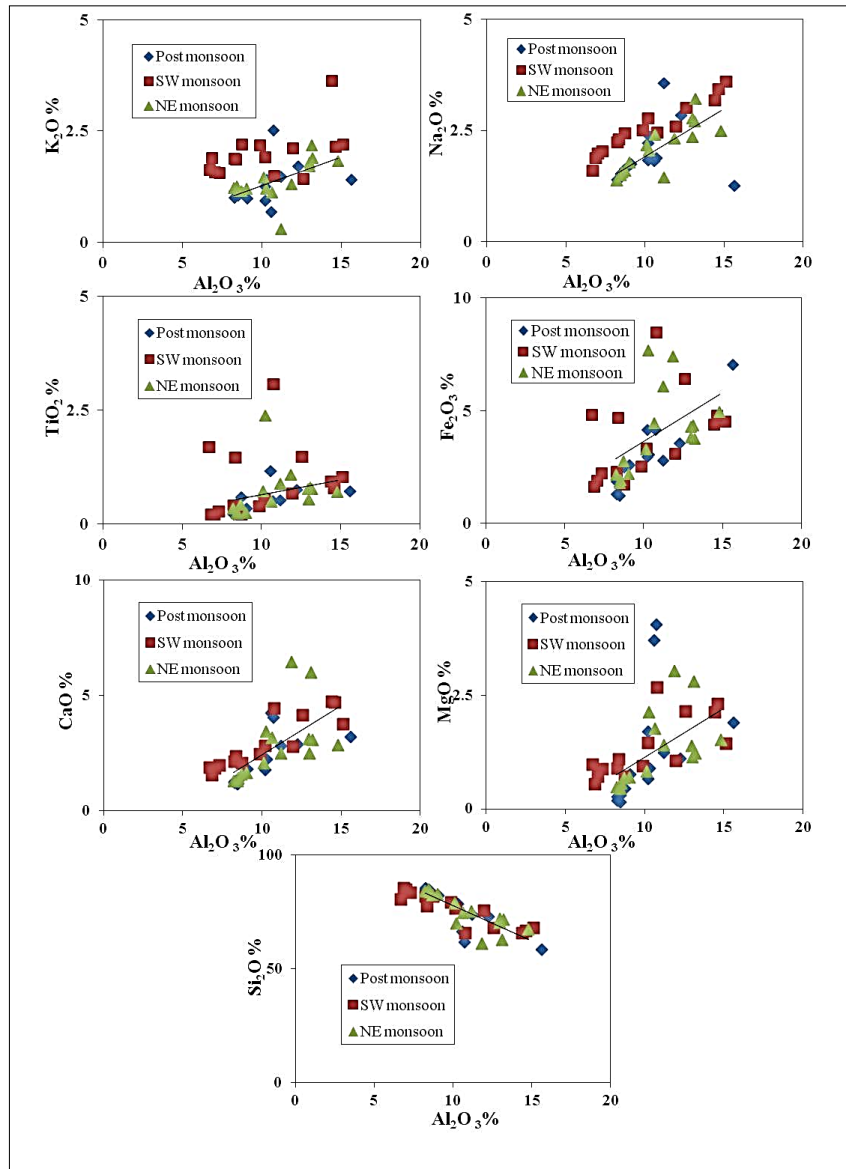


Fig. 5 Al₂O₃ v/s Major oxides

The relationship between $\text{Al}_2\text{O}_3\%$ and major oxides supports the occurrence of clay minerals in the sediments. The $\text{Al}_2\text{O}_3\%$ is positively correlated with Na_2O , K_2O , TiO_2 , Fe_2O_3 and MgO , except SiO_2 . These relationships between the oxides characterize the sediments encompass clay minerals (Fig. 5). The negative correlation between $\text{Al}_2\text{O}_3\%$ with $\text{SiO}_2\%$ reflects that the sediments are higher in quartz (Adel

et. al., 2011). The positive correlation between K_2O (%) and Rb (ppm) in the sediments of all the seasons (Fig. 6), construes to the occurrence of illite mineral in the Cauvery River sediments (Cox and Lowe, 1995). The bivariate diagram of Al_2O_3 vs. TiO_2 deduced that the sediments are derived from granite and granodiorite rocks (Fig. 8 & 9).

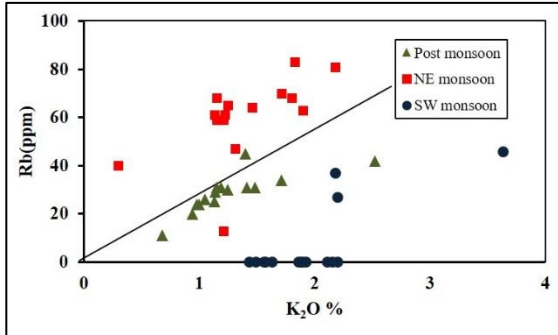


Fig. 6. Bivariate plots of Rb (ppm) vs. $\text{K}_2\text{O}\%$.

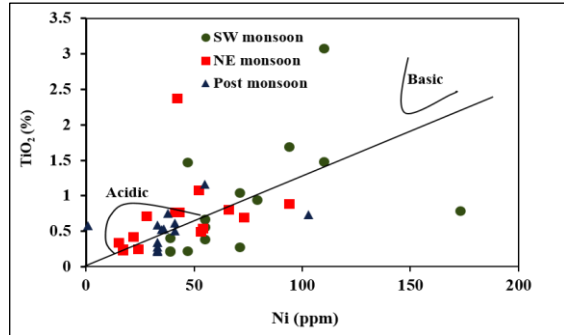


Fig.7. Classification of acidic and basic sources; Ni (ppm) vs. TiO_2 (%)

Sediment Geochemistry: implication to provenance

The relationship between TiO_2 vs. Ni signifies that the Cauvery River sediments are

derived from the acidic rocks (Floyd et al., 1989) (Figure 4.9). Further, the bivariate variation between K_2O vs. Rb entails acid-intermediate composition of the source rocks (Fig.7) (Bhuiyan et al., 2011).

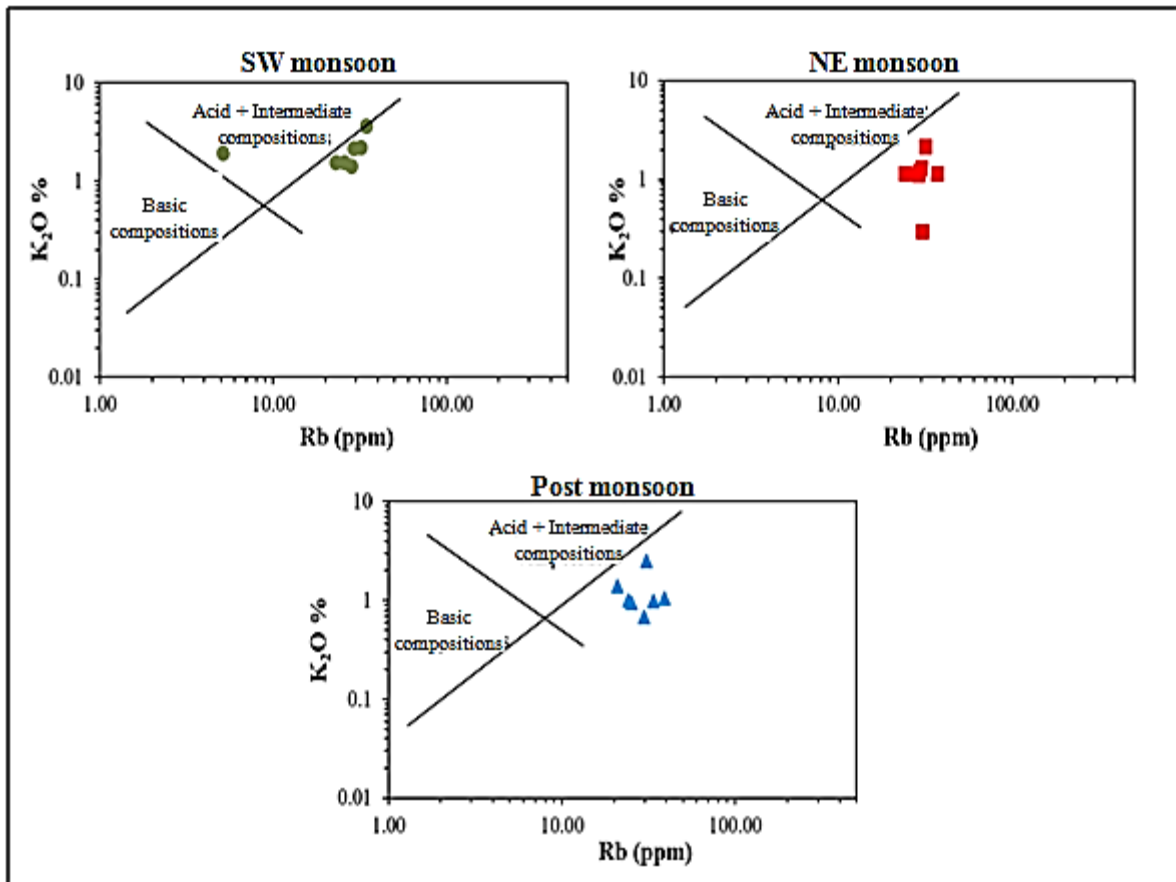


Fig. 8 Plot of K_2O vs. Rb in Cauvery River sediments

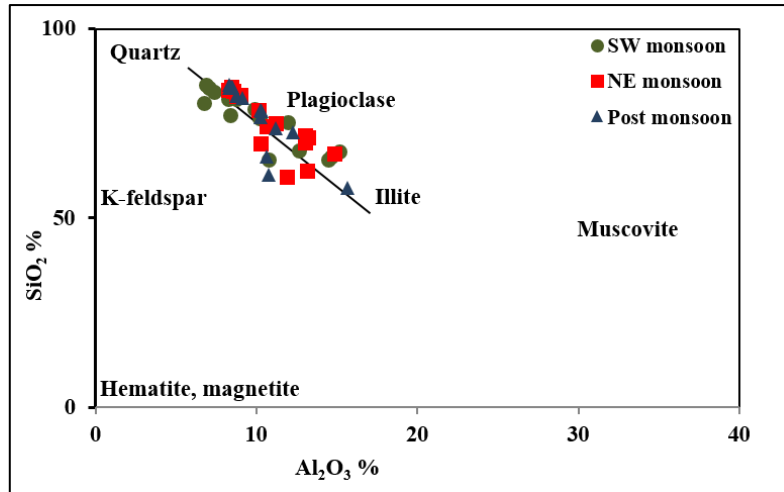


Fig. 9 Provenance of Cauvery River sediments (Floyd et al., 1989).

Source rock Weathering

The degree of weathering is controlled by the mineral composition of the source rocks, climatic conditions, and duration of weathering (Wronkiewicz and Condie, 1989). During the weathering, Ca, K, and Na was impasse from the source rocks, and tracing these elements in the sediments is a sensitive index of the intensity of weathering (Nesbit et al., 1997). The

bivariate plots of SiO_2 vs. Al_2O_3 have been useful in discriminating the weathering of rocks and sediments. The Cauvery River sediments of SW, NE and Post-monsoon seasons follow the trend from quartz, plagioclase, K-feldspar to illite mineral (Fig. 10), which demonstrates that the sediments were weathered from quartz, feldspar, illite and other minerals in the rocks (Cullers and Podkovyrov, 2000).

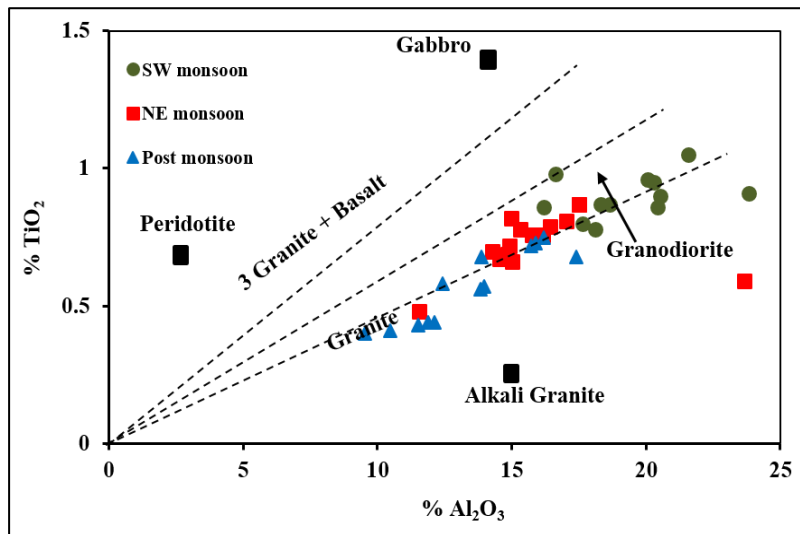


Fig. 10. Weathering trend: Al_2O_3 v/s. SiO_2 in Cauvery River sediments

The weathering of Cauvery River sediments follows the trend towards the illite mineral formation (Fig. 10). Further, the ternary plot displays the degree of weathering quantified by chemical index alteration (CIA) (Nesbitt & Young 1982) by using alumina and alkali minerals, which reflect the change in the proportions of feldspar and clay minerals during the weathering. The CIA is calculated by the following equation:

$$\text{CIA} = (\text{Al}_2\text{O}_3 / (\text{Al}_2\text{O}_3 + \text{CaO} + \text{Na}_2\text{O} + \text{K}_2\text{O})) * 100$$

The CIA is used for evaluation of chemical weathering within the specific drainage basin

(McLennan, 1993). The results of the Cauvery River sediment CIA is 55.58%-61.32% (SW monsoon), 60.54%-72.58% (NE monsoon) and 44.47%-72.73% (post-monsoon) indicate weak to intermediate weathering intensity (Fig.11). The CIA results of the sediments of different seasons are attributed to the chemical weathering controlled by the monsoon. The average CIA values of 57.73% (SW), 64.79% (NE) and 64.17% (post-monsoon) represent the rapid weathering intensity during the NE monsoon and post-monsoon (McLennan, 1993).

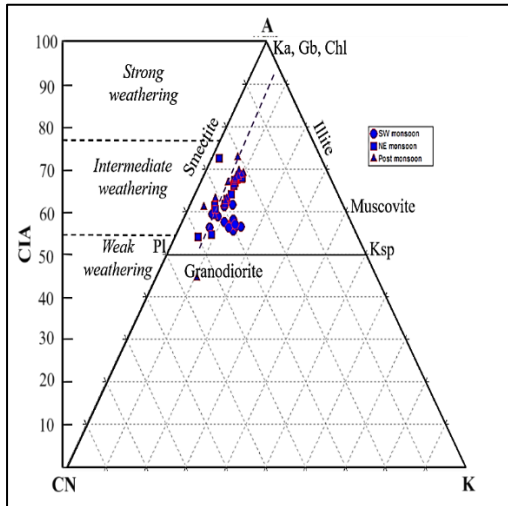


Fig. 11 A-CN-K relationship and weathering trend

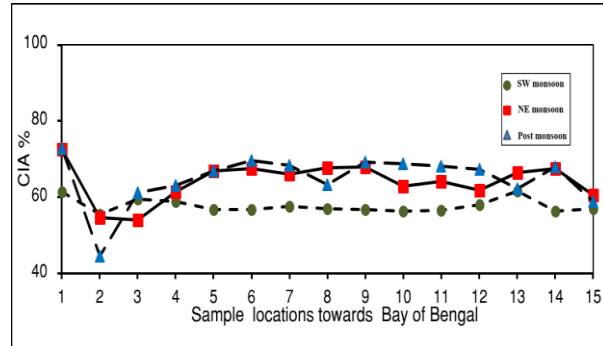


Fig. 12 Comparisons of CIA of Cauvery River sediments.

For understanding the controlling factor of weathering processes on rocks and sediments, the CIA values of sediments are spatially compared among the SW, NE, and post-monsoon samples (Fig. 12). The CIA of NE monsoon is rather higher (64.79%) than the other two seasons. The NE monsoon receives the advanced rainfall than SW and post-monsoon which suggests the weathering of rocks along the Cauvery River is controlled by the expanse of precipitation.

The average CIA value of World Rivers is 72.1%. The CIA values of African rivers are 83.4% (higher than the other continents), 71.7% for Asian rivers (closer to the average World Rivers) and 66.0% for North American (McLennan, 1993; Savenko, 2006; Viers et al., 2008; Chao li & Shouye yang, 2010). The average CIA value of Cauvery River is (60.95%) which is below the world average CIA of river sediments and very close to the Indus River sediments (Table 8, Fig. 13).

Table. 8 The average CIA values of global rivers sediment

World Rivers	Al ₂ O ₃ %	Na ₂ O%	CaO%	K ₂ O%	CIA%
Mississippi	15.49	0.75	1.47	1.92	77.2
Columbia	16.9	2.9	3.3	2.9	57.1
Amazon	14.6	1.1	1.1	2.2	70.9
Parana	16.76	1.21	1.04	2.9	70.4
Danube	12.1	2.38	6.39	2.51	53.4
Seine	11.58	0.26	13.18	1.47	82.5
Congo	25.1	0.32	1.34	1.64	89.9
Nile	18.8	1.0	5.68	2.32	76.4
Kala	55.65	13.75	25.76	13.38	48.2
Irtys	11.6	0.49	1.8	1.51	78.1
Ganges	16.0	1.58	4.07	2.77	66.7
Indus	17.63	2.04	2.37	4.07	61.3
Brahmaputra	19.08	1.48	1.06	3.31	70.5
Cauvery	10.4	2.13	2.75	1.55	60.95

Conclusions

The high concentration of Si, Al, and K in the sediments infers that the sediments are derived from the source rock by the chemical weathering processes. The high concentration in Fe₂O₃ signifies that the sediments are affected by oxidation, leaching and hydration processes during their weathering. The negative correlation between the Al₂O₃% and SiO₂%

of the sediments is attributed to the Cauvery River sediments enrichment with quartz. The relationship between Al₂O₃ vs. TiO₂ infers that the provenance of Cauvery River sediments is represented by granite and granodiorite rocks. The trend of weathering of sediments is eminent by the occurrence of illite clay minerals.

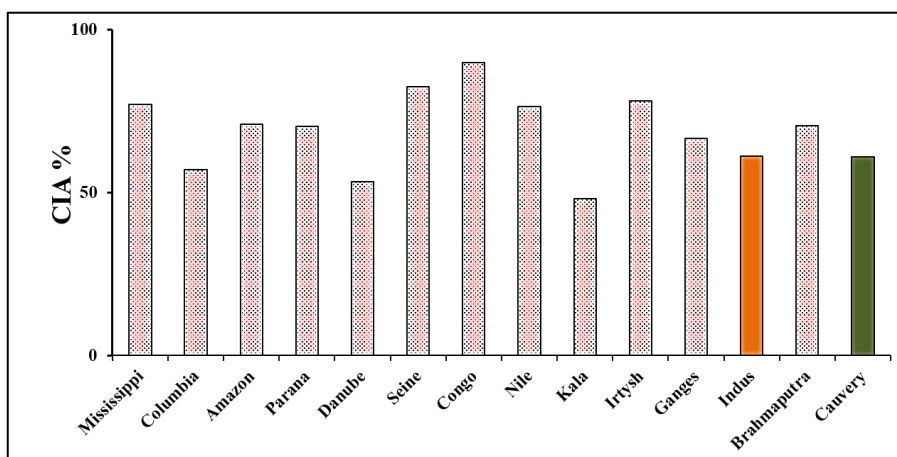


Fig.13. CIA values of Cauvery River sediments with global rivers

The CIA of Cauvery River sediments of SW (57.73%), NE (64.17%) and post-monsoon (64.79%) indicates weak to intermediate weathering intensity. These low CIA values are attributed to the impact of weathering on the Cauvery River rocks controlled by precipitation. The average CIA value of Cauvery River sediments (60.95%) is below the average CIA values of world Rivers (72.1%) and it's near to the Indus River (61.3%). The concentration of Ba in the Cauvery River sediments varies from 459.45 ppm to 856.95ppm reflecting the presence of K-feldspar in the source rocks. The decreasing trend of trace elements in the downstream is influenced by the variation of sorting, whereas the sediments at Poombugar (L-15) show higher concentration influenced by the Bay of Bengal.

Acknowledgement

Authors are thankful to National Remote Sensing Centre, Hyderabad, India for the award of the research project on Cauvery River basin studies.

References

- Adel I.M, Akarish and Amr El-Gohary (2011) Provenance and source area weathering-derived from the geochemistry of Pre-Cenomanian sandstones, East Sinai, Egypt. *J. of Appl. Science*, v.11 (7), pp.3070-3088.
- Bhuiyan., M.A.H, Rahman M.J.J, Dampare SB, Suzuki S (2011) Provenance, tectonics and source weathering of modern fluvial sediments of the Brahmaputra-Jamuna River, Bangladesh: inference from geochemistry, *J Geochem Explor*, v.111, pp.113-137.
- Chao Li and Shouye Yang (2010) Is chemical index of alteration (CIA) a Reliable proxy for chemical weathering in global drainage basins. *Amer. J of Science*, v.310, pp.111-127.
- Cox R, and Lowe D.R. (1995) Compositional evolution of coarse clastic sediments in the southwestern United States from 1.8 to 2.3GA and implications for relationships between the development of crustal blocks and their sedimentary cover. *Jour. Sed. Res A*, v.65, pp.477-494.

- Cullers, R.L, and Podkovyrov, V.M. (2000) Geochemistry of the Mesoproterozoic Lakhanda shales in south-eastern Yakutia, Russia: implications for mineralogical and provenance control, and recycling. *Precambrian. Res*, v.104, pp.77-93.
- Floyd, P.A, Winchester, J.A, and Park, R.G. (1989) Geochemistry and tectonic setting of Lewisian clastic metasediments from the early Proterozoic Loch Maree Group of Gairloch. *Precambrian Research*, v.45, pp.203-214.
- Johnn, M.M, Balakrishnan, S, and Bhadra, B.K. (2005) Contrasting metamorphism across Cauvery Shear Zone, south India. *J. Earth Syst. Science*, v.114 (2), pp.1-16.
- Mahabaleshwar, B, Jayananda, M, Peucat, J.J, and Sadaksharswamy (1995) Archean high-grade gneiss complexes from Santur-Halgur, Sivasudram areas, Karnataka, South India: petrogenesis and crustal evolution. *J. Geol. Soc. India*, v.45, pp.33-49.
- McLennan, S.M. (1993) Weathering and global denudation. *J. Geol.*, v.101, pp.169-200.
- McLennan, S, M. Taylor, S.R., (1983) Geochemical evolution of the Archean shales from South Africa. I. The Swaziland and Pongola supergroups. *Precambrian Research*, v.22, pp.93-124.
- Mengying He, Hongbo Zheng, Peter D Clift, Ryuji Tada, Weihua Wu, and Chao Luo (2015) Geochemistry of fine-grained sediments in the Yangtze River and the implications for provenance and chemical weathering in East Asia. *Progress in Earth and Planetary Science*, v.2, pp.32.
- Mikkel S, and Henderson, J.B. (1983) Archean chemical weathering at three localities on the Canadian shield. *Precambrian Research.*, v.20, pp.189-224.
- Nemeo, D. (1975) Barium in K-Feldspar megacrystals from granitic and syenitic rocks of the Bohemian massif. *Tschermaks Min. Petrol. Mitt.*, v.22.
- Nesbitt, H.M, & Young, G.M. (1982) Early Proterozoic climates and plate motions inferred from major element chemistry of lutites. *Nature*, v.299, pp.715-717.
- Nesbitt, H.W, Young, G.M. (1996) Petrogenesis of sediments in the absence of chemical weathering: effects of abrasion and sorting on bulk composition and mineralogy. *Sedimentology*, v.43, pp.341-358.

- Prakash Narasimha, Schoichi Kobayashi K, Tetsuya Shoji, Munetake Sasaki, and Sethumadhav M.S. (2009) XRD, EPMA and FTIR studies on Garnet from Bettadabidu, Sargur area, Karnataka, India. *Journal of Applied Geochemistry*, v.11 (1), pp.1-11.
- Pramod Singh (2010) Geochemistry and provenance of stream sediments of the Ganga River and its major tributaries in the Himalayan region, India. *Chemical Geology*, v.269 (3-4), pp.220-236.
- Radhakrishna, B.P. (1992) Cauvery- it's geological past. *J. Geol. Society. India*, v. 40(1), pp.1-12.
- Rahman, M.J.J, & Suzuki, S. (2007) Geochemistry of sandstones from the Miocene Surma Group, Bengal Basin, Bangladesh: implications for provenance, tectonic setting and weathering. *Geochem, J.*, v.41, pp.415-428.
- Ramakrishna, M, and Swaminath, J (1981) Tectonics and Crustal evolution. *Geol. Surv. India, Mem.*, v.112, pp. 261-271.
- Savenko, V.S. (2006) Principal features of the chemical composition of suspended loads in World Rivers. *Doklady Earth Sciences*, v.407, pp.450-454.
- Schieber, J. (1992) A Combined petrographical-geochemical provenance study of the Newland Formation, Mid-Proterozoic of Montana. *Geol. Mag.*, v.129, pp. 223-237.
- Shilpa Vuba, Masood Ahmad S, & Nageswara Rao Anipindi (2015) Geochemical and mineralogical studies in recent clastic sediments from upper Godavari River in Peninsular India. *Journal of Geological Soc. of India*, v.86, pp.107-114.
- Valdiya, K.S. (1998) Late Quaternary movements and landscape rejuvenation in southern Karnataka and adjoining Tamil Nadu in southern Indian Shield. *J. Geol. Soc. India*, v.51, pp.139-166.
- Viers J, Dupre B and Gaillardet J. (2008) Chemical composition of suspended sediments in World Rivers: New insights from a new database. *Science of the Total Environment*, v.407, pp.853-868.
- Wronkiewicz, D.J, Condie, K.C. (1987) Geochemistry of Archean shales from the Witwaterstrand Supergroup, South Africa: source area weathering and provenance. *Geochimica et Cosmochimica Acta*, v.51, pp.2401-2416.
-

Gravity flows: Types, definitions, origins, identification markers, and problems

G. Shanmugam

Department of Earth and Environmental Sciences, The University of Texas at Arlington,
Arlington, TX 76019, USA
E-mail: shanshanmugam@aol.com

Abstract

This review covers 135 years of research on gravity flows since the first reporting of density plumes in the Lake Geneva, Switzerland by Forel (1885). Six basic types of gravity flows have been identified in subaerial and subaqueous environments. They are: (1) hyperpycnal flows, (2) turbidity currents, (3) debris flows, (4) liquefied/fluidized flows, (5) grain flows, and (6) thermohaline contour currents. The first five types are flows in which the density is caused by sediment in the flow, whereas in the sixth type, the density is caused by variations in temperature and salinity. Although all six types originate initially as downslope gravity flows, only the first five types are truly downslope processes, whereas the sixth type eventually becomes an alongslope process. (1) Hyperpycnal flows are triggered by river floods in which density of incoming river water is greater than the basin water. These flows are confined to proximity of the shoreline. They transport mud, and they do not transport sand into the deep sea. There are no sedimentological criteria yet to identify hyperpycnites in the ancient sedimentary record. (2) A turbidity current is a sediment-gravity flow with Newtonian rheology and turbulent state in which sediment is supported by flow turbulence and from which deposition occurs through suspension settling. Typical turbidity currents can function as truly turbulent suspensions only when their sediment concentration by volume is below 9% or $C < 9\%$. This requirement firmly excludes the existence of 'high-density turbidity currents'. Turbidites are recognized by their distinct normal grading in deep-water deposits. (3) A debris flow (c. 25-100%) is a sediment-gravity flow with plastic rheology and laminar state from which deposition occurs through freezing *en masse*. The terms debris flow and mass flow are used interchangeably. General characteristics of muddy and sandy debrites are floating clasts, planar clast fabric, inverse grading, etc. Most sandy deep-water deposits are sandy debrites and they comprise important petroleum reservoirs worldwide. (4) A liquefied/fluidized flow (>25%) is a sediment-gravity flow in which sediment is supported by upward-moving intergranular fluid. They are commonly triggered by seismicity. Water-escape structures, dish and pillar structures, and SSDS are common. (5) A grain flow (c. 50-100%) is a sediment-gravity flow in which grains are supported by dispersive pressure caused by grain collision. These flows are common on the slip face of aeolian dunes. Massive sand and inverse grading are potential identification markers. (6) Thermohaline contour currents originate in the Antarctic region due to shelf freezing and the related increase in the density of cold saline (i.e., thermohaline) water. Although they begin their journey as downslope gravity flows, they eventually flow alongslope as contour currents. Hybridites are deposits that result from intersection of downslope gravity flows and alongslope contour currents. Hybridites mimic the "Bouma Sequence" with traction structures (Tb and Tc). Facies models of hyperpycnites, turbidites, and contourites are obsolete. Of the six types of density flows, hyperpycnal flows and their deposits are the least understood.

Keywords: Debris flow, Gravity flow, Fluidized/Liquefied flow, Grain flow, Hyperpycnal flow, Thermohaline contour current, Turbidity current

Introduction

Gravity flows are the most consequential sedimentary phenomena in the geologic record. From a sedimentological perspective, density flows are ubiquitous in both subaerial and subaqueous environments. Importantly, gravity flows dominate in shelf, slope, and basin environments. They are caused not only by sediment density, but also by changes in temperature and salinity. Furthermore, density flows travel not only downslope, but also alongslope. Therefore, the key objectives of this article are (1) to identify and discuss basic types of density flows, (2) to provide a clear definition of each flow type, (3) to identify their origins or triggering mechanisms, (4) to suggest identification markers of their deposits, and (5)

to identify the remaining unresolved problems in aiding future research. I have attempted to accomplish these objectives by integrating:

- 1) theoretical considerations,
- 2) experimental verifications,
- 3) modern submarine observations,
- 4) modern subaerial observations,
- 5) ancient outcrop examples, and
- 6) modern and ancient subsurface (sediment core) examples.

I have selected the following six basic types of density flows for discussion in this review (Table 1). The density value cited for each example is to provide a relative sense, and they should not be considered typical of the example.

Table 1. Six types of gravity (density) flows and their characteristics.

Flow type	Flow attributes	Environment	Origins (Triggers)	Reliability of identification markers
1. Hyperpycnal flow	Density of river water > Density of basin water SSC (Suspended sediment concentration) (ρ): 0.025 g/cm ³ (Wright and Nittrouer, 1995)	Subaqueous only, near shoreline	River floods	Unreliable facies model because of absence of modern sediment core and experimental observations (Shanmugam, 2018a)
2. Turbidity current	Newtonian rheology Turbulent state C < 9% by volume (Bagnold, 1962) Flow density (ρ): 1.1 g/cm ³ (Kuenen, 1966) Deposition by settling	Subaqueous only, shelf, slope, and basin	Earthquake, slope instability, oversupply of sediment, volcanism, meteorite impact, tsunamis, cyclones	Reliable normal grading
3. Debris flow	Plastic rheology Laminar state C: 25-100% Flow density (ρ): 2 g/cm ³ (Hampton, 1972) En masse freezing	Subaerial and subaqueous	Earthquake, slope instability, oversupply of sediment, volcanism, meteorite impact, tsunamis, cyclones	Reliable markers because of modern examples and experimental observations (Shanmugam, 2000; Marr et al., 2001)
4. Liquefied/Fluidized flow	Upward moving fluid Flow density (ρ): 1.8 g/cm ³ (Breien et al., 2010)	Subaerial and Subaqueous	Earthquakes, volcanism, meteorite impacts, tsunamis, cyclones,	Reliable markers because of modern examples in earthquake-induced SSDS (Shanmugam, 2017)
5. Grain flow	Frictional strength Grain collision (Dispersive pressure) Flow (ρ): 2.1—2.3 g/cm ³ (Parsons et al., 2001)	Subaerial and subaqueous, aeolian dunes and submarine canyons	Climate, wind, steep gradients	Reliable markers because of modern examples in aeolian dunes and in submarine canyons

6. Thermohaline contour current (THCC)	Current reworking Antarctic Bottom Water (AABW) density (ρ): 0.03 g/cm ³ (Purkey et al., 2018) Bottom Water density in Ross Sea, Antarctica at 4,000 m water depth (ρ): 0.03 g/cm ³ (Henze, 2015, her Fig. 2.14)	Subaqueous only, shelf edge, slope, basin.	Shelf freezing (Temperature and salinity) in Antarctica. Note that THCC began as downslope gravity flows (Fig. 36), but became a contour current.	Reliable markers because of modern sediment cores (Hollister, 1967)
--	--	--	---	---

This review should be helpful from both an academic and an applied point of view. For example, identification markers of deposits of density flows are of practical value because sandy debrites and associated mass-transport deposits are important petroleum reservoirs in the North Sea (Shanmugam et al., 1995), Nigeria (Shanmugam, 2012), Bay of Bengal (Shanmugam et al., 2009), Gulf of Mexico, Russia and Australia (Meckel, 2010; Meckel et al. 2011) and China (Zou et al., 2012). Global economic significance of sandy contourites has been discussed by Viana (2008), Stow et al. (2011), and Shanmugam (2017c). In terms of regional importance, Mullins et al. (1980) discussed carbonate sandy contourites in the Straits of Florida, and Shanmugam et al. (1993) documented measured porosity and permeability values of petroleum-producing sandy contourites in the Ewing Bank area of the Gulf of Mexico.

Gravity flows

The term “gravity flow” is used here for a continuous, irreversible deformation of sediment-water mixture that occurs in response to applied shear stress, which is gravity in most cases (Pierson and Costa 1987, p. 2). In this article, density flows and gravity flows are considered to be one and the same, although density represents mass per unit volume and gravity represents a force. Gravity flows have been of great interest to sedimentologists and engineers for over 100 years, since the first discussion of theory of turbulence in fluid mechanics (Prandtl, 1925, 1926). Selected publications on this domain are of Kuenen (1951 and 1953), Bates (1953), Bagnold (1954 and 1962), Dott (1963), Sanders

(1965), Middleton (1965, 1966, 1967, 1970, 1993), Klein (1966 and 1975), Middleton and Bouma (1973), Hampton (1972), Middleton and Hampton (1973), Lowe (1976a, 1976b, 1982), Kneller (1995), Shanmugam 1996, 2000, 2002, 2006, 2012, 2015, 2018a, b, 2019a, b), Iverson (1997), Rebesco et al. (2008), and Zenk (2008).

Gravity-driven downslope processes

Because all six types begin their journey as downslope gravity flows, some basic principles are briefly discussed here on gravity-driven downslope processes.

Mass transport and turbidity currents

Dott (1963) proposed the most meaningful and practical classification of subaqueous mass-transport processes. In this scheme, subaqueous processes are broadly classified into (1) elastic, (2) elastic and plastic, (3) plastic, and (4) viscous fluid types based on mechanical behavior (Fig. 1). The elastic behavior represents rockfall; the elastic and plastic behavior comprises slide and slump; the plastic behavior represents debris flow; and the viscous fluid represents Newtonian turbidity current. The importance of Dott’s (1963) classification is that mass-transport processes do not include turbidity currents (Fig. 1C). In this article, although mass-transport processes are composed of three basic types: (1) slide, (2) slump, and (3) debris flow (Fig. 1), only debris flow is considered as a ‘flow’. The reason is that slides and slumps are coherent masses and they are not composed of sediment-water mixtures, a condition that is a prerequisite in defining a ‘flow’.

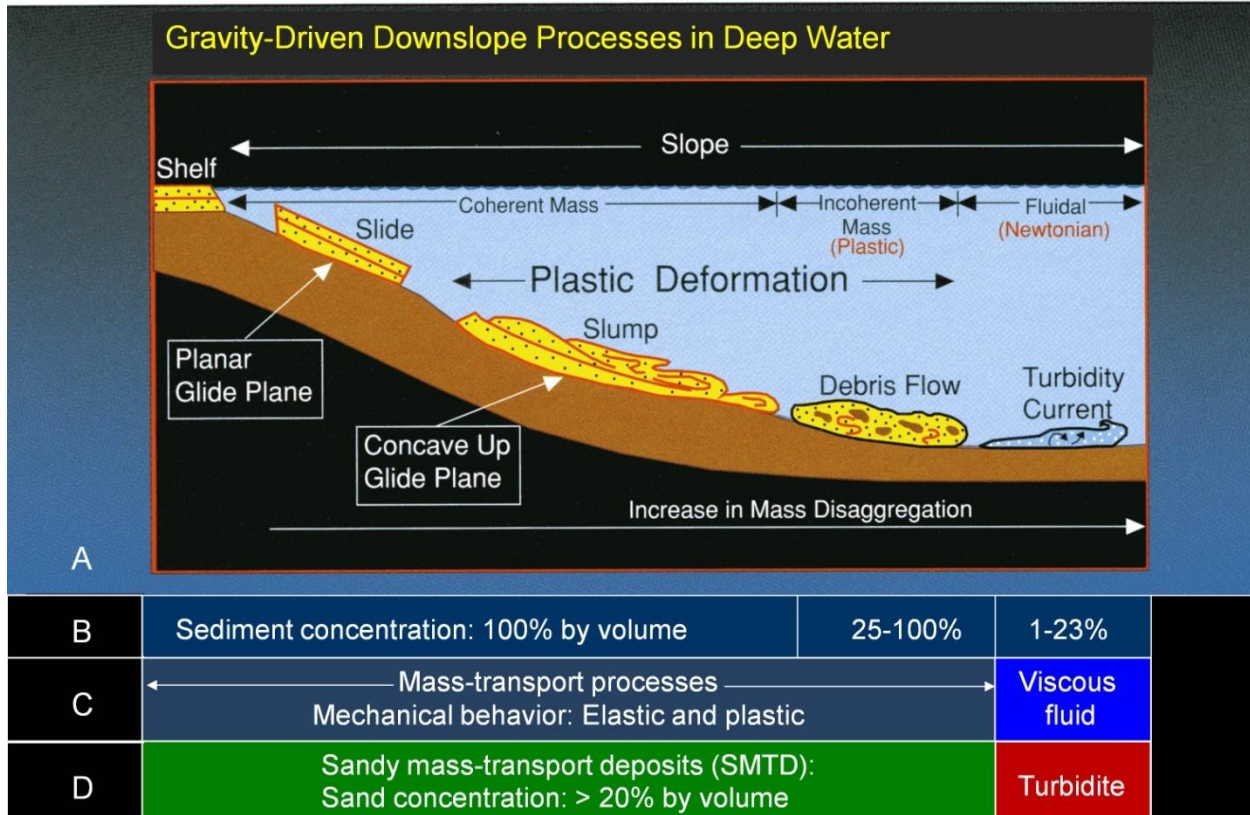


Fig. 1. (A) Schematic diagram showing four common types of gravity-driven downslope processes that transport sediment into deep-marine environments. A slide represents a coherent translational mass transport of a block or strata on a planar glide plane (shear surface) without internal deformation. A slide may be transformed into a slump, which represents a coherent rotational mass transport of a block or strata on a concave-up glide plane (shear surface) with internal deformation. Upon addition of fluid during downslope movement, slumped material may transform into a debris flow, which transports sediment as an incoherent body in which intergranular movements predominate over shear-surface movements. A debris flow behaves as a plastic laminar flow with strength. As fluid content increases in debris flow, the flow may evolve into Newtonian turbidity current. Not all turbidity currents, however, evolve from debris flows. Some turbidity currents may evolve directly from sediment failures. Turbidity currents can develop near the shelf edge, on the slope, or in distal basinal settings. (B) Sediment concentration (% by volume) in gravity-driven processes. Slides and slumps are composed entirely of sediment (100% by volume). Debris flows show a range of sediment concentration from 25% to 100% by volume. Note that turbidity currents are low in sediment concentration (1%–23% by volume), implying low-density flows. These values are based on published data (see Shanmugam, 2000, his Fig. 4). (C) Based on mechanical behavior of gravity-driven downslope processes, mass-transport processes include slide, slump, and debris flow, but not turbidity currents (Dott, 1963). (D) The prefix “sandy” is used for mass-transport deposits (SMTDs) that have grain (> 0.06 mm: sand and gravel) concentration value equal to or above 20% by volume. The 20% value is adopted from the original field classification of sedimentary rocks by Krynine (1948). (A) Reproduced from Shanmugam et al. (1994).

The underpinning principle of Dott’s (1963) classification is the separation of solid from fluid mode of transport based on sediment concentration. In the solid (elastic and plastic) mode of transport, high sediment concentration is the norm (25-100% by volume, Fig. 1B). Mass-transport mechanisms are characterized by solid blocks or aggregate of particles (mass). In contrast, individual particles are held in

suspension by fluid turbulence in turbidity currents (Dott, 1963; Sanders, 1965). Turbidity currents are characterized by low sediment concentration (Bagnold, 1962).

Mass transport can operate in both subaerial and subaqueous environments, but turbidity current can operate only in subaqueous environments. The advantage of this classification is that physical features preserved in a deposit directly represent the physics of

sediment movement that existed at the final moments of deposition. The link between the deposit and the physics of the depositional process can be established by practicing the principle of process sedimentology, which is detailed bed-by-bed description of sedimentary rocks and their process interpretation (Shanmugam, 2006).

Sediment-gravity flows

Middleton and Hampton (1973) distinguished sediment-gravity flows from fluid gravity flows. In a *fluid-gravity flow* (e.g., river currents and some deep-ocean currents), fluid is directly driven by gravity, whereas in a *sediment-gravity flow* the interstitial fluid is driven by the grains moving downslope under the influence of gravity. Furthermore, Middleton and Hampton classified sediment-gravity flows into four types based on sediment-support mechanisms (Fig. 2). They are: (1) *turbidity current* with turbulence; (2) *fluidized sediment flow* with upward moving intergranular flow; (3) *grain flow* with grain interaction (i.e., dispersive pressure); and (4) *debris flow* with matrix strength. Sandy debris flows occupy an intermediate region between debris flows and grain flows (Fig. 2).

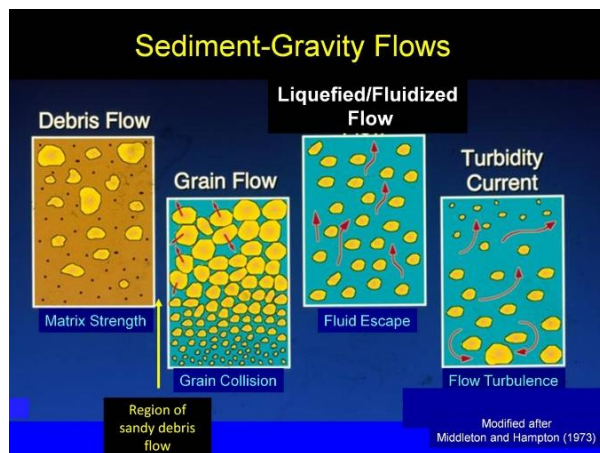


Fig. 2. Classification of sediment-gravity flows based on sediment-support mechanisms by Middleton and Hampton (1973). The position of sandy debris flow is shown for comparison.

Newtonian vs. plastic fluid rheology

In this article, the focus is on debris flows and turbidity currents because of their importance. These two processes are distinguished from one another on the basis of fluid rheology and flow state. The rheology of fluids can be expressed as a relationship between applied shear stress and rate of shear strain (Fig. 3). Newtonian fluids (i.e., fluids with no inherent strength), like water, will begin to deform the moment shear stress

is applied, and the deformation is linear. In contrast, some naturally occurring materials (i.e., fluids with strength) will not deform until their yield stress has been exceeded (Fig. 3); once their yield stress is exceeded, deformation is linear. Such materials (e.g., wet concrete) with strength are considered to be Bingham plastics (Fig. 3). For flows that exhibit plastic rheology, the term plastic flow is appropriate. Using rheology as the basis, deep-water sediment flows are divided into two broad groups, namely, (1) Newtonian flows that represent turbidity currents and (2) plastic flows that represent debris flows.

Turbulent vs. laminar flow state

In addition to fluid rheology, flow state is used in distinguishing laminar debris flows from turbulent turbidity currents. The difference between laminar and turbulent flows was demonstrated in 1883 by Osborne Reynolds, an Irish engineer, by injecting a thin stream of dye into the flow of water through a glass tube. At low rates of flow, the dye stream traveled in a straight

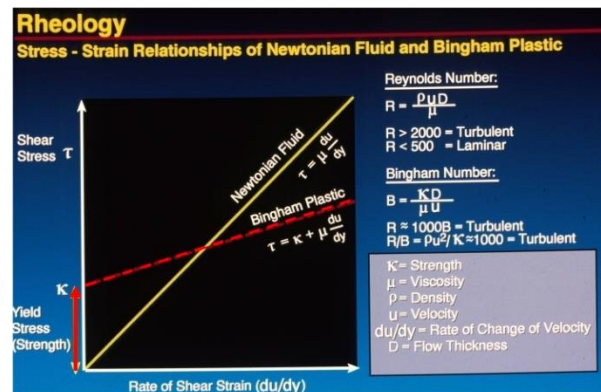


Fig. 3. Rheology (stress-strain relationships) of Newtonian fluids and Bingham plastics. Graph shows that the fundamental rheological difference between debris flows (Bingham plastics) and turbidity currents (Newtonian fluids) is that debris flows exhibit strength, whereas turbidity currents do not. Reynolds number is used for determining whether a flow is turbulent (turbidity current) or laminar (debris flow) in state. Compiled from several sources (Dott, 1963; Enos, 1977; Pierson and Costa, 1987; Phillips and Davies, 1991; Middleton and Wilcock, 1994). After Shanmugam (1997).

path. This regular motion of fluid in parallel layers, without macroscopic mixing across the layers, is called a laminar flow. At higher flow rates, the dye stream broke up into chaotic eddies. Such an irregular fluid motion, with macroscopic mixing across the layers, is called a turbulent flow. The change from laminar to turbulent flow occurs at a critical Reynolds number (the

ratio between inertia and viscous forces) of about 2000 (Fig. 4).

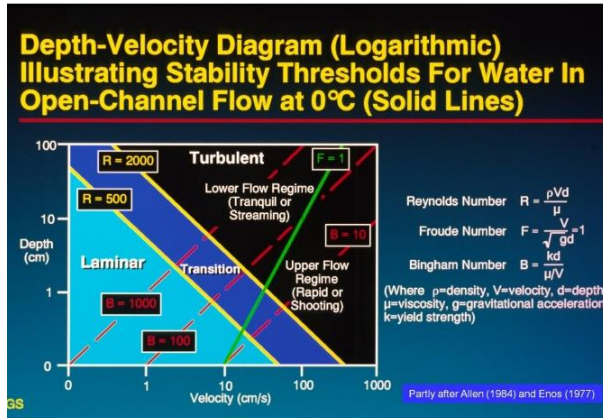


Fig. 4. Depth-velocity diagram showing laminar and turbulent fields of fluids. Partly after Allen (1984) and Enos (1977).

Sediment concentration

Sediment concentration is the most important property in controlling fluid rheology (Fig. 5). Classification of gravity-driven sediment flows into Newtonian and plastic types is based on fluid rheology. Turbidity currents are Newtonian flows, whereas all mass flows (muddy debris flows, sandy debris flows, and grain flows) are plastic flows. Turbidity currents occur only as subaqueous flows, whereas debris flows and grain flows can occur both as subaerial and as subaqueous flows. High-density turbidity currents are not meaningful in this rheological classification because their sediment concentration values represent both Newtonian and plastic flows (see Shanmugam, 1996).

In the following discussion, each density flow is evaluated with the above principles in mind.

Hyperpycnal flows

Definition

Forel (1885, 1892) first reported the phenomenon of density plumes in the Lake Geneva (Loc. Léman), Switzerland. In advocating a rational theory for delta formation, Bates (1953) suggested three types: (1) hypopycnal plume for floating river water that has lower density than basin water (Fig. 6a); (2) homopycnal plume for mixing river water that has equal density as basin water (Fig. 6b); and (3) hyperpycnal plume for sinking river water that has higher density than basin water (Fig. 6c). A. plume is a

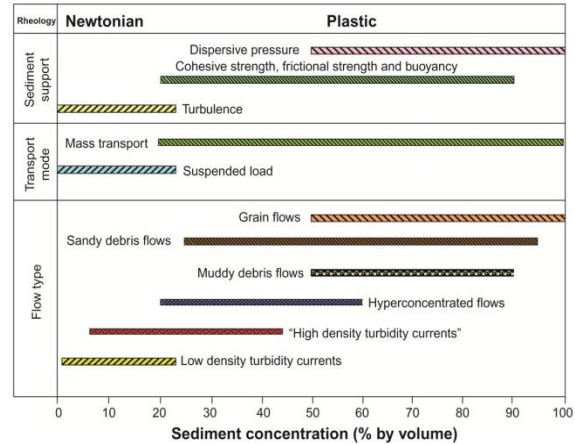


Fig. 5. Classification of gravity-driven sediment flows, based on sediment concentration, into Newtonian and plastic types. Sediment concentration is the most important property in controlling fluid rheology. High-density turbidity currents are included here solely for purposes of discussion. Also, for purposes of comparison, subaerial flows (river currents and hyper-concentrated flows) are considered. Published values of sediment concentration by volume percent are: (1) river currents (1-5%; e.g., Galay, 1987), (2) low-density turbidity currents (1-23%; e.g., Middleton, 1967, 1993), (3) high-density turbidity currents (6-44%; Kuenen, 1966; Middleton, 1967), (4) hyperconcentrated flows (20-60%; Pierson and Costa, 1987), (5) muddy debris flows (50-90%; Coussot and Muenier, 1996), (6) sandy debris flows (25-95%; Shanmugam, 1997; which was partly based on reinterpretations of various processes that exhibit plastic rheology in papers by Middleton, 1966, 1967; Wallis, 1969; Lowe, 1982; Shultz, 1984), (7) grain flows (50-100%; partly based on Rodine and Johnson, 1976; Shultz, 1984; Pierson and Costa, 1987). After Shanmugam (2000). Reproduced with permission from Elsevier.

fluid enriched in sediment, ash, biological or chemical matter that enters another fluid. However, the term "flow" is used for a continuous, irreversible deformation of sediment-water mixture that occurs in response to applied shear stress, which is gravity in most cases (Pierson and Costa 1987, p. 2). Not all plumes are flows. For example, floating hypopycnal plumes are not driven by gravity (Fig. 6a). However, both terms "flow" and "plume" are applicable to hyperpycnal type. This is because hyperpycnal type behaves as bed load due to higher sediment concentration (Fig. 6C). The other practice is to employ terms "overflow", "interflow", and "underflow" for hypopycnal, homopycnal, and hyperpycnal plumes, respectively. Again, the term flow is not appropriate for hypopycnal plume that is unaffected by gravity.

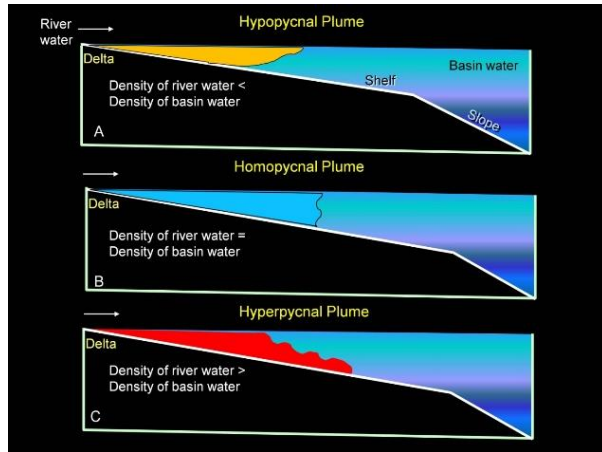


Fig. 6. Concepts and examples of density plumes. a, b, and c Schematic diagrams showing three types of density variations in riverine plumes in deltaic environments based on concepts of Bates (1953). Figure from Shanmugam (2012) with permission from Elsevier

Origin

Hyperpycnal flows originate from river floods at the plunge points near the shoreline. Mulder et al. (2003) expanded the applicability of the concept of hyperpycnal plumes from shallow water (deltaic) to deep-water (continental slope and abyssal plain) environments. In this new development, hyperpycnal flows are considered analogous to turbidity currents in many respects (Mulder et al., 2003; Steel et al., 2016; Zavala and Arcuri, 2016).

It is worth noting that Middleton and Hampton (1973) did not consider hyperpycnal flows in their original classification of sediment-gravity flows (Fig. 2), although hyperpycnal flows are indeed driven by sediment gravity. For the following reasons, hyperpycnal flows are considered as sediment-gravity flows in this article.

1. River-mouth hyperpycnal flows are caused by higher density of the entering river flows in comparison to density of seawater (Bates, 1953). Sediment particles in the flow are the cause of higher flow density.
2. The other option for higher density of entering flow is by changes in salinity and/or temperature, such as thermohaline ocean-bottom contour currents (Gordon, 2019), which is unlikely to occur at river mouths.
3. By applying the concept of Middleton and Hampton (1973), where the river waters enter the ocean, density of ambient fluid changes from air (1.225 kg/m^3) to seawater (1030 kg/m^3) (Beicher, 2000). In other words, at river-mouth plunge points, fluid-gravity flows could transform into sediment-gravity flows (Fig. 7). However, fluid mechanics of

hyperpycnal flows is mired in controversies (Shanmugam, 2018a, 2019b). Importantly, this flow transformation does not imply that all river flows routinely become turbidity currents.

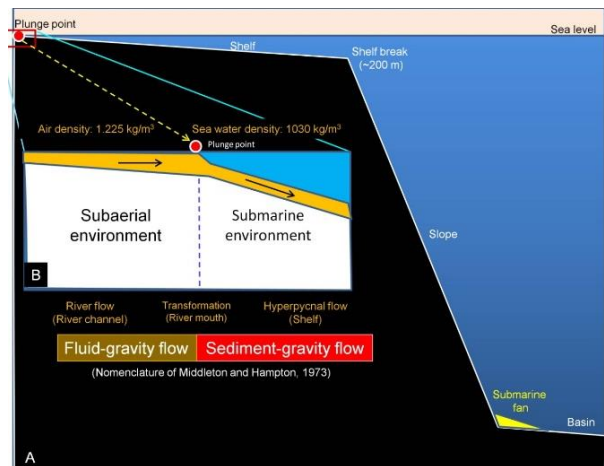


Fig. 7. Conceptual diagram of a continental margin showing relative positions of plunge point (red filled circle) at river mouth and submarine fan at base-of-slope. Note that fluid-gravity flows can transform into sediment-gravity flows at plunge points and deposit sediments as hyperpycnites near the shoreline in shallow-water environments. From Shanmugam (Shanmugam, 2020).

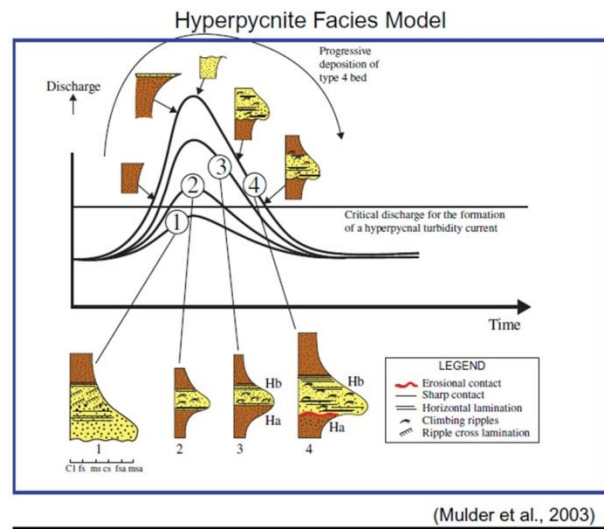


Fig. 8. Hyperpycnite facies model showing inverse to normal grading with erosional contact in the middle. Note identical inverse to normal grading trend in the contourite facies model (Fig. 44). From Mulder et al. (2003)

Identification

- Facies model (Mulder et al., 2003)
- Inverse- to normal- grading (Fig. 8)

- Internal erosion surface (Fig. 8)

Problem

Although there are modern plumes that may be termed hyperpycnal flows (Fig. 9), there are problems associated with recognizing hyperpycnal flows using aerial photographs and satellite images because these

images do not provide information on fluid rheology, low state, and sediment concentration in distinguishing hyperpycnal flows from turbidity currents. The basic issue is that hyperpycnal plumes are defined purely based on density (Bates, 1953).



Fig. 9. Sediment plume triggered by Elwha Dam demolition in the State of Washington (USA), (A) Index map showing Elwha Dam (arrow). The 108-foot dam, built in 1910 and demolished in 2012, is located approximately 7.9 km upstream from the river mouth. Credit: U.S. Geological Survey Public Domain map, (B) Aerial photograph of the Olympic Peninsula and the Strait of Juan de Fuca. Note the Elwha River mouth is shown by a filled yellow circle. From Duda et al. (2011) with additional labels by G. Shanmugam, (C) Elwha sediment plume triggered by the demolition of Elwha Dam in 2012. Red arrow shows easterly deflecting plume, away from the Pacific Ocean. This deflection could be attributed to tidal currents in this estuarine environment. Also, the Strait of Juan de Fuca is subjected to easterly upwelling winds. Photo credit: Tom Roorda. Aerial photo was taken on March 30, 2012. From Hickey (2013), UW News, March 7, 2013, University of Washington, Seattle, WA, (D) Aerial photo of Elwha River mouth showing absence of sediment plume in 2019 (compare with Fig. 9C). Photo courtesy of Tom Roorda, Roorda Aerial, Port Angeles, WA. Aerial photo was taken on February 28, 2019.

Although such a definition was adequate in 1953, it is no longer sufficient in light of advances that have been made on fluid dynamics discussed earlier. Major unresolved problems are:

- (1). Facies model has not been reproduced in experiments.
- (2). There has not been any verification of inverse to normal grading based on sediment core from modern hyperpycnites.

(4) The nomenclatural problem is further muddled by classifying turbidity currents and debris flows as "hyperpycnal flows" based on provenance (i.e., land derived) (Fig. 11) by Zavala (2020). The reason is that debris flows and turbidity currents were traditionally classified as sediment-gravity flows based on sediment-support mechanisms by Middleton and Hampton (1973), which is the standard reference in process sedimentology.

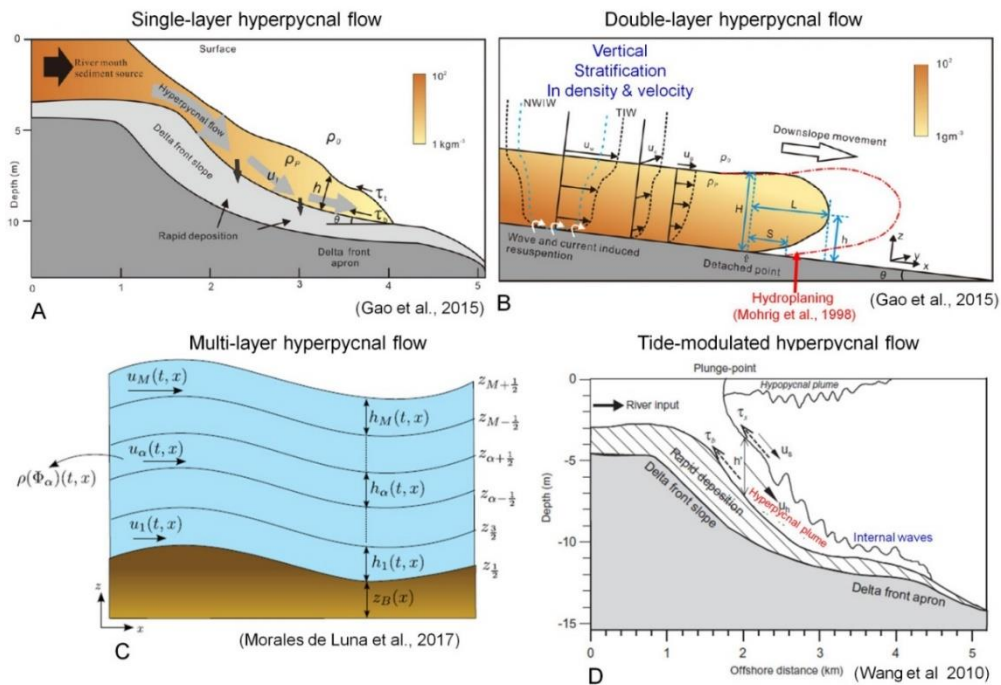


Fig. 10. Four types of hyperpycnal flows. From Shanmugam (2018a). (Correction in reference Wang et al., 2010 in Figure)

(3). There are 16 types of hyperpycnal flows, but their fluid dynamical properties have not been verified in experiments. Specifically, deposits of single layer type, double layer type, multi-layer type, etc. (Fig. 10) have not been documented.

(5). Finally, there are 22 external controls (Fig. 12) and their role on deposits of hyperpycnal flows has never been studied.

Types of hyperpycnal flows			Flow origin		
Newtonian (Fluid flows)	Subcritical	Non-Newtonian (plastic)	Cohesive debris flows (CDF)	High-density short-lived flows entering the basin	
		Supercritical	Laminar	Hyperconcentrated flows (HCF)	- Alluvial fans - Small mountainous rivers - Flash floods
			Turbulent	Concentrated (granular) flows (CF)	Require steep slopes to accelerate, incorporate ambient water, and transform into dilute turbulent flows
	Turbulent	Sediment-laden turbulent flows (SLTF)	Pebbly	Low-density long-lived flows entering the basin	
			Sandy	- Medium- to large-size rivers	
			Muddy	No steep slopes are necessary. Flow can travel for long distances since the flow is sustained by the river discharge	

Fig. 11. Classification of debris flows and turbidity currents as "hyperpycnal flows" by Zavala (2020), causing confusion. Note that sediment-gravity flows were originally classified on the basis of sediment-support mechanisms by Middleton and Hampton (1973), whereas Zavala (2020) has classified types of sediment-gravity flows as "hyperpycnal flows" on the basis of their provenance (i.e., land derived). Other problems associated with hyperpycnal flows were addressed by Shanmugam (2018a and 2019b). Figure

Turbidity Currents

Definition

A turbidity current is a sediment flow with Newtonian rheology (Fig. 3) and turbulent state (Figs

13 and 14) in which sediment is supported by turbulence and from which deposition occurs through suspension settling (Dott, 1963; Sanders, 1965; Middleton and Hampton, 1973; Shanmugam, 1996).

Environment	Composition	Provenance	External Control	Type
1. Marine	1. Siliciclastic	1. River flood	1. Wind forcing	1. Simple lobe
2. Lacustrine	2. Calciclastic	2. Common delta	2. Wind waves	2. Horse's tail
3. Estuarine	3. Volcaniclastic	3. Braid delta	3. Longshore curr.	3. Deflecting
4. Lagoon	4. Planktonic	4. Tidal estuary	4. Cyclonic curr.	4. Dissipating
5. Bay	5. Hydrogen sulfide	5. Subglacial	5. Monsoonal curr.	5. U-Turn
6. Reef	6. Gas hydrate	6. Eolian	6. Upwelling curr.	6. Swirly
		7. Volcanic	7. Seiche	7. Cloudy
		8. Planktonic	8. Tidal shear front	8. Massive
		9. Carbonate platform/Reef	9. Tidal current	9. Tidal lobe
		10. Hydrogen sulfide	10. Internal waves and tides	10. Cascading
		11. Gas hydrate	11. Ocean curr.	11. Backwash
			12. Tsunami	12. Meltwater
			13. Braid delta	13. Coalescing irreg.
			14. Volcanism	14. Blanketing
			15. Glacial melt	15. Linear
			16. Coral reef	16. Anastomosing
			17. Fish activity	17. Coalescing lobe
			18. Pockmarks	18. Whitings
			19. Phytoplankton	19. Ring
			20. Hydrogen sulfide	20. Tendril
			21. Gas hydrate	21. Eolian dust
			22. Anthropogenic	22. Feathery
				23. Volcanic ash
				24. Gas hydrate

Fig. 12. Summary diagram showing complex natural variability of plumes in terms of their environmental settings, their composition, their source, their external control, and types. Modified after Shanmugam (2018a, b).

Turbidity currents exhibit unsteady and non-uniform flow behavior (Fig. 13), and they are surge-type waning flows. As they flow downslope, turbidity currents (Fig. 13) invariably entrain ambient fluid (sea water) in their frontal head portion due to turbulent mixing (Allen, 1985). With increasing fluid content, plastic debris flows may tend to become turbidity currents with high turbulence (Fig. 14). However, not all turbidity currents evolve from debris flows. Some turbidity currents may evolve directly from sediment failures. Although turbidity currents may constitute a distal end member in basinal areas, they can occur in any part of the system (i.e., shelf edge, slope, and basin).

Origin (Triggers)

The origins of four sediment-gravity flows are

closely related to sediment failures and slope instability. There are 21 triggering mechanisms in causing sediment failures (Shanmugam, 2015), but only important mechanisms are listed in each case.

- Earthquake,
- oversupply of sediment,
- volcanism,
- meteorite impact,
- tsunamis, and
- cyclones

Identification Turbidity currents cannot transport gravel and coarse-grained sand in suspension because they do not possess the strength like debris flows. General characteristics of turbidites are:

Problem

- 1) Misapplication of the term 'turbidite' for deposits of all four types of sediment-gravity flows, including debris flows (Fig. 18) by Mutti et al. (1999) and by Zavala (2019).
- 2) There is no agreement on the density value that separates "low-density" from "high-density" turbidity currents (Fig. 19A). Turbidity currents are inherently low in sediment concentration or low in flow density (Fig. 19A), According to Bagnold (1962), typical turbidity currents can function as truly turbulent suspensions only when their sediment concentration by volume is below 9% or c. < 9% (Fig. 19A). Therefore, high-density turbidity currents (Fig. 19B) cannot exist in nature.
- 3) Flume experiments have revealed that the so-called "high-density turbidity currents" are indeed composed of a basal laminar layer, typical of debris flows (Shanmugam, 1996), not turbulent turbidity currents. Experiment also provided evidence for deposition of floating clasts (Postma et al., 1988) at the rheological interface (Fig. 19B), which is common in debris flows.



Fig. 17. Outcrop photograph showing tilted thin-bedded turbidite sandstone beds with sheet-like geometry, Lower Eocene, Zumaya, northern Spain. Reproduced from Shanmugam (2006). Elsevier. Photo by G. Shanmugam.

- 4) The complete "Bouma sequence" (with Ta, Tb, Tc, Td, and Te divisions) has never been documented in modern deep-sea sediments. Nor has it been reproduced in flume experiments. Furthermore, this model suffers from a lack of sound theoretical basis (Leclair and Arnott, 2005; Sanders, 1965; Shanmugam, 1997). Leclair and Arnott (2005, p. 4) state that "...the debate on the upward change from massive (Ta) to parallel laminated (Tb) sand in a Bouma-type turbidite remains

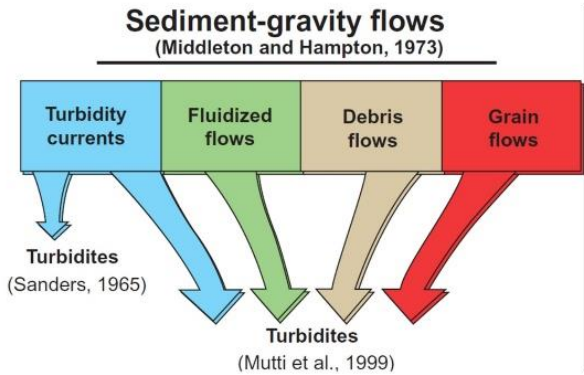


Fig. 18. Original classification of sediment-gravity flows by Middleton and Hampton (1973). Confusing application of the term 'turbidites' to deposits of all four types by Mutti et al. (1999) without regard for fluid mechanics, which Zavala (2019) has adopted in his comment. I have adopted Sanders' (1965) classification in which only deposits of turbidity currents are considered as turbidites. From Shanmugam (2002).

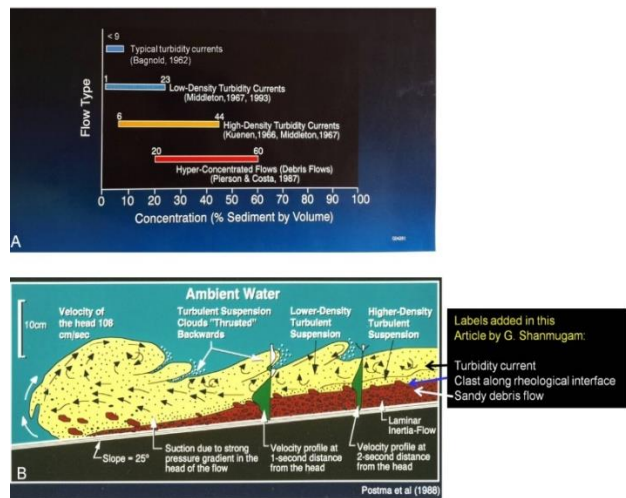


Fig. 19. (A)-Plot of sediment concentration for different flow types. Note that a typical turbidity current can exist only in sediment concentration less than 9% by volume (Bagnold, 1962). Note overlap in sediment concentration among low-density, turbidity currents, high-density turbidity currents, and hyper-concentrated flows. Modified after Shanmugam (1996). Reproduced with permission from SEPM. (B)-Experimental stratified flows with a basal laminar-inertia flow and an upper (turbulent) turbidity current that have been termed as "high-density turbidity currents." Note clasts near the top of sandy debris flows along the rheological interface. Compare with Fig. 29 and related text. Figure from Postma et al. (1988). Publication: Sedimentary Geology. Elsevier
 unresolved." The ultimate objective of facies models is to interpret ancient strata (i.e., the unknown). However,

the turbidite facies models, developed exclusively from the ancient strata without validation from the modern environment (i.e., the known), promote circular reasoning

- 5) The ideal turbidite bed with 16 divisions (Fig. 20) is untenable from a fluid dynamic point of view. No one has ever documented the vertical facies model showing the R1, R2, R3, S1, S2, and S3 divisions of the Lowe (1982) sequence and the Ta, Tb, Tc, Td, and Te divisions of the Bouma (1962) sequence in ascending order in modern deep-sea sediments.
- 6) No one has ever replicated in flume experiments of turbulent turbidity currents that could carry coarse sand and gravel in suspension in laboratory flume experiments that could produce the R1, R2, R3, S1, S2, and S3 divisions in ascending order.

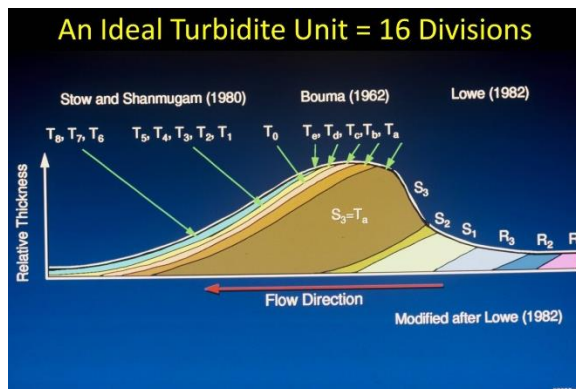


Fig. 20. An ideal turbidite bed should develop 16 divisions. However, no one has ever documented such a turbidite bed with 16 divisions in the field or in flume experiments. After Shanmugam (2000), reproduced with permission from Elsevier

Debris Flows

Definition

A debris flow is a sediment flow with plastic rheology and laminar state from which deposition occurs through freezing en masse. The terms debris flow and mass flow are used interchangeably because each exhibits plastic flow behavior with shear stress distributed throughout the mass (Nardin et al., 1979). In debris flows, inter-granular movements predominate over shear-surface movements. Although most debris flows move as incoherent mass, some plastic flows may be transitional in behavior between coherent mass movements and incoherent sediment flows (Marr et al., 2001). Debris flows may be mud-rich (i.e., muddy debris flows), sand-rich (i.e., sandy debris flows), or

mixed types. In multibeam bathymetric data, recognition of debrites is possible.

Sandy debris flows are defined because of their importance in petroleum geology (Shanmugam et al., 2009). Sandy debris flow represents an intermediate stage between grain flow and cohesive debris flow (Fig. 2). The concept of sandy debris flows was first introduced by Hampton (1972). Sandy debris flows are defined here on the basis of (1) plastic rheology; (2) multiple sediment-support mechanisms (cohesive strength, frictional strength, hindered settling, and buoyancy); (3) mass-transport mode; (4) more than 25-30% sand and gravel; (5) 25-95% sediment (gravel, sand, and mud) concentration by volume (Fig. 5); and (6) variable clay content (as low as 0.5% by weight) (Shanmugam, 2000). Sandy debris flows could develop in slurries of any grain size (very fine sand to gravel), any sorting (poor to well), any clay content (low to high), and any modality (unimodal and bimodal). Sandy debris flow was misclassified as “high-density turbidity currents” (Shanmugam, 1996).

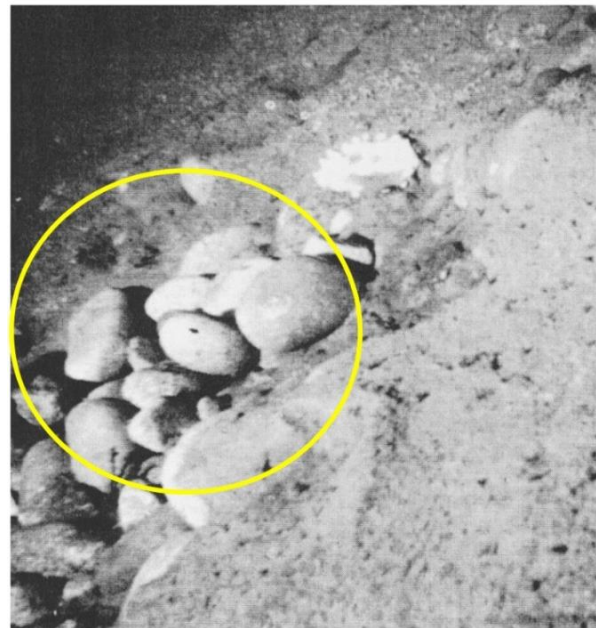


Fig. 21. Underwater photograph showing a pocket of rounded cobbles up to 15 cm in diameter in massive sandy matrix at a depth of 130 m (427 ft) in Los Frailes Canyon, Baja California. Note projected nature of clasts from the upper sediment surface. Photo by R.F. Dill. After Shepard and Dill (1966), Rand McNally & Company, Published in Shanmugam, G. (2012). New perspectives on deep-water sandstones: Origin, recognition, initiation, and reservoir quality. In: Handbook of petroleum exploration and production, vol. 9, 524 p. Amsterdam: Elsevier.

Origin

- Earthquake,
- slope instability on alluvial fans,
- oversupply of sediment,
- volcanism,
- meteorite impact,
- tsunamis, and
- cyclones.



Fig. 22. Flume used in the experiments of sandy debris flows. See Shanmugam (2000) and Marr et al. (2001) for details on experiments. Photo by G. Shanmugam.

Identification

Debris flows are capable of transporting gravel and coarse-grained sand because of their inherent strength. General characteristics of muddy and sandy debrites are:

- Gravel to mud lithofacies.
- The reliability of identification of ancient debrites in the rock record is high. This is because reliable field criteria have been developed on the basis of modern analogs of gravelly debrites (Fig. 21) and on the basis of large laboratory flume (Fig. 22) experiments in reproducing excellent examples of sandy debris flows with various diagnostic features, such as snout (Fig. 23) and other identification markers (Fig. 23).
- Floating or rafted mudstone clasts near the tops of sandy or muddy beds (core and outcrop) (Fig. 25)
- Floating armored mudstone balls in sandy matrix (core and outcrop)
- Projected clasts (core and outcrop) (Fig. 25)
- Planar clast fabric (core and outcrop) (Fig. 26A)
- Imbricate clasts (experiment)
- Brecciated mudstone clasts in sandy matrix (core and outcrop) (Fig. 27)
- Concentration of larger clasts (pumice blocks) near the front of volcanic debris flows or lahars, which would result in inverse grading of clasts in the rock record
- Inverse grading of clasts and rock fragments with random fabric (core and outcrop) (Fig. 28)
- Inverse grading of quartz granules in sandy matrix (core and outcrop)
- Inverse grading, normal grading, inverse to normal grading, and absence of any grading of matrix (core and outcrop)
- Unusually large blobs of heterolithic facies in muddy matrix
- Floating quartz granules in sandy matrix (core and outcrop)
- Pockets of gravels in sandy matrix (core and outcrop) (Fig. 21)
- Preservation of delicate mud fragments with planar fabric in sandy matrix (core and outcrop)
- Irregular, sharp upper contacts (core and outcrop)
- Side-by-side occurrence of garnet granules (density: 3.5–4.3) and quartz granules (density: 2.65) (core and outcrop)
- Lenticular to sheet-like in geometry
- Lobe-like geometry (map view) in the Gulf of Mexico Tongue-like geometry (map view) in the North Atlantic (Fig. 27A).

Experimental sandy debris flow

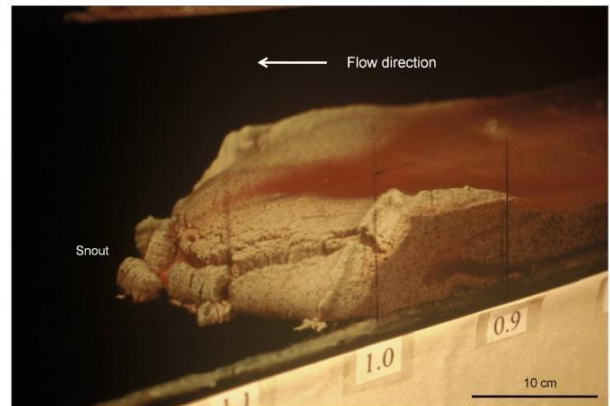


Fig. 23. Side view of flume tank showing strong debris flows with well-developed snout. Note the absence of turbulent suspension on top. Also note irregular upper surface caused by sudden freezing of the flow. Deformation in the front suggests strongly coherent character of flow, which may be called a slump. Reproduced from Shanmugam, G. (2006). Deep-water processes and facies models: Implications for sandstone petroleum reservoirs. In: Handbook of petroleum exploration and production, vol. 5, 476 p. Amsterdam: Elsevier

Features	Observation	Interpretation
	Sharp Upper Contact	Freezing of Flow and Plastic Rheology
	Irregular Upper Contact and Lateral Pinch-out Geometry	Freezing of Primary Relief and Plastic Rheology
	Irregular Front (Snout)	Freezing of Primary Relief and Plastic Rheology
	Non-Erosive Base and Water Entrapment (↙)	Laminar Flow and Hydroplaning
	Dish Structures and Water Entrapment (↙)	Hydroplaning and Water Escape
	Vertical Pipes	Hydroplaning and Water Escape
	Grain Segregation and Normal Grading	Grain Settling from Weak Flow
	Planar Fabric and Inverse Grading	Laminar Flow and Flow Strength
	Random Fabric	Flow Strength and Freezing of Flow
	Internal Layers	Mass Movement and Secondary Glide Planes
	Imbricate Slices	Mass Movement and Compression
	Isolated Blocks	Mass Movement and Tension
Flow Direction →	120 μm Silica Sand 500 μm Coal Slag (bulk density: 2.6 g/cm ³)	

Fig. 24. Summary of identification markers associated with debris flows based on experiments. From Shanmugam (2000). Elsevier.

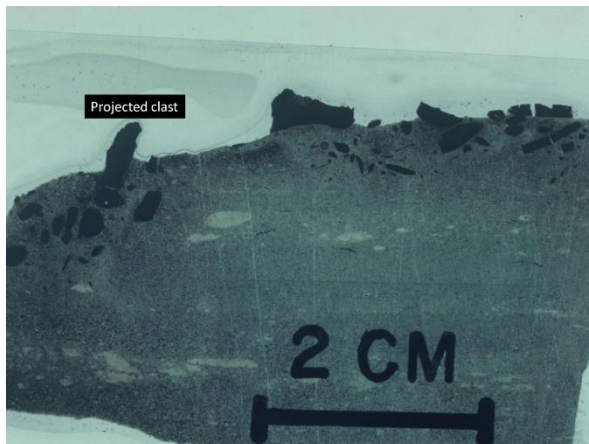


Fig. 25. Polished slab showing projected clasts, interpreted as freezing by debris flows. From Shanmugam and Benedict (1978). SEPM.

The modern Amazon submarine channel has two major debrite deposits (east and west) (Damuth and Embley, 1981; Piper et al., 1997). The western debrite unit is about 250 km long, 100 km wide and 125 m thick. In the U.S. Atlantic margin, debrite units are about 500 km long, 10-100 km wide, and 20 m thick. On the NW African Continental margin, the Canary

debrite is 60-100 km wide, 5-20 m thick, and traveled about 600 km (Masson et al., 1997).

Based on (1) experimental sandy debris flows showing detached blocks (Shanmugam, 2000), (2) documented long runout natural sandy debris flows in modern oceans (Gee et al., 1999) and (3) interpreted example in the ancient record (Teale and Young, 1987), long runout sandy debrite blocks are viable candidates for developing thick, isolated, sandstone petroleum reservoirs in deep-water environments. Because of clay-poor nature (Marr et al., 2001), isolated outrunner sandy debrites have great potential for serving as sandstone petroleum reservoirs.

Problem

There are three major problem areas regarding interpreting coarse-grained deposits either as high-density turbidites or as sandy debrites in deep-water strata.

First, are high-density turbidity currents sandy debris flows? Conventionally, stratified flows have been classified as high-density turbidity currents. I (Shanmugam, 1996) argued against such classifications. The prevailing differences of opinion on nomenclature can be explained by our flume experiments (Shanmugam, 2000; Marr et al., 2001). For example, the stratified flow with lower laminar layer and an upper turbulent layer in our experiment (Fig. 29) would be classified differently by different researchers as follows:

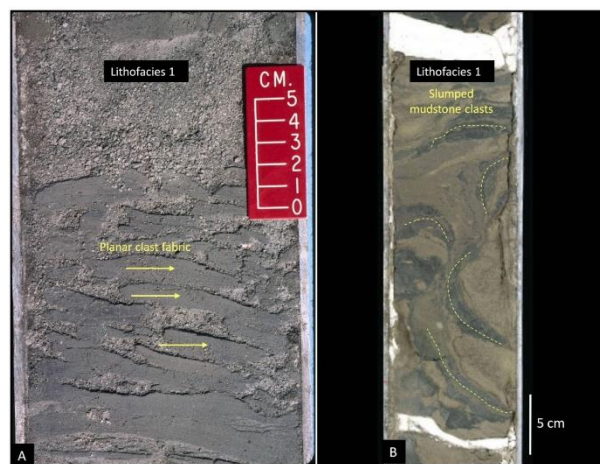


Fig. 26. Core photos showing planar clast fabric (A) and associated slump facies (B). Pliocene reservoir sands in upper-slope canyon environments, Offshore Krishna-Godavari Basin, Bay of Bengal (India). From Shanmugam et al. (2009).

1. Group 1 of researchers would recognize the importance of bottom layer with different rheology and flow state (Bagnold, 1956; Sanders, 1965; 3; Shanmugam, 1996).
2. Group 2 would not (Kuenen, 1956; Postma et al., 1988; Mutti et al., 1999; Zavala, 2019). Postma et al. (1988) would combine both layers and classify them together as "High-density turbidity currents" (Fig. 19B).

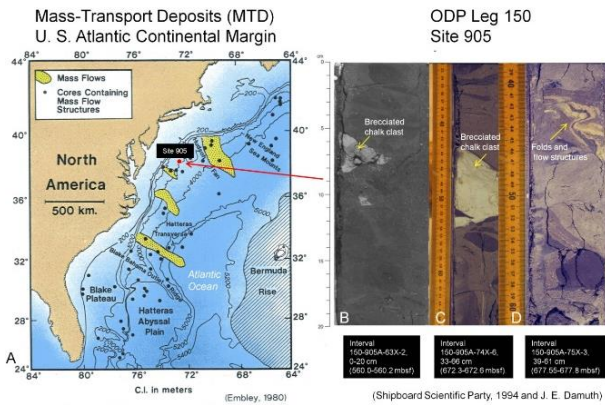


Fig. 27. (A) Map showing the distribution of MTD on the U.S. Atlantic Continental margin. Note position of ODP Leg 150, Site 905 (filled red circle) added in this study. (B) Core photograph showing brecciated chalk clast. (C) Core photograph showing brecciated chalk clast (Eocene) in sandy clay matrix. (D) Core photograph showing folds and flow structures in sandy clay matrix. Color photograph courtesy of J.E. Damuth. Red arrow points to site location. From Shanmugam (2017a). Elsevier.

Second, are floating clasts in deep-water sandstones representing sandy debrites? Experiments have shown that clasts indeed form along rheological boundaries on top of sandy debris flows (Fig. 19B).

Third, the major unresolved issue is flow transformation in sediment-gravity flows. Fisher (1983) proposed four types of transformations for sediment-gravity flows: (1) body transformation; (2) gravity transformation; (3) surface transformation; and (4) elutriation transformation. Flow transformations cannot be established without knowing: (1) initial flow behavior; (2) transport mechanisms; and (3) final flow behavior. There are, however, no established criteria for recognizing initial flow behavior and transport mechanisms in the depositional record (Dott, 1963; Middleton and Hampton, 1973).

In discussing the physics of debris flows, Iverson (1997) states, 'When mass movement occurs, the sediment-water mixtures transform to a flowing, liquid-like state, but eventually they transform back to

nearly rigid deposits.' Although such transformations can occur during transport, evidence for flow transformations cannot be inferred from the final deposit. We may never resolve this issue of flow transformation.



Fig. 28. Outcrop photograph showing inverse grading with floating boulder-size clasts near the top of sandstone unit (arrow). Note random fabric of clasts. Middle Miocene, San Onofre Breccia, Dana Point, California. This lithofacies has been interpreted to be sandy debrite associated with alluvial fan and fan delta. Reproduced from Shanmugam, G. (2012). New perspectives on deep-water sandstones: origin, recognition, initiation, and reservoir quality. In: Handbook of petroleum exploration and production, vol. 9, 524 p. Amsterdam: Elsevier

Liquefied/Fluidized Flows

Definition

In contrast to the classification of Middleton and Hampton (1973), Lowe (1976a) made a clear distinction between liquefied and fluidized systems. In liquefied beds and flows, the solids settle downward through the fluid, displacing it upward, whereas in fluidized beds, the fluid moves upward through the solids, which are temporarily suspended without net downward movement.

Origin

- Earthquake,
- sediment loading,
- volcanism,
- meteorite impacts,
- tsunamis, and
- cyclones,

In understanding this type of phenomenon, one needs to discuss liquefaction. Allen (1984)

provided an accurate account of soft-sediment deformation in terms of physics.

- 1) Stratigraphical and sedimentological studies over many years have shown that soft sediments often become deformed non-tectonically. The structures induced take myriad forms and are increasingly called “soft-sediment deformations”.
- 2) Soft-sediment deformation is associated in time with the earliest stages of sediment consolidation, when the deposit is weakest and pore fluid is being expelled most rapidly. This process is popularly known as “prelithification deformation”. Lowe (1975) classified such soft-sediment deformations as “water-escape structures”.
- 3) Liquefaction is significant in the production of many kinds of soft-sediment deformations.

He and Qiao (2015, their Fig. 1) classified deformations of seismites, based on structural styles, preserved positions, activity times, formation mechanisms and dynamics of soft-sediment deformation structures triggered by seismic activity, into 5 primary types:

- (1) liquefied deformation,
 - (2) thixotropic deformation,
 - (3) hydroplastic deformation,
 - (4) superimposed gravity driving deformation, and,
 - (5) brittle deformation.
- Further, based on the main genetic types, composition of sediments and deformation styles, the authors proposed 35 secondary types (e.g., liquefied breccia, liquefied droplet, homogenite, tepee structure, fault grading, shatter breccia, etc.).

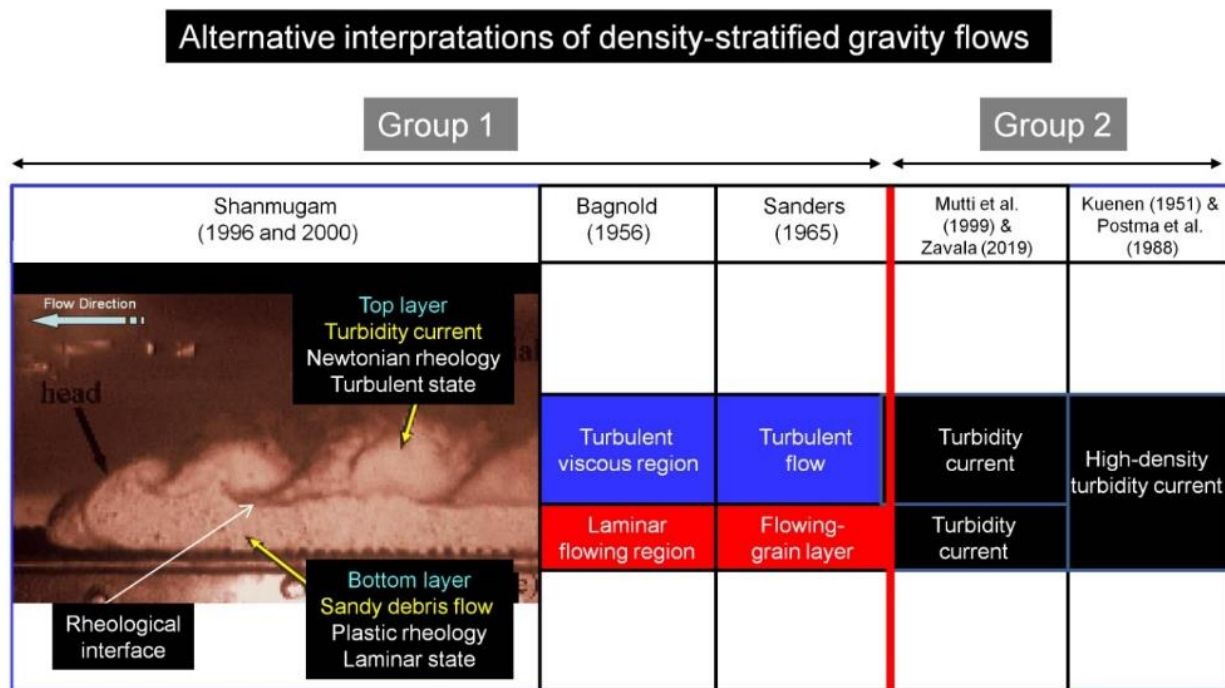


Fig. 29. Diagram illustrating the importance of distinguishing bottom layer based on fluid rheology and flow state in density-stratified gravity flows, which is based on a photograph of experimental density-stratified gravity flows showing the rheological difference between plastic debris flow (bottom layer) in massive sand and Newtonian turbidity current (top layer). Note that only Group 1 of researchers would recognize the importance of bottom layer with different rheology and flow state. Note that Postma et al. (1988) would classify both layers together as 'high-density turbidity current' (see Fig. 19B). This Mobil-funded experimental flume study was carried out at St. Anthony Falls Laboratory (SAFL), University of Minnesota (1996-1998) under the direction of Professor G. Parker to evaluate the fluid dynamical properties of sandy debris flows. Results were published in two major articles (Shanmugam, 2000; Marr et al., 2001).

Identification

- Fluid escape structures
- Dish and pillar structures (Fig. 30A)
- Dewatering pipes (Fig. 30B)
- Soft-sediment deformation structures (SSDS) (Fig. 31), (Shanmugam, 2017a).

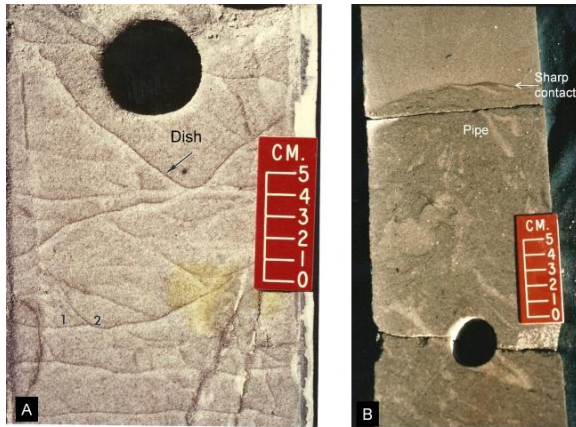


Fig. 30. (A)-Core photograph showing water-escape dish structures by liquidization in fine-grained, well-sorted sand. The arrow shows a concave-up (dish structure) color couplet with left wing dipping at 45° from the core horizontal due to deformation. Note cross-cutting relationship between two dish structures in which an earlier formed dish structure (1) has been terminated by a later one (2). Eocene, U.K. North Sea. From Shanmugam (2006), with permission from Elsevier; (B)-Core photograph showing pipes (water-escape structures). Paleocene, U.K. Atlantic Margin. Figures from Shanmugam (2012), with permission from Elsevier.

Su and Sun (2012) proposed that the following SSDS are common identification markers associated with earthquake-induced liquefaction:

- diapirs,
- clastic dikes,
- convolute bedding,
- compressional deformation features (accordion folds, plate-spine breccias, mound-and-sag structures), and
- extensional plastic features (loop-bedding).

Li et al. (2008) suggested the following criteria for recognizing features induced by seismicity:

- Seismic micro-fractures,
- microcorrugated laminations,
- liquefied veins, “vibrated liquefied layers”,
- deformed cross laminations,
- convolute laminations,
- load structures,
- flame structures, breccias,
- slump structures,
- seismo-disconformity.

Problem

Fluidized flows are transitional and transient in nature (Lowe, 1982). They also are not important sediment transport processes. For these reasons, I combined the two processes and call it 'Liquefied/Fluidized flow'. In the rock record, it is a challenge to distinguish liquefaction features induced by earthquakes from those generated by rapid sedimentation. The other problem is that there are no objective criteria to recognize earthquakes as a unique triggering mechanism (among 20 others) of soft-sediment deformation structures (SSDS) (Shanmugam, 2017b). Major problems in recognizing seismicity-induced SSDS are discussed by Shanmugam (2016a).

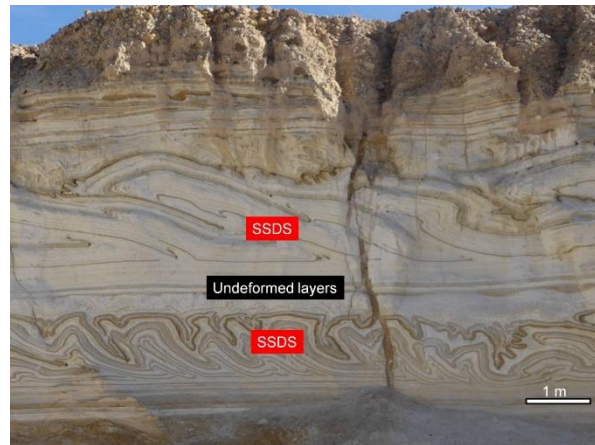


Fig. 31. Outcrop photograph showing two layers of seismicity-induced soft-sediment deformation structures (SSDS) with an intervening interval of undeformed layers. Perazim Wadi in the Quaternary Lisan Formation, a dry wash in the Ami'az Plain SW of Ein Boquet in Israel. Although this formation is not of deep-water origin, it illustrates the seismicity-induced sediment deformation in tectonically active settings. Photo courtesy of Professor Emeritus R. D. Hatcher, Jr., Department of Earth and Planetary Sciences, The University of Tennessee, Knoxville.

Grain Flows

Definition

According to Lowe (1976b), the term grain flow is restricted to sediment gravity flows in which a dispersion of cohesionless grains is maintained against gravity by grain dispersive pressure and in which the fluid interstitial to the grains is the same as the ambient

fluid above the flow. Modified flows include those in which a dense interstitial fluid, current, or escaping pure fluid aids in maintaining the dispersion.

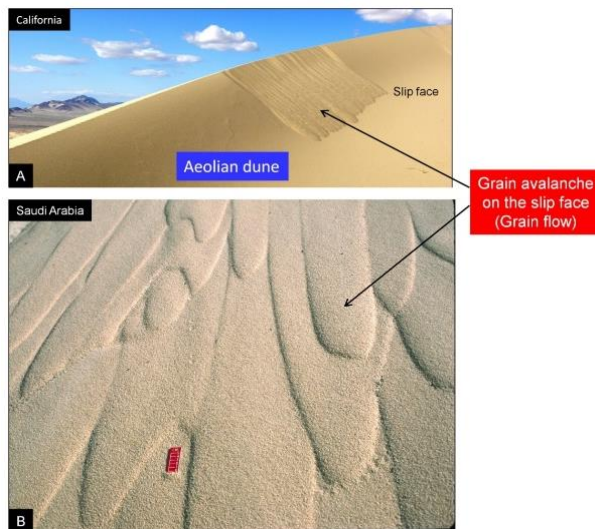


Fig. 32. Grain flows. (A). Photograph showing grain avalanches (i.e., grain flows) on the 'slip face' or lee side of an aeolian dune. Photo was taken at Kelso in the Mojave desert, California by Mark. A. Wilson. Wikipedia. Public domain. (B). Photograph showing grain avalanches (i.e., grain flows) on the 'slip face' or lee side of an aeolian dune. Saudi Arabia. Red scale = 5 cm.



Fig. 33. Underwater photograph showing a cascading sand fall at a depth of 40 m (130 ft) in gully leading down into San Lucas Canyon, Baja California. Such pure sand falls would develop massive sand intervals in the rock record. Photo by R.F. Dill. After Shepard and Dill (1966), Rand McNally & Company.

Origin

- Arid climate, wind, aeolian dunes (Fig. 32)
- Steep gradients associated with submarine canyon-heads where sand fall occurs (Fig. 33). Submarine sand falls are considered somewhat analogous to grain flows.

Identification

- Massive sand layers
- Thin layers (< 5 cm)
- Well sorted
- Inverse grading

Problem

Deposits of grain flows are volumetrically insignificant in submarine environments, but included here for completeness.

Thermohaline- Contour currents

Definition

Thermohaline-induced bottom currents that follow regional bathymetric contours in deep-water (200 bathymetry) environments. They are called thermohaline contour currents (THCC) in this article.

Origin

Wüst (1936) first documented the importance of deep-water masses in the Atlantic Ocean. Deep-water masses in the world's oceans are caused by differences in temperature and salinity. When sea ice forms in the polar regions due to freezing of shelf waters, seawater experiences a concurrent increase in salinity due to salt rejection and a decrease in temperature. The increase in the density of cold saline (i.e., thermohaline) water directly beneath the ice triggers the sinking of the water mass down the continental slope (Fig. 34) and the spreading of the water masses to other parts of the ocean (Fig. 35). These are called thermohaline water masses.

.Antarctic Bottom Water (AABW)

The origin of thermohaline water masses are best studied using the Antarctic Bottom Water (AABW) (Gordon, 2001, 2019; Gordon et al. 2013; Purkey et al. 2018, among others). The AABW is initiated as downslope gravity flows on the continental slope (Fig. 36). The AABW has a density of 0.03 g/cm^3 with temperatures ranging from -0.8 to $2 \text{ }^\circ\text{C}$ ($35 \text{ }^\circ\text{F}$), salinities from 34.6 to 34.7 psu. Being the densest water mass of the oceans (Purkey et al., 2018, AABW is found to occupy the depth range below 4000 m. The ABW (Antarctic bottom water) is formed

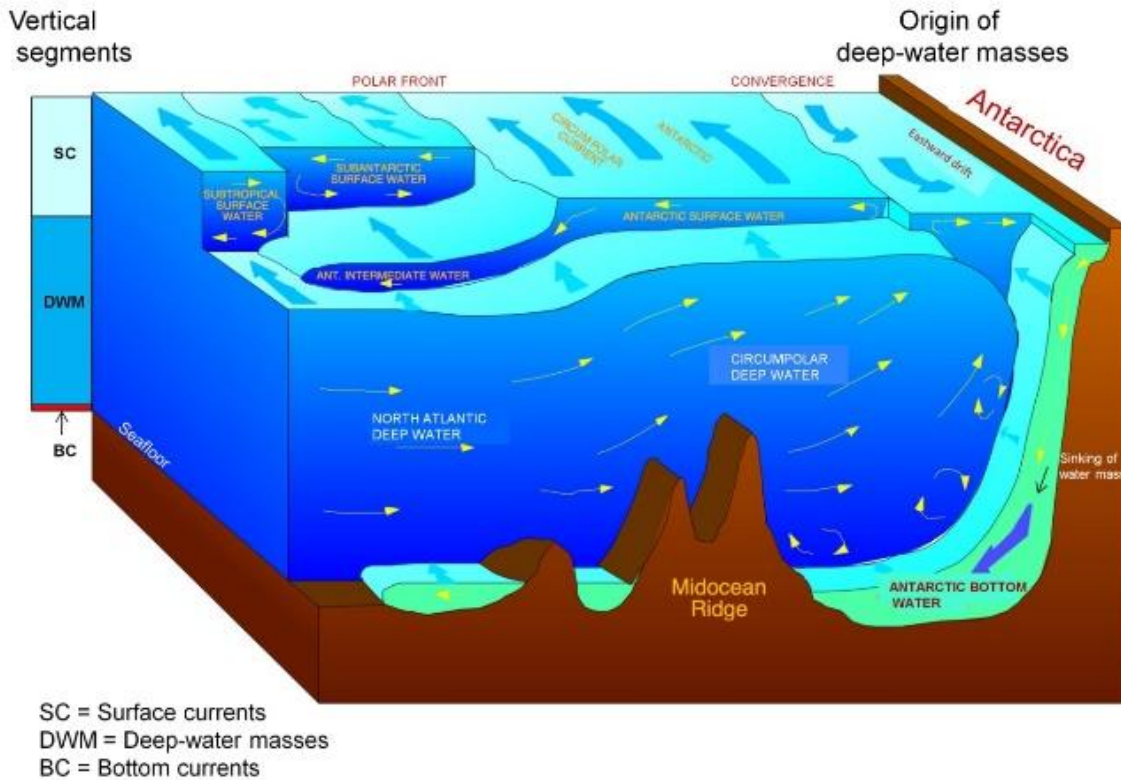


Fig. 34. A conceptual model of the Southern Ocean showing three vertical segments, composed of the upper surface currents, the middle deep-water masses, and the lower bottom currents, forming a vertical continuum (left). Note the origin of AABW by freezing of shelf waters (right). As a consequence, the increase in the density of cold saline (i.e., thermohaline) water triggers the sinking of the water mass down the continental slope and the spreading of the water masses to other parts of the ocean. Modified after Hannes Grobe, September 5, 2015. From Shanmugam (2012), with permission from Elsevier.

in the Weddell and Ross Seas, off the Adélie Coast and by Cape Darnley from surface water cooling in polynyas and below the ice shelf. A unique feature of Antarctic bottom water is the cold surface wind blowing off the Antarctic continent (Fig. 36). The surface wind creates the polynyas (i.e., an area of open water surrounded by sea ice), which opens up the water surface to more wind. This Antarctic wind is stronger during the winter months and thus the Antarctic bottom water formation is more pronounced during the Antarctic winter season. Stommel (1958) first developed the concept of the global circulation of thermohaline water masses and the vertical transformation of light surface waters into heavy deepwater masses in the oceans. Broecker (1991) presented a unifying concept of the global oceanic “conveyor belt” by linking the wind-driven surface circulation with the thermohaline-driven deep circulation regimes.

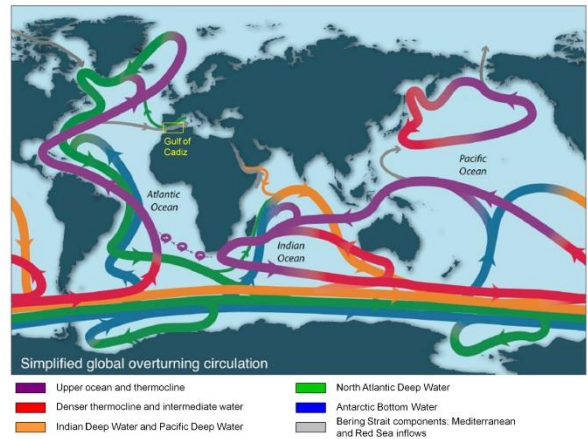


Fig. 35. Map showing the global overturning circulation (GOC). Note, the location of Gulf of Cadiz which served as the type locality for the contourite facies model. Modified after Talley (2013), with permission from the Oceanography Society.

The large-scale horizontal transport of water masses, which also sink and rise at select locations, is known as the “thermohaline circulation” or THC. Aspects of thermohaline circulation are discussed by Zenk (2008). The global overturning circulation has been presented by Talley (2013) (Fig. 35). Examples of selected deep-water masses in various parts of the world’s oceans and their acronyms are given below.

AABW: Antarctic bottom water

ABW: Arctic bottom water

AAIW: Antarctic intermediate water (Brazilian margin)

ACC: Antarctic circumpolar current (Antarctica)

AW: Atlantic water (Mediterranean sea)

BC: Brazil current

BICC: Brazil intermediate counter current

CDW or CPDW: Circumpolar deep water

DGSRF: Deep Gulf Stream return flow

DWBUC or DWBC: Deep western boundary undercurrent

IDW: Indian deep water

ITF: Indonesian through flow

LCDW: Lower circumpolar deep water

LIW: Levantine intermediate water (Mediterranean sea)

MOW: Mediterranean outflow water

MUC: Mediterranean undercurrent

NADW: North Atlantic deep water

NAdDW: North Adriatic dense water

NPDW: North Pacific deep water (Japan)

NSDW: Norwegian sea deep water

PDW: Pacific deep water

SACW: South Atlantic central water (Brazilian margin)

SOW: Sea overflow water

UCDW: Upper circumpolar deep water

WBUC: or WBU Western boundary undercurrent

WDW: Warm deep water (Antarctica)

WSBW: Weddell sea bottom water (Antarctica)

WSDW: Weddell sea deep water (Antarctica)

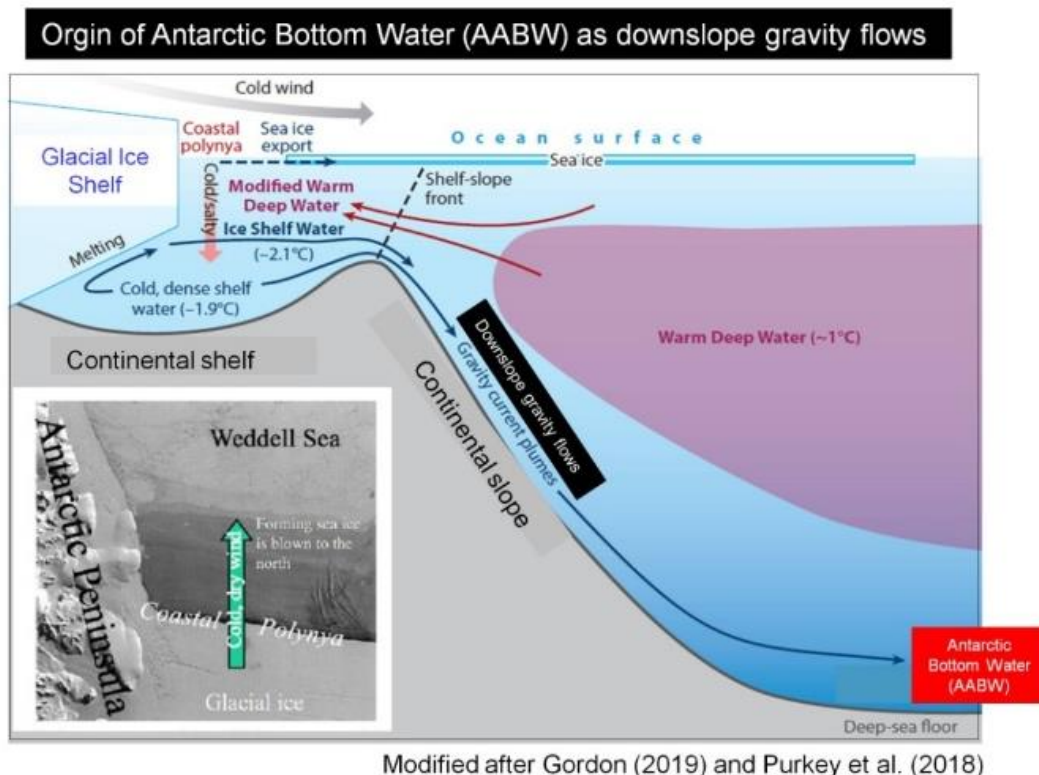


Fig. 36. Schematic of the origin of the Antarctic Bottom Water as downslope gravity flows on the continental slope. Cold shelf water forms through brine rejection in coastal polynyas during ice formation and export. The shelf water flows down the slope in dense plumes, mixing with ambient Warm Deep Water (also referred to as modified Circumpolar Deep Water). Potential temperatures pertinent to Weddell Sea Bottom Water formation are also shown. Modified after Gordon (2001, 2013) and Purkey et al. (2018) with additional labels by G. Shanmugam. Figure from Shanmugam (2020a).

The deep-water component of these water masses that winnow, rework, and deposit sediment on the seafloor for a sustained period of time is called 'thermohaline-induced bottom currents'. They often intersect with downslope turbidity currents or debris flows (Fig. 37) causing 'hybrid flows'. These thermohaline currents are known as 'contour currents' because of their tendency to follow bathymetric contours of continental slope and rise (Heezen et al., 1966). In addition to thermohaline-induced bottom currents or contour currents, there are three other major types, namely wind-driven, tide-

driven, and internal tide-driven bottom currents (Shanmugam, 2016b). The genetic term 'contourite' was originally introduced for deposits of thermohaline-induced contour currents in the deep oceans (Hollister, 1967). Measured current velocities usually range from 1 to 20 cm/s (Hollister and Heezen, 1972); however, exceptionally strong, near-bottom currents with maximum velocities of up to 300 cm/s were recorded in the Strait of Gibraltar (Gonthier et al., 1984). Therefore, contour currents are quite capable of reworking sand and forming traction structures.

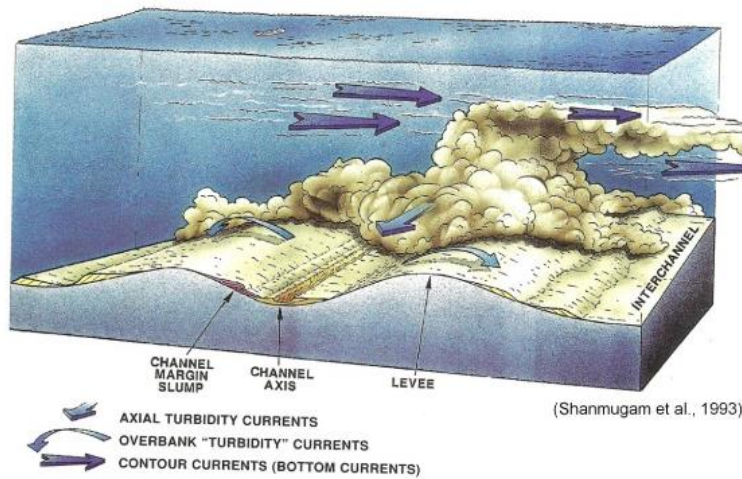
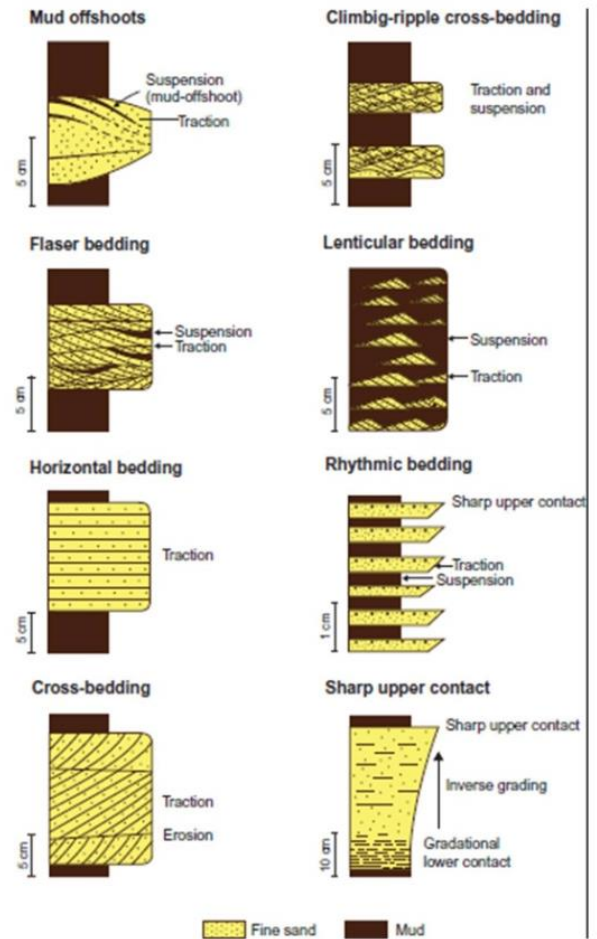


Fig. 37. Conceptual model showing the spatial relationship between downslope turbidity currents and along-slope contour currents. Intersection of these two flows are ideal for generating hybrid flows and their deposits (see Fig. 40), known as hybridites. After Shanmugam et al. (1993), AAPG

Identification

Traction structures (Fig. 38), such as ripple cross laminae and associated sharp upper contacts (Fig. 39), are common in contourites. The importance of traction structures in contourite has been documented worldwide (Hsü, 1964; Hubert, 1964; Klein 1966; Hollister 1967; Mutti, 1992; Shanmugam et al., 1993; Ito, 2002; Martin-Chivelet et al., 2008; Shanmugam, 2008)

Fig. 38. Summary of traction features interpreted as indicative of deep-water bottom-current reworking by all types of bottom currents, namely thermohaline contour currents, wind-driven currents, tidal currents, and baroclinic currents (Shanmugam et al., 1993). Each feature occurs randomly and should not be considered as part of a vertical facies model. From Shanmugam et al., 1993, with permission from AAPG.



Problem

General problems associated with deep-water contourites are discussed by Shanmugam (2016b):

(1) In areas where both downslope sandy debris flows and alongslope bottom currents operate concurrently (Fig. 40A), the reworking of the tops of sandy debrites by bottom currents may be expected. Such a scenario, common on continental margins, could generate a basal massive sand division and an upper reworked division, mimicking a partial Bouma Sequence (Fig. 40B). Such offspring deposits of two flow types, namely sandy debris flows and contour currents (i.e., hybrid flows), are termed as “hybridites.” These genuine hybrid flows should not be confused with the usage of the term “hybrid flows” by Houghton et al. (2009) for flow transformation from one gravity low into another. The distinction is that flow transformation represents a transitional stage between two flows, whereas, hybrid flows represent two hydrodynamically different flows without flow transition. The other difference is that hybrid flows travel at right angle to each other (i.e., downslope vs alongslope (Fig. 40A). Analogous to the

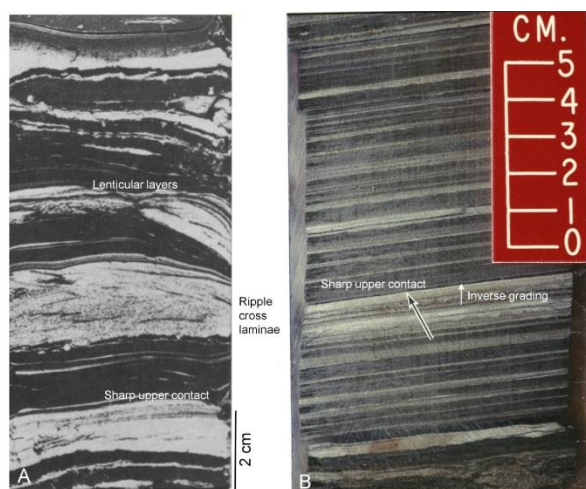


Fig. 39. (A) Core photograph showing well-sorted fine-grained sand and silt layers (light gray) with interbedded mud layers (dark gray). Note sand layers with sharp upper contacts, internal ripple cross-laminae, and mud offshoots. Also note lenticular nature of some sand layers. Pleistocene, continental rise off Georges Bank, Vema 18-374, 710 cm, water depth 4756 m. After Hollister (1967, his Figure VI-1, p. 208) and Bouma and Hollister (1973), reproduced with permission from SEPM. (B) Core photograph showing rhythmic layers of sand and mud, inverse grading, and sharp upper contacts of sand layers (arrow), interpreted as bottom-current reworked sands. Paleocene, North Sea. Figure from Shanmugam (2008).

concept of Houghton et al. (2009), Talling (2013) also proposed a transitional hybrid-flow model, using flow

transformation, between turbidity currents and cohesive debris flows. Hybridites are common in the geologic record and could be easily misinterpreted as turbidites.

According to the Cambridge Dictionary, the term “hybrid” (Etymology: Latin word "Hybrida")

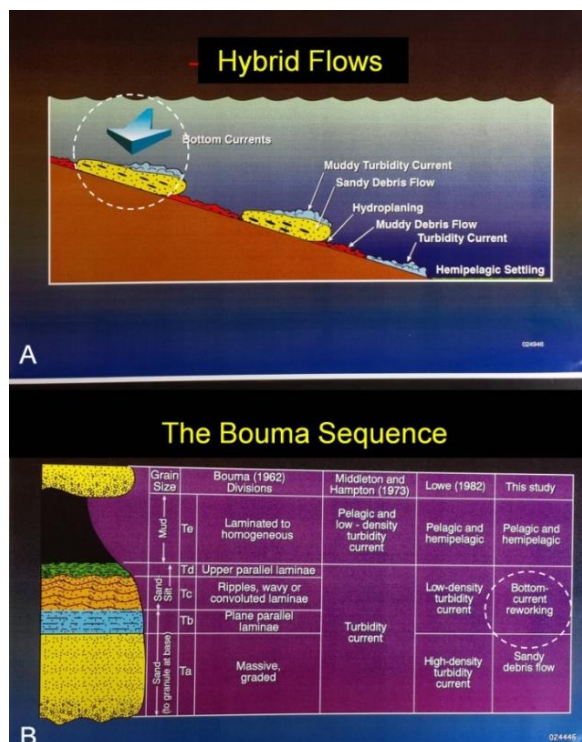


Fig. 40. (A) Conceptual model of genuine hybrid flows showing reworking (white circle) the tops of downslope sandy debris flows by alongslope bottom currents. (B) Such complex deposits would generate a sandy unit with a basal massive division and upper reworked divisions with traction structures (parallel or ripple laminae), mimicking the “Bouma sequence.” (This may explain the upward transition of Ta to Tb, as discussed by Leclair and Arnott (2005). Source: (A) From Shanmugam (2006), with permission from Elsevier. (B) From Shanmugam (1997), with permission from Elsevier.

represents the hybrid offspring byproducts of two different plants, animals, or other entities (<https://dictionary.cambridge.org/dictionary/learner-english/hybrid>, accessed June 2, 2020). In animals, for example, a mule is the hybrid offspring of a male donkey and a female horse. By contrast, a debris flow often transforms downslope into a stratified flow with a lower debris-flow layer and an upper turbidity-current layer (Fig. 29) (see also Norem et al., 1990). In other words, the concept of “hybrid” begins with two different parental species yielding a single hybrid offspring whereas, the concept of “flow transformation”

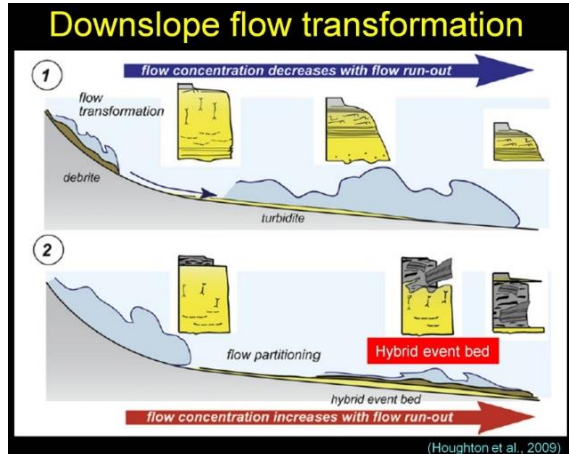


Fig. 41. Diagram showing "hybrid event beds" developed during flow transformation. Note that hybrid event beds do not follow the conventional etymological explanation of the term "hybrid" (see Fig. 42). From Houghton et al. (2009). Additional labels by G. Shanmugam.

begins with a single parent flow that transforms downslope into two sediment-gravity flows. Stratified flows are often called "high-density turbidity currents" (HDTC). Controversies surrounding HDTC were discussed by Shanmugam (1996). Flow transformations cannot be inferred from the final deposit. As noted earlier, we may never resolve this issue of flow transformation because it would be like attempting to establish the previous life history of a human being after reincarnation!

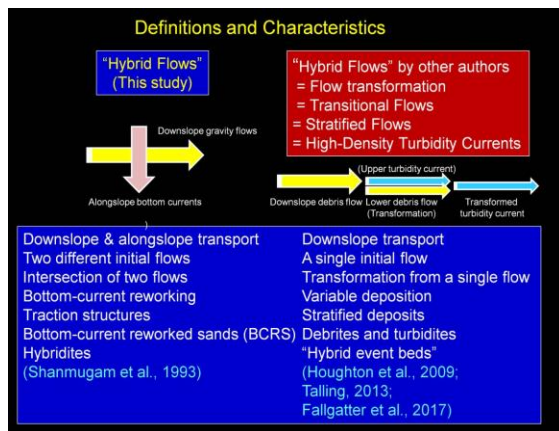
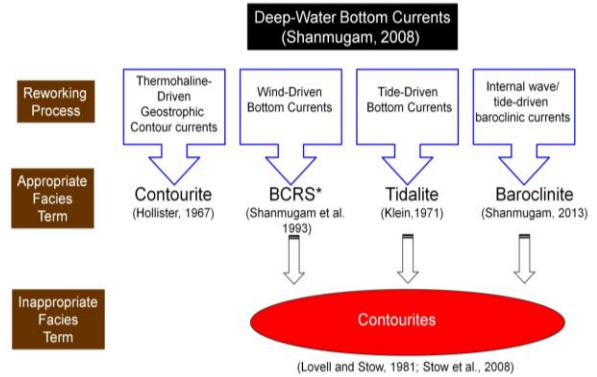


Fig. 42. Left: Genuine hybrid flows as used in this study by following etymology. Right: Equating hybrid flows with flow transformation as used by other authors by ignoring etymology



* BCRS = Bottom-current reworked sands. This general term is appropriate for all four types.

Fig. 43. Four types of bottom currents and their depositional facies. The facies term "contourites" is appropriate only for deposits of thermohaline-driven geostrophic contour currents, but not for deposits of other three types of bottom currents (i.e., wind, tide, or baroclinic). The basic problem began with a false narrative by Lovell and Stow (1981, p. 349) who state that "... the cause of the current is not necessarily critical to the application of the term." In other words, the term "contourites" can be applied to any kind of bottom-current deposit, irrespective of their origin (see also Stow et al., 2008).

(2) Traction structures are ubiquitous in bottom-current deposits of all kinds (Fig. 38). This has created problems in distinguishing deep-sea sediments with traction structures either as contourites (Bouma and Hollister, 1973) or as deposits of wind-driven bottom currents or as deposits of tidal bottom currents (see Shanmugam, 2008).

(3) In contrast to the original definition of contourites by Hollister (1967), Lovell and Stow (1981, p. 349) concluded that contourites can be produced by any kind of bottom current (Fig. 43), irrespective of their origin (i.e., thermohaline, wind, tide, or baroclinic). In maintaining clarity, it is suggested in this article to follow the original definition of contourites by Hollister (1967), which is to restrict the term "contourites" exclusively to the deposits of thermohaline-induced geostrophic contour currents in deep-water environments.

(4) The Gulf of Cadiz (Fig. 35), which served as the type locality for the contourite facie model (Fig. 44), is a highly complicated oceanographic location for studying depositional and erosional aspects of genuine contour currents. Furthermore, the vertical facies model suffers for the following reasons. First, the conventional explanation of the vertical change in grain size of the contourite facies model by changes in current velocity (Fig. 44) fails to consider alternative possibilities, such as increased sediment supply (Mulder et al., 2013)."

Second, the hydrodynamic origin of the five internal divisions is not understood in the Gulf of Cadiz. Third, the presence of internal hiatuses (Fig. 44) argues against the model being the product of a single depositional event. Fourth, bioturbation, considered to be a characteristic feature of contourites, is also common in turbidites and hyperpycnites (Shanmugam, 2018c). Fifth, the currents that operate in the Gulf of Cadiz are not genuine contour currents (Zenk, 2008), they represent a complex transitional type due to mixing and spreading (Shanmugam, 2016b, his Fig. 9.18). The five internal divisions (C1, C2, C3, C4, C5) in the model are not evident in the published core details from the IODP (Integrated Ocean Drilling Program) Expedition 339 (Shanmugam, 2016b).

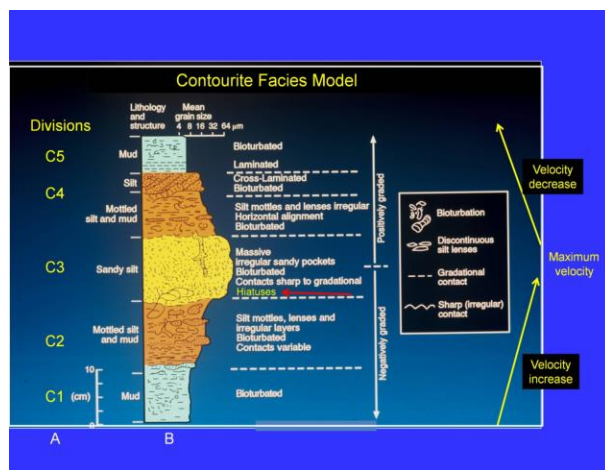


Fig. 44. (A). Revised contourite facies model with five divisions proposed by Stow and Faugères (2008). (B). Original contourite facies model by Gonthier et al. (1984). Note that the original authors of this model did not include the five internal divisions (Gonthier et al., 1984). The most recent version of this model by Faugères and Mulder (2011) contains neither the five internal divisions nor the hiatuses in the C3 division (red arrow inserted in this article). Note the similarity in vertical grain-size trend (inverse to normal grading) between hyperpycnite model (Fig. 8) and contourite model. Note that the ascending five divisions C1 to C5 in Fig. 44A were inadvertently listed in descending order in Shanmugam (2020a, his Fig. 8.17). Also note that the original muddy contourite facies model was published in the same year 1984 by both Gonthier et al. (1984) and by Faugères et al. (1984), Figure 44 B from Faugères et al. (1984), with permission from the Geological Society of America.

(5) Surprisingly, no one could explain the striking similarity in vertical grain-size trend (inverse to normal

grading) between hyperpycnite model (Fig. 8) and contourite model (Fig. 44). Although Mulder et al. (2003) originally proposed the hyperpycnite facies model with inverse to normal grading (Fig. 8), Mulder et al. (2011) critiqued the contourite facies model with identical inverse to normal grading (Fig. 44).

(6) Gonthier et al. (1984, their Fig. 12) originally published the model *without* five internal divisions of C1-C5 and *without* hiatus at the bottom of the sandy interval (C5) in the middle (Fig. 44B). Stow and Faugères (2008, their Fig. 13. 9) published the model *with* five internal divisions of C1-C5 and *with* hiatus at the bottom of the sandy interval (C5) in the middle (Fig. 44A). One wonders as to why it took 24 years for Stow and Faugères (2008) to recognize five internal divisions and hiatus, if these features have been an integral part of contourite facies since its emplacement?

(7) Stow and Smillie (2020) proposed large-scale cross bedding in medium- to coarse sands for “The sandy contourite family” based on the study of Brackenridge et al. (2018). However, Brackenridge et al. (2018) did not document large-scale cross bedding in contourite sands. Stow and Smillie (2020) may prove to be correct because the likelihood of developing large-scale cross bedding by bottom currents is much greater than by turbidity currents.

(8) Stow and Smillie (2020, their Fig. 13) proposed base-cut-out contourites and top-cut-out contourites. Walker (1965) originally applied this “cut-out” logic to the Bouma Sequence. This approach assumes that the entire sequence was present at the time of deposition, but portions were cut-out. If this were true, one could assume anything to arrive at a desired interpretation, such as turbidite, contourite, tidalite, or seismite! Process interpretations must be based on observations and not on assumptions. In practice, it is difficult to verify one's assumptions without objective criteria.

(9) de Castro et al. (2020) reported bottom- current reworked sands (BCRS) in the Gulf of Cadiz (their Fig. 13). Although they reported starved ripples in the sandy intervals, but were unable to document with the empirical photographic evidence due to poor preservation of primary sedimentary structures in unconsolidated sediment intervals. It is important, however, to note that these authors were able to document wispy and lenticular laminae in their Facies 4 of sandy intervals (their Fig. 4), indicating bottom-current reworking in a sand-starved system.

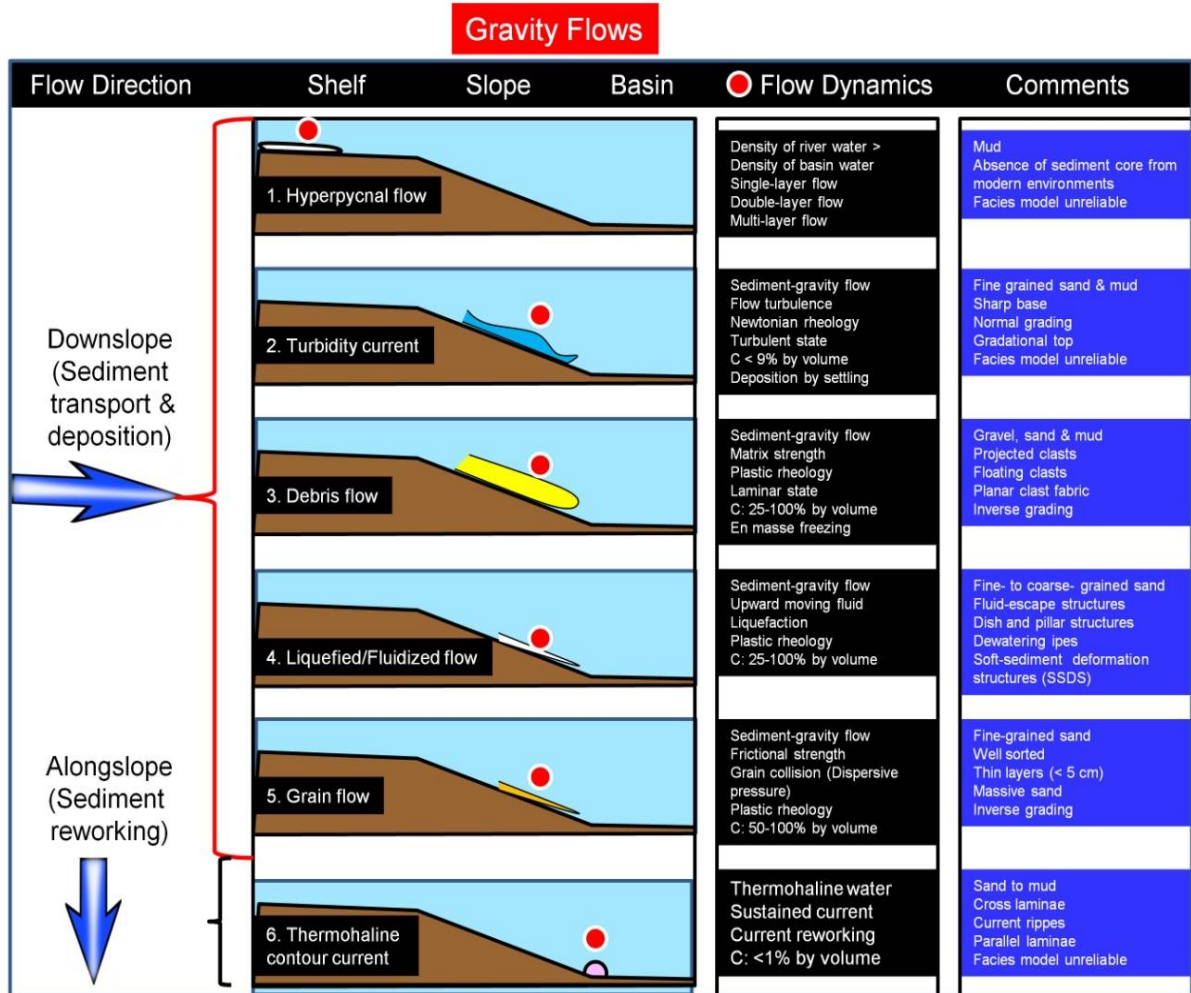


Fig. 45. Summary diagram of six types of gravity flows and their characteristics. Red dot denotes position of flow. From Shanmugam (2020a).

Concluding remarks

Gravity flows constitute the single most important sediment-transport mechanism on land, shelf, slope, and basin environments. They play important roles not only in downslope, but also in alongslope directions (Fig. 45). In terms of transporting large volumes of coarse-grained sediment in the deep sea, debris flows and related mass movements are the most important of all other processes. Also, identification markers of debrites discussed in this review are of value for recognizing them in the ancient sedimentary record because sandy debrites are important petroleum reservoirs worldwide. Of the six density flow types discussed, hyperpycnal flow is the least understood.

Acknowledgements

I thank Prof. G. M. Bhat, Managing Editor of JIAS, for encouraging me to submit this review. I also

thank Prof. F.J. Hernández-Molina and Dr. S. de Castro, both of Royal Holloway, University of London, UK, who helped me with research material from IODP Expedition 339, Gulf of Cadiz. I wish to thank Professor Emeritus R. D. Hatcher, Jr., Department of Earth and Planetary Sciences, The University of Tennessee, Knoxville, TN, for providing a photo of SSDS from Israel. Photo of Elwha River plume was courtesy of Tom Roorda, Roorda Aerial, Port Angeles, WA. A Mobil-funded experimental flume study was carried out at St. Anthony Falls Laboratory (SAFL), University of Minnesota (1996–1998) under the direction of Professor G. Parker to evaluate the fluid dynamical properties of sandy debris flows. Results were published in two major articles (Shanmugam 2000; Marr et al. 2001). I am grateful to the Reliance Industries Ltd. (RIL) in Mumbai (India) for the opportunity to examine cores from the offshore Krishna-Godavari Basin, Bay of

Bengal (Fig. 26)). As always, I am thankful to my wife Jean Shanmugam for her general comments.

References

- Allen, J.R.L. (1970). *Physical Processes of Sedimentation*. Elsevier, New York, p. 239.
- Allen, J.R.L., 1984. *Sedimentary Structures, their Character and Physical Basis*. Elsevier, Amsterdam, I, p. 593 and II, p. 663.
- Allen, J.R.L. (1985a). Loose-boundary hydraulics and fluid mechanics, selected advances since 1961. In: Brenchley, P.J., Williams, P.J. (Eds.), *Sedimentology, Recent Developments and Applied Aspects*, Published for the Geological Society. Blackwell Scientific Publications, Oxford, pp. 7-28.
- Allen, J.R.L. (1985b). *Principles of Physical Sedimentology*. George Allen & Unwin, London, p. 272.
- Bagnold, R. A. (1954). Experiments on a gravity-free dispersion of large solid spheres in a Newtonian fluid under shear. *Proc. R. Soc. Lond. A* 225, 49–63.
- Bagnold, R.A. (1956). The flow of cohesionless grains in fluids. *Phil. Trans. Royal Society of London, Series A. Mathematical and Physical Sciences*, 249, 235–297.
- Bagnold, R.A. (1962). Auto-suspension of transported sediment. *Philosophical Transactions of the Royal Society of London, Series A, Mathematical and Physical Sciences*, 265, 315-319.
- Bates, C.C. (1953). Rational theory of delta formation. *AAPG Bulletin*, 37 (9), 2119–2162
- Bouma, A.H. (1962). *Sedimentology of Some Flysch Deposits: A graphic approach to facies interpretation*. Elsevier, Amsterdam, p. 168.
- Beicher, R. J. (2000). *Physics for Scientists and Engineers*. Orlando: Saunders College.
- Bouma, A.H., Hollister, C.D. (1973). Deep ocean basin sedimentation. In: Emiddleton, G.V., Bouma, A.H. (Eds.), *Turbidites and Deep-Water Sedimentation*. SEPM, Anaheim, CA, SEPM Pacific Section Short Course, pp. 79-118.
- Breien, H., De Blasio, F. V., Elverhøi, A., Nystuen, J. P., and Harbitz, C. B. (2010). Transport mechanisms of sand in deep-marine environments—insights based on laboratory experiments: *Journal of Sedimentary Research*, 80, 975–990.
- Broecker, W.S. (1991). The great ocean conveyor. *Oceanography*, 4, 79–89.
- Coussot, P., Meunier, M. (1996). Recognition, classification and mechanical description of debris flows. *Earth-Sci. Rev.* 40, 209-227.
- Dott Jr., R.H. (1963). Mechanics of subaqueous gravity depositional processes. *AAPG Bulletin*, 47, 104-128.
- Damuth, J.E. Embley, R.W. (1981). Mass-transport processes on Amazon Cone: Western Equatorial Atlantic. *American Association of Petroleum Geologists Bulletin*, 65, 629–643.
- Duda, J.J., Warrick, J.A., Magirl, C.S. (2011). Coastal and Lower Elwha River, Washington, Prior to Dam Removal—History, Status, and Defining Characteristics. In: Duda, J.J., Warrick, J.A., Magirl, C.S., (Eds.), *Coastal Habitats of the Elwha River: Biological and Physical Patterns and Processes Prior to Dam Removal*. U.S. Geological Survey Scientific Investigations Report 2011-5120. Chapter 1.
- Embley, R.W. (1980). The role of mass transport in the distribution and character of deep-ocean sediments with special reference to the north Atlantic. *Marine Geology*, 38, 23–50.
- Enos, P. (1977). Flow regimes in debris flow. *Sedimentology*, 24, 133_142.
- Faugères, J.-C., Mulder, T. (2011). Contour currents and contourite drifts. In: Hüneke, H., Mulder, T. (eds.), *Deep-Sea Sediments, Developments in Sedimentology 63*: Elsevier, Amsterdam, pp. 149-214. Chapter 3.
- Faugères, J.-C., Gonthier, E., Stow, D. A. V. (1984). Contourite drift moulded by deep Mediterranean outflow. *Geology*, 12, 296–300.
- Feng, Z-Z. (2019). "Words of the Editor-in-Chief — Some ideas about the comments and discussions of hyperpycnal flows and hyperpycnites". *Journal of Palaeogeography*, 8
- Fisher, R.V., (1983). Flow transformations in sediment gravity flows. *Geology*, 11, 273-274.
- Forel, F.A. 1885. Les ravins sous-lacustres des fleuves glaciaires. *Comptes Rendus de l'Académie des Sciences Paris*, 101 (16), 725–728.
- Forel, F.A. 1892. *Le Léman: monographie limnologique*. Vol. 1, 543. Lausanne: F. Rouge.
- Galay, V. (1987). *Erosion and Sedimentation in the Nepal Himalaya*. Kefford Press, Singapore, p. 10, 11.
- Gao, S., D. Wang, Y. Yang, L. Zhou, Y. Zhao, W. Gao, Z. Han, Q. Yu, and G. Li. (2015). Holocene sedimentary systems on a broad continental shelf with abundant river input: Process-product relationships. In *River-dominated shelf sediments of east Asian seas*, ed. P.D. Clift, J. Harff, J. Wu, and Y. Qui, vol. 429, 223–259. London: Geological Society, Spl Publ..
- Gee, M.J.R., Masson, D.G., Watts, A.B., Allen, P.A. (1999). The Saharan debris flow: an insight into the mechanics of long-runout submarine debris flows. *Sedimentology* 46, 317-335.
- Gordon, A.L. (2001). Bottom water formation. In *Encyclopedia of Ocean Sciences*, 2nd edition, 334-340. Elsevier
- Gordon, A.L. (2013). Bottom water formation. In *Encyclopedia of Ocean Sciences*, ed. JH Steele, KK Turekian, SA Thorpe, pp. 415–21. San Diego, CA: Academic. 2nd ed. <https://doi.org/10.1016/B978-0-12-409548-9.04019-7>
- Gordon, A.L. (2019). Bottom water formation. *Encyclopedia of Ocean Sciences*, Third Edition, 6, 120-126.
- Hampton, M. A. (1972). The role of subaqueous debris flows in generating turbidity currents. *Journal of Sedimentary Petrology*, 42, 775-793.
- He, B.Z., Qiao, X.F. (2015). Advances and overview of the study on paleo-earthquake events: a review of seismites. *Acta Geologica Sinica (English Edition)*, 89, 1702-1746.
- Heezen, B.C., Ewing, M. (1952). Turbidity currents and submarine slumps, and the 1929 grand banks earthquake. *American Journal of Science*, 250, 849-873.
- Heezen, B.C., Hollister, C.D., Ruddiman, W.F. (1966). Shaping of the continental rise by deep geostrophic contour currents. *Science*, 152, 502-508. Henze, C. (2015). Antarctic Bottom Water in CMIP5 models: characteristics, formation, evolution. University of East Anglia, School of Environmental Sciences, Ph.D. Thesis. Norwich, England, UK. 226 p.
- Hollister, C. D. (1967). *Sediment distribution and deep circulation in the western North Atlantic*, p. 467. Ph.D. dissertation, Columbia University, New York.
- Houghton, P., Davis, C., McCaffrey, W. & Barker, S. (2009). Hybrid sediment gravity flow deposits – Classification, origin

- and significance. *Marine and Petroleum Geology*, 26, 1900–1918.
- Hsü, K. J. (1964). Cross-laminated sequence in graded bed sequence. *Journal of Sedimentary Petrology*, 34, 379–388.
- Hubert, J.F. (1964). Textural evidence for deposition of many western North Atlantic deep-sea sands by ocean-bottom currents rather than turbidity currents. *The Journal of Geology*, 72, 757–785
- Ito, M. (2002). Kuroshio current-influenced sandy contourites from the Plio-Pleistocene Kazusa forearc basin, Boso Peninsula, Japan. In: D.A.V. Stow, C.J. Pudsey, J.A. Howe, J.-C. Faugères, A.R. Viana (eds.). *Deep-Water Contourite Systems: Modern Drifts and Ancient Series*, Seismic and Sedimentary Characteristics Geological Society Memoir vol. 22, pp. 421–432
- Iverson, R. M. (1997). The physics of debris flows. *Reviews of Geophysics*, 35, 245–296.
- Klein, G.D. (1966). Dispersal and petrology of sandstones of Stanley-Jackfork boundary, Ouachita foldbelt, Arkansas and Oklahoma. *AAPG Bulletin*, 50, 308–326.
- Klein, G.D. (1971). A sedimentary model for determining paleotidal range. *Geological Society of America Bulletin*, 82, 2585–2592.
- Klein, G.D. (1975). Resedimented pelagic carbonate and volcanoclastic sediments and sedimentary structures in Leg 30 DSDP cores from the western equatorial Pacific. *Geology*, 3, 39–42.
- Kneller, B. (1995). Beyond the turbidite paradigm: physical models for deposition of turbidites and their implications for reservoir prediction. In: Hartley, A.J., Prosser, D.J. (Eds.), *Characterization of Deep-Marine Clastic Systems*, Geological Society Special Publication No. 94, pp. 31–49.
- Kuenen, Ph. H. (1951). Properties of turbidity currents of high density. In: Hough, J.L. (Ed.), *Turbidity currents and the transportation of coarse sediments to deep water*. A Symposium, SEPM Special Publication 2, pp. 14–33.
- Kuenen, Ph. H. (1953). Significant features of graded bedding. *AAPG Bulletin*, 37: 1044–1066.
- Kuenen, Ph.H. (1966). Experimental turbidite lamination in a circular flume. *J.Geol.* 74, 523–545. Leclair, S. Arnott, R.W.C (2005). Parallel lamination formed by high-density turbidity currents. *Journal of Sedimentary Research*, 75, 1–5.
- Li, S., Du, Y., Zhang, Z., Wu, J. (2008). Earthquake-related soft sediment deformation structures in Palaeogene on the continental shelf of the East China Sea. *Frontiers of Earth Science*, 2(2) : 177–186. <http://dx.doi.org/10.1007/s11707-008-0026-9> (in Chinese with English abstract).
- Lovell, J.P.B. and Stow, D.A.V. (1981). Identification of ancient sandy contourites. *Geology*, 9, 347–349.
- Lowe, D.R. (1975). Water escape structures in coarse grained sediments. *Sedimentology*, 22, 157–204.
- Lowe, D.R. (1976a). Subaqueous liquefied and fluidized sediment flows and their deposits. *Sedimentology*, 23, 285–308.
- Lowe, D.R. (1976b). Grain flow and grain flow deposits. *Journal of Sedimentary Petrology*, 46, 188–199.
- Lowe, D.R. (1979). Sediment gravity flows: their classification, and some problems of application to natural flows and deposits. In: Doyle, L.J., Pilkey, O.H. (Eds.), *Geology of Continental Slopes*, SEPM Special Publication 27, pp. 75–82.
- Lowe, D.R. (1982). Sediment gravity flows: II. depositional models with special reference to the deposits of high-density turbidity currents. *Journal of Sedimentary Petrology*, 52, 279–297.
- Marr, J.G., Harff, P.A., Shanmugam, G., Parker, G. (2001). Experiments on subaqueous sandy gravity flows: the role of clay and water content in flow dynamics and depositional structures. *GSA Bulletin*, 113, 1377–1386
- Masson, D.G., van Niel, B., and Weaver, P.P.E. (1997). Flow processes and sediment deformation in the canary debris flow on the NW African continental rise. *Sedimentary Geology*, 110, 163–179.
- Meckel, T. (2010). Classifying and characterizing sand-prone submarine mass-transport deposits, AAPG Annual Convention and Exhibition, New Orleans, LA, 11–14 April 2010 (Search and Discovery Article #50270 (Posted 16 July 2010) http://www.searchanddiscovery.com/documents/2010/50270meckel/ndx_meckel.pdf (Accessed June 19, 2019).
- Meckel, L.D. III, Shipp, et al. (2011). Reservoir characteristics and classification of sand-prone submarine mass-transport deposits. In: *Mass-transport deposits in deepwater settings*, pp. 423–454. Tulsa, OK: SEPM. Special Publication No. 96.
- Middleton, G.V. (Ed.), (1965). *Primary Sedimentary Structures and their Hydrodynamic Interpretation*. SEPM Special Publication 12, p. 265.
- Middleton, G.V. (1966). Experiments on density and turbidity currents. I. Motion of the head. *Canadian Journal of the Earth Science*, 3, 523–546.
- Middleton, G.V. (1967). Experiments on density and turbidity currents: III. deposition of sediment. *Canadian Journal of Earth Sciences*, 4, 475–505.
- Middleton, G.V. (1970). Experimental studies related to problems of flysch sedimentation. In: Lajoie, J. (Ed.), *Flysch Sedimentology in North America*, Geological Association of Canada Special Paper No. 7, pp. 253–272.
- Middleton, G.V. (1993). Sediment deposition from turbidity currents. *Annual Review Earth Planetary Sciences*, 21, 89–114.
- Middleton, G.V., Bouma, A.H. (Eds.), (1973). *Turbidites and Deep-water Sedimentation*. SEPM Pacific section Short Course, Anaheim, California, p. 157.
- Middleton, G.V., Hampton, M.A. (1973). Sediment gravity flows: mechanics of flow and deposition. In: Middleton, G.V., Bouma, A.H. (Eds.), *Turbidites and Deep-water Sedimentation*, SEPM Pacific section Short Course, Anaheim, California, pp. 1–38.
- Middleton, G.V., Wilcock, P.R. (1994). *Mechanics in the Earth and Environmental Sciences*. Cambridge University Press, Cambridge, p. 459.
- Morales de Luna, T., E.D. Fernández Nieto, and M.J. Castro Díaz. (2017). Derivation of a multilayer approach to model suspended sediment transport: Application to hyperpycnal and hypopycnal plumes. *Communications in Computational Physics*, 22 (5), 1439–1485.
- Mulder, T., J.P.M. Syvitski, S. Migeon, J.-C. Faugères, and B. Savoye. (2003). Marine hyperpycnal flows: Initiation, behavior and related deposits. A review. *Marine and Petroleum Geology*, 20, 861–882.
- Mulder, T., Hassan, R., Ducassou, E., Zaragosi, S., Gonthier, E., Hanquiez, V., Marchès, E., and Toucanne, S. (2013). Contourites in the Gulf of Cadiz: A cautionary note on

- potentially ambiguous indicators of bottom current velocity. *Geo-Marine Letter*, 33, 357–367.
- Mullins, H.T., Neumann A.C., Wilber R.J., Hine A.C., and Chinburg S.J. (1980). Carbonate sediment drifts in the northern Straits of Florida. *AAPG Bulletin*, 64, 1701–1717.
- Mutti, E. (1992). *Turbidite Sandstones*. Agip Special Publication, Milan, Italy, p. 275.
- Parsons, J.D., Whipple, K., Simoni, A. (2001). Experimental Study of the Grain-Flow, Fluid-Mud Transition in Debris Flows. [*The Journal of Geology*, 109, 427–447.
- Phillips, C.J., Davies, T.R.H. (1991). Determining rheological parameters of debris flow material. *Geomorphology*, 4, 101–110.
- Piper, D.J.W., Pirmez, C., Manley, P.L., Long, D., Flood, R.D., Normark, W.R., et al. (1997). Mass transport deposits of the Amazon Fan. In: Flood, R.D., Piper, D.J.W., Klaus, A., Peterson, L.C. (Eds.), *Proceedings of the Ocean Drilling Program, Scientific Results*, 155, pp. 109–143.
- Postma, G. (1986). Classification of sediment gravity-flow deposits based on flow conditions during sedimentation. *Geology*, 14, 291–294.
- Prandtl, L. (1925). Bericht fiber Untersuchungen zur ausgebildeten Turbulenz. *ZAMM*, 5, 136–139.
- Prandtl, L. (1926). Bericht fiber neuere Turbulenzforschung. In: *Hydraulische Probleme*, VDI-Verlag, Berlin, pp. 1–13.
- Purkey, S.G., W.M. Smethie, G. Gebbie, A.L. Gordon, R.E. Sonnerup, M.J. Warner, and J.L. Bullister, (2018), A Synoptic View of the Ventilation and Circulation of Antarctic Bottom Water from Chlorofluorocarbons, *Annual Review of Marine Science*, 10, 503–527.
- Rebesco M, Camerlenghi A, and Van Loon AJ (2008). Contourite research: A field in full development. In: Rebesco M and Camerlenghi A (eds.) *Contourites, developments in sedimentology*. vol. 60, pp. 3–10. Amsterdam: Elsevier.
- Rebesco, M., Hernández-Molina, F.J., Van Rooij, D., Wåhlin, A., (2014). Contourites and associated sediments controlled by deep-water circulation processes: state-of-the-art and future considerations. *Marine Geology*, 352, 111–154.
- Rodine, J.D., Johnson, A.M. (1976). The ability of debris, heavily freighted with coarse clastic material to flow on gentle slopes. *Sedimentology*, 23, 213–234.
- Sanders, J.E. (1965). Primary sedimentary structures formed by turbidity currents and related resedimentation mechanisms. In: Middleton, G.V. (Ed.), *Primary Sedimentary Structures and Their Hydrodynamic Interpretation*, 12. SEPM Special Publication, Tulsa, OK, pp. 192–219.
- Shanmugam, G. (1996). High-density turbidity currents: are they sandy debris flows? *Journal of Sedimentary Research*, 66, 2–10.
- Shanmugam, G. (1997). The Bouma sequence and the turbidite mind set. *Earth- Science Reviews*, 42, 201–229.
- Shanmugam, G. (2000). 50 years of the turbidite paradigm (1950s–1990s): deep-water processes and facies models—a critical perspective. *Marine and Petroleum Geology*, 17, 285–342.
- Shanmugam, G. (2002). Ten turbidite myths. *Earth-Science Reviews*, 58, 311–341.
- Shanmugam, G. (2003). Deep-marine tidal bottom currents and their reworked sands in modern and ancient submarine canyons. *Marine and Petroleum Geology*, 20, 471–491.
- Shanmugam, G. (2006). *Deep-water Processes and Facies Models, Implications for Sandstone Petroleum Reservoirs*, vol. 5. Elsevier, *Handbook of Petroleum Exploration and Production*, Amsterdam, 476 p.
- Shanmugam, G. (2012). New Perspectives on Deep-water Sandstones, Origin, Recognition, Initiation, and Reservoir Quality. In: *Handbook of Petroleum Exploration and Production*, vol. 9. Elsevier, Amsterdam, p. 524.
- Shanmugam, G. (2013). Modern internal waves and internal tides along oceanic pycnoclines, challenges and implications for ancient deep-marine baroclinic sands. *AAPG Bulletin*, 97 (5), 767–811.
- Shanmugam, G. (2015). The landslide problem. *Journal of Palaeogeography*, 4(2), 109–166.
- Shanmugam, G. (2016a). The seismite problem. *Journal of Palaeogeography*, 5(4), 318–362.
- Shanmugam, G. (2016b). The contourite problem. In: R. Mazumder (Ed.), *Sediment provenance*, chapter 9, 183–254. Elsevier.
- Shanmugam, G. (2017a). Global case studies of soft-sediment deformation structures (SSDS): Definitions, classifications, advances, origins, and problems. *Journal of Palaeogeography*, 6(4), 251–320.
- Shanmugam, G. (2017b). The fallacy of interpreting SSDS with different types of breccias as seismites amid the multifarious origins of earthquakes: implications. *Journal of Palaeogeography*, 6(1), 12–44.
- Shanmugam, G. (2017c). Contourites: Physical oceanography, process sedimentology, and petroleum geology. *Petroleum Exploration and Development*, 44(2), 183–216.
- Shanmugam, G. (2018a). The hyperpycnite problem. *Journal of Palaeogeography*, 7 (3), 197–238.
- Shanmugam, G. (2018b). A global satellite survey of density plumes at river mouths and at other environments: Plume configurations, external controls, and implications for deep-water sedimentation. *Petroleum Exploration and development*, 45 (4): 640–661.
- Shanmugam, G. (2018c). Bioturbation and trace fossils in deep-water contourites, turbidites, and hyperpycnites: A cautionary note. In: Special Issue dedicated to George Devries Klein by the Journal of the Indian Association of Sedimentologists (JIAS). *Journal of the Indian Association of Sedimentologists*, Vol. 35, No. 2: 13–32.
- Shanmugam, G. (2019a). Slides, Slumps, Debris Flows, Turbidity Currents, Hyperpycnal Flows, and Bottom Currents. In: *Encyclopedia of Ocean Sciences (Third Edition) Volume 4*, 228–257.
- Shanmugam, G. (2019b). Reply to discussions by Zavala (2019) and by Van Loon, Hüeneke, and Mulder (2019) on Shanmugam, G. (2018, *Journal of Palaeogeography*, 7 (3): 197–238): 'The hyperpycnite problem' *Journal of Palaeogeography*, 8 (3), 408–421.
- Shanmugam, G. (2020). *Mass transport, gravity flows, and bottom currents*. Elsevier, 608 p.
- Shanmugam, G., Benedict, G.L. (1978). Fine-grained carbonate debris flow, Ordovician basin margin, Southern Appalachians. *J. Sedimentary Petrol.* 48, 1233–1240.
- Shanmugam, G., Spalding, T.D., Rofheart, D.H. (1993). Process sedimentology and reservoir quality of deep-marine bottom-

- current reworked sands (sandy contourites): an example from the Gulf of Mexico. *AAPG Bulletin*, 77, 1241-1259.
- Shanmugam, G., Lehtonen, L.R., Straume, T., Syversten, S.E., Hodgkinson, R.J., Skibeli, M. (1994). Slump and debris flow dominated upper slope facies in the Cretaceous of the Norwegian and Northern North Seas (61°-67° N), implications for sand distribution. *AAPG Bulletin*, 78, 910-937
- Shanmugam, G., Bloch, R.B., Mitchell, S.M., Beamish, G.W.J., Hodgkinson, R.J., Damuth, J.E., Straume, T., Syversten, S.E., Shields, K.E. (1995). Basin-floor fans in the North Sea, sequence stratigraphic models vs. sedimentary facies. *AAPG Bulletin*, 79, 477-512.
- Shanmugam, G., Shrivastava, S.K., Das, B. (2009). Sandy debrites and talites of Pliocene reservoir sands in upper-slope canyon environments, Offshore Krishna-Godavari Basin (India): Implications. *J. Sedimentary Res.* 79, 736-756.
- Shepard, F.P., Dill, R.F. (1966). Submarine Canyons and Other Sea Valleys. *Rand McNally & Co.*, Chicago, p. 381.
- Shultz, A.W. (1984). Subaerial debris-flow deposition in the upper Paleozoic Cutler Formation, Western Colorado. *J. Sedimentary Petrol.* 54, 759-772.
- Steel, E., A.R. Simms, J. Warrick, and Y. Yokoyama. 920160. Highstand shelf fans: The role of buoyancy reversal in the deposition of a new type of shelf sand body. *GSA Bulletin*, 128, 1717-1724.
- Shipboard Scientific Party 919940. In: Mountain GS, Miller KG, and Blum P, et al. (eds.) Site 905, Proceedings of ocean drilling program, initial reports, College Station, Texas vol. 134, 255-308. <https://doi.org/10.2973/odp.proc.ir.150.109.1994>.
- Stommel, H. 919580. The abyssal circulation. *Deep-Sea Research*, 5, 80-82.
- Stow, D.A.V. 91985). Deep-sea clastics, where are we and where are we going? In: Brenchly, P.J., Williams, P.J. (Eds.), *Sedimentology, Recent Developments and Applied Aspects*. Published for the Geological Society by Blackwell Scientific Publications, Oxford, UK, pp. 67-94.
- Stow, D.A.V., Shanmugam, G. (1980). Sequence of structures in fine-grained turbidites, comparison of recent deep-sea and ancient flysch sediments. *Sedimentary Geology*, 25, 23-42.
- Stow, D. A. V., Faugères, J. C. (2008). Contourite facies and the facies model. In: Rebesco, M., Camerlenghi, A. (eds.), *Contourites*. Elsevier, Amsterdam, *Developments in Sedimentology* 60, pp. 223-256. Chapter 13.
- Stow, D.A.V., Hunter S, Wilkinson D, and Hernández-Molina F.J. (2008). The nature of contourite deposition. In: Rebesco M and Camerlenghi A (eds.) *Contourites: Developments in sedimentology*. vol. 60, pp. 143-156. Amsterdam: Elsevier. (Chapter 9)
- Stow, D.A.V. Brackenridge R Hernandez-Molina FJ. (2011). Contourite sheet sands: new deepwater exploration target. Abstract American Association of Petroleum Geologists Annual Conference, Houston 2011.
- Su, D.C., Sun, A.P. (2012). Typical earthquake-induced soft sediment deformation structures in the Mesoproterozoic Wumishan Formation, Yongding River Valley, Beijing, China and interpreted earthquake frequency. *Journal of Palaeogeography*, 1, 71e89.
- Talley, L.D. (2013). Closure of the global overturning circulation through the Indian, Pacific, and Southern Oceans: schematics and transports. *Oceanography*, 26 (1), 80-97.
- Talling, P. J. (2013). Hybrid submarine flows comprising turbidity current and cohesive debris flow: Deposits, theoretical and experimental analyses, and generalized models. *Geosphere*, 3 (3), 460-488.
- Teale, T. Young, J.R. (1987). Isolated olistoliths from the Longobucco Basin Calabria, S. Italy. In: Leggett, J.K. and Zuffa, G.G. (eds.) *Advances in marine clastic sedimentology*, pp. 75-88. London, UK: Graham & Trotman.
- Van Loon, A. J. (Tom), Hüeneke, H., and Mulder, T. (2019). The hyperpycnite problem: Comment. *Journal of Palaeogeography*, 8
- Viana, A.R. (2008). Economic relevance of contourites. In: Rebesco M and Camerlenghi A (eds.) *Contourites: Developments in sedimentology*. vol. 60, pp. 493-510. Amsterdam: Elsevier. (Chapter 23).
- Walker, R.G. (1965). The origin and significance of the internal sedimentary structures of turbidites. *Proceedings of the Yorkshire Geological Society*, 35, 1-32.
- Wallis, G.B. (1969). *One-dimensional Two-phase Flow*. McGraw-Hill, New York, p. 408.
- Wang, H., N. Bi, Y. Wang, Y. Saito, and Z. Yang. (2010). Tide-modulated hyperpycnal flows off the Huanghe (Yellow River) Mouth, China. *Earth Surface Processes and Landforms*, 35 (11), 1315-1329.
- Warrick, J.A., A.R. Simms, A. Ritchie, E. Steel, P. Dartnell, J.E. Conrad, and D.P. Finlayson. (2013). Hyperpycnal plume-derived fans in the Santa Barbara channel, California. *Geophysical Research Letters*, 40, 2081-2086.
- Wright, L.D., Nittrouer CA. (1995). Dispersal of river sediments in coastal seas: six contrasting cases. *Estuaries*, 18(3), 494-508.
- Wüst, G. (1936). Schichtung und Zirkulation des Atlantischen Ozeans. Das Bodenwasser und die Stratosphäre: *Duetschen Atlantischen Expedition. Tiefsee. Geologische Rundschau*, 47, 187-195.
- Zavala, C. (2019). The new knowledge is written on sedimentary rocks- a comment on Shanmugam's paper "The hyperpycnite problem". *Jour. of Palaeogeography*, 8, 306-313.
- Zavala, C., (2020). Hyperpycnal (over density) flows and deposits. *Journal of Palaeogeography* (2020) 9:17. <https://doi.org/10.1186/s42501-020-00065-x>
- Zavala, C., and M. Arcuri. (2016). Intrabasinal and extrabasinal turbidites: Origin and distinctive characteristics. *Sedimentary Geology*, 337, 36-54.
- Zenk, W. (2008). Abyssal and contour currents. In: Rebesco M and Camerlenghi A (eds.) *Contourites: Developments in sedimentology*. vol. 60, pp. 37-57. Amsterdam: Elsevier. (Chapter 4).
- Zou, C., Wang, L., Li, Y., Tao, S., and Hou, L. (2012). Deep-lacustrine transformation of sandy debrites into turbidites, pper Triassic, Central China. *Sedimentary Geology* 265 266, 14.

Provenance, tectonics and palaeoenvironment of Mesoproterozoic Saundatti Quartzite Member of Kaladgi Basin, India: a petrographic view.

Purushottam Verlekar and Mahender Kotha

School of Earth, Ocean and Atmospheric Science, Goa University
Email: geology.purushottam@unigoa.ac.in

Abstract

The Kaladgi basin, one of the important Proterozoic Sedimentary basins of Peninsular India, exposes a thick sequence of Proterozoic succession composed of a variety of lithologies with predominance of arenaceous rocks interbedded with carbonate sediments at different stratigraphic levels. The present work focuses mainly on understanding the sedimentological nature and diagenetic character of the lower part of the Lokapur Sub-group rocks that are exposed in and around Savadatti Town, Belagavi District of Karnataka. These rocks are mainly composed of arenite sequences of varying grain size. The clastic succession comprises of sandstones with minor conglomeratic facies at the lower part of the sequence. An attempt was made to identify the petrographic character of the sandstones to understand the provenance and depositional environments. Our study suggests that the coarse clastic conglomerates are essentially of polymictic type and the sandstones are sub-mature to mature (mineralogically), medium to coarse grained and can be categorized mainly into lithic/feldspathic and quartz arenites. Minor occurrence of feldspars as the framework constituent also suggests that the rocks have undergone considerable transport. However, with their variable degree of alteration (from fresh to partially to completely altered grains) associated with textural maturity and nature of quartz point towards the possibility of derivation of these sediments from two different sources. Palaeocurrent data that indicate a NW palaeoslope suggest the derivation of sediments from a variety of granitic and gneissic crystalline complexes occurring along the basin margin. The maturity of the sandstones (quartz arenites) is attributed to the recycling and re-working of the older sediments. Analysis of textural parameters of these rocks point towards deposition under beach environments. The lack in preservation of much amount of feldspar in these sandstones indicates a remote source and relatively dry-arid climate of the source area.

Keywords: Proterozoic, Saundatti Quartzite Member, Petrography, Kaladgi Basin, Lithic Arenites, Diagenesis

Introduction

The Kaladgi is one of the major Proterozoic basins (Purana) in northern Karnataka region of India comprising of thick clastic and non-clastic rock succession known as the Kaladgi Supergroup (Jayaprakash et al., 1987). The succession is divided into Older Bagalkot Group and Younger Badami Group and the two are separated by an angular unconformity (Vishwanathiah, 1968). Rb–Sr isotopic age calculated with respect to CHUR for the shales from Bagalkot Group suggested that their deposition was younger than 1800 ± 100 Ma (Padmakumari et al., 1998 and Sambasiva Rao et al., 1999). Various structural, sedimentological and aspects related to evolution of this basin have been studied by previous workers. However, detailed petrographic work from individual formations from this succession has not been reported. Petrographic work is an integral part of any comprehensive sedimentological study and is of paramount importance for studying provenance,

palaeoclimate and tectonics (Basu *et al.*, 1975; Dickinson and Suczek, 1979; Zuffa, 1980; Dickinson, 1985; Ingersoll et al., 1984; Uddin and Lunberg, 1998; Das 2008, ; Das and Sarma, 2009; Bokanda et al., 2018; Chima *et al.*, 2018; Chaudhuri *et al.*, 2018, Chaudhuri *et al.*, 2020).

The present study is focused primarily on petrography of Saundatti Quartzite Member of Ramdurg Formation exposed in and around Saundatti town (It. 15.7522° N, lon. 75.1253° E), Karnataka along the southern margin of Kaladgi basin. The sandstones under investigation do not exhibit wide variation in their composition and texture but the minor changes have been critically studied to identify petrographic changes in relation to changing environmental dynamics. Besides, the analysis of time or environment related changes; a major emphasis of the present study is directed towards provenance studies, recognition of palaeoclimate and the tectonic regime. The most of the Saundatti Quartzite Member is exposed mainly in the hill sections in and

around Savadatti town as outliers and extending northward up to Ramdurg. Rocks of this unit include slightly deformed Quartz arenite and conglomerates containing Jasper clasts demarcating the basin boundary of the Bagalkot Group and forming a marker horizon due to its prominent geomorphic expression and topographic character.

Geology of the Study Area

The Kaladgi basin is an epicratonic basin formed due to trough faulting. Presently the basin is exposed in an area of about 8000 km² whereas, the estimated maximum area is 20,000 km² (Kale 1991). The basin is nearly 200 km long and about 100 km wide (Fig.1). The maximum aggregate stratigraphic thickness is ~4500 m (Jayaprakash et al., 1987; Radhakrishna and Vaidyanadhan, 1994). Metasediments, granitic gneisses and schistose rocks form the basement for these sedimentary deposits. In western and northern parts, the sediments are concealed

beneath the lava flows of Deccan traps. At places where the lava flows are removed due to weathering the exposures are seen to occur as inliers within trappean rocks. Stratigraphically, the Kaladgi Supergroup is divided into older Bagalkot Group and younger Badami Group separated by an unconformity (Kale and Phansalkar, 1991). Rock types in this basin include conglomerate, sandstone and shale (argillite) as clastic facies and non clastic facies is represented by limestone and dolomite.

The basal Ramdurg Formation comprises partially metamorphosed beds of sandstones with conglomerate at the base and shale as subordinate constituent. The succession unconformably overlies gneisses, granitoids and, schists of Hungund schist belt of the Archaean basement complex. This formation is classified into three members based upon their lithological character. The Salgundi conglomerate is oldest in the sequence followed by Saundatti quartzite and Manoli argillite members. The detailed stratigraphic column of the area is given in Table 1.

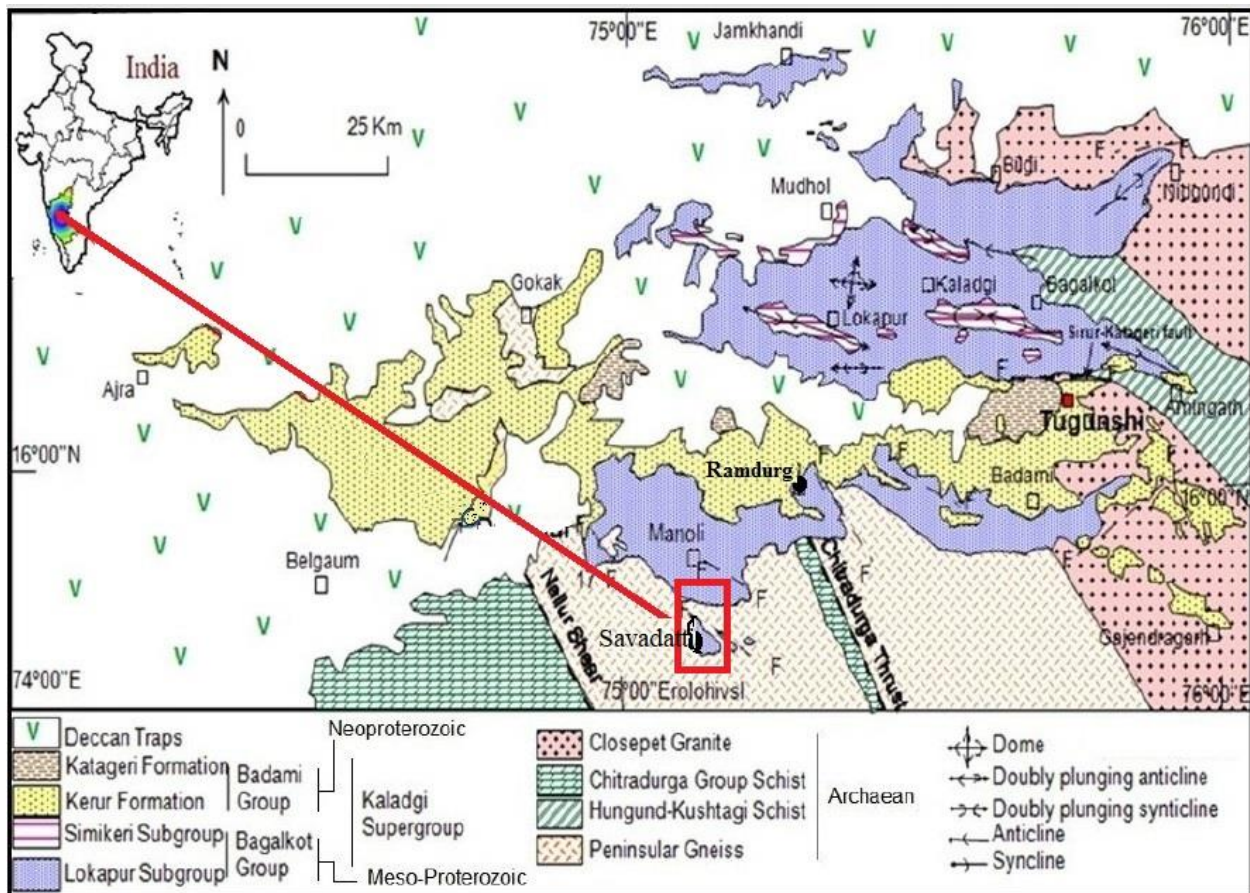


Figure 1: Geological Map of the study area (after Jayaprakash et al., 1987; Dey et al., 2009)

Table 1: Generalized Stratigraphic succession of Kaladgi Supergroup. (Jayaprakash et al., 1987)

	Group	Subgroup	Formation	
Kaladgi Supergroup	Badami Group		Katageri	
			Kerur	
	<i>Angular Unconformity</i>			
	Bagalkot Group	Simikeri Subgroup		Hosakatti
				Arilkatti
				Kundargi
		<i>Disconformity</i>		
		Lokapur Subgroup		Yadhalli
				Muddapur
				Yendigeri
				Yargatti
				Ramdurg
		<i>Erosional unconformity</i>		
	Archean: Granitoids, gneisses, metasediments			

Field Observations

The outcrops exposed around Savadatti, Hooli and Ramdurg representing the Saundatti quartzite member are selected for the present study. The rocks exposed here directly overly the basement of Precambrian gneissic complex. The Saundatti quartzite beds are gently dipping towards east and display a variety of well-preserved primary sedimentary depositional structures represented by imbrications, ripple marks and cross-bedding. Thickly bedded planar parallel bedding is characteristic bedding observed in these rocks (Figure 2b). Thickness of beds varies from 30 to 50 cm. The bedding plane is smooth, parallel and sharp planar. Further examination of bedding plane revealed presence of ripple marks (Figure 2c). These are wave formed symmetrical ripples with straight and bifurcating crests. Ripple index was estimated at 3-5, having more rounded troughs and flattened crests. A tangential cross-stratification structure was better

exposed at a stream cut section (figure 2d). The co-set thickness as measured is around 40cm with a set thickness of 20cm. The cross laminae are 5-10 cm thick. The palaeocurrent analyses of the cross-bedding structures suggest northwesterly (310⁰) direction of the sediment transport.

Methodology

Petrographic study has been made in thin sections prepared from the sandstone samples collected from field outcrops. A total of 50 samples were collected from surface outcrops of Savadatti town and its outskirts which belong to Saundatti quartzite member of lower Kaladgi sequence. In all 25 thin sections were prepared representing entire ~380 m thick section and all were subjected to detailed petrographic analysis with optical microscopy. Around nine hundred points were counted for mineralogical analyses on 16 sandstone samples using conventional point counting method following Dickinson and Suczek (1979) and Dickinson *et al.* (1983). The grain roundness was measured by visual comparison of all the grains used in size measurement with the standard chart of Powers (1953). SEM analyses of selected samples were made to study textural parameters and grain to grain relationship in selected samples. The framework constituents of these rocks are quarts which include monocrystalline (Qm) as well as polycrystalline (Qp) varieties, feldspars and lithic fragments are also seen as part of framework constituents in less amounts. The volumetric percentages of the various framework components as identified and measured under the microscope for use in interpretation of provenance and depositional environments are presented in Table 2. The recalculated data from Table 2 for classification is given in Table 3. Grain size was analyzed by measuring apparent long axes of 100–150 grains per thin section using Digimizer software. Grain size parameters viz., mean size (Mz), standard deviation, skewness and kurtosis were calculated by the standard method of moments (Krumbein *et al.*, 1983) as given in Table 4.

Mineralogical classification, framework composition, tectonic setting and provenance were interpreted based on the plotting of modal analysis data in triangular diagram of Folk (1980), James *et al.*, (1986), Dickinson and Suczek (1979), Dickinson *et al.* (1983) and Dickinson (1985). Suttner and Dutta (1986) plot has been used for understanding the Palaeoclimate.



Table 2: Modal analysis of studied samples of Saundatti quartzite member

Sample No.	Sample ID	Quartz		Total	Feldspar	Lithic Fragments
		Monocrystalline	Polycrystalline			
1.	RDG-1	50	8	58	5	9
2.	RDG-2	70	6	76	5	2
3.	HOO-1	20	3	23	0	2
4.	HOO-1B	15	2	17	0	0
5.	HOO-2A	43	2	45	0	14
6.	HOO-2B	44	2	46	0	4
7.	HOO-2C	52	0	52	0	2
8.	HOO-2D	72	0	72	2	11
9.	HOO-3	70	1	71	0	2
10.	SAU-5	48	1	49	0	3
11.	SAU-5B	56	1	57	3	4
12.	SAU-5C	62	2	64	1	4
13.	SAU-6A	55	9	64	1	4
14.	SAU-6B	78	2	80	0	7
15.	SAU-8A	35	4	39	0	7
16.	SAU-7	30	1	31	0	4

Table 3: Recalculated tabulated data from modal analysis

Sample no.	Sample ID	Data for QFR diagram			Data for QmFRt diagram		
		Q	F	Rt	Qmt	F	Rt
1.	RDG-1	82	6	12	78	8	14
2.	RDG-2	91	6	3	91	8	1
3.	HOO-1	92	0	8	91	0	9
4.	HOO-1B	100	0	0	100	0	0
5.	HOO-2A	76	0	24	64	0	36
6.	HOO-2B	92	0	8	92	0	8
7.	HOO-2C	96	0	4	93	0	7
8.	HOO-2D	85	2	13	87	2	11
9.	HOO-3	97	0	3	97	0	3
10.	SAU-5	94	0	6	94	0	6
11.	SAU-5B	90	4	6	93	3	4
12.	SAU-5C	93	1	6	94	1	5
13.	SAU-6A	93	1	6	93	2	5
14.	SAU-6B	92	0	8	88	0	12
15.	SAU-8A	85	0	15	83	0	17
16.	SAU-7	89	0	11	86	0	14

Table 4: Detailed textural data of sandstone samples of Saundatti quartzite member.

Sr. no.	Sample Id	Mean Mz	Median	Standard deviation σI		Skewness SKI		Kurtosis KG	
1.	HOO-1B	0.91	0.81	0.54	MWs	0.48	Fine Skewed	0.41	Leptokurtic
2.	HOO-2A	1.66	1.30	0.56	MWs	-0.36	Very Coarse Skewed	-0.72	Platykurtic
3.	HOO-2C	1.82	1.82	0.31	Very Ws	-0.075	Near symmetrical	0.30	Platykurtic
4.	HOO-2D	1.56	1.56	0.42	Ws	-0.31	Very Coarse Skewed	0.76	Platykurtic
5.	HOO-3	1.23	1.19	0.35	Ws	0.11	Near symmetrical	0.13	Platykurtic
6.	KDG-1A	1.54	1.59	0.43	Ws	-0.41	Very Coarse Skewed	-0.73	Very platykurtic
7.	RDG-2	1.02	0.98	0.61	MWs	-0.22	Coarse Skewed	-0.16	Very platykurtic
8.	SAU-1	1.60	1.51	0.51	MWs	-0.34	Coarse Skewed	-0.67	Very platykurtic
9.	SAU-2	2.06	2.05	0.29	Very Ws	0.01	Near symmetrical	-0.20	Very platykurtic
10.	SAU-5	1.49	1.44	0.47	Ws	0.31	Fine Skewed	-0.09	Very platykurtic
11.	SAU-5C	1.15	1.16	0.33	Very Ws	-0.02	Near symmetrical	0.23	platykurtic
12.	SAU-6A	1.11	1.07	0.36	Very Ws	0.36	Very Coarse Skewed	-0.54	Very platykurtic
13.	SAU-6B	1.37	1.38	0.34	Very Ws	0.08	Near symmetrical	-0.038	Very platykurtic
14.	SAU-8A	0.99	0.99	0.55	M Ws	-0.21	Coarse Skewed	0.46	platykurtic
15.	SAU-8B	1.24	1.87	0.54	M Ws	0.24	Coarse Skewed	-0.87	Very platykurtic

(Mz-mean size, σI -standard deviation, SKI-skewness, KG-kurtosis, Ws- Well sorted, MWs- Moderately well Sorted)

Petrography

Petrographic analyses of sandstones were carried out for mineralogical composition, diagenesis and classification. The analyzed sandstone samples revealed that these sandstones from Saundatti quartzite member are medium to coarse grained, sub-angular to sub-rounded, moderate to moderately well sorted. Long grain contacts dominate while sutured and concavo-convex contacts are also observed in these rocks (Table 5; Figure 3a, 3b) with subordinate amount of matrix. Mineralogical constituents of this member thus identified are primary detrital constituents which include variety of quartz and feldspars, lithic fragments, matrix and cement. Quartz is the most abundant grain type and it is identified based on number of distinctive features like undulose extinction, strained nature of crystal shape. Sandstone were classified using Folk (1980) scheme (Figure 4). The rocks belonging to Saundatti quartzite member are mainly sublitharenites with subordinate amounts of quartz arenites and have average framework composition of $Q_{90.43}F_{1.25}R_{8.32}$. The framework grains are mainly quartz, and less frequently rock fragments, feldspars and heavy minerals. Framework constituents make up the dominant part of the rock and detrital material making up matrix is subordinate.

Quartz is the most abundant framework grain in these sandstones constituting an average 90.43% of the rock volume. The quartz grains are commonly subangular to sub-rounded in shape (Figure 3a). Most of these quartz grain show multiple deformation features (Figure 3b, 6a). Among quartz grains, monocrystalline quartz (Qm) is dominant (94.78%) over polycrystalline quartz (Qp) of 5.22%. Most of the Qm grains show undulatory extinction (Figure 5a). Some of these grains contain mineral inclusions (Figure 5b). Long and sutured contacts are common (Figure 5a, 5c) and are caused by compaction and pressure solution. Few sections also display concavo-convex contacts due to increased compaction. Some of these grains show corroded margins (Figure 5c) while some quartz grains show syntaxial overgrowths (Figure 5d). Heavy minerals (viz. zircon, sphene, and tourmaline) occur as accessories. Quartz grains which show two or more units under cross nicols but look like a single grain under polarized light are called as polycrystalline quartz (Conolly, 1965). Among these, composite quartz and pressure quartz are the two main varieties identified in these rocks. Grains of composite quartz are identified by the presence of two or more internal quartz grains.

They show a single grain outline under polarized light while the internal units are distinctly visible under cross-nicols (Figure 5d). Pressure quartz is identified by the presence of internal elongated units of different optical orientation which gives it a mosaic like appearance. The grains show extreme undulose extinction (Figure 5e). The internal boundaries are smooth and units show both unit and undulose extinction.

Feldspar grains are present only in few thin sections (Table 2). They are subangular and devoid of inclusions. Both K-feldspar and plagioclase are present in sandstones. Plagioclase feldspar is characterized by lamellar twinning (Figure 5f) while the orthoclase is untwined and shows cloudy appearance. Few grains of feldspar are altered indicating restricted chemical weathering in these rocks. Absence of feldspars in most of the thin sections indicates an extensive alteration with enhanced chemical weathering and/or recycling.

Lithic or rock fragments are the pieces of disintegrated source rock and are of immense importance in provenance study along with tectonic setting of the source area. Rock fragments are recorded in majority of samples from Saundatti quartzite member (Table 2). These include chert and metamorphic rock fragments (Figure 5g & h). They range from 0 to 24 % with an average of 8.31%. Volcanic rock fragments are absent in the Saundatti quartzite member. Generally, these lithic fragments are subrounded however, few rounded-clasts are also observed.

Heavy minerals form a minor constituent of these sandstones that include sub rounded grains of zircon, sphene, chloritoids, tourmaline (Figure 6 a,b,c,d). Grains of heavy minerals are very fine and show moderate abrasion. The assemblage is suggestive of mixed sedimentary and metamorphic source. Siliceous cement is predominant. Cementing material occurs as pore fillings of silica, clay and iron oxide (Figure 7a). Kaolinite and chlorite are the main Clay mineral species observed in the sandstones. Kaolinite dominates over chlorite in terms of abundance. Samples as observed under SEM show kaolinite occupying the intergranular spaces between framework grains (Figure 7b). Kaolinite is present in variety of forms which include vermiform (Figure 7c), book shaped, well crystallized and blocky forms (Figure 7d). Predominance of kaolinite with little or no illite indicate the sedimentary origin under continental conditions (Lonnie, 1982; Tsuzuki and Kawabe, 1983, Amer *et al.*, 1989).

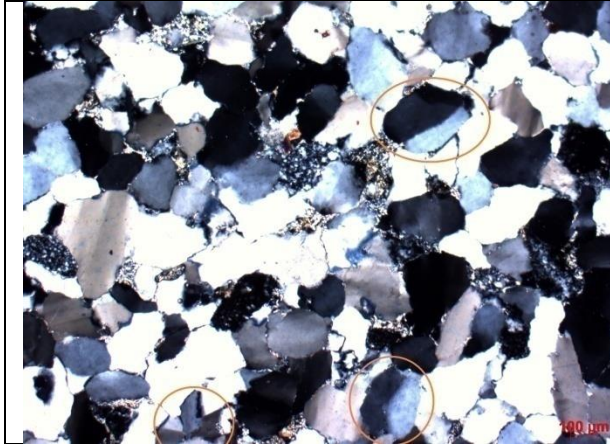


Figure 5a: Grains of monocrystalline quartz exhibiting undulose extinction, also note long and sutured grain contacts



Figure 5b: Zoning observed in crystal of zircon



Figure 5c: Corroded grain boundaries filled by clay minerals precipitated secondary minerals

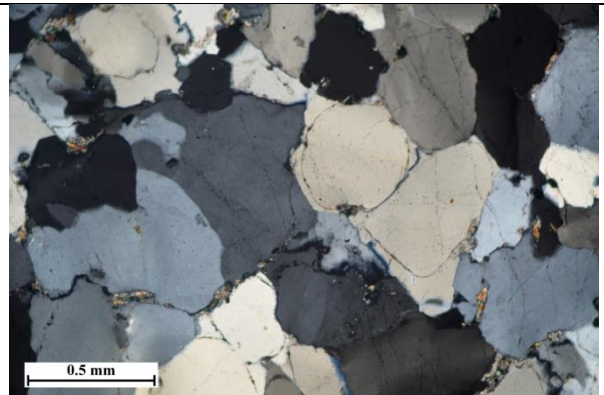


Figure 5d: Quartz overgrowth around detrital grains. Original grain boundaries can also be seen

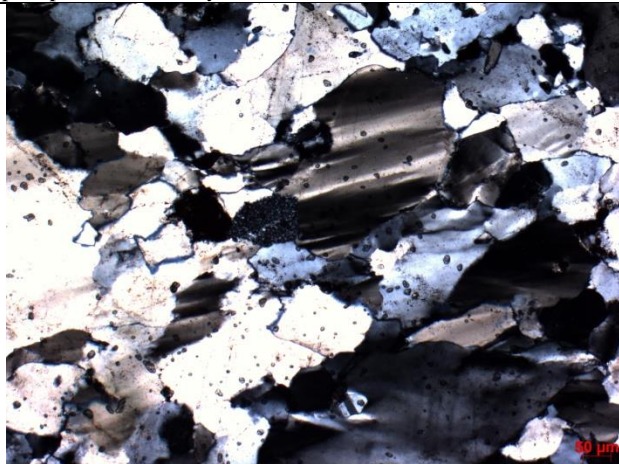


Figure 5e: Extreme undulose extinction shown by pressure quartz

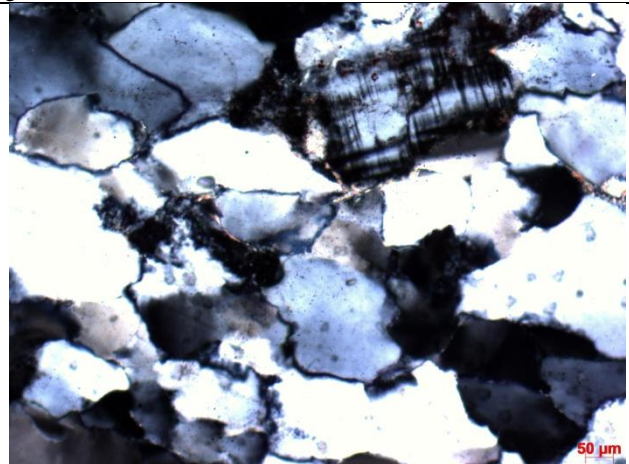


Figure 5f: Grain of plagioclase feldspar showing lamellar twinning

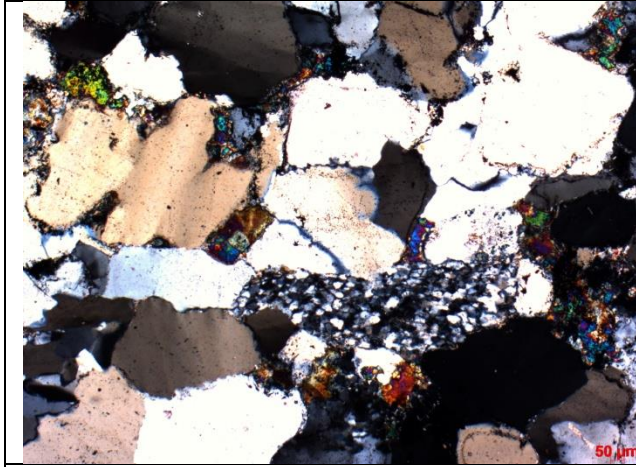


Figure 5g: Metamorphic rock fragment as a part of framework constituent

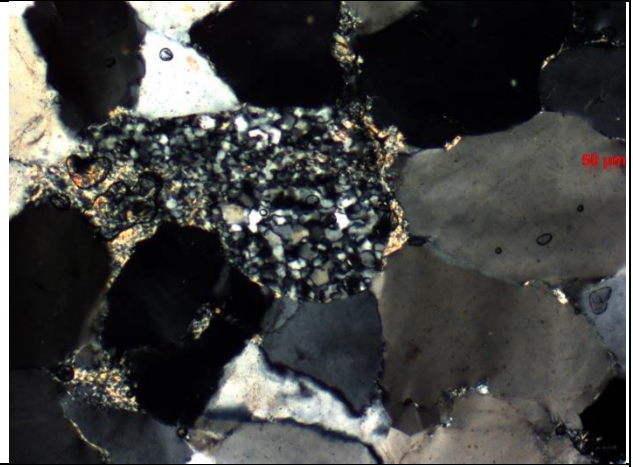


Figure 5h: Metamorphic rock fragment showing alteration

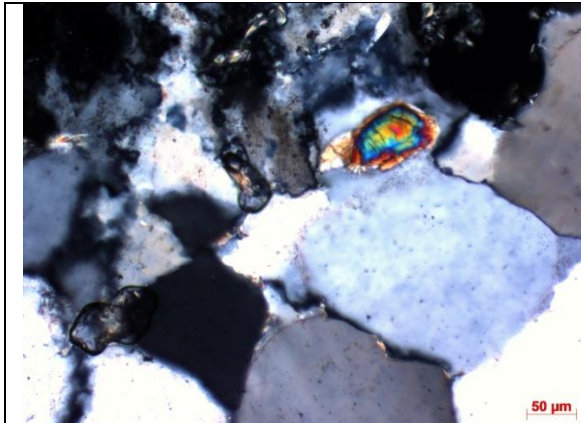


Figure 6a: Zoning observed in crystal of zircon



Figure 6b: Pale green, characteristic wedge shaped grain of sphene

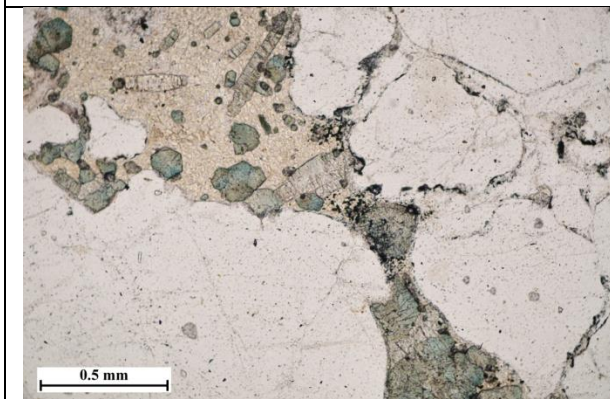
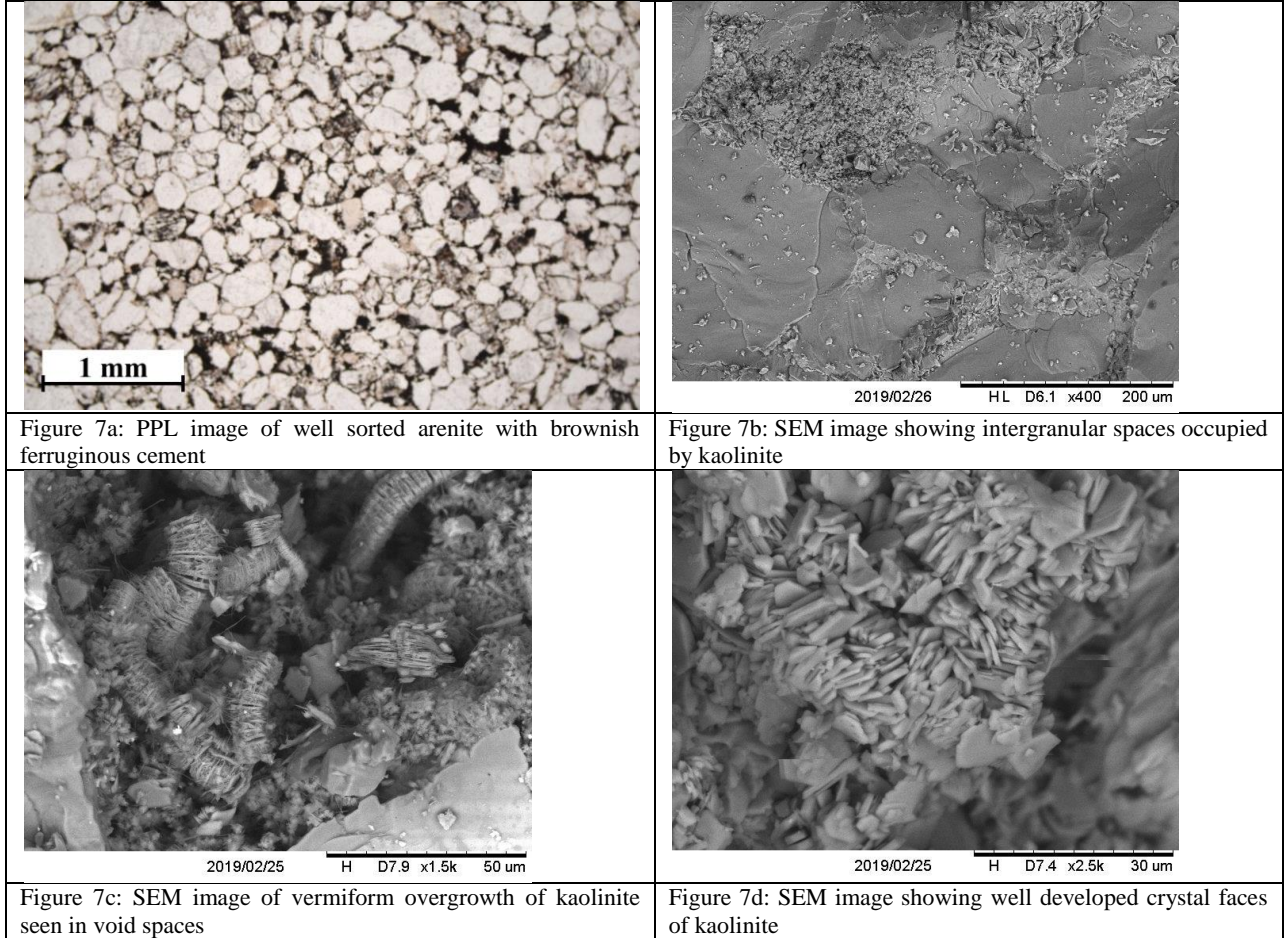


Figure 6c: Distinct greenish to yellow coloured specs of chloritoids, note flowage around quartz grains



Figure 6d: Slender prismatic habit of tourmaline grain



Tectonic Setting and Provenance

The petrographic study reveals that the studied rocks are characterized by higher proportion of monocrystalline quartz followed by polycrystalline quartz, considerable number of lithic fragments and subordinate feldspar. Much work has been done on the composition of sandstone and its implications on the tectonic setting of a depositional basin. Important amongst these are the works of Crook (1974), Young (1976), Dickinson and Suczek (1979), Mack (1984), Dickinson (1985) Trop and Ridgway (1997). The key relationship between provenance and basins are governed by plate tectonics which ultimately controls the distribution of different types of sandstones (Dickinson and Suczek, 1979).

To interpret the tectonics of the source area, mineral composition of the samples collected from Saundatti quartzite member were plotted on Qt-F-L and Qm-F-Lt ternary diagrams of Dickinson et al. (1983) (Fig 4 c, d). On the QtFL diagram of Dickinson and Suczek (1979), most of the studied samples fall within recycled orogen field and few fall in craton interior

field. The framework grain properties like subordinate presence of feldspars, polycrystalline quartz and rock fragments of studied units are consistent with those of sediments deposited in a recycled orogen setup. Such a craton type reflects mature sandstone derived from relatively low lying granitoid and gneissic sources, supplemented by recycled sands from associated platform or passive margin basins (Dickinson et al., 1983). Low percentage of unstable grains, the dominance of monocrystalline quartz and alteration of feldspar grains suggests that the source area underwent a long period of intensive chemical weathering in a warm humid climate (Pettijohn et al., 1987).

It is known that the ratios of feldspar and lithic fragments to polycrystalline quartz or total quartz are sensitive indicator of climatic signature of the sandstones (Young et al., 1975 and Basu, 1985). Following Suttner and Datta (1986) data was plotted in QFR diagram and plotted points indicate a metamorphic source in a sub humid to humid conditions (Fig 4b).

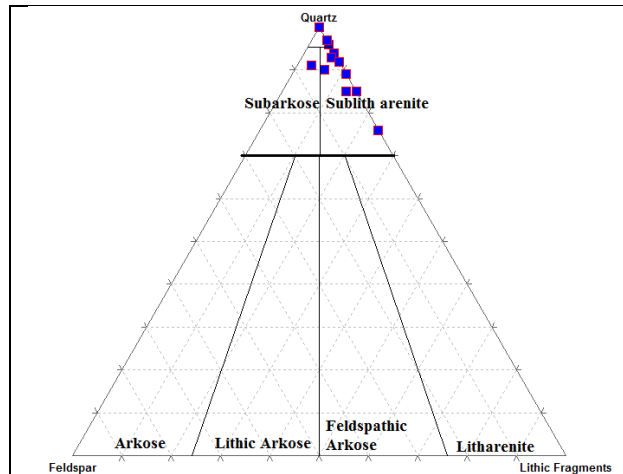


Figure 4a: Classification of studied sample as per Folk (1980) scheme

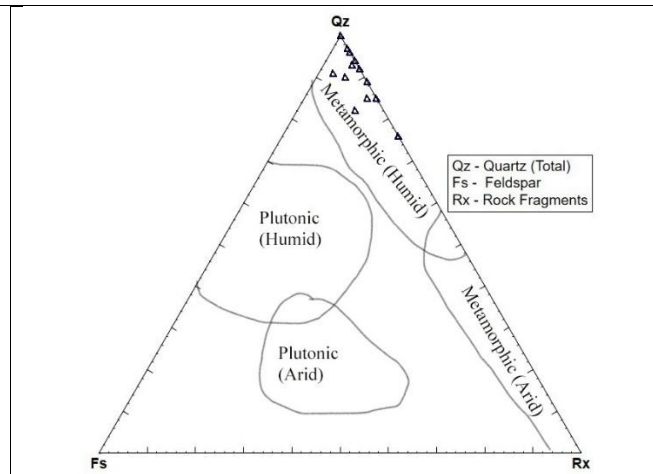


Figure 4b: The effect of source rock on the composition after Suttner et. al. (1981)

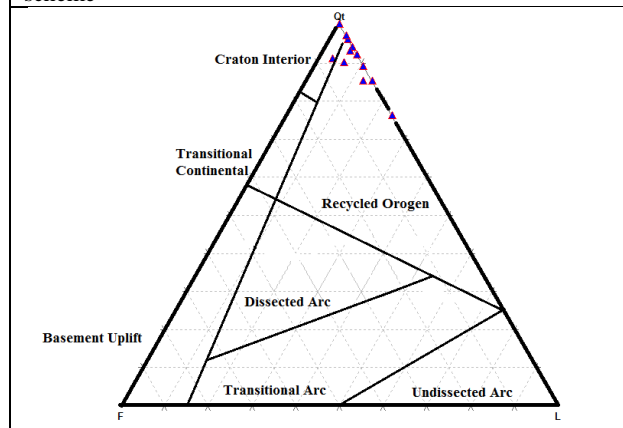


Figure 4c: Tectonic setting discrimination diagram based on Qt-F-L after Dickinson and Suczek (1979)

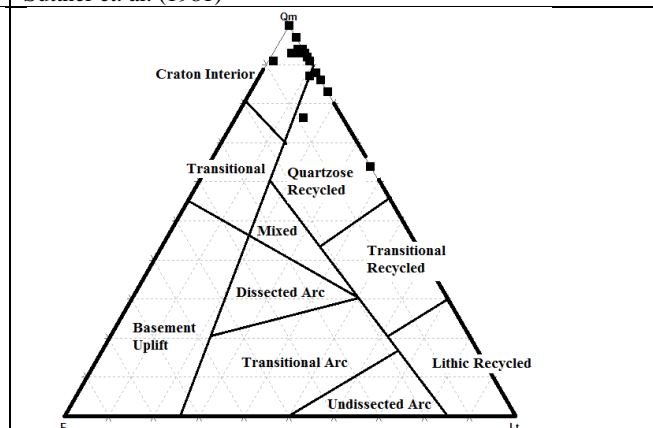


Figure 4d: Qm-F-Lt ternary diagram after Dickinson et. al. (1983)

A high percentage of quartz (90.43%) and textural features such as coarse to fine grain texture, moderate to moderately well sorting and sub-rounded to sub-angular shape and low percentage of feldspars (Table 2, 3) point towards a distant source and extensive transportation and/or reworking of the sediments. The sandstones of Saundatti quartzites member is probably derived from the platform or uplifted basement rocks and has been extensively recycled. Polycrystalline quartz grains with more crystal units indicate metamorphic provenance. Elongated nature of polycrystalline grains and suturing of grain boundaries further suggest metamorphic derivation of sediments of these rocks. The studied samples also show the effect of pressure on some grains before and after deposition. Therefore, the sediments could have possibly been derived from metamorphic source rocks of Dharwarian basement probably peninsular gneissic complex.

Conclusions

Presence of Primary sedimentary structures like asymmetrical ripple marks, cross bedding in the Saundatti quartzite member indicate that it was dominantly formed under the influence of tidal processes. The overall environment of deposition for these sediments thus can be attributed a fluvial i.e., a continental set up. The Sandstones of Saundatti quartzite member are medium to coarse grained, moderately sorted to moderately well sorted. The sand grains are subangular to sub-rounded. The framework constituents of the studied samples are mainly composed of various types of quartz, followed by feldspars and rock fragments. Heavy minerals are seen to be occurring as minor constituents. The provenance is crystalline rocks of Archaean-Dharwar craton.

The sediments of the sandstones were derived from metamorphic and igneous source. Tectonic domain discrimination based on Qt-F-L and Qm-F-Lt

plots suggest sediment supply from the recycled orogen and from basement granites exhumed in the craton interior. The cementing material in these sandstones is Silica and iron oxide.

Mechanical compaction was the dominant diagenetic process during the early stage of diagenesis. During mechanical compaction rearrangement of grains took place and long, sutured and concave-convex contacts developed. The climate plots concentrate mainly in the humid zone. However, the composition got further modified during transportation and subsequent sedimentation

References

- Amer, K. M., Abu-Zeid, M. M., El-Mohammady, R. A. (1989), Particle-size distribution and depositional environment of the sandstones of "Nubia" facies in west central Sinai. Earth Science Series 3, Middle East Research Centre, Ain Shams University, 146-160.
- Ahmed, A. H. M., Rais, S., Safdar Azam, M., and Majid, A. (2008), Provenance and Diagenesis of Athleta Sandstone (Chari Formation), Fakirwari Dome, Kachchh, Gujarat, Jour. Indian Association of Sedimentologist, 27, 77-86.
- Bakkiraj, D. and Nagendra, R. (2008), Geochemistry and Provenance History of Sandstone, Sillakkudi Formation, Ariyalur Area, Cauvery Basin, Jour. Indian Association of Sedimentologist, 27, 39-49
- Basu, A., (1985), Influence of climate and relief on the composition of sands released at source areas; In: Provenance of Arenites (ed.) G GZuffa (Reidel Publishing Co.), 231-247.
- Blatt, H., (1967), Original Characteristics of Clastic Quartz grains, Jour. Sed. Petrol, 37, 401-424.
- Bokanda, E. E., Ekomane, E., Romuald, K., Isaac, N., Ethel, A., Paul, T., Bentrant, B., Gabriel, N., Shelly, O. N., Cedric, B. B. (2019), Provenance, paleoclimate and diagenetic signatures of sandstones in the Mamfe Basin (West Africa). Heliyon, Article No. e01140.
- Chaudhuri, A., Banerjee, S., Chauhan, G. (2020), Compositional evolution of siliciclastic sediments recording the tectonic stability of a pericratonic rift: Mesozoic Kutch Basin, western India. , Marine and Petroleum Geology, 111, 476-495
- Chaudhuri, A., Banerjee, S., Le Pera, E. (2018), Petrography of Middle Jurassic to Early Cretaceous sandstones in the Kutch Basin, western India: Implications on provenance and basin evolution., Journal of Palaeogeography, 7, 2-14.
- Cherian A., (2003); Sedimentological studies in the beaches between Valinokkam and Tuticorin, Tamil Nadu; unpublished Ph.D. thesis, Tamil University, Tamil Nadu, India.
- Chima, P., Baiyegunhi, C., Liu K., and Gwavava, O. (2018), Petrography, modal composition and tectonic provenance of some selected sandstones from the Molteno, Elliot and Clarens Formations, Karoo Supergroup, in the Eastern Cape Province, South Africa, Open Geosci., 10, 821-833
- Conolly, J. R., (1965), The occurrence of polycrystallinity and undulatory extinction in quartz in sandstone, Journal of Sed. Petrol., 35, 116-135.
- Das, P. K. (2008); Petrography of Sandstones of Thekopali Formation, Jaintia Hills district, Meghalaya. Bull. Of Pure and applied sciences-Geology, vol 27 p. 19
- Das, P.K. and Sharma, A., (2009), Petrographic study of the Sandstones from Shella Formation, Lumshnong area. South Jaintia Hills, Meghalaya, Gond. Geol. Magazine, 24(2);
- Datta B., (2005), Provenance, Tectonics and Palaeoclimate of Proterozoic Chandrapur Sandstones, Chattisgarh Basin: A petrographic view, Journ. Of Earth System sci. 114, 227-245.
- Devli, M., Mahender, K., (2018), Paleocurrent, Deformation and Geochemical studies of Lower part of Bagalkot Group of Kaladgi Basin at Ramthal and Salgundi: Implications on Sedimentation History, Jour. Indian Assoc. Of Sedimentologists, 35, 77-88.
- Dey, S., (2015), Geological History of the Kaladgi-Badami and Bhima basins, south India: Sedimentation in a Proterozoic intracratonic setup., Precambrian basins of India: Stratigraphic and Tectonic context. Geol. Soc. London, Memoirs, 43, 283-296.
- Dickinson, W. R., Beard, L. S., Brakenridge, G.R., Erjavek, J. L., Ferguson, R. C., Inman, K. F., Knepp, R. A., Lindberg, F. A. and Ryberg, P. T. (1983), Provenance of North American Phanerozoic Sandstones in relation to Tectonic setting, Geol. Soc. America Bull., 94, 222-235.
- Folk, R. L. and Ward, W., (1957), Brasos River bar, a study in the significance of grain size parameters, J. Sed. Petrol., 27, 3-26.
- Friedman, G. M., (1961), Dynamic processes and statistical parameters compared for size frequency distribution of beach and river sands. J. Sed. Petrol., 32, 327-354.
- Gogoi, K. D. and Borgohain, P. (1996), Sedimentology of the Barail Sandstones in Some Parts of Nagaland, Jour. Indian Association of Sedimentologist, 15, 131-142.
- Inman D.L., (1952), Measures describing size of sediments. J. Sed. Petrol., 19, 125-147.
- Ingersoll, R. V., Bullard, T. F., Ford, R. L., Grimm, J. P., Pickle, J. D., Sares S. W. (1984), The effect of grain size on detrital modes: a test of the Gazzi-Dickinson point counting method, Journ. of Sedimentary Petrology, 54, 103-116.
- Jayaprakash, A. V., Sundaram, V., Hans, S.K., and Mishra, R. N., (1987), Geology of the Kaladgi Basin, Karnataka, In: Purana Basins of Peninsular India (Middle to Late Proterozoic), Memoir 6, Gsi, 201- 225.
- Nagalakshmi, K., Pramod Kumar, M., Lakshmi Prasad, T., Jayaraju, N., Lakshmana, N. and Sreenivasulu, G., (2018), A study on textural parameters of beach sands along some parts of the Nellore coast, east coast of India: Implications to Depositional Environment, Journ. Of Indian Geophy. Union., v.22, no.5, pp: 558-567.
- Kale, V. S. and Pillai, S. P., (2011), A reinterpretation of two Chert breccias from the Proterozoic basins of India. Jour. Geol. Soc. India., 78, 429-445.
- Lonnie, T. P., (1982), Mineral and chemical composition of clay beds on the south shore of Long Island, New York: Journ. of Sedimentary Petrology, 52(2), 529-536.
- Mahender, K. and Fernandes, B., (2002), Petrography, Diagenesis and depositional Environment of the Late proterozoic Cave-Temple arenites of Badami Group,

- Karnataka, Recent researches on the Proterozoic Basins of India. 17-25.
- Mason, C. C. and Folk, R. L. (1958), Differentiation of Beach, Dune and Aeolian Flat Environments by Size Analysis, Mustang Island, Texas. *Journal of Sedimentary Research*, 28, 211-226.
- Moiola, R.J. and Weiser, D. (1968), Textural parameters and evaluation. *Jour. Sed. Pet.*, V-38, p 45-53.
- Mukherjee, M. K., Das, S., and Modak, K., (2016), Basement-Cover Structural relationships in the Kaladgi Basin, Southwestern India: Indication towards a Mesoproterozoic gravity gliding of the cover along a detached unconformity. *Precambrian research*, 281, 495-520.
- Padmakumari, V. M., Sambasiva Rao, V. V., and Srinivasan, R. (1998), Model Nd and Rb-Sr ages of shales of the Bagalkot Group, Kaladgi Supergroup, Karnataka. In *Abstracts: National Symposium Late Quaternary Geology and Sea Level Changes*, Cochin University, Kochi, 70p.
- Periyasami, V. and Venkateshwarlu, M., (2017); Petrography and Geochemistry of Jurassic Sandstones from Jhuran Formation of Jara Dome, Kachch Basin, India: Implications for provenance and tectonic setting. *Journ. of Earth System sci.* 44, 126.
- Pettijohn F. J. (1987), *Sand and sandstone*. Springer- verlag, New York, Heidelberg, 553.
- Pillai Patil, S., and Kale, V.S., (2011), Seismites in the Lokapur Subgroup of the Proterozoic Kaladgi Basin, South India: A testimony to syn- sedimentary tectonism., *Sedimentary Geology*, 240, 1-13.
- Powers, M. C. (1953), A new roundness scale for sedimentary particles, *Journ. Of Sedimentary Petrology*, 23, 117-119.
- Rajamanickam, G. V. and Gujar, A. R. (1984); Sediment depositional environment in some bays in the Central West Coast of India; *Indian J. Mar. Sci.* 13 53-59
- Raza, M., Bhardwaj, V. R., Ahmad, A. H. M., Mondal, M. E. A., Khan, A., Khan, S. M., (2010), Provenance and Weathering history of Archaean Naharmgra Quartzite of Aravalli craton, NW Indian Shield: Petrographic and Geochemical evidence., *Geochemical Journal*, 44, 331-345.
- Sambasiva Rao, V. V., Sreenivas, B., Balaram, V., Govil, P. K. and Srinivasan, R. (1999), The nature of the Archean upper crust as revealed by the geochemistry of the Proterozoic shales of the Kaladgi basin, Karnataka, south India; *Precamb. Res.* 98 53-65.
- Sen, S., Nath M., Das, P. K., Borah, M., Konwar, S. (2017), Petrography of the Barail Sandstones Occuring in and around Mandardisa, North Cachar Hills, Assam, India., *Internation Journal of Scientific and Engineering research.*, 8, 969-978.
- Suttner S., Basu A, Mack G. H., (1981), Climate and the origin of Quartz arenites, *journ. Sedim.Petrol.* 51, 1235-1246
- Tsuzuki, Y. and Kawabe, I. (1983), Polymorphic transformations of kaolin minerals in aqueous solutions, *Geochimica et Cosmochimica Acta.* 47 (1), 59-66.
- Tucker, M. E. (1981), *Sedimentary Petrology: An Introduction*, Blackwells, Oxford. 252p
- Tucker, E. M., (2011). *Sedimentary rocks in the Field: A practical Guide.* 4th Edition, Wiley-Blackwell Publishing Company.
- Young, S., (1976), Petrographic textures of detrital Polycrystalline quartz as an aid in interpreting crystalline source rock, *Journ. Of Sedim.Petrol.* 46, 595-603.
- Zaid, M. S., Al Ghatani (2014); Provenance, Diagenesis, Tectonic setting and Geochemistry of Hawksbury Sandstones, Southern Sydney Basin, Australia. *Turkish Journal of Earth Science*, 24, 72-98.
-

Lithological variations and drainage evolution in a marginal region: A case study from Chandrapur block of the Pranhita-Godavari Basin, Central India

Vijay Sharma^{*1}, Aditya K. Verma²

^{*1}The Maharaja Sayajirao University of Baroda, Vadodara

²Department of Earth Sciences, Indian Institute of Technology, Roorkee

Abstract

Field mapping and interpretation of sedimentary structures in Gojoli region of Chandrapur block along the eastern margin of the Pranhita-Godavari valley suggests westward flowing channels during the Neoproterozoic. Present channels in this part of Chandrapur block are south/ southeast flowing and possess clear imprints of the basin-margin faults and lineaments. Drainage parameters in its Neoproterozoic stratigraphic sequence suggest impervious substrates probably due to high degree of consolidation and filling of rock-fractures by hydrothermal solution activities. However, the same for the Gondwana's friable sandstone (towards western region) and Archaean gneisses (in the eastern part) has been observed consistent probably due to its porous nature and development of thick weathering profile. The affiliation of drainage with tectonism is therefore, from Neoproterozoic to present day within contrasting lithology, was out of synchronization intermittently.

Key words: Pranhita-Godavari basin, Drainage, Hydrothermal.

Introduction

Drainage network at the Earth's surface exerts a first order control on relief dynamics and the erosion of mountain belts. It is mainly controlled by the coupling between surface and deep crustal processes such as tectonic and climatic variations (Viaplana-Muzas et al., 2015). The topographic gradients and structural attributes of a region also contribute to the development of the drainage system. The study area of Chandrapur block exhibits predominant structural controls over drainage network due to its protofabric. As cratons came closer from Mesoproterozoic onwards, initial paleo-mesoproterozoic cratonic amalgamation governed it temporally (Torsvik et al., 2001). The drainage patterns may reflect original slope and structure or the successive episodes of perturbations, which has caused the surface modifications by uplift, subsidence, tilting, warping, folding, faulting, and jointing, as well as deposition by the sea, glaciers, volcanoes, wind, and rivers. Manifestations of such tectonic activities are exposed regionally in the Cratons, especially along the Cratonic margins similar to the present scenario. Their impacts are in ample abundance in this region due to its proximity to the boundary of the Craton (Sharma et al., 2018).

In such conditions, the paleo-drainage characteristics can be deduced from the distribution of the paleochannels, associated facies and sedimentary structures. Also, presence of streams in a landscape imparts the effects of a long geologic history while decrypting the structure and surface conditions (Schumm

et al., 1987). The sedimentary, geomorphic and structural features observed in parts of Chandrapur block provide significant implications for topographic evolution and associated subsurface processes from Neoproterozoic to Cenozoic era.

The drainage density exhibited by a region is the balance between climate, geomorphology and hydrology, which in turn shows the degree of fluvial dissection of a region (Lin and Oguchi, 2004). The rate at which erosion proceeds depends on the susceptibility of the rock surface to erode and the runoff intensity (Strahler, 1956). Convergence and offsetting patterns of streams are common in faulted terrains (Pati et al., 2011; Bhosle et al., 2009; Singh et al., 2006), which are very much prominent along the boundary faults in the study area. Slope influences rates of runoff, soil creep (depends on the cohesiveness and angle of repose), and soil flowage (Strahler, 1956). It changes due to faulting and differential erosion changes the local geography and hence the drainage geomorphology.

Being a discrete and active part of Godavari watershed, where the differential erosion are effective throughout the region (Ghosh and Paul, 2020), it is imperative to understand the tectono-sedimentary setup and Neoproterozoic channel behaviour with its geology. Therefore, in this study, we have compared the orientation of the Neoproterozoic drainage system of Gojoli region where most of the streams are non-perennial. This has been done with the help of morphometric parameters to describe processes (Ghosh

and Paul, 2020) as well as their underlying link between geology and basin geomorphology (Rai et al., 2019). An integration of morphometric analysis, sedimentary evidence, geomorphological and geochemical analyses is carried out to understand the geomorphic evolution in terms of drainage under marginal tectonic controls of the basin.

Study Area

The Study area lies between the longitude 79°30' to 79°45' and latitude 19°30' to 20°00' in Chandrapur district, Maharashtra, Central East India and covers ~160 km² (Fig. 1). It falls in parts of the Survey of India toposheet 56M/9 and 56M/10. Geologically, the study area is lying along the eastern margin of the Pranhita-Godavari basin infringing the Western Bastar craton within the Cratonic nuclei. The deposition

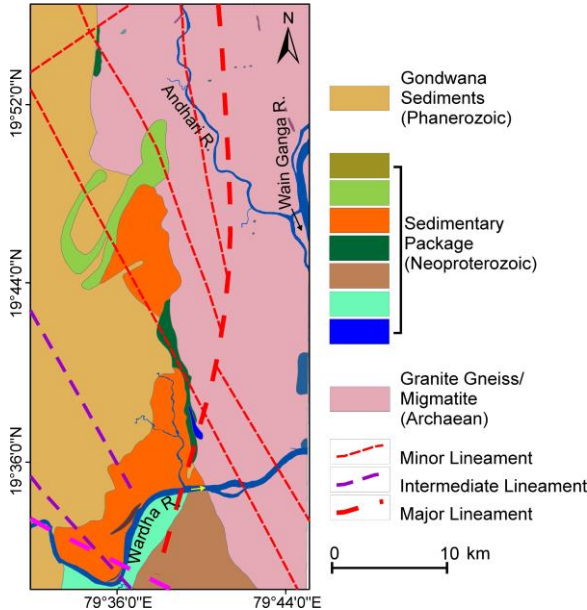


Figure 1 Lithological assemblage (GSI, 1983), and lineaments of the study area. (Lineaments are redrawn from Seismotectonic Atlas of India and after Das et al., 2003)

probably started from late Mesoproterozoic and early Neoproterozoic to Cenozoic Era. It has been evident from the depositional ages of ~970 Ma from detrital Zircons of the Cycle III of Sullavai Group over which the Gondwanas are resting separated by unconformable surface (Amarasinghe et al., 2015).

The Archean cover in the eastern, Neoproterozoic sediments in the middle (PG-basin margin sediments) part and the Lower Gondwana sequences in the western part are resting within the intra-cratonic settings in this block. These three prominent litho-chrono-sequences can be distinguished by their present-day drainage characteristics (Fig. 1). The

Gondwana Formation in the western part show moderate to semi-sparse presence of streams revealing dendritic to sub-dendritic type of drainage pattern, the Archean granite gneiss and migmatites show mostly dendritic to parallel and sub-parallel drainage patterns. The central

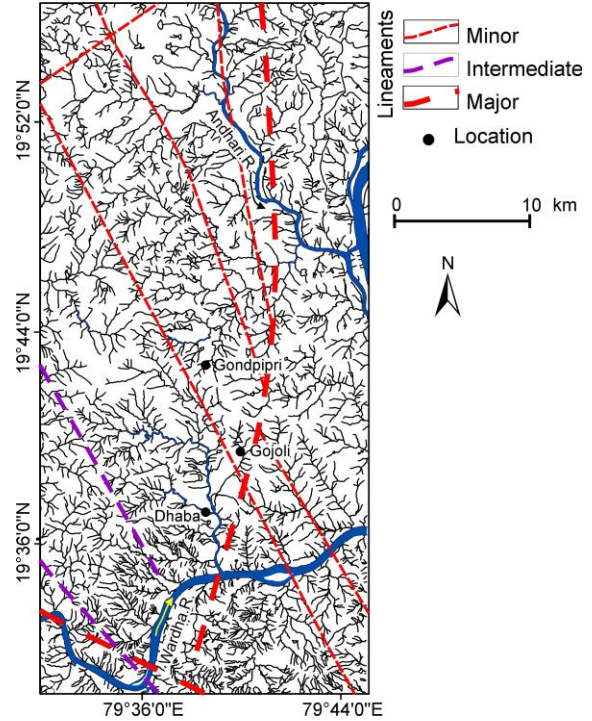


Figure 2 Drainage map of the study area (drawn from the Survey of India toposheet and Landsat TM image) superimposed by the lineaments. The lineaments are characterized by water divides and channel convergence, offset and straightness of river courses.

marginal region of Neoproterozoic sequences is characterized by dendritic drainage (Fig. 2). Hence, overall drainage of the region could be considered as dendritic type because impervious to moderate permeability of the strata with flat or rolling topography generally expresses it. The NW-SE trending prominent lineaments are characterized by convergent and straight channels. Drainage divide certainly owes its existence to various physical properties of its lithology and tectonic control over topography. The region has been bounded by faults and lineaments and partial parallel drainage along its lithological boundary within the basin margin. The draining streams has behaved according to the gradient and permeability of various lithologies considering the factors of erosion rate and precipitation. Presence of several deformation features in the Proterozoic belts as well as extensional structures on different scales within the bounded basin (Deb., 2003) has integratively governed overall slope of the region other than protofabric related tectonism. The varied slope of topography in the study area can be attributed to the

subsidence and intra-deformational activities, leading to development of dendritic and parallel drainage pattern in the basin. The region is segmented by five sets of lineaments (Das et al., 2003; Neogi and Das., 1998) and in the present study area, four sets are prominently present.

The study area is mainly composed of three prominent chrono-sequences i.e. Archean granite gneiss and migmatites in the eastern margin (Bastar Craton). Its presence has promoted the hydrothermal activity initially at the base of the deposited limestones in the basin

the active zones of weakness giving channel-ways to few metallizing solutions or hydrothermal fluids. The Proterozoic age has been given by the radiometric dating for surrounding major Proterozoic basins ($1276 > 20$ Ma) in this region like this P-G basin. However, the upper part of Sullavai group, along the margin, unconformably lies over the Pakhal sequence has K-Ar dates of 871 ± 14 Ma (Chaudhuri and Howard, 1985) correlates with subarkosic sandstones (Fig. 3 a, b) found in Dubarpet, in this part of Chandrapur block., which are partially affected by mild metamorphic effect and micro

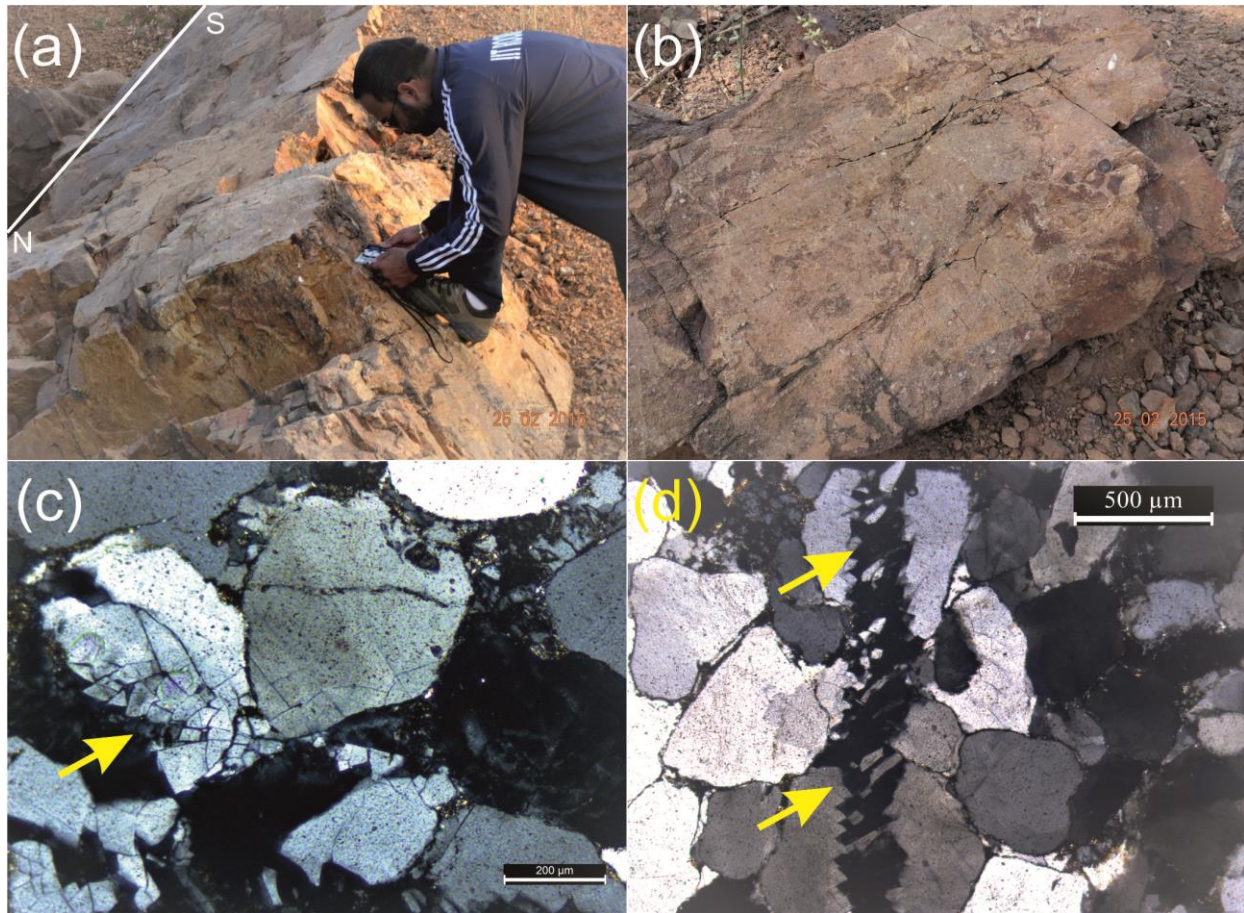


Figure 3 (a) Massive sandstone with its trend direction (b) Sandstone showing ungraded behaviour due to the presence of gravels and lithic fragments present between the matrix indicating varying energy conditions and depositional fluctuations (c, d) Fractured zones within the thin section showing the impact of tectonic disturbances and effect of shearing.

marginal region (central strip of the study area) which was of Neoproterozoic age (Amarasinghe et al., 2014) probably due to faster mantle upwelling affecting the average thinner crust. Although, such activity were the result of diagenesis and solution movement induced by accumulation of heat and extensive partial melting at lower crustal levels within unconformity bound surfaces in the intra-cratonic basinal settings (Deb, 2003). The evidences are also visible in the form of the Iron enrichment in major fractures within this zone. These are

fracturing (Fig. 3 c, d), provides the basic idea of later disturbance and the formational time frame in space. It has larger clasts in between matrix show depositional instability due to intermittent fluctuating energy conditions and tectonism. The Meso-Neoproterozoic platformal successions occur in the two belts along the margins of the P-G Valley. The medial part of the valley



Figure 4 (a) Cross bedding of sandstone showing westward flowing channels near Dubarpeth (b) near Dongargaon. (c) & (d) imbricated pebbles (yellow lines) in the conglomerate beds at Dongargaon hill showing flow direction.

contains Permo-Triassic Gondwana Supergroup (Deb., 2003) which is the youngest deposit recently exposed other than Quaternary to Recent alluvium over it.

Meso-Neoproterozoic. The presence of trough cross-bedding (Fig. 4 a, b) and the imbricated conglomerate (Fig. 4 c, d) associated with the basin-margin fluvial

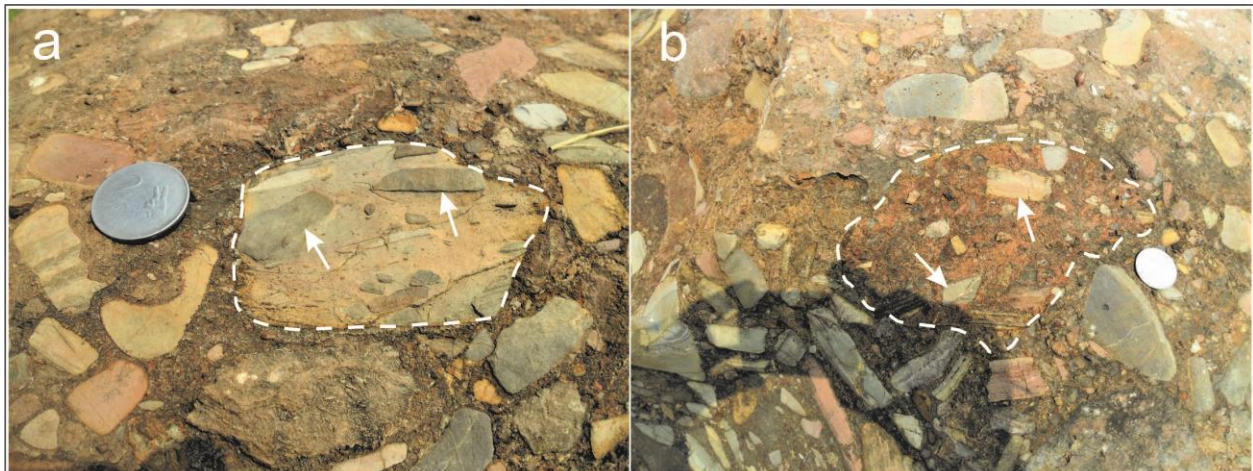


Figure 5 Autoclastic conglomerate showing clast within the clast configuration near to the basin margin. The mass flow sequence has played major role for its formation.

Lithology and facies association suggests rivers in the study area followed the slopes from the Bastar Craton in the east to the PG-basin in the west during

sequences around Dubarpeth and Dongargaon region are sedimentary evidence. They indicate west (towards the shelf) flowing channels during Proterozoic. It is

supported by mass flow sequence towards the shelf and clast in clast containing larger clasts of limestone. However, as the whole sequence is unexposed, detailed nature of the paleochannels (channel width and depth ratio) cannot be studied due to lack of sufficient outcrop

flowing streams. Dhaba and Andhari rivers in the central part of the area represent the similar settings within basin marginal faults and its proximity. Also, sedimentary structures in ancient and modern environments, other than exposed within marine settings, has explained about

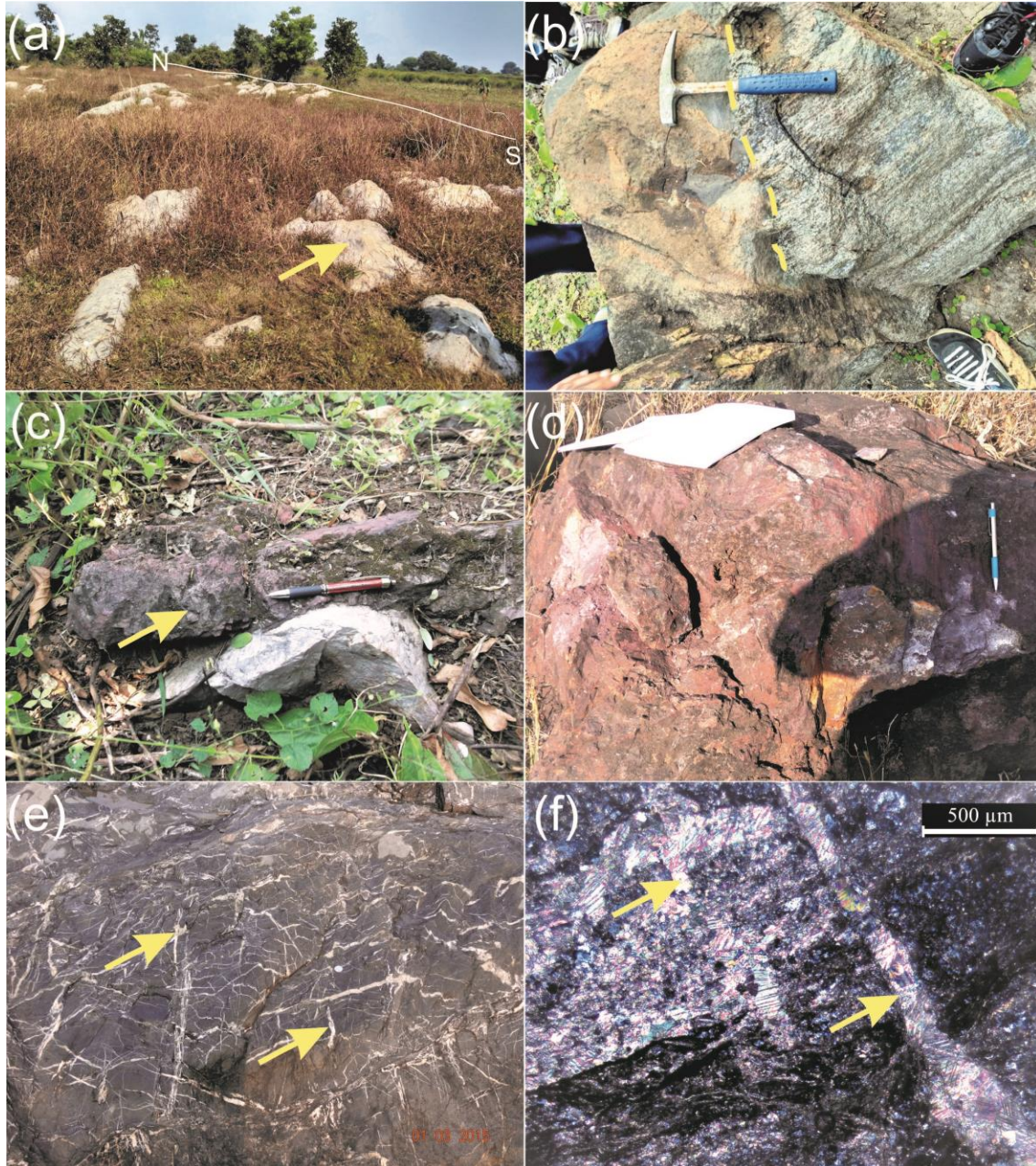


Figure 6 (a) Central Neoproterozoic terrain of massive west-dipping dolomitic limestone. (b) Contact between Archean Basement (TTG) and dolomitic limestone visible at some places due to exhumation. The Archean basement has been exposed towards the eastern part of the study area. (c) Presence of Iron enriched lithology in between the weak zones of dolomitic limestone showing hydrothermal solution impact. (d) Iron-enriched lithology observed in between the dolomitic limestone. (e) Presence of cross-cutting veins in dolomitic limestone showing multiple episodes of hydrothermal activity. (f) Photomicrograph showing the presence of calcitic-veins in dolomitic limestone proving hydrothermal activity under thin-section.

exposure in the area. Primitive structural control in relict form can be seen in some of the straight and fault guided

the slope and geomorphic conditions of the area. Previously, presence of various rounded clasts and clast

within clast at the base of marginal environment indicates that the topography was not rolling and the underlying tectonic activity due to active faults was quite appreciable (Fig. 5). It was supported by the fact that

Methodology

Initial work stimulus was to observe the study area using remote sensing and GIS data through ArcGIS platform. Landsat-TM imageries were the primary



Figure 7 (a) Massive marginal sandstone (b) Zones of chloritization and shearing in parts of massive sandstone.

marginal clastic mass accumulation along fault and its deposition with lithified scree and fine groundmass pertaining to multiple mass flow events were also present. It had a valid amount of slope affiliation which has been evident from the 36°–40° degrees dipping dolomitic limestone in eastern (Proterozoic) part of the block (Fig. 6). The presence of abundant water enabled easy transportation of the material. It implies that intermittent tectonic activity and geomorphological factors controlled the evolution of drainage in the region. Due to temporally prevailing more or less flat-lying character of Proterozoic basins in the peninsula, available visible evidences out of these sedimentary sequences which was the implication of the drainage and tectonic play observed in this part of P-G basin. There is visible perturbatory evidence, along major lineaments, over the drainage paths. The regional exhumation of the basement (TTG) and subsequent carbonate precipitation formed the platformal ramps over the slopes. Later, tectonic micro fracturing has caused iron enriched zones due to differential hydrothermal fluid movements through crosscutting veins in the form of micro conduits.

Solution induced fracture-filling at about supergene depth has played a major role in the infiltration process which in turn affected the drainage characteristics. This supergene effect at shallow depth is exposed at certain places due to upliftment and exhumation along the fan-deltaic settings of the marginal area with lot of effects like chloritization which has been now visible. The chloritization and sericitization of rocks in northern part of the block (in Dubarpet) indicates the impact of differential weathering along tectonically affected zone (Fig. 7a, b).

reckoning guide for the same. Further, creation of 3-D model was an imperative element to understand the correlation of the study area with imagery using surfer platform. Basic layers of regional spot heights and contour data were also reproduced using SOI toposheets of 1:50,000 scale. Correlation of data extracted from Landsat-TM imagery with the 3-D model acquired with the help of surfer platform helped the demarcation of major geomorphological pattern and major slope characteristics of the region. Field work for the collection of sedimentological, morphometric, and other data were done. Later, regional behaviour of drainage with lithological variation coupled with the impacts of tectonism in the study area were interpreted. Hence, discussion of the same enhances the regional sedimentological and geomorphological behaviour.

Results

Morphometric Interpretations

Geomorphic analysis

In this study, Landsat-TM image (Path 143 and Row 47) acquired in May-2011 was used for preliminary investigations (Fig. 8a). Contrast of colour tone and texture represents different lithologies in the central part. Since, the area is almost flat with some relict hillocks, conventional digital elevation model (DEM) provided by SRTM was not effective to detect the minor topographic variations in the plains due to its low height resolution. Therefore, point heights were retrieved from the Survey of India toposheets using ArcGIS 10.2. Kriging interpolation method was used to prepare a Digital Elevation Model (DEM) for regional study of the topography (Fig. 8b). Structural impressions of the faults (Das et al., 2003; Verma et al., 2017) can be interpreted with the help of DEM.

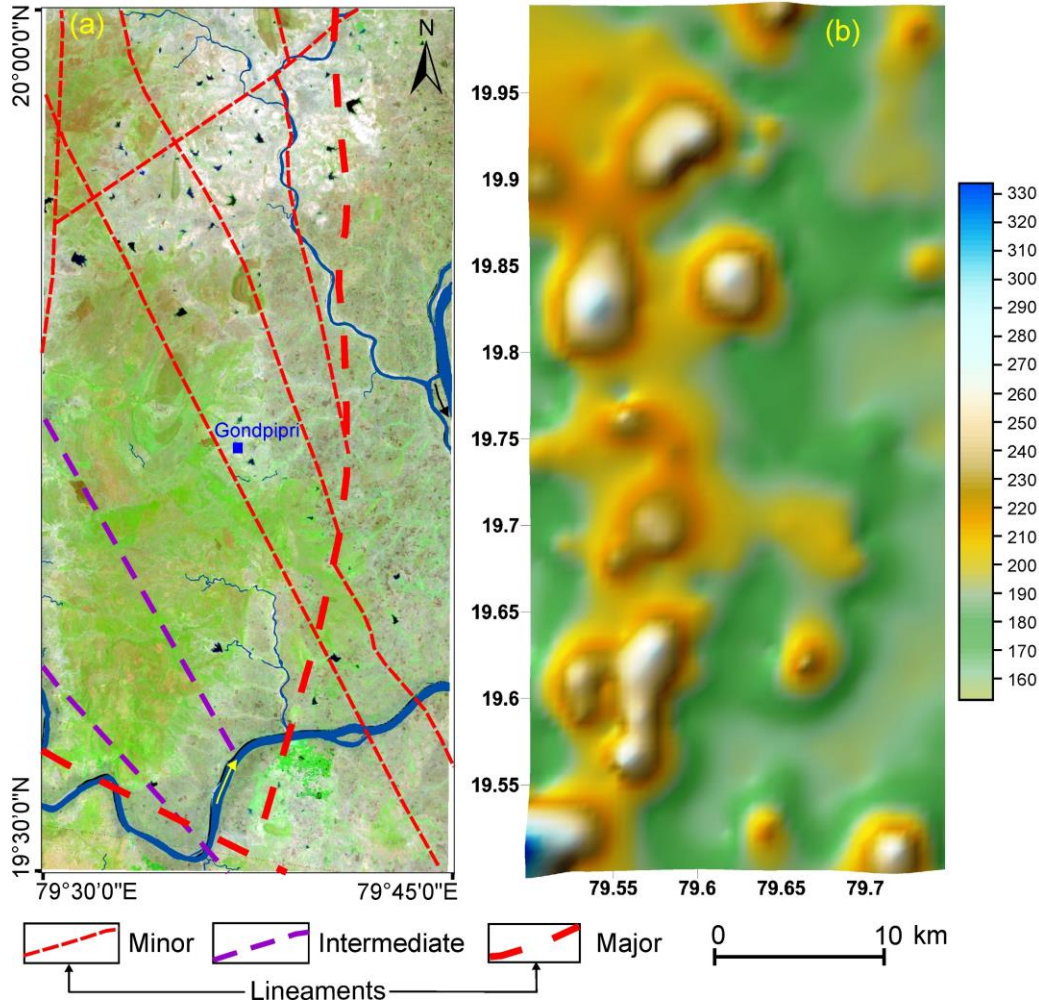


Figure 8 (a) Standard FCC (R:7 G:4 B:3) of Landsat TM image of the study area with lineaments superimposed (b) Digital elevation model (DEM) of the study area showing topographic variation.

Drainage analysis

The morphological studies are ready reckoning tool for the assessment of hydrological response of any watershed as well as the geomorphic maturity (Khurana et al., 2020). Geomorphologically, the terrain is rugged with hills and frequently changing lithology within the small area giving rise to varying drainage patterns. The valleys are filled with varying thickness of sediment cover. The drainage network is also prepared from the SOI toposheets at a scale of 1:50,000. The peninsular terrain of the Cratonic nuclei has displayed dendritic to sub-dendritic and sub-parallel drainage pattern over deposited lithology in the study area. Morphometric analysis is imperative to understand the basic relationship between the geology and its drainage.

Drainage anomalies are local offset deviations or deviation from basic stream pattern which elsewhere accord with the known regional geology or topography (Howard, 1967). Therefore, the impact of tectonism and lithology over drainage within geomorphological

constraints converge to the evolutionary understanding. Parameters like drainage patterns, drainage density, stream frequency, channel sinuosity, and infiltration number show and validate each other signifying the structural, lithological and slope variability for the region. It has been observed that major streams are more or less following the Proterozoic belt trend of NW-SE if overviewed in the PG-Basin as a whole. But it is interesting to see one of the major streams showing N-S trend merging with the locally eastward flowing Wardha River in this region. The anomaly in the regional streams indicates lithological and/or structural control over the drainage evolution.

Drainage pattern and drainage density

Drainage pattern depends mainly upon the lithological variation, geomorphology of the region, its structures and climate mainly. In general, surficial low-gradient of around 5°-10° in the area has helped the development of mostly dendritic to sub-dendritic

drainage pattern in the area (Fig. 2) which is observable in standard FCC of Landsat TM image. Convergence of channels along a linear zone mainly indicates structural

protofabric or fault zone has moderate effect on the channel geometry when feeble amount of structure is observable due to sediment cover just like a torned sheet

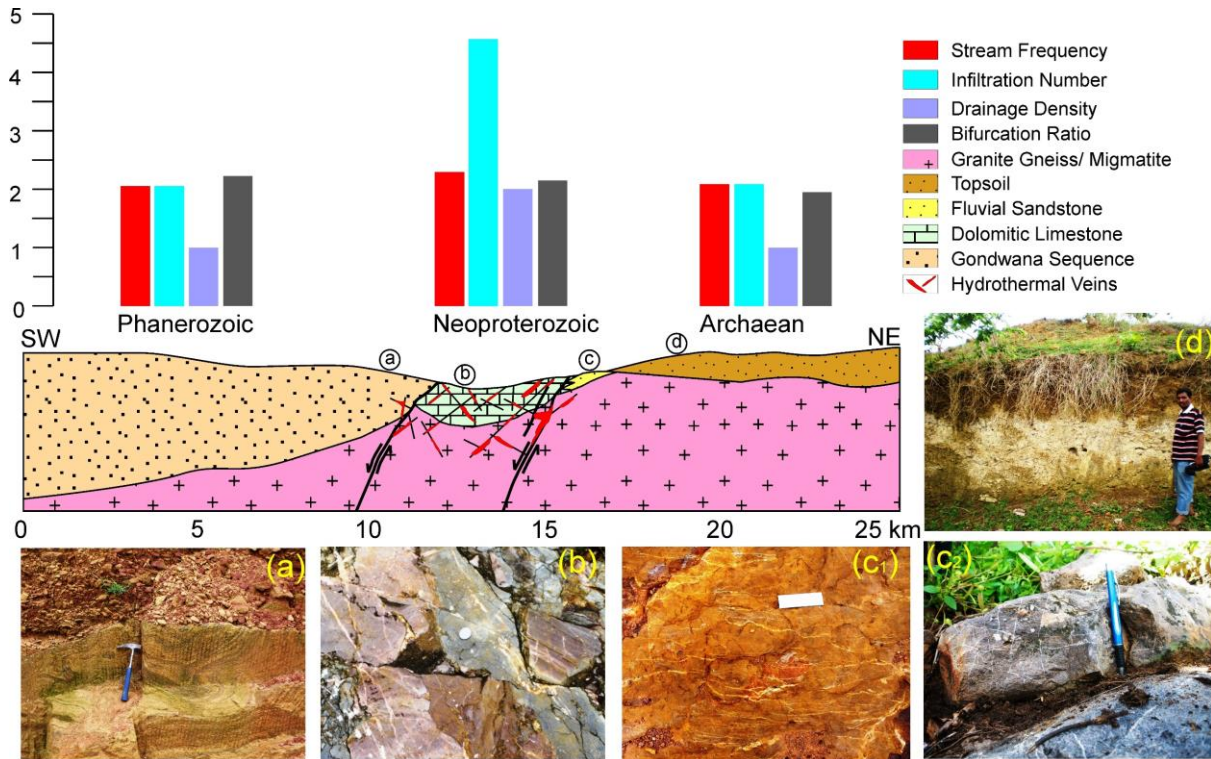


Figure 9 Diagrammatic representation of the lithological and structural disposition of the area with variation of drainage parameters. Circles represent the position of photographs shown below the figure. (a) Gondwana sandstone at Kirmiri, (b) Hydrothermal veins within the basin boundary limestone near Gojoli, (c1) Hydrothermal veins within the basin boundary sandstone surface at Dongargaon hill (c2) at Dubarpeth (below the surface) (d) Development of thick weathering profile on Archaean gneiss terrain near Dongargaon.

discontinuity (fault) along the basin margin. Fault controlled areas along the basin margin shows offsetting of channels of Dhaba and Andhari rivers (Fig. 2). Some lineaments represent the regional water divides. Apart from the structures, convergence of many first and second order streams are seen in the south-eastern and eastern part of the area due to variation in slope. Also, there is a strong similarity of structural control concordance with the streams as we follow the same marginal N-S faults towards northern or southern part. The same has also been followed by the adjacent major streams as well. Therefore, previous structural fabric has overall control on the topography as well as lithology causing present drainage pattern in the study area.

Channel sinuosity

Sinuosity (S) is a measure used to quantify the difference between meandering and straight channels. Hence, it also gives some account of tectonism in the given region and movement along certain lineaments. Here, the major streams in the study area show an average sinuosity of 1.25 to 1.35. Hence, relict of the

in which shallower torned part is filled with sediments when overviewed from top.

Stream frequency

The drainage frequency introduced by Horton (Horton, 1932) means stream frequency or channel frequency (Fs) as the number of stream segments (Nu) per unit area (A).

$$Fs = Nu/A$$

In the present study area shows low stream frequency i.e. varies from 2.1-2.3 /km². The Gondwana sequence and the basement part show similar value (Fs=2.1) but the Proterozoic sequence in the middle show relatively high (Fs=2.3) stream frequency. The development of the stream segments in the area is influenced by lithology, slope, rainfall, and temperature as well as the amount of perviousness developed due to secondary fracturing or weathering followed by post-solutional fracture filling (Fig. 6 e, f).

Basins having fault bounded nature and reduced draining of internal fluids to the external region along the margin harbours such conditions. Comprehensively, the

region shows higher impact of physical weathering but erosion (Sharma et al., 2018) leading to high infiltration and lesser stream frequency in some areas.

Infiltration number

Infiltration number of a drainage basin is the product of drainage density (Dd) and stream frequency (Fs) given by relation

$$\text{Infiltration number (If)} = Fs \times Dd \text{ (Faniran, 1968).}$$

It is a parameter which gives information about infiltration characteristics of an area. The infiltration number is 4.6 in the Proterozoic part, which indicates low infiltration and high runoff in the regions of crystalline nature. Similar characteristics for the Archaean and the Gondwana show even lower values ($If=2.1$). This indicate porous and permeable nature of the Gondwana sandstone (Fig. 9) and development of thick weathering profile (Fig. 9) on the Archaean gneissic terrain, which support subsurface infiltration, rather than surface flow. As the lithology of the Proterozoic sequence is less permeable, higher values of infiltration number indicate the lower infiltration and the higher surface runoff (Das and Mukherjee, 2005).

Bifurcation Ratio

Bifurcation ratio is the ratio between number of streams of a given order (Nu) to the number of segments of the next higher order ($Nu+1$) (Reddy et al., 2004; Strahler, 1964)

$$Rb = Nu / Nu+1.$$

In the study area Rb varies from 0.82 to 2.54. High bifurcation ratio in any particular area indicates high drainage density (Chopda et al., 2005). In the present area, bifurcation ratio varies from 1.92 (Archaean gneiss) to 2.18 (Proterozoic sequence) which indicate a rolling or flat region without any structural control (Kalaiivanan et al., 2014). Many times, the structural relicts are not visible over the surface due to thickness of sediment cover or thick weathering profile, although, presence of structure can never be ruled out which prevails in this region very well. Drainage density of the region too supports the bifurcation ratio. Usually these values are common in the areas where geologic structure and tectonics remain confined within the major streams only rather than affecting the later developed drainage pattern within the thick sediment profiles. The thick sediment cover which has been developed temporally accommodates small activities whose signatures merely show up unless major subsidence or upliftment. Such

activities are mainly due to protofabric structure migration.

Lithological Correlation and Evolution

Drainage analysis is always useful in structural interpretation, local or regional, particularly in areas of low relief. The lack of outcrop exposure and vast forest cover does not allow the detailed field study of paleo-drainage characteristics in the area. However, westward flowing channels could be readily interpreted in the Gojoli region from the available sedimentary structures and facies assemblage within the Chandrapur tectono-sedimentary block. The associated facies assemblage (sandstone and matrix supported conglomerate showing imbrication) suggest that the channels originated from the Archaean basement and supracrustal rocks in the east. The presence of major transport pathways of the sediment from the east and south, dating back to Meso to Paleoproterozoic, especially for the Somanpalli, Sullavai and Penganga Group within the P-G Basin (Amarasinghe et al., 2014) gives an overview of the regional framework originating from the time when collision took place between SE India and Enderby land in Antarctica (Henderson et al., 2014).

The trough cross-bedding in the sandstone (Fig. 4a) also points the flow direction from east to west. Presence of clast within clast towards the dipping direction which is also the flow direction towards the shelf or basin interior is another evidence (Fig. 5). Moreover, matrix supported conglomerate supports a short distance of transport before debouching into the basin towards shelf region. Even the regional streams of various orders would have appended themselves into the major drainage while sediment transport from east towards west. These evidences support the origin of the channels to be not far from the basin and were flowing on a higher slope so that; matrix and clast were not separated. If overviewed, the P-G Valley itself has been formed due to the sediment transport from multi-directional sediment influx from multiple easterly provenances of Enderbyland (Amarasinghe et al., 2014) which was opposite to the present flow direction of the streams.

The major structures (faults and lineaments) along the basin boundary are characterized by parallel to sub-parallel drainage pattern flowing towards south. Surface of the fault-bounded blocks shows dendritic to sub-dendritic drainage. This leads to the fact that even if the area is peneplained to much extent due to various surface and subsurface processes from the Proterozoic to Recent, the effects of structural features still persists on topography. The change of slope in and around the area is the result of temporal tectonic activity and erosion.

Also, morphometric study of the present-day east and southward flowing drainage characteristics well correlates to the geology and geomorphology. The

Neoproterozoic counterpart, however, and then active various surface processes, hence, gets decoded instinctively. This has been supported by geological responses in the form of sedimentary structures for west-flowing Neoproterozoic channels. These channels later debouched along the eastern margin of the P-G Valley towards the shelf from Gajoli, Dubarpet and Dongargaon.

The morphometric study includes drainage patterns, drainage density, stream frequency, channel sinuosity, and infiltration number (Table-1) for its geological correlation.

These morphometric properties, lithological characteristics, and geomorphological conditions enable us to delineate three major zones i.e., Archean, Neoproterozoic and Phanerozoic chronologically in the study area correctly syncing with particular values in each region respectively (Fig. 9). In the eastern part or gneissic basement part, stream frequency is 2.14 whereas basin margin region or central Neoproterozoic part of study area shows 2.3 and western part or Phanerozoic part shows 2.1 and their corresponding infiltration number values are 2.14, 4.6, and 2.1 respectively. This shows that lower surface runoff in the eastern and western parts but the central Neoproterozoic marginal zone. Drainage density value in the central part ($Dd=2$) shows higher runoff and low infiltration supports high infiltration number 4.6. This pertains to then effect of these sub-basinal paleoweathering conditions, hence, subsequently changing lithology and drainage. The low value of drainage suggests that the region is composed of highly resistant sub-soil materials (Srivastava, 1997) and rocks supported by diagenetic effects as seen in dolomitic limestones and sandstones. As the Neoproterozoic sequence was affected by fault movements, causing the rock fractures to be filled by hydrothermal solutions. The central strip of Neoproterozoic lithology can also be observed under the satellite image (Fig. 8a). The easterly juxtaposed Late-Proterozoic igneous activity fed the hot fluidal influx in to the fracture channel-ways as the structural perturbations has created conduits and chnnelways for the same temporally. Eventually, the whole process probably reduced the rock permeability and restricted the surface water to percolate downward thereby increasing the surface runoff. The Neoproterozoic sedimentary succession in the middle shows twice the drainage density (Table-1) compared to western and eastern part of the study area. This implies that impervious lithology and moderate slope aptly correlates with the observed drainage density in the area, and thus it can be deduced that lithology is another major controlling factor for drainage development.

Table 1: Table showing various values of morphometric parameters in different regions

Factor	Phanerozoic	Neoproterozoic	Archean
Stream frequency (F_s)	2.1	2.3	2.14
Drainage density (Dd)	1	2	1
Infiltration Number (I_f)	2.1	4.6	2.14
Bifurcation Ratio	2.18	2.12	1.92

Normally, if the bifurcation ratio (R_b) is low, the basin produces a sharp peak of discharge, and if R_b is high, the basin yields a low but extended peak flow (Agarwal, 1998). In the present study area, bifurcation ratio value shows the area to be almost flat or rolling type character (Kalaivanan et al., 2014; Horton, 1945) producing above moderate yield. Therefore, due to thick sedimentary cover in the region, the geological structures and tectonics has exercised dominant influence on the present drainage pattern but visible within or along the major streams only. This gives an insight of probable protofabric migration. Also, stream sinuosity of 1.25 to 1.35 in the study area shows less sinuous streams (Schumm, 1963; Leopold and Wolman, 1957) which is another indicative of less undulating topography due to denudational effect within later deposited restricted sediment cover.

Therefore, overall relict of the basin boundary faults still has certain influence on the present drainage system as proved by convergence, offsetting and straightness of the channel courses other than the lithology. All major channels in the block are south flowing following the basin boundary faults which when observed for the Neoproterozoic times were west flowing, based on evidence given by the facies and sedimentary structures. This shows a change in evolutionary pattern in topography and slope from the Proterozoic to Cenozoic era.

Conclusive Remarks

Based on remote sensing and GIS studies, tectono-sedimentary structural setup of block, and field study of the sedimentary terrain, it can be concluded that the Proterozoic channels were west-flowing as shown by the sedimentary structures. Facies assemblage and the present channels in the block are south and east flowing. Morphometric studies suggest, the present-day drainage characteristics are mainly controlled by lithology, slope and tectonic control conditions. Most of them are contained within the overlying sedimentary cover only.

The basin boundary faults still influence the major channels as shown by the stream convergence and offsetting patterns. It indicates that the proto-fabric of the region has control over the development of present-day drainage. Lithological contrast can be seen through the drainage density contrast in the block. The filling of rock-fractures by hydrothermal solutions in the fault zone had significant impact on drainage characteristics mainly in, the Neoproterozoic sequence, Surface of the fault-bounded blocks show dendritic to sub-dendritic drainage pattern, whereas, the boundary zone shows straight drainage controlled by faults. Therefore, topographic change from Proterozoic to Recent is due to tectonism, lithology, and erosion. Varied diagenesis in the different lithounits had also helped in the differential rates of weathering causing behavioural differences in the lithounits.

References

- Agarwal, C. S. (1998), Study of drainage pattern through aerial data in Naugarh area of Varanasi district, UP. *Journal of the Indian Society of Remote Sensing*, v. 26, p. 169-75.
- Bhosle, B., Parkash, B., Awasthi, A. K. and Pati, P. (2009), Use of digital elevation models and drainage patterns for locating active faults in the Upper Gangetic Plain, India. *International Journal of Remote Sensing*, v. 30, p. 673-91.
- Chopra, R., Dhiman, R. D. and Sharma, P.K. (2005), Morphometric analysis of sub-watersheds in Gurdaspur district, Punjab using remote sensing and GIS techniques. *Journal of the Indian Society of Remote Sensing*, v. 33, p. 531-9.
- Das, A. K. and Mukherjee, S. (2005), Drainage morphometry using satellite data and GIS in Raigad district, Maharashtra. *Geological Society of India*, v. 65, p. 577-586.
- Das, D. P., Chakraborty, D.K. and Sarkar K. (2003), Significance of the regional lineament tectonics in the evolution of the Pranhita-Godavari sedimentary basin interpreted from the satellite data. *Journal of Asian Earth Sciences*, v. 21, p. 553-6.
- Faniran, A. (1968), The index of drainage intensity-A provisional new drainage factor. *Australian Journal of Science*, v. 31, p. 328-330.
- Ghosh, S. and Paul, A.K., 2020. Tectonic control over drainage basin of South Andaman Island: study toward hydro-morphometric analysis. *Applied Water Science*, v. 10, p. 5.
- Horton, R. E. (1932), Drainage-basin characteristics. *Eos, Transactions American Geophysical Union*, v. 13, p. 350-361.
- Horton, R. E. (1945), Erosional development of streams and their drainage basins: Hydro-physical approach to quantitative morphology, *Geological Society of American Bulletin*, v. 56, p. 275-370.
- Howard, A. D. (1967), Drainage analysis in geologic interpretation: a summation. *AAPG bulletin*, v. 51, p. 2246-59.
- Kalaivanan, K., Gurugnanam, B., and Suresh, M. (2014), GIS based morphometric analysis of gadilam river basin, Tamil Nadu, India, *International Journal of Advanced Research*, v. 7, p. 1015-1022.
- Khurana, D., Rawat, S.S., Raina, G., Sharma, R. and Jose, P.G. (2020), GIS-Based Morphometric Analysis and Prioritization of Upper Ravi Catchment, Himachal Pradesh, India. In *Advances in Water Resources Engineering and Management*, Springer, Singapore, p. 163-185.
- Lane, E. W. (1957), A study of the shape of channels formed by natural streams flowing in erodible material: U. S. Army Corps of Engineers (Omaha), Missouri River Division, Sediment Series No. 9, p. 106
- Leopold, L. B. and Wolman, M. G. (1957), River channel patterns: braided, meandering, and straight. US Government Printing Office.
- Lin, Z. and Oguchi, T. (2004), Drainage density, slope angle, and relative basin position in Japanese bare lands from high-resolution DEMs. *Geomorphology*, v. 63, p. 159-73.
- Neogi, S. and Das, N. (1998), Lithotectonic domains and metamorphic history of the boundary zone of the Eastern Ghats orogen and Bastar craton. Deobhog area, Madhya Pradesh and its implication. *Precambrian Crust in Eastern and Central India*, p.180-204.
- Pati, P., Parkash, B., Awasthi, A.K., Acharya, V., Singh, S. (2011), Concealed thrusts in the Middle Gangetic plain, India-A ground penetrating radar study proves the truth against the geomorphic features supporting normal faulting. *Journal of Asian Earth Sciences*, v. 40, p. 315-25.
- Rai, P.K., Singh, P., Mishra, V.N., Singh, A., Sajan, B. and Shahi, A.P. (2019), Geospatial Approach for Quantitative Drainage Morphometric Analysis of Varuna River Basin, India. *Journal of Landscape Ecology*, v. 12, p.1-25.
- Reddy, G. P., Maji, A.K. and Gajbhiye, K.S. (2004), Drainage morphometry and its influence on landform characteristics in a basaltic terrain, Central India-a remote sensing and GIS approach. *International Journal of Applied Earth Observation and Geoinformation*, v. 6, p. 1-6.
- Schumm, S. A. (1963), Sinuosity of alluvial rivers on the Great Plains. *Geological Society of America Bulletin*, v. 74, p. 1089-1100.
- Schumm, S. A., Mosley, M.P. and Weaver, W. (1987), *Experimental fluvial geomorphology*.
- Sharma, V., Pati, P., Dora, M.L., Patel, N.K., Dash, C., Alam, P., Verma, A.K. and Gupta, A. (2018), Paleoweathering and Paleoclimatic Reconstructions using Neoproterozoic Paleosol in the Eastern Margin of the Pranhita-Godavari Basin, India. *Journal of the Geological Society of India*, v. 92, p. 201-208.
- Singh, R., Jhorar, R. K., Van Dam, J. C., Feddes, R. A. (2006), Distributed ecohydrological modelling to evaluate irrigation system performance in Sirsa district, India II: Impact of viable water management scenarios. *Journal of Hydrology*, v. 329, p. 714-23.
- Strahler, A. N. (1956), The nature of induced erosion and aggradation. *Man's Role in Changing the Face of the Earth*. Univ. Chicago Press, Chicago, p. 621-38.

- Strahler, A.N. (1964), Quantitative geomorphology of drainage basin and channel networks. Handbook of applied hydrology.
- Strahler, A. N. (1956), Quantitative slope analysis. Geological Society of America Bulletin, v. 67, p. 571-96.
- Srivastava, V. K. (1997), Study of drainage pattern of Jharia Coalfield (Bihar), India, through remote sensing technology, Journal of the Indian Society of Remote Sensing, v. 25, p. 41-6.
- Verma, A.K., Pati, P. and Sharma, V. (2017), Soft sediment deformation associated with the East Patna Fault south of the Ganga River, northern India: Influence of the Himalayan tectonics on the southern Ganga plain. Journal of Asian Earth Sciences, v. 143, p. 109-121.
- Viaplana-Muzas, M., Babault, J., Dominguez, S., Van den Driessche, J., Legrand, X., Drainage network evolution and patterns of sedimentation in an experimental wedge. Tectonophysics. 2015 Nov 28; 664: p. 109-24.

Sedimentological and Geochemical Characterization of Manaveli and Cuddalore Formations, Puducherry Basin, India

Shyam N. Mude, Shyam Yawale and Vishal Choudhari

Department of Geology, Fergusson College (Autonomous), Pune- 411004, India

Email: shyam.mude@fergusson.edu; shyammude25@yahoo.co.in

Abstract

The rocks of Puducherry basin have been classified as Valudavur, Mettuveli, Karasur, Manaveli, Cuddalore formations in chronological order. The sedimentological and geochemical studies of the sediments from Manaveli (Paleocene) and Cuddalore (Mio-Pliocene) formations were carried out to understand the grain-size variation and distribution of major oxides to deduce depositional environment, provenance, paleoclimate and source area weathering conditions. The sieve analysis was used to study grain size variations evaluated for various geo-statistical parameters to understand the depositional environment. The discriminant function analysis of the sediments from the Cuddalore Formation infers that mostly the sedimentation occurred in fluvio-deltaic

environment with incursions of shallow marine environment whereas bivariate plots suggest that the deposition occurred in riverine to deltaic environments. The values of CIA (chemical index of alteration), CIW (chemical index of weathering), ICV (index of compositional variability) and PIA (plagioclase index of alteration) of the sediments infer intense weathering conditions prevailed in the source area during the deposition of Manaveli and Cuddalore formations. The ratio of $(Al_2O_3+K_2O+Na_2O)/SiO_2$ indicate semi-humid climatic conditions during deposition of the Cuddalore Formation whereas Manaveli Formation was deposited in semi-arid climatic conditions. The discriminant function diagram suggests sedimentary provenance for Cuddalore and Mafic igneous provenance for Manaveli Formation.

Keywords: Grain-size, Depositional environment, Geochemistry, Manaveli, Cuddalore, Puducherry Basin

Introduction

The Cretaceous-Paleocene sediments of the Cauvery Basin are classified into five formations viz., Sillakudi, Kallankurichchi, Ottakoil, Kallamedu and Niniyur (Sundaram and Rao 1986). A lot of work has been carried out in the field of stratigraphy, sedimentology and palaeontology (Ayyasamy, 1990; Blanford, 1862; Chandrasekaran et al., 1996; Govindan et al., 1996, 2000; Hart et al., 2000; Kossmat, 1897; Muthuvairvasamy et al., 2003; Mammgain et al., 1968, 1973; Nair and Vijayam 1980; Radulovic and Ramamoorthy 1992; Ramasamy and Banerji, 1991; Sastry and Rao 1964; Sastry et al., 1972, 1968, 1977; Srivastava and Tewari, 1967; Tewari et al., 1996; Venkatachala, 1974; Venkatachalapathy and Ragothaman 1995; Yadagiri and Govindan, 2000; Nagendra et al., 2010, 2011; Prasad et al., 2013; Reddy et al., 2013; Sarkar et al., 2014, Nagendra and Reddy, 2017; Jaiprakash et al., 2016; Nagendra et al., 2019). Cretaceous fossil calcareous algae from the Cauvery Basin has been documented by various researchers (Rajanikanth 1992; Rao and Prasannakumar 1932; Rao and Pia. 1936; Rao and Gowda, 1954; Misra and Kumar, 1988; Misra et al., 2004 and 2006) whereas Cenozoic fossil calcareous algae have been also reported from Cauvery Basin (Misra et al., 2000, 2001, 2003;

Kishor et al., 2003; Kishor, 2004a, 2004b; Kishor and Singh, 2004).

Puducherry region is situated on the Coromandel Coast between 11°45' to 12°03'N and 79°37' to 79°53'E with an area of 293 sq. km. The Cauvery rift basin trending NE-SW, ranges from Late Jurassic to Early Cretaceous (Powell et al., 1988). A complete section of upper Cretaceous to Paleocene is exposed in the Ariyalur – Puducherry sub basin (Sastry & Rao, 1964). The rocks exposed in and around Puducherry are represented by Valudavur, Mettuveli, Karasur, Manaveli, Cuddalore formations in chronological order. Grain size data play a significant role in interpretation of depositional environment and specific grain size distribution can be used to estimate the environment of deposition of clastic rocks (Udden, 1898; Krumbein, 1934; Folk and Ward, 1957; Greenwood, 1969; Visher, 1969 and Friedman, 1979, Ghosh and Chatterjee, 1994; Ghaznavi et al., 2019; Quasim et al., 2020). On the basis of grain size, interpretation can be obtained by two methods, first is statistical method which includes mean, standard deviation, skewness, kurtosis etc. It can be calculated by graphic or moment method and with the combination of statistical methods like mean vs standard deviation, standard deviation vs skewness, skewness vs kurtosis

(Friedman, 1962, 1967, 1979). The second method is qualitative observation of shape of cumulative frequency curves on probability paper (Spencer, 1963 and Visser, 1969). Multivariate discriminant analysis is also useful to understand depositional environment using parameters like mean, standard deviation, skewness, kurtosis by graphic or moment method (Mahalanobis, 1930; Greenwood, 1969). The interpretation of depositional environment, the interrelationship of specific grain size parameter is very important, as textural parameters of sediment are much sensitive towards depositional environment (Folk and Ward, 1957; Mason and Folk, 1958; Friedman, 1967; Moiola and Weiser, 1968; Visser, 1969; Rajamanickam and Gujar, 1984; Srivastava and Mankar, 2008; Rajganapati, 2013; Ghaznavi et al., 2019). The geochemical studies of sedimentary rocks are significant to interpret the provenance, source rock composition, weathering intensity and the tectonic settings. (Dickinson and Suczek, 1979; Nesbitt and Young, 1982; Bhatia, 1983; Bhatia and Crook, 1986; Roser and Korsch, 1986, 1988; McLennan and Taylor, 1991; McLennan, 1989, 1993, 2001; McLennan et al., 1993; Madhavaraju and Ramasamy, 2002; Nagarajan et al., 2007a,b; Madhavaraju and Lee, 2010; Madhavaraju and Gonzalez-Leon, 2012; Madhavaraju et al., 2016; Armstrong-Altrin et al., 2013, 2015; Madhavaraju, 2015; Pandey and Parcha, 2017; Lone et al., 2017; Shah et al., 2017; Khan et al., 2019; Mude et al., 2019). The mutual relationship of the major, trace and rare earth elements play a significant role in understanding the weathering condition of the source area and provenance (Nesbitt and Young, 1982; McLennan, 1993).

Grain size variation and geochemical changes form the sediments of Manaveli and Cuddalore formations were not carried out earlier although these two parameters are very significant to deduce depositional and paleoenvironment. Only Selvaraj and Ramasamy (1998) have carried out granulometric analysis of Cuddalore Formation from Neyveli and Ariyalur area. Therefore, in the present paper, it is attempted to understand geochemical variation in the sediments of Manaveli and Cuddalore formations to interpret source area weathering conditions and paleoclimate. Further it is attempted to study the grain size variation from these sediments to know depositional environment.

Geological Setting

The sediments of Ariyalur Group (Late Cretaceous and Paleogene) are poorly exposed as an inlier of NW Puducherry, which is surrounded by Quaternary alluvium and Cuddalore Formation (Miocene-Pliocene). The sediments of Puducherry area are further divided into Valudavur, Mettuveli, Karasur and Manaveli formations (Figure 1). The Valudavur Formation contains informal units A and B of Warth (1895) (Rajagopalan, 1965). The lower bed of the

formation is pale yellow, fine to very coarse sandstone consisting of mica as minor component and rounded quartz pebbles. Upper bed has pale sandstone generally uncemented and bioturbated. It also contains concretionary shale and this formation has thickness of about 180m (Sundaram et al., 2001). Neogene strata of the Cuddalore Formation overlap the Valudavur Formation from north and west. Mettuveli Formation is conformably overlying Valudavur Formation. Upper part of the formation contains Ammonites of Late Maastrichtian age whereas the lower part consists of plankton foraminifera (*Globotruncana tricarinata*) of the late Campanian (Govindan, 1972).

The Mettuveli Formation consists of sandy shale and fine sandstone consisting of moulds and phosphatic cast of shell debris. The thickness of formation is around 150m with more amounts of Molluscan fossils (Sundaram et al., 2001). On the basis of planktonic foraminiferal zone of *Abathomphalus mayaroensis* the age of the Mettuveli Formation is determined as Late Maastrichtian (Govindan, 1972). The Karasur Formation consists of coarse impure calc-arenites, bioturbated at places and contains corals. It is massive bedded, exhibiting nodular fabric and thickness is about 120m (Sundaram et al., 2001). Contact of the formation is conformable both below and above. On the basis of Planktonic foraminifera, the age for the Karasur Formation is assigned as Paleocene (Rajagopalan, 1965; Govindan, 1972). The Manaveli Formation consists of buff sandy shale, poorly lithified with siltstone and fine grained sandstone containing poorly preserved molluscan fossils. The thickness of this formation is approximately 100m (Sundaram et al., 2001). It has conformable contact with the Karasur Formation and dis-conformable contact with Cuddalore Formation. Rajagopalan (1968) suggested Paleocene age for the Manaveli Formation on the basis of planktonic foraminifera. The Cuddalore Formation consists of ferruginous arkosic sandstone associated with clay and gravel beds. The sedimentary structures viz., planar cross bedding, small scale herringbone cross bedding, cross lamination and ripple drift lamination are well developed and the thickness of formation is about 150m. It has dis-conformable contact with Manaveli Formation below and conformable with alluvium above. The Cuddalore Formation is dated as Miocene-Pliocene (Vredenburg 1908; Wadia 1953; Krishnan 1960; Ramanujam 1968).

Methods and Material

Total thirteen samples were taken from the Cuddalore Formation and selected for grain size studies. The Sieve analysis of these samples was carried out in Department of Geology, Fergusson College (Autonomous), Pune. Thirteen samples from the Cuddalore Formation were selected for sieve analysis. Hundred and fifty grams of sample were

taken from sediments by coning and quartering. These samples were treated with 10N HCL to remove any carbonate impurities and coatings of grains. The samples were dried in laboratory oven at 70°C. Hundred grams of samples were taken for sieve analysis using sieves of 2mm, 1mm, 500µ, 250µ,

125µ and 63µ mesh. Samples were put into the sieve-shaker to shake in circular motion for 15 min on 50Hz frequency. After sieving, fraction from each sieve was collected and by using electronic balance, the weight of the sample was calculated and used for further calculations.

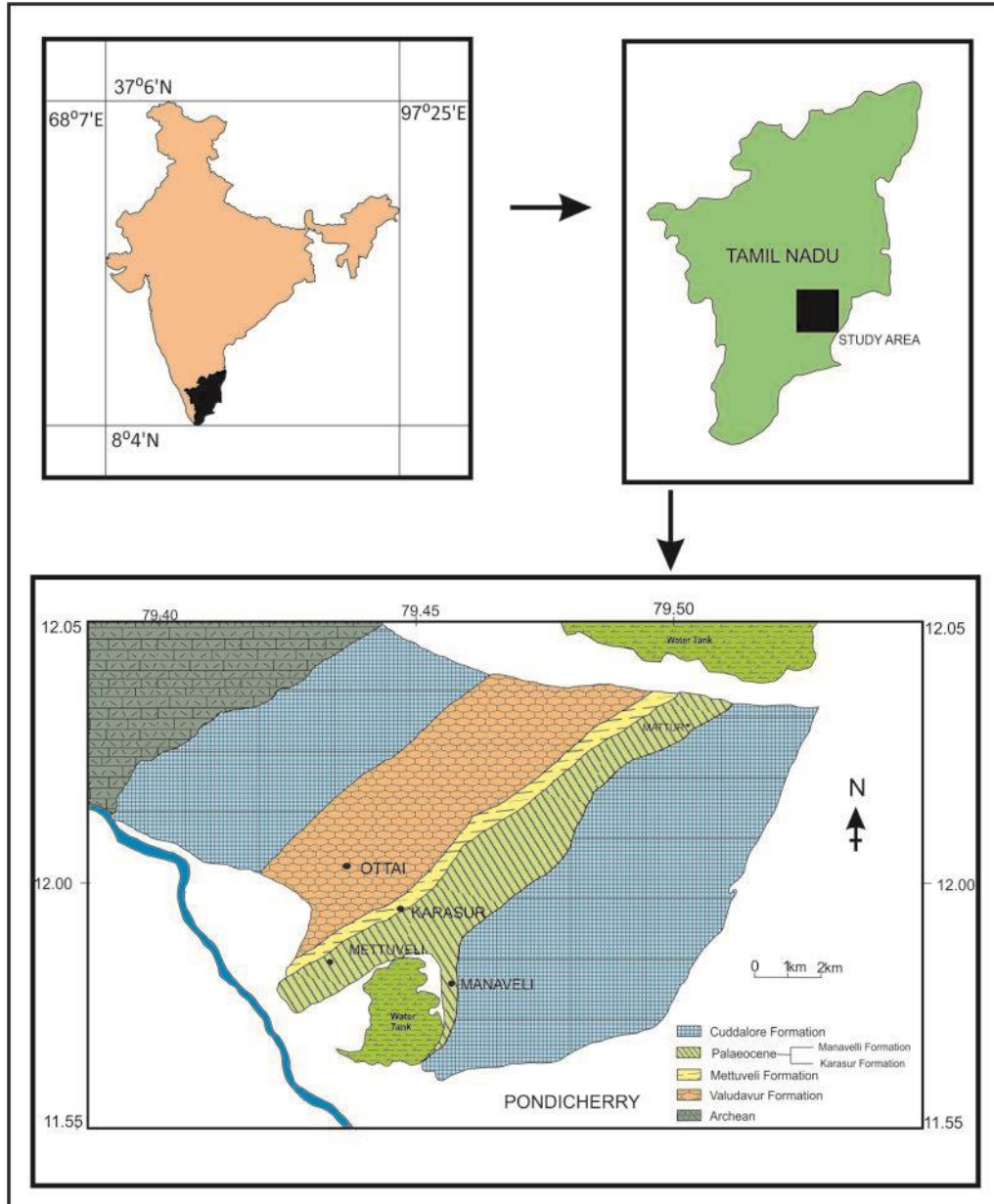


Figure 1: Geological map of the Puducherry area (after Malarkodi, et al., 2009)

Seven samples from Cuddalore Formation and six samples from Manaveli Formation were selected for geochemical analysis. The XRF analysis of these samples for major and trace elements were carried out in the Wadia Institute of Himalayan Geology, Dehradun. Ten grams of the sample were prepared by powdering in an agate mortar. The pressed power pellet mode for sample preparation was employed for the major and trace elements analysis (Watsan, J. S., 1996). The average error of the analysed major and trace elements was less than $\pm 5\%$.

Field Observations

Manaveli Formation

This section is exposed on Manaveli main road, 100m N-E of Puducherry maritime academy (latitude - 11°58'0.15" N; longitude - 79°46'13.67" E; elevation - 24m) and the section is about 3 m thick. The section consists of 4 lithounits of alternate white and yellow clays and 1 unit of iron concretion. At the base of this section, 0.3m thick unit of yellow clay is present and horizontal as well as vertical burrows were seen. This unit is followed by 0.6m thick white clay. Above this unit 0.3m thick bed of yellow clay is present, which is followed by 0.9m thick unit of white clays and upper most units is about 0.9m thick consisting of pebbles and iron concretions.

Manaveli Formation

The section of the Manaveli Formation is exposed on NE of Manaveli village around 800m (latitude - 11°58'21.20" N; longitude - 79°46'32.02" E; elevation - 33m). The thickness of the section is 2.2 m. Three samples were collected from two lithounits of this section. Lower unit of this section is 1.2m thick, white colored claystone; upper unit of this section is 1m thick red colored sandy pebbly horizon, pebbles are more than 3mm in size, rounded and moderately sorted.

Cuddalore Formation

The section of the Cuddalore Formation is exposed in a quarry section, 1.2 km from Manaveli village (latitude - 11°57'56" N; longitude - 79°46'49.5" E; elevation - 32m) towards east and hardly 3-4 km west of Puducherry airport. The thickness of the section is about 18 m and 8 samples were collected from the different stratigraphic levels of this section. At the base of the section, 0.5m thick reddish weathered sandstone is exposed, which is poorly sorted and has medium to coarse, angular grains. Above this red sandstone, there is 0.1m thin layer of gravels and pebbles, which is followed by 0.8m thick red sandstone consisting of minor amount gravels and pebbles. This lithounit shows laminations and has fine to medium grained, moderately sorted angular to sub angular grains of quartz and feldspar, rock fragments and at the top of this lithounit, laminations are present. Above this unit, there is 1.2m thick pale brown coloured, very poorly sorted gravelly/pebbly horizon present, some grains are more than 3cm across, they are rounded to sub-rounded which are slightly laminated. Above this unit 0.6m thick moderately sorted, fine to medium, sub-angular, red

colored sandstone is present. This unit is followed by reddish brown colored, moderately sorted, medium size; sub-angular sandy horizon which is 3m thick containing 5 to 10 % small pebbles. Above this unit 1.8m thick brown colored moderately sorted, medium size, sub-angular sandy pebbly horizon which contains 30 to 35% small to medium pebbles about 2mm across. This unit is followed by sandy horizon, brown colored, poorly sorted, medium to fine grains and containing 5 to 10% pebbles, clay material is also present, and this unit is 2.5m thick. Upper most units is red brown colored, moderately sorted and medium to fine grain silty-sandy horizon, this unit is 7.3m thick.

Cuddalore Formation

In a quarry section, 300m towards west of Pon Pure Chemical Private Limited (latitude - 11°56'14.5" N; longitude - 79°45'29.3" E; elevation - 17m) sequence of Cuddalore Formation is exposed. This section is about 6.8m thick and 8 samples were collected from different stratigraphic levels. At the base of this section 1m thick reddish-brown colored, moderately sorted, medium to coarse grained fossiliferous sandstone is present with some calcareous matter. Above this unit 2m thick red colored, well sorted, fine grained, laminated unfossiliferous, friable sandstone is present. This unit is followed by white colored laminated shale having thickness of about 0.3m which is further followed by sandstone with intercalation of shale. Sandstone in this unit is reddish in color, moderately sorted and fine to medium grained whereas, white shale has a thickness about 0.6 m. Above this unit, 1m thick reddish white colored claystone is present. This unit is followed by yellowish red, well sorted, fine to medium, rounded grained sandstone having thickness of 0.3m. Above this unit, 1m thick bed of reddish white claystone is present. On the top of this formation, 0.6m thick bed of yellowish red colored, well sorted, medium to fine grain sandstone is present.

Recent Deposits

Recent sediments are exposed on Manaveli main road near Mettuveli village in front of Foseco India Limited (latitude - 11°57'27.3" N; longitude - 79°46'59" E; elevation - 42 m). Total thickness of the sequence is 3.5m and 3 samples were collected from this section. This horizon is reddish brown colored, coarse to fine grained; weathered sandy and silty clay.

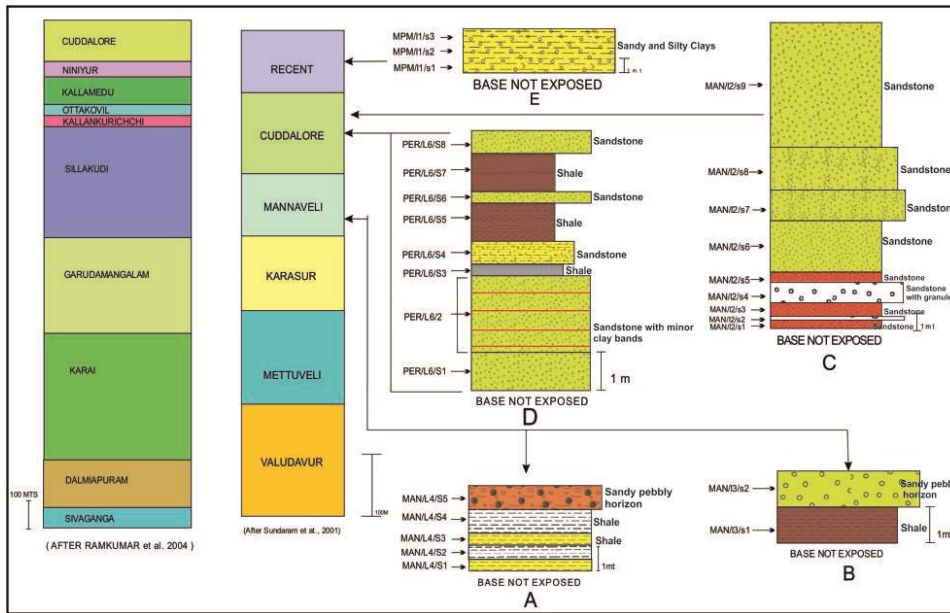


Figure 2: Lithologs of studied section of Manaveli Formation, Cuddalore Formation and recent deposits from Puducherry basin; A: litholog of Manaveli Formation at Manaveli village, 100m NE of Puducherry maritime academy; B: litholog of Manaveli Formation at 800m towards N-E of Manaveli village and 600m east of Kasipalayam village; C: litholog of Cuddalore Formation at quarry section 1.2 km from Manaveli village towards east and hardly 3-4 km west of Puducherry airport; D: litholog of Cuddalore Formation at quarry section, 300m towards west of Pon-Pure Chemical Private Limited, near Perambai village; E: litholog of recent deposits at open pit on Manaveli main road near Mettuveli village in front of Foseco India Limited.

Recent Deposits

Recent sediments are exposed on Manaveli main road near Mettuveli village in front of Foseco India Limited (latitude - 11°57'27.3" N; longitude - 79°46'59" E; elevation - 42 m). Total thickness of the sequence is 3.5m and 3 samples were collected from this section. This horizon is reddish brown colored, coarse to fine grained; weathered sandy and silty clay.

Results

Grain Size Analysis

The standard methodology of granulometric analysis was used and grain size distribution is given in Table 1. Cumulative weight percent and frequency of each sample were individually plotted on a graph and ϕ values from the graph were calculated. Value of ϕ_5 , ϕ_{16} , ϕ_{25} , ϕ_{50} , ϕ_{75} , ϕ_{84} , ϕ_{95} from the cumulative curves were obtained & used to calculate four graphic measures (Folk and Ward 1957) viz., Mean (M_z) = $(\phi_{16} + \phi_{50} + \phi_{84})/3$. Std deviation (S_i) = $(\phi_{84} - \phi_{16})/4 + (\phi_{95} - \phi_5)/6.6$ Skewness (Sk_G) = $(\phi_{84} + \phi_{16} - 2\phi_{50})/2(\phi_{84} - \phi_{16}) + (\phi_{95} + \phi_5 - 2\phi_{50})/2(\phi_{96} - \phi_5)$. Kurtosis (K_G) = $(\phi_{95} - \phi_5)/2.44(\phi_{75} - \phi_{25})$.

Sahu (1964) described the depositional environments on the basis of discriminant functions.

On the basis of graphic measurements (Folk and Ward, 1957), Y_1 , Y_2 and Y_3 discriminant functions were calculated as follows (Sahu, 1964),
 $Y_1 = -3.5688(M_z) + 3.701(S_i) - 2.0766(Sk_G) + 3.1135(K_G)$
 $Y_2 = 15.6534(M_z) + 65.7091(S_i) + 18.1070(Sk_G) + 18.5043(K_G)$
 $Y_3 = 0.2852(M_z) - 8.7694(S_i) - 4.8932(Sk_G) + 0.0482(K_G)$

If Y_1 is less than -2.7411, it indicates depositional environment is aeolian and when it is greater than -2.7411 it suggested as beach environment. If Y_2 is less than 65.3650 it suggests beach environment and greater than 65.3650 shallow marine environment. If value of Y_3 is less than -7.419 it suggests fluvio-deltaic deposits and greater than -7.419 is shallow marine depositional environment.

Bivariate plots viz., Mean (M_z) Vs. Standard Deviation (S_i); Graphic Skewness (Sk_G) Vs. Graphic Standard Deviation (S_i); Graphic Kurtosis (K_G) Vs. Graphic Skewness (Sk_G); Graphic Skewness (Sk_G) Vs. Mean (M_z) were extensively used to understand the depositional environment of sediments (Folk and Ward, 1957; Mason and Folk, 1958; Friedman, 1967; Muiola and Weiser, 1968; Visher, 1969; Rajamanickam and Gujar, 1984).

Table 1: Grain size distribution of samples from Cuddalore Formation

Sample No.	PER/L6/S1		PER/L6/S2		PER/L6/S4		PER/L6/S6		PER/L6/S8	
Phi no.	Wt%	Cum Wt %								
-1	8.16	8.15	2.84	2.84	4.11	4.1	0.43	0.43	0.70	0.7
0	25.13	33.25	6.08	8.92	20.56	24.6	5.52	5.943	7.48	8.18
1	40.55	73.75	32.59	41.48	39.83	64.32	47.71	35.52	33.22	41.4
2	16.16	89.89	36.79	78.24	17.59	81.86	30.48	83.92	40.78	82.18
3	4.70	94.59	15.58	93.81	9.22	91.06	8.22	92.123	11.41	93.59
4	3.22	97.81	5.19	99.00	7.62	98.66	7.10	99.208	5.19	98.78
5	2.05	99.86	0.91	99.91	1.04	99.70	0.51	99.718	1.20	99.98
Sample No.	MAN/L2/S1		MAN/L2/S2		MAN/L2/S3		MAN/L2/S4			
Phi no.	Wt%	Cum Wt %								
-1	11.17	11.17	2.97	2.97	52.25	51.94	2.71	2.71		
0	20.06	31.22	9.944	12.9	13.66	65.52	10.50	13.21		
1	50.59	81.78	38.03	50.88	18.68	84.09	57.80	70.96		
2	12.60	94.38	39.74	90.57	7.92	91.97	17.64	88.59		
3	3.53	97.91	6.97	97.53	3.78	95.73	4.80	93.39		
4	0.08	97.99	2.17	99.7	3.18	98.9	4.35	97.74		
5	1.95	99.94	0.15	99.85	0.60	99.5	2.17	99.91		
Sample No.	MAN/L2/S5		MAN/L2/S6		MAN/L2/S7		MAN/L2/S8			
Phi no.	Wt%	Cum Wt %								
-1	3.24	3.24	63.08	62.83	5.66	5.65	1.52	1.52		
0	8.09	11.33	11.00	73.79	11.19	16.81	16.57	18.09		
1	55.93	67.23	14.00	87.74	38.30	54.98	38.97	57.05		
2	23.81	91.03	6.71	94.43	20.83	75.74	19.75	76.8		
3	4.90	95.93	3.56	97.98	15.00	90.69	13.67	90.46		
4	3.82	99.75	1.64	99.62	8.48	99.15	8.69	99.15		
5	0.20	99.95	0.04	99.66	0.51	99.66	0.73	99.88		

Table 2: Calculated phi (ϕ) values of the samples

Name of sample	5 ϕ	16 ϕ	25 ϕ	50 ϕ	75 ϕ	84 ϕ	95 ϕ
PER/16/s1	1.22436	-0.57536	-0.25765	0.39853	1.09069	1.46591	2.5268
PER/16/s2	-0.4587	0.26153	0.58505	1.22817	1.87938	2.21571	3.01935
PER/16/s4	-1.04164	-0.39132	-0.04557	0.69566	1.49578	1.93319	3.18333
PER/16/s6	-0.05781	0.5141	0.76516	1.26253	1.77302	2.04558	2.78577
PER/16/s8	-0.29375	0.33005	0.61586	1.1893	1.77743	2.08667	2.87033
MAN/12/s1	-1.28148	-0.46946	-0.18734	0.33707	0.85498	1.12602	1.82794
MAN/12/s2	-0.51492	0.15872	0.43547	0.96942	1.49931	1.76952	2.39726
MAN/12/s3	-1.93993	-1.73689	-1.5501	-0.88349	0.24697	0.96497	2.76128
MAN/12/s4	-0.44528	0.04767	0.25751	0.67229	1.10965	1.35885	2.41796
MAN/12/s5	-0.41058	0.10598	0.32121	0.74109	1.17028	1.40107	2.05489
MAN/12/s6	-1.95608	-1.80487	-1.66532	-1.16315	-0.28811	0.29487	2.00942
MAN/12/s7	-0.99042	-0.22457	0.16811	0.99094	1.84899	2.29509	3.35611
MAN/12/s8	-0.86928	-0.20584	0.15521	0.9353	1.76976	2.21249	3.32291

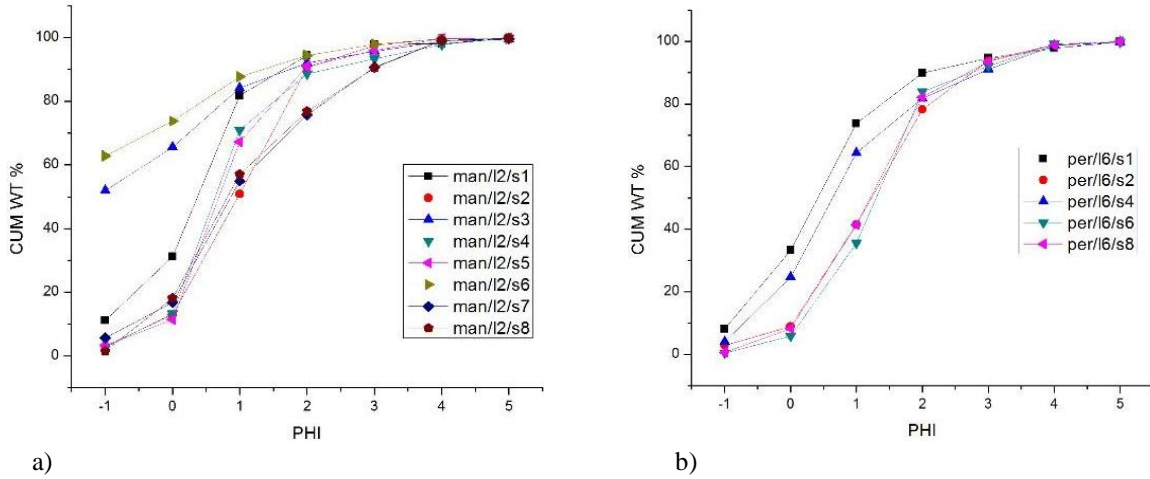


Figure 3: Phi (ϕ) values vs cumulative weight percentage of Cuddalore Formation.

Table 3: Calculated values of Mean, Standard Deviation, Skewness and Kurtosis of Cuddalore Formation

Name of sample	Median	Mean (Mz)	Standard Deviation (S_i)	Skewness (SK_Z)	Kurtosis (K_G)
PER/16/s1	0.39	-0.2241	1.0786	0.09026	1.1401
PER/16/s2	1.2281	1.2351	1.0155	0.0203	1.1012
PER/16/s4	0.6956	0.7458	1.2212	0.1211	0.1233
PER/16/s6	1.2625	1.274	0.8137	0.0468	1.1563
PER/16/s8	1.1893	1.202	0.9185	0.0421	1.1163
MAN/12/s1	0.337	0.3312	0.8694	-0.2805	1.2226
MAN/12/s2	0.9694	0.9658	0.8439	-0.0129	1.1218
MAN/12/s3	-0.8834	-0.5518	1.3877	1.1934	1.0721
MAN/12/s4	0.6722	0.6924	0.7616	0.1333	0.9999
MAN/12/s5	0.741	0.7493	0.6973	0.0424	0.6391
MAN/12/s6	-1.1631	-0.891	1.1257	0.4944	1.18
MAN/12/s7	0.9909	1.0204	1.2884	0.0617	1.0597
MAN/12/s8	0.9353	0.9806	1.2397	0.0976	1.0641

Table 4: Discriminant Function values of Cuddalore Formation.

Name of sample	Y1	Y2	Y3
PER/16/s1	8.153934	90.097	-9.9093
PER/16/s2	2.736972	106.8056	-8.59933
PER/16/s4	1.990468	96.3926	-11.0831
PER/16/s6	1.967808	95.65386	-6.94558
PER/16/s8	2.497846	100.5878	-7.86408
MAN/12/s1	6.424714	79.85624	-6.09819
MAN/12/s2	3.196039	91.09451	-7.00786
MAN/12/s3	7.96491	123.9943	-18.1145
MAN/12/s4	3.184022	81.79858	-7.08537
MAN/12/s5	1.808395	70.14188	-6.07787
MAN/12/s6	9.993275	90.80873	-12.4881
MAN/12/s7	4.298015	121.3585	-11.2583
MAN/12/s8	4.198964	118.267	-11.018

Geochemical Analysis

The average percentage of major oxides was compared with Post-Archean Australian Shale

(PAAS) and Upper Continental Crust (UCC) (Table.5). The average percentage of Na_2O , MgO , Al_2O_3 , P_2O_5 , K_2O , CaO , MgO and Fe_2O_3 is less

compared to PAAS and UCC (Taylor and McLennan,1985). The average percentage of SiO₂ is more as compared to PAAS and UCC (Taylor and

McLennan, 1985) whereas the average percentage of TiO₂ is more than UCC and less than PAAS.

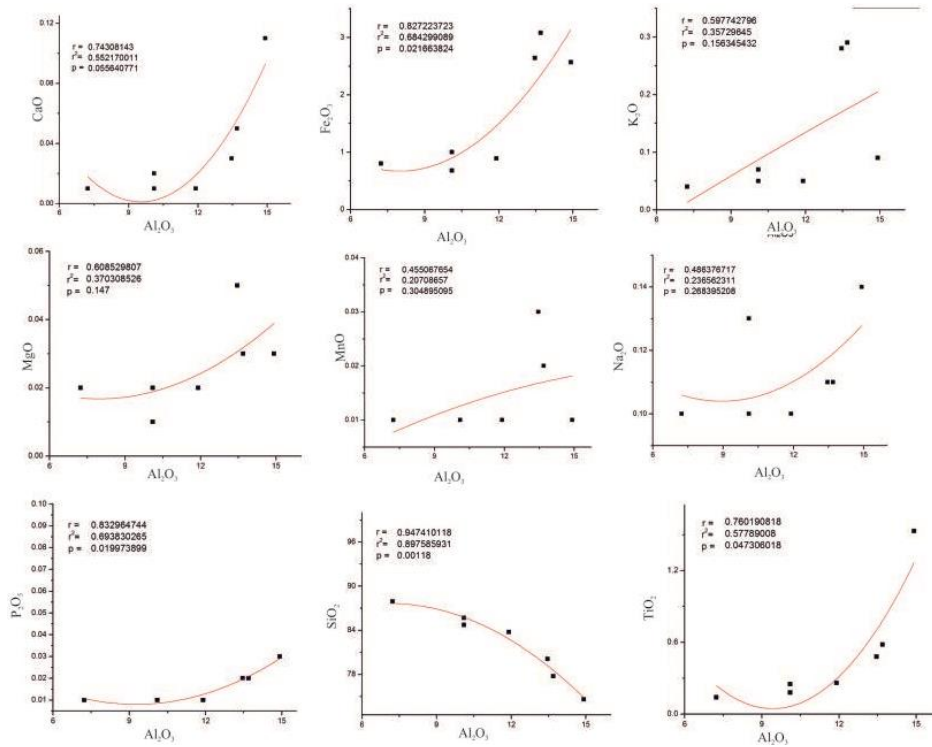


Figure 4: Distribution of major elements against Al₂O₃ from sediments of Cuddalore Formation (Litholog C)

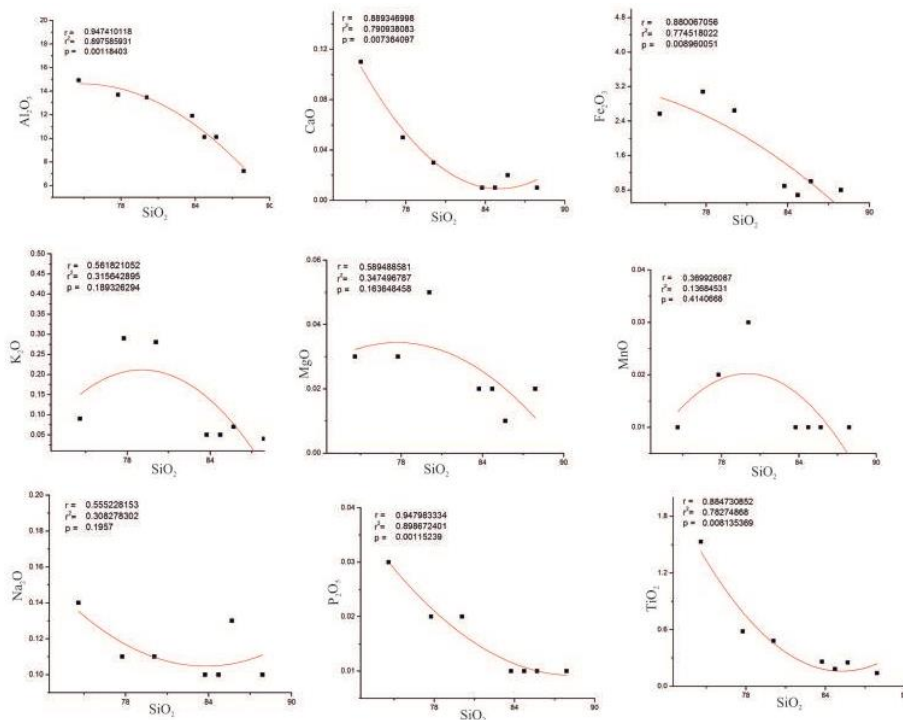


Figure 5: Distribution of major elements against SiO₂ of the Samples of Cuddalore Formation. (Litholog C)

Table 5: Major and trace element distribution of the Cuddalore and Manaveli sediments (PAAS and UCC data from; Taylor and McLennan 1985).

Sample	MAN/ L2/S1	MAN/ L2/S2	MAN/ LL2/S3	MAN/ LL2/S4	MAN/ LL2/S5	MAN/ LL2/S6	MAN/ LL2/S7	MAN/ L3/S1	MAN/ L3/S2	MAN/ L4/S1	MAN/ L4/S2	MAN/ L4/S3	MAN/ L4/S4	AVG	PAAS	UCC	
	Cuddalore Formation							Manaveli Formation									
Na ₂ O %	0.13	0.10	0.14	0.10	0.10	0.11	0.11	0.42	0.29	0.78	0.48	0.26	0.43	0.2653	1.2	3.90	
MgO %	0.01	0.02	0.03	0.02	0.02	0.03	0.05	1.09	1.21	1.09	1.96	2.16	1.45	0.7030	2.2	2.2	
Al ₂ O ₃ %	10.10	7.23	14.92	10.10	11.91	13.69	13.46	19.84	22.16	16.92	18.60	16.55	19.70	15.013	18.90	15.20	
SiO ₂ %	85.69	87.91	74.59	84.73	83.76	77.76	80.08	60.09	57.72	62.39	58.19	50.34	59.47	70.978	62.3	66	
P ₂ O ₅ %	0.01	0.01	0.03	0.01	0.01	0.02	0.02	0.01	0.01	0.02	0.02	0.04	0.03	0.018	0.16	0.17	
K ₂ O %	0.07	0.04	0.09	0.05	0.05	0.29	0.28	1.97	1.62	2.09	1.80	1.56	1.90	0.908	3.70	3.40	
CaO %	0.02	0.01	0.11	0.01	0.01	0.05	0.03	1.26	1.36	1.30	1.59	1.50	1.42	0.666	1.30	4.20	
TiO ₂ %	0.25	0.14	1.53	0.18	0.26	0.58	0.48	0.58	0.56	0.48	0.67	0.54	0.55	0.523	1.00	0.50	
MnO %	0.01	0.01	0.01	0.01	0.01	0.02	0.03	0.01	0.01	0.01	0.01	0.01	0.01	0.012	0.11	0.1	
Fe ₂ O ₃ %	1.00	0.80	2.57	0.68	0.89	3.08	2.64	4.04	4.46	5.46	4.58	12.85	5.48	3.733	7.23	4.5	
SiO ₂ /Al ₂ O ₃	8.48	12.15	4.99	8.38	7.03	5.68	5.94	3.02	2.60	3.68	3.12	3.04	3.018	--	--	--	
K ₂ O/Na ₂ O	0.53	0.4	0.64	0.5	0.5	2.63	2.54	4.69	5.58	2.67	3.75	6	4.41	--	--	--	
K ₂ O/Al ₂ O ₃	0.0069	0.005	0.006	0.005	0.004	0.021	0.02	0.099	0.073	0.123	0.096	0.094	0.09	--	--	--	
Fe ₂ O ₃ /K ₂ O	14.28	20	28.55	13.6	17.8	10.62	9.42	2.05	2.75	2.61	2.54	8.23	2.88	--	--	--	
Na ₂ O/K ₂ O	1.85	2.5	1.55	2	2	0.37	0.39	0.21	0.17	0.37	0.26	0.16	0.22	--	--	--	
Al ₂ O ₃ /TiO ₂	40.4	51.64	9.75	56.11	45.80	23.60	28.04	34.20	39.57	35.25	27.76	30.64	35.81	--	--	--	
CIA	97.86	97.96	97.77	98.44	98.67	96.81	96.97	84.46	87.14	80.22	82.77	83.29	84	--	--	--	
ICV	0.98	0.83	1.05	0.69	0.62	2.83	2.74	11.81	8.78	14.79	11.59	12.13	11.59	--	--	--	
PIA	98.52	98.49	98.34	98.91	99.08	98.82	98.94	91.40	92.56	87.69	89.03	89.49	90.58	--	--	--	
CIW	98.53	98.50	98.35	98.92	99.08	98.84	98.97	92.19	93.07	89.05	89.98	90.38	91.41	--	--	--	

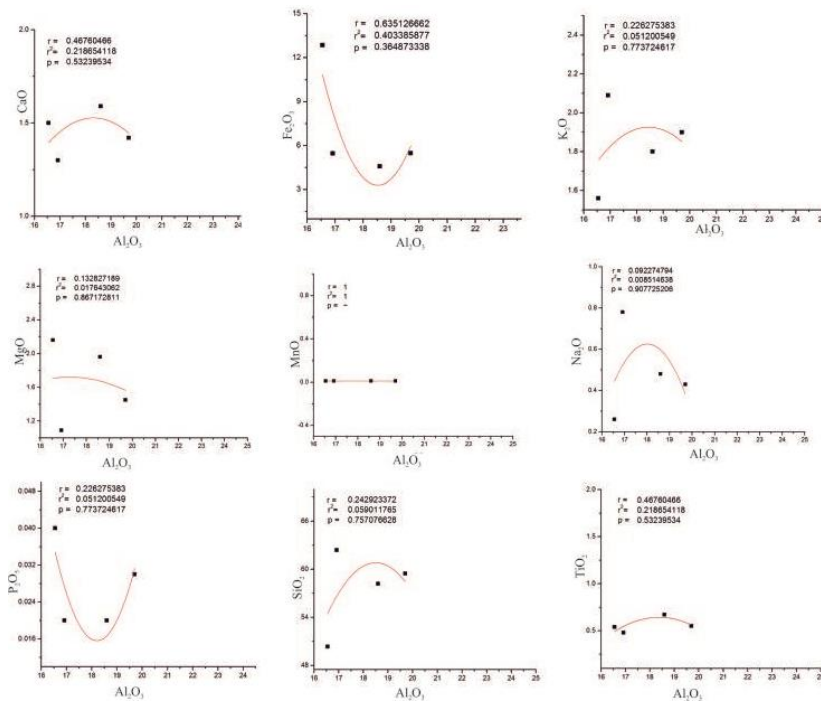


Figure 6: Distribution of major elements against Al_2O_3 of the Samples of Manaveli Formation. (Litholog A)

Discussion

The depositional environments of the Manaveli and Cuddalore formations were discussed here based on granulometric data whereas weathering intensity, compositional maturity, paleoclimate and provenance were deduced on the basis of geochemical data.

Depositional Environment

Discriminant Function Y1, Y2 and Y3 calculated using formula given by Sahu (1964), based on graphic measurements (Folk and Ward, 1957) were employed to understand depositional environment of sediments.

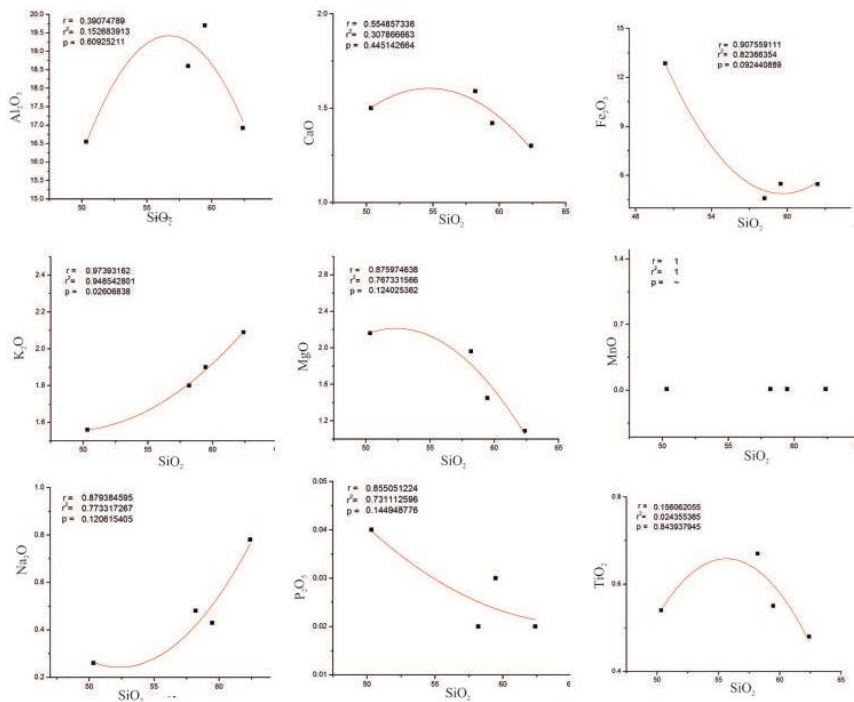


Figure 7: Distribution of major elements against SiO_2 of the Samples of Manaveli Formation (Litholog A)

Litholog C: Discriminant Function values suggested that 100% of MAN/L2 samples of Cuddalore Formation used to calculate Y1 fall in beach environment. 100 % Y2 values fall in shallow marine environment and 50% Y3 values fall in fluvio-deltaic environment and 50% of samples fall in shallow marine environment. Litholog D: Discriminant

function values suggested that 100% of PER/L6 samples of Cuddalore Formation used to calculate Y1 fall in beach environment. 100 % Y2 values fall in shallow marine environment and 83.4% Y3 values fall in fluvio-deltaic environment and 16.6% of samples fall in shallow marine environment.

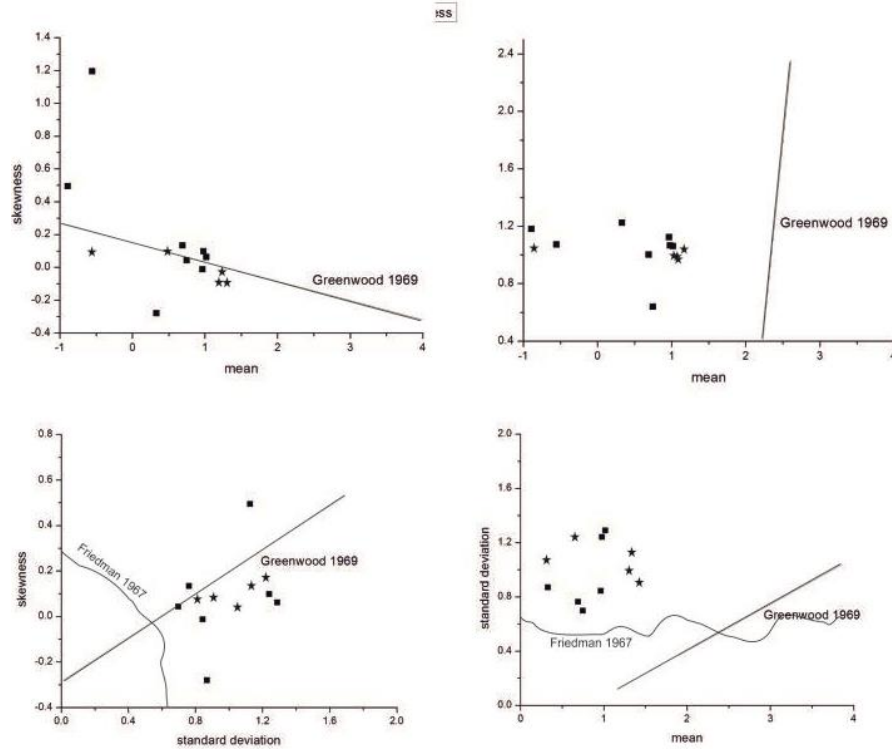


Figure 8: Grain size bivariate plot of MAN/L2 section of Cuddalore Formation (Litholog C), Bivariate plots viz., mean vs. kurtosis, mean vs. skewness, mean vs. standard deviation and standard deviations vs. skewness are prepared in figure 8. The samples from section MAN/L2 and PER/L6 of Cuddalore Formation show deposition of sediments dominantly in riverine to deltaic environment.

Weathering Intensity and Compositional Maturity

The discriminant function analyses of the sediments from the Cuddalore Formation infer that mostly the sedimentation was in fluvio-deltaic environment with incursions of shallow marine environment. Bivariate plots / graphs are widely used to understand the depositional environments (Friedman,1961,1962 and 1967; Greenwood ,1969). Various bivariate plots were prepared and interpreted as follows. In order to interpret the degree of chemical weathering and compositional maturity, various chemical weathering indices have been proposed (Nesbitt and Young, 1982). These Chemical weathering indices characterizes different weathering profiles (Price and Velbel, 2003). The Chemical Index of Alteration (CIA = { Al₂O₃ / (Al₂O₃+ CaO*+Na₂O+K₂O) } × 100) by Nesbitt and Young (1982), Index of Compositional Variability (ICV={ (Fe₂O₃ +K₂O+Na₂O + CaO*+MgO+MnO+TiO₂) /Al₂O₃ } × 100) by Cox and Lowe, (1995),

Plagioclase Index of Alteration (PIA={ (Al₂O₃-K₂O)/ (Al₂O₃ + CaO* +Na₂O-K₂O) } × 100) by Fedo et al., (1995) The Chemical Index of Weathering (CIW = { (Al₂O₃ / (Al₂O₃+ CaO* + Na₂O) } × 100) (Harnois 1988) were used in the present work to deduce source area weathering conditions.

These chemical signatures of sedimentary records have been found useful to define the source area weathering conditions (Nesbitt and Young, 1982, 1984; McLennan et al.,1993; Fedo et al., 1995).

The CIA values of sediments from Cuddalore Formation (Fig. 9, A) were plotted against Al₂O₃ to understand weathering condition of source rock. All plotted CIA values occupied space in the region of intensive weathering, thus it indicates that the sediments of the Cuddalore Formation were derived from the area which was intensively weathered.

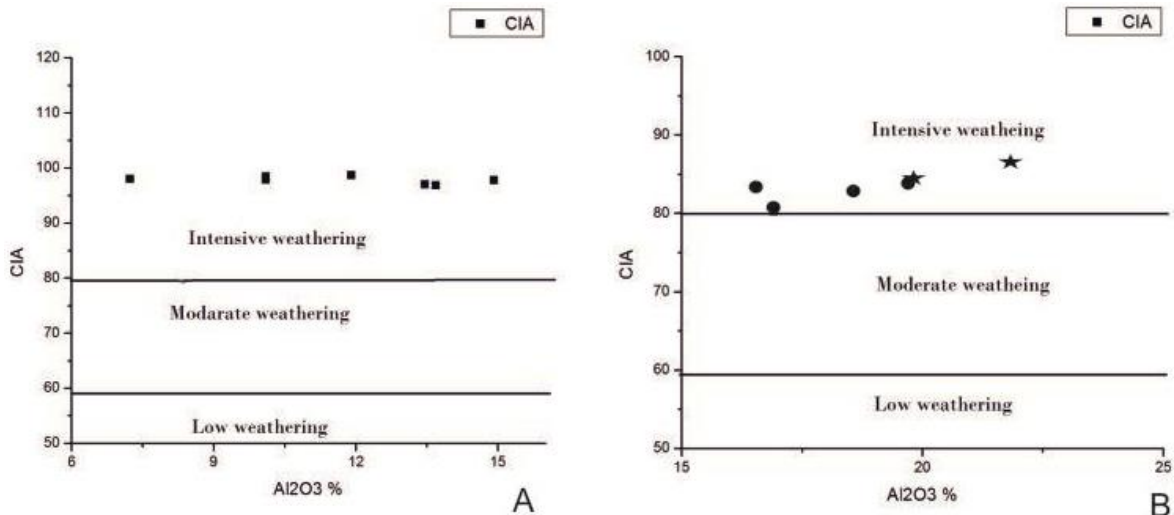


Figure 9: Bivariate plot of CIA against Al₂O₃ showing weathering conditions of source rock of Cuddalore (A) and Manaveli formations (B) (after Nesbitt and Young 1982).

The CIA values of sediments from Manaveli Formation (Fig. 9, B) were plotted against Al₂O₃ to understand weathering condition of source rock. All plotted CIA values occupied space in the region of intensive weathering, thus it indicates that the sediments of the Manaveli Formation were derived from the area which was intensively weathered.

In the present study, the ICV value of the sediments from Cuddalore Formation varies from 0.61 to 2.4 (average 1.39) indicating that sediments of Cuddalore Formation are compositionally moderate to well matured whereas the ICV values of the sediments from Manaveli Formation ranges from 8.77 to 14.79 (average 11.78) suggesting that sediments are compositionally moderately matured. The K₂O/Na₂O ratios for the studied samples from the Cuddalore Formation vary from 0.4 to 2.63,

which infer moderate to high maturity whereas the values K₂O/Na₂O ratios for Manaveli Formation range from 2.67 to 6 indicate moderate maturity. The PIA and CIW values range from 98.34 to 98.94 and 98.53 to 98.97 for the Cuddalore Formation whereas, 87.69 to 92.56 and 89.05 to 92.19 for the Manaveli Formation, infer intense source area weathering.

The binary relation of major oxides ratios and their logs can be implemented to understand the chemical maturity of the sediments. The logs of SiO₂/Al₂O₃, Na₂O/K₂O and Fe₂O₃/K₂O are commonly used for determining the chemical maturity. Bivariate plots of these ratios are useful to discriminate mature and immature sediments (Pettijohn et al., 1972; Herron, 1988; Vital and Stattegger, 2000).

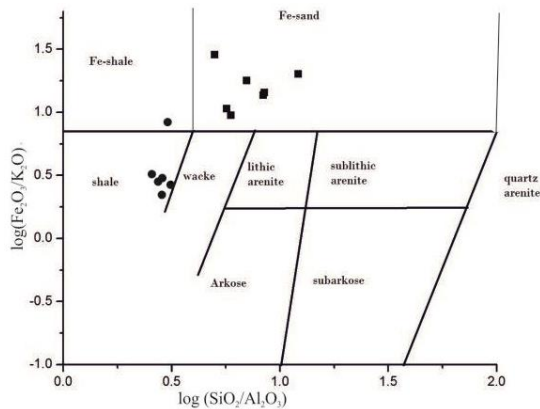


Figure 10a: Bivariate plots of log (SiO₂/Al₂O₃) vs. log (Fe₂O₃/K₂O) of the MAN/L2 sample of Cuddalore and Manaveli formations (after Herron, 1988).

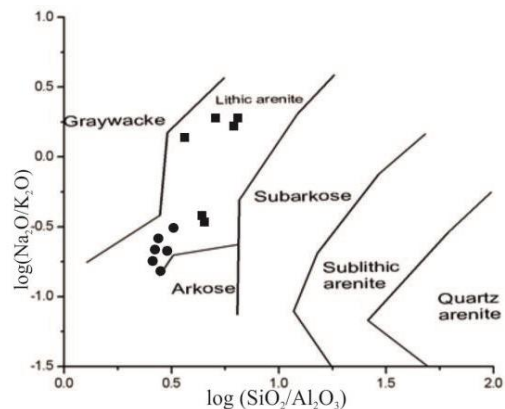


Figure 10b: Bivariate plot of log (SiO₂/Al₂O₃) vs. log (Na₂O/K₂O) of the MAN/L2 sample of Cuddalore and Manaveli formations (after Pettijohn et al., 1972)

Paleoclimate and Provenance

Bivariate plots of log (SiO₂/Al₂O₃) vs. log (Fe₂O₃/K₂O) and log (SiO₂/Al₂O₃) vs. log

(Na₂O/K₂O) indicate that the sediments from Cuddalore and Manaveli formations were moderately matured.

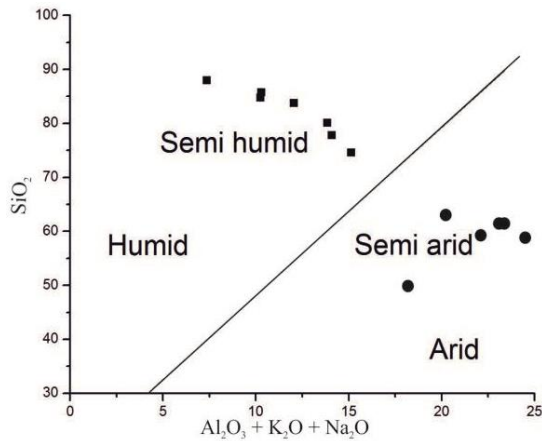


Figure 11 Bivariate plot of $\text{Al}_2\text{O}_3 + \text{K}_2\text{O} + \text{Na}_2\text{O}$ against SiO_2 showing climatic condition of Cuddalore and Manaveli formations (after Suttner and Dutta, 1986).

Suttner and Dutta (1986) have established a relationship between $(\text{Al}_2\text{O}_3 + \text{K}_2\text{O} + \text{Na}_2\text{O})$ and SiO_2 that can be used to discuss chemical maturity and climatic condition of source rock area. In the Bivariate plot of $(\text{Al}_2\text{O}_3 + \text{K}_2\text{O} + \text{Na}_2\text{O})$ against SiO_2 (Suttner and Dutta, 1986), all the samples of the Cuddalore Formation fall in semi-humid zone (Fig.11) and Manaveli Formation fall in semi-arid zone (Fig.11). Thus, the bivariate plot of the samples of the Cuddalore Formation infers that the sediments are chemically well mature and deposited in semi-humid and samples of Manaveli Formation are chemically moderately mature and deposited in semi-arid climatic conditions.

The discriminant function diagram is widely used in the provenance study. Roser and Korsch (1988) have given the discriminant function diagram. They have proposed 2 discriminant functions which are as $F1 = (-1.733\text{TiO}_2 + 0.607\text{Al}_2\text{O}_3 + 0.76\text{Fe}_2\text{O}_3 - 1.5\text{MgO} + 0.616\text{CaO} + 0.509\text{Na}_2\text{O} - 1.224\text{K}_2\text{O} - 9.09)$ and $F2 = (0.445\text{TiO}_2 + 0.07\text{Al}_2\text{O}_3 - 0.25\text{Fe}_2\text{O}_3 - 1.142\text{MgO} + 0.438\text{CaO} + 1.475\text{Na}_2\text{O} + 1.426\text{K}_2\text{O} - 6.86)$ and 4 provenance fields which are as (P1) Mafic igneous provenance, (P2) Intermediate igneous provenance, (P3) Felsic igneous provenance, and (P4) Quartzose sedimentary provenance. The bivariate plot (Roser and Korsch, 1988) of F1 against F2 can be used for interpreting the provenance.

In the discriminant function diagram, all the samples of Cuddalore Formation fall in P4 region indicating the sedimentary provenance and samples of Manaveli Formation fall in P1 region indicating the Mafic igneous provenance. Hayashi et al. (1997) suggested $\text{Al}_2\text{O}_3 / \text{TiO}_2$ ratio increases from 3 to 8 for mafic igneous rocks, from 8 to 21 for intermediate rocks and from 21 to 70 for felsic igneous rocks. The

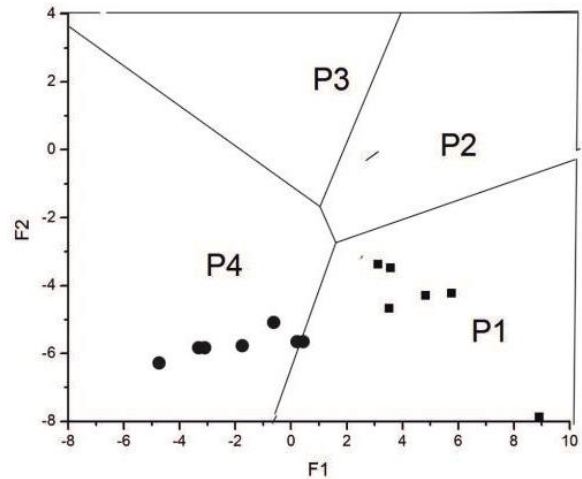


Figure 12: Discriminant function F1 against discriminant function F2 variation diagram of Cuddalore Formation and Manaveli Formation, fields after Roser and Korsch (1988), Provenance fields: (P1) Mafic igneous provenance, (P2) Intermediate igneous provenance, (P3) Felsic igneous provenance, and (P4) Quartzose sedimentary provenance (after Roser and Korsch, 1988).

values of $\text{Al}_2\text{O}_3 / \text{TiO}_2$ ratios vary from 9.75 to 51.64 (average 36.47) for Cuddalore Formation and 27.76 to 39.57 (average 33.87) for Manaveli Formation, inferring felsic igneous provenance for both.

Conclusions

The discriminant function analysis of the sediments from the Cuddalore Formation infers that mostly the sedimentation occurred in fluvio-deltaic environment with incursions of shallow marine environment whereas bivariate plots suggests that the deposition occurred in riverine to deltaic environment. The weathering indices of the sediments from Manaveli and Cuddalore formations infer high/intense weathering prevailed in source area of sediments for Manaveli and Cuddalore formations. The sediments of Cuddalore Formations are chemically moderately to well mature whereas, the sediments from Manaveli Formation are moderately mature. The ratio $(\text{Al}_2\text{O}_3 + \text{K}_2\text{O} + \text{Na}_2\text{O}) / \text{SiO}_2$ indicate semi-humid climatic conditions during deposition of Cuddalore Formation whereas, Manaveli Formation was deposited in semi-arid climatic conditions. The discriminant function diagram suggests quartzose sedimentary provenance for Cuddalore and Mafic igneous provenance for Manaveli Formation. The $\text{Al}_2\text{O}_3 / \text{TiO}_2$ ratios of Cuddalore and Manaveli formations, infer felsic igneous provenance for both.

Acknowledgments

We would like to thank Principal and Head of Geology Department, Fergusson College (Autonomous) Pune for his moral support and constant encouragement. We are also thankful for financial assistance from BCUD Savitribai Phule Pune University, Pune under Minor Research Project

2016-2018. We are greatly indebted to anonymous

reviewer for critical reviews of the manuscripts.

References

- Armstrong-Altrin, J. S., Nagarajan, R., Madhavaraju, J., Rosales-Hoz, L., Lee, Y. I., Balam, V., Cruz-Martínez, A. and Avila-Ramírez, G. (2013). Geochemistry of the Jurassic and Upper Cretaceous shales from the Molango Region, Hidalgo, eastern Mexico: Implications for source-area weathering, provenance, and tectonic setting. *Comptes. Rendus. Geosci.*, v. 345, 185–202.
- Armstrong-Altrin, J. S., Machain-Castillo, M. L., Rosales-Hoz, L., Carranza-Edwards, A., Sanchez-Cabeza, J. A. and Ruiz-Fernández, A. C. (2015). Geochemistry of deep sea sediments from the south-western Gulf of Mexico, Mexico: Implication for depositional environment. *Cont. Shelf. Res.*, 95, 15–26.
- Ayyasamy, K. (1990). Cretaceous heteromorph ammonoid biostratigraphy of southern India: *Newsletters on Stratigraphy*, 22 (2-3), 111-118.
- Bhatia, M. R. (1983). Plate tectonics and geochemical composition of sandstones. *Jour. Geol.*, 91, 611–627.
- Bhatia, M. R. and Crook, K. A. W. (1986). Trace element characteristics of graywackes and tectonic setting discriminant of sedimentary basins. *Contrib. Mineral. Petrol.*, 92, 181–193.
- Blanford, H. F. (1862). On the Cretaceous and other rocks of the South Arcot and Trichinopoly districts. *Memoirs of the Geological Survey of India*, 4, 1–217.
- Chandrasekaran, V.A. Ramkumar, M. and Jacob, M., (1996). Sediment deformational structures from the Sillakkudi Formation (Campanian) Ariyalur Group, Tiruchy district, Tamil Nadu. *Journal of the Indian Association of Sedimentologists*, 15, 43–49.
- Cox, R. and Lowe, D. R. (1995). A conceptual review of regional scale controls on the composition of clastic sediment and the coevolution of continental blocks and their sedimentary cover. *Jour. Sediment. Res.*, 65, 1–12.
- Condie, K. C. (1993). Chemical composition and evolution of the upper continental crust: contrasting results from surface samples and shales. *Chem. Geol.*, 104, 1-37.
- Dickinson, W. R. and Suczek, C. A. (1979). Plate tectonics and sandstone composition. *AAPG Bull.*, 63, 2164–2182.
- Fedo, C. M., Nesbitt, H. W. and Young, G. M. (1995). Unraveling the effects of potassium metasomatism in sedimentary rocks and paleosols, with implications for paleoweathering conditions and provenance. *Geology.*, 23, 921–924.
- Folk, R. L. and Ward, H. W. (1957). Brazos river bar: a study in the significance of grain size parameter. *Jour. Sedim. Petrol.*, 27, 3-26.
- Friedman, G.M. (1961). Distinction between dune, beach, and river sands from their textural characteristics. *Jour. Sedi. Petrol.*, 31, 514-529.
- Friedman, G.M. (1962). On sorting coefficient and the log normality of grain size distribution in sandstones. *Jour. Geo.*, 70, 737-753.
- Friedman, G.M. (1967). Dynamic processes and parameters compared for size frequency distribution of beach and river sands. *Jour. Sedi. Petrol.*, 37(2), 327-354.
- Friedman, G. M. (1979.) Differences in size distributions of populations of particles among sands of various origins. *Sedimentol*, 26,3–32,
- Greenwood, B. (1969). Sediment parameters and environment discrimination: an application of multivariate statistics. *Canadian Jour. of Earth Sciences*, 6, 1347-1358.
- Ghaznavi, A. A., Quasim, M. A., Ahmad, A. H. M., and Ghosh, S. K. (2019). Granulometric and facies analysis of Middle–Upper Jurassic rocks of Ler Dome, Kachchh, western India: An attempt to reconstruct the depositional environment. *Geologos*, 25(1), 51–73.
- Ghosh, S. K., and Chatterjee, B. K. (1994). Depositional mechanism as revealed from grain-size measures of the Palaeoproterozoic Kolhan siliciclastics, Keonjhar District, Orissa, India. *Sedimentary Geology*, 89,181–196.
- Govindan, A., Ananthanarayanan, S. and Vijayalakshmi, K.G., (2000). Cretaceous petroleum system in Cauvery basin, India. In: Govindhan, A. (ed.), *Cretaceous stratigraphy – An update*. *Memoirs of the Geological Society of India*, 46, 365–382.
- Govindan, A., Ravindran, C.N. and Rangaraju, M.K., (1996). Cretaceous stratigraphy and planktonic foraminiferal zonation of Cauvery basin, South India. In: Sahni, A. (ed.), *Cretaceous stratigraphy and palaeoenvironments*. *Memoirs of the Geological Society of India*, 37, 155–187.
- Govindan, A. (1972). Upper Cretaceous planktonic foraminifera from the Pondicherry area, south India. *Micropaleontology*, 18, 160–183.
- Hart, M.B., Bhaskar, A. and Watkinson, M.P., (2000). Larger foraminifera from the upper Cretaceous of the Cauvery basin, S.E. India. In: Govindhan, A. (ed.), *Cretaceous stratigraphy – An update*. *Memoirs of the Geological Society of India*, 46, 159–171.
- Hayashi Ken-I, H., Fujisawa H.D., Holland & H. Ohmoto (1997) Geochemistry of 1.9 Ga sedimentary rocks from northeastern Labrador, Canada *Geochim Cosmochim. Acta* 61, 4115–4137
- Harnois, L. (1988). The CIW index: A new chemical index of weathering. *Sediment. Geol.*, 55, 319–322.
- Herron, M. M. (1988). Geochemical classification of terrigenous sands and shales from core or log data. *Jour. Sediment. Petrol.*, 58, 820-829.
- Jaiprakash, B. C., Venkatesh, P., Maya V. P., Gilbert, H. and Selvin, S. P. (2016) Biochron and tectonic framework for the origin of KTB Canyon in Nagapattinam sub-basin, Cauvery Basin. *Proceedings of Indian National Science Academy*, 82: 905–921.
- Kishor, S. (2004a). Palaeo-ecological significance of Palaeocene Calcareous algae from th Cauvery Basin, India, *Ecoprint*, 11 (1), 59-63.
- Kishor, S. (2004b). Occurrence and significance of the Palaeocene Green alage (Dasycladacean and Utoteacean) from Cauvery Basin, India. *Geophytology*, 33 (1&2), 39-46.
- Kishor, S. and Singh S.K. (2004). Coralline alage from the Ninniyur Formation (Thnetian) of the Cauvery Basin, South India., *Our Nature*, 2, 1-6.
- Kishor, S., Misra, P.K., Jauhri, A.K. and Singh, S. K. (2003). Calcareous algal association from the Ninniyur Formation (Palaeocene) of the Cauvaery Basin, India, *Ecoprint*, 10(1), 13-17.
- Khan Z, Quasim M.A., Amir M, and Ahmad AHM. (2019) Provenance, tectonic setting, and source areaweathering of Middle Jurassic siliciclastic rocks of Chari Formation, Jumara Dome, Kachchh Basin, Western India: Sedimentological, mineralogical, and geochemical constraints. *Geological Journal*, 55 (5), 3537-3538.
- Krishnan, M.S. (1960). *Geology of India and Burmah*. Higginbothams Pvt. Ltd., Madras.
- Krumbein, W. C. (1936). Application of logarithmic moments to size- frequency distribution of sediments. *Jour. Sediment. Petrol.*, 6, 35-47.
- Kossmat, F. (1897) *The Cretaceous deposits of Pondicherry*. *Records of the Geological Survey of India*, 30, 51–110.
- Lone, A., Babeesh, C., Achyuthan, H. and Chandra, R. (2017). Evaluation of environmental status and geochemical assessment of sediments, Manasbal Lake, Kashmir, India, *Arab J Geosci*, 10:92, 1-18, DOI 10.1007/s12517-016-2826-7.
- Madhavaraju, J. (2015). Geochemistry of Campanian–Maastrichtian sedimentary rocks in the Cauvery basin, south India; In: *Constraints on paleoweathering, provenance and Cretaceous environments* (ed.) Ramkumar M, *Chemostratigraphy: Concepts, Techniques and Applications; Elsevier Spl. Volume.*, 185–214.
- Madhavaraju, J. and Ramasamy, S. (2002). Petrography and major element geochemistry of Late Maastrichtian–Early Paleocene sediments of Tiruchirapalli, Tamil Nadu – Paleoweathering and provenance implication. *Jour. Geol. Soc.*, 9, 133–142.
- Madhavaraju, J. and Lee, Y. I. (2010). Influence of Deccan volcanism in the sedimentary rocks of Late Maastrichtian–

- Danian age of Cauvery basin, southeastern India: Constraints from Geochemistry. *Curr. Sci.*, 98, 528–537
- Madhavaraju, J. and Gonz'alez-Le'on, C. M. (2012). Depositional conditions and source of rare earth elements in carbonate strata of the Aptian–Albian Mural Formation, Pitaycachi section, northeastern Sonora, Mexico. *Rev. Mex. Cienc. Geol.*, 29, 478–491.
- Madhavaraju, J., Erik Ramirez-Montoya, E., Monreal, R., Gonz'alez-Leon, C. M., Pi-Puig, T., spinoza-Maldonado, I. G. and Grijalva-Noriega, F. J. (2016). Paleoclimate, paleoweathering and paleoredox conditions of Lower Cretaceous shales from the Mural Limestone, Tuape section, northern Sonora, Mexico: Constraints from clay mineralogy and geochemistry. *Rev. Mex. Cienc. Geol.*, 33(1), 34–48.
- Mahalanobis, P. C. (1930). On tests and measures of group divergence. *J. and Proc. Asiatic Soc. of Bengal*, 27, 541–588.
- Malarkodi, N., Patel, S. J., Fayazudeen P. J. and Mallikarjuna U. B. (2009). Paleoenvironmental Significance of Trace fossils from the Palaeocene sediments of the Pondicherry area, South India. *Jour. Geol. Soc. Ind.* 74, 738–748.
- Mamgain, V. D., Rao, B. R. J. & Sastry, M. V. A. (1968). The Niniyur Group of Trichinopoly, south India (Cretaceous–Tertiary formations of South India). *Memoirs of the Geological Society of India*, 2, 85–91.
- Mamgain, V. D., Sastry, M. V. A. and Subbaraman, J. V. (1973). Report of ammonites from Gondwana plant beds at Terani, Tiruchirapalli district, Tamil Nadu. *Journal of the Geological Society of India*, 14, 189–200.
- Mason, C.C., Folk, R.L., (1958). Differentiation of beach, dune and aeolian flat environments by size analysis. *Mustang Island, Texas. Journal of Sedimentary Petrology*, 28, 211–226.
- McLennan, S. M. and Taylor, S. R. (1991). Sedimentary rocks and crustal evolution: Tectonic setting and secular trends. *Jour. Geol.*, 99, 1–21.
- McLennan, S. M., Hemming, S., McDaniel, D. K. and Hanson, G. N. (1993). Geochemical approaches to sedimentation, provenance and tectonics; In: *Processes Controlling the Composition of Clastic Sediments* (eds) Johnson M J and Basu A, Geological Society of America Special Paper, USA , 21–40.
- McLennan, S. M. (1989). Rare earth elements in the sedimentary rocks: Influence of provenance and sedimentary processes. *Rev. Mineral.*, 21, 169–200.
- McLennan, S. M. (1993). Weathering and global denudation. *Jour. Geol.*, 101, 295–303.
- McLennan, S. M. (2001). Relationships between the trace element compositions of sedimentary rocks and upper continental crust. *Geochem. Geophys. Geosyst.*, 2, 2000GC000109.
- Misra, P.K. and Kumar, P. (1988). Fossil algae from the Cretaceous of Varagur, Tiruchirapalli District, Tamil Nadu. *Palaeobot.*, 37(1), 36–51.
- Misra, P.K., Jauhri, A.K., Kishor, S. and Chowdhury, A. (2000). Calcareous algae (Dasycladaceans and Gymnocodiacean) from the Palaeocene deposits of the Tiruchirapalli (= Trichinopoly) area, Tamil Nadu, India. *Journal of Palaeontological Society of India*, 45, 151–164.
- Misra, P.K., Jauhri, A.K., Chowdhury, A. and Kishor, S. (2001). Palaeocene Rhodophycean algae from the Ninniyur Formation of the Cauvery Basin, Southern India. *Palaeobotanists*, 50 (2 and 3), 311–339.
- Misra, P.K., Kishor, S., Jauhri, A.K. and Singh, S. K. (2003). Coralline algae from the Ninniyur Formation, Cauvery Basin, South India, 48, 89–97.
- Misra, P.K., Rajanikanth, A., Jauhri, A.K., Kishore, S. and Singh, S.K. (2004). Albian limestone building algae of Cauvery Basin, South India. *Curr. Sci.*, 87, 1516–1518.
- Misra, P.K., Jauhri, A.K., Singh, S.K., Kishore, S. and Rajanikanth, A. (2006). Non-geniculate coralline algae from the Uttatur Group (Early Cretaceous), south India. *Palaeobotanist*, 55(1-3), 29–40.
- Moiola, R.J. and Weiser, D., (1968). Textural parameters: An evaluation. *Journal of Sedimentary Petrology*, 38(1), 45–53.
- Mude, S. N., Parcha, S. K., Pandey, S. and Madane, S. (2019). Geochemistry, Provenance, Compositional Maturity and Source area weathering of Mastani Lake sediments, India. *Journal of Geosciences Research, India*, 4 (2): 143–154.
- Muthuvairasamy, R., Stüben, D. and Berner, Z., 2003. Lithostratigraphy, depositional history and sea level changes of the Cauvery Basin, southern India: Geoloski anali Balkanskog poluostrva, 65, 1–27.
- Nagarajan, R., Madhavaraju, J., Nagendra, R., Armstrong-Altrin, J. S. and Moutte, J. (2007a). Geochemistry of Neoproterozoic shales of the Rabanpalli Formation, Bhima basin, Northern Karnataka, southern India: Implications for provenance and paleoredox conditions. *Rev. Mex. Cienc. Geol.*, 24, 150–160.
- Nagarajan, R., Armstrong-Altrin, J. S., Nagendra, R., Madhavaraju, J. and Moutte, J. (2007b). Petrography and geochemistry of terrigenous sedimentary rocks in the Neoproterozoic Rabanpalli Formation, Bhima basin, southern India: Implications for paleoweathering condition, provenance, and source rock composition. *Jour. Geol. Soc.*, 70, 297–312.
- Nagendra, R., Reddy, A. N., Jaiprakash, B. C., Gilbert, H., Zakharov, Y. D. and Venkateshwarlu, M. (2019). Integrated Cretaceous stratigraphy of the Cauvery Basin, South India. *Stratigraphy*, 15 (4) : 245–259.
- Nagendra, R., Kamalakkannan, B. V., Gargi Sen, G., Bakkiaraj, H., Nallapa Reddy, A. and Jaiprakash, B. C. (2011). Sequence surfaces and paleobathymetric trends in Albian to Maastrichtian sediments of Ariyalur area, Cauvery Basin, India. *Journal of Marine and Petroleum Geology*, 28: 895–905.
- Nagendra, R. and Nallapa Reddy, A. (2017). Major geological events of the Cauvery Basin, India and their correlation with global signatures—A review. *Journal of Palaeogeography*, 6: 69–83.
- Nagendra, R., Patel, S. J., Deepankar, R. and Reddy, A. N. (2010). Bathymetric significance of the ichnofossil assemblages of the Kulakkalnattam sandstone, Ariyalur area, Cauvery Basin. *Journal of Geological Society of India*, 76: 525–535.
- Nair, K.M. and Vijayam, B.E., (1980). Sedimentology of limestones in Ninniyur Formation, Palaeocene, Cauvery basin, South India. *Journal of the Geological Society of India*, 21, 503–510.
- Nesbitt, H. W. and Young, G. M. (1982). Early Proterozoic climates and plate motions inferred from major element chemistry of lutites. *Nature*, 299, 715–717.
- Nesbitt, H. W. and Young, G. M. (1984). Prediction of some weathering trends of plutonic and volcanic rocks based on thermodynamic and kinetic considerations. *Geochim. Cosmochim. Acta.*, 8, 1523–1534.
- Pandey, S. and Parcha, S. K. (2017). Provenance, tectonic setting and source-area weathering of the lower Cambrian sediments of the Parahio valley in the Spiti basin, India. *Jour. Earth. Syst. Sci.*, 126 (27), 1–16.
- Pettijohn, F. J., Potter, P. E. and Siever, R. (1972). *Sand and Sandstones*. New York Springer-Verlag, 618.
- Price, J. R. and Velbel, M. A. (2003). Chemical weathering indices applied to weathering profiles developed on heterogeneous felsic metamorphic parent rocks. *Chem. Geol.*, 202 (3&4), 397–416.
- Prasad, G. V. R., Verma, O., John, J. F. and Anjali, G. (2013). A new Late Cretaceous vertebrate fauna from the Cauvery Basin, South India: Implications for Gondwanan paleobiogeography. *Journal of Vertebrate Paleontology*, 33: 1260–1268.
- Powell, C. McA., Roots, S. R. and Veevers, J. J. (1988). Pre-breakup continental extension in east Gondwanaland and the early opening of the Indian Ocean. *Tectonophysics.*, 155, 261–283.
- Quasim M. A., Ghosh S.K., Ahmad A.H.M, Srivastava, V.K. and Albaroot M.(2020) Integrated approach of lithofacies and granulometric analysis of the sediments of the Proterozoic Upper Kaimur Group of Vindhyan Supergroup, Son Valley, India: Palaeo-environmental implications. *Geological Journal*, 55 (9), 5591–6021. <https://doi.org/10.1002/gj.3781>
- Radulovic, V. and Ramamoorthy, K., (1992). Late Cretaceous (Early Maastrichtian) brachiopods from south India. *Senckenbergiana Lethaea*, 72, 77–89.

- Rajnikanth, A. (1992). Rock building Cretaceous-Tertiary algae from India - An ecological perspective. *Palaeobotany*, 40, 399-412.
- Rajagopalan, N. (1965). Late Cretaceous and Early Tertiary Stratigraphy of Pondicherry, South India, *Jour. Geol. Soc. India.*, 6, 104-121.
- Rajagopalan, N. (1968) A restudy of the Pondicherry Formation. *Mem. Geol. Soc. India.*, 2, 128-129.
- Rajamanickam, G. V. and Gujar, A. R. (1984) Sediment depositional environment in some bays in the Central West Coast of India; *Indian J. Mar. Sci.* 13, 53-59.
- Rajganapathi, V.C., Jitheshkumar, N., Sundararajan, M., Bhat, K.H. and Velusamy, S. (2013) Grain size analysis and characterization of sedimentary environment along Thiruchendur coast, Tamilnadu, India. *Arabian Journal of Geosciences*, 6: 4717-4728, DOI 10.1007/s12517-012-0709-0
- Ramasamy, S. and Banerji, R.K., (1991). Geology, petrography and systematic stratigraphy of pre-Ariyalur sequence in Trichirapalli district, Tamil Nadu, India. *Journal of the Geological Society of India*, 37, 577-594.
- Ramanujam, C.G.K. (1968). Some observations on the flora of the Cuddalore Series. *Memoir of Geological Society of India*, 2, 271-285.
- Rao, L.R. and Prasannakumar, C. (1932). Occurrence of Lithothamnion in the South Indian Cretaceous. *Nature*, 129, 776-777.
- Rao, L.R. and Pia, J. (1936). Fossil algae from the uppermost Cretaceous beds (The Ninniyur Group) of the Trichinopoly District, S. India. *Mem. Geol. Surv. India, Pal. India*, 21(4), 13-40.
- Rao, L.R. and Gowda, S.S. (1954). Solenoporaceae in the Cretaceous rocks of south India. *Curr. Sci.*, 23, 177-178.
- Reddy, A. N., Jaiprakash, B. C., Rao, M. V., Chidambaram, L. and Bhaktavatsala, K. V., (2013) Sequence stratigraphy of Late Cretaceous successions in the Ramnad Sub-basin, Cauvery Basin, India. *Geological Society of India Special Publication*, 1: 78-97.
- Roser, B. P. and Korsch, R. J. (1986). Determination of tectonic setting of sandstone-mudstone suites using SiO₂ content and K₂O/Na₂O ratio. *Jour. Geol.*, 94, 635-650.
- Roser, B. P. and Korsch, R. J. (1988). Provenance signature of sandstone-mudstone suite determined using discriminant function analysis of major element data. *Chem. Geol.*, 67, 119-139.
- Sastry, M.V.A. and Rao, B.R.J., (1964). Cretaceous-Tertiary boundary in south India. *Proceedings on the XII International Geological Congress on Cretaceous-Tertiary boundary including volcanic activity*, 3 (3),92-103.
- Sastry, M.V.A., Mamgain, V.D. & Rao, B.R.J., (1972). Ostracod fauna of the Ariyalur Group (Upper Cretaceous), Trichinopoly district, Tamil Nadu. *Palaeontologica Indica*, 40, 1-48.
- Sastry, M.V.A., Rao, B.R.J. & Mamgain, V.D., (1968). Biostratigraphy zonation of the Upper Cretaceous formation of the Trichinopoly district, south India. *Memoirs of the Geological Society of India*, 2, 10-17.
- Sastry, V.V., Raju, A.T.R., Sinha, R.N. & Venkatachala, B.S., (1977). Biostratigraphy and evolution of the Cauvery basin, India. *Journal of the Geological Society of India*, 18, 355-377.
- Sarkar, S., Nivedita, C., Mandal, A., Banerjee, S. and Bose, P.K. (2014) Siliciclastic-carbonate mixing modes in the river-mouth bar paleogeography of the Upper Cretaceous Garudamangalam Sandstone (Ariyalur, India). *Journal of Paleogeography*, 3: 233-256.
- Shah, R. A., Achyuthan, H., Lone, A. M., Ramanibai, R. (2017). Diatoms, spatial distribution and physicochemical characteristics of the Wular lake sediments, Kashmir valley, Jammu and Kashmir. *Jour. Geol. Soc. India*, 90(2), 159-168.
- Sahu, B. K. (1964). Depositional mechanical from the size analysis of the classic sediments. *Jour. Geol. Sedi. Petro.*, 36, 73-83.
- Selvaraj, K. and Ramasamy, S. (1998). Depositional environment of Cuddalore Sandstone Formation, Tamil Nadu, *Jiur. Geol. Soc. India*, 50, 803-812.
- Spencer, D.W. (1963). The interpretation of grain size distribution curves of clastic sediment. *J. Sediment. Petro.*, 37, 180-190.
- Srivastava, R. P. and Tewari, B. S. (1967). Biostratigraphy of the Ariyalur Stage, Cretaceous of Trichinopoly. *Jour. Paleo. Soc. India.*, 12, 48-54.
- Srivastava, A.K. and Mankar, R.S. (2008) Grain size analysis and depositional pattern of upper Gondwana sediments (Early Cretaceous) of Salbardi area, districts Amravati, Maharashtra and Betul, Madhya Pradesh. *Journal of Geological Society of India* 73: 393-406.
- Sundaram, R. and Rao, P. S. (1986). Lithostratigraphy of Cretaceous and Paleocene rocks of Tiruchirapalli district, Tamil Nadu, south India. *Records of the Geological Survey of India*, 116, 11-23.
- Sundaram, R., Henderson, R.A., Ayyasami, K. and Stilwell, J.D. (2001). A lithostratigraphic revision and palaeoenvironmental assessment of the Cretaceous System exposed in the onshore Cauvery Basin, southern India: *Cretaceous Research*, 22, 742-762
- Suttner, L. J. and Dutta, P. K. (1986). Alluvial sandstone composition and paleoclimate. I Framework mineralogy. *Jour. Sediment. Petro.*, 56, 329-345.
- Taylor, S. R. and McLennan, S. M. (1985). *The Continental Crust: Its Composition and Evolution*. Oxford, Blackwell, 349.
- Tewari, A., Hart, M. B. and Watkinson, M. P. (1996). A revised lithostratigraphic classification of the Cretaceous rocks of the Trichinopoly district, Cauvery Basin, southeast India. *In Contributions to the XV Colloquium on Micropaleontology and Stratigraphy*, 789-800. (Published by Paleontological Society of India).
- Udden, J. (1898). *Mechanical composition of wind deposits*. *Aug. Lib. Publ.*, 1, 69.
- Venkatachala, B.S., (1974). Palynological zonation of the Mesozoic and Tertiary subsurface sediments in the Cauvery basin. *In: Surange, K.R. et al. (eds.), Aspects and appraisal of Indian Palaeobotony*, 476-495. (Published by British Institute of Palaeontology, Lucknow).
- Venkatachalapathy, R. and Ragothaman, V. (1995). A foraminiferal zonal scheme for the mid-Cretaceous sediments of the Cauvery Basin, India. *Cretaceous Research.*, 16, 415-433.
- Vital, H. and Statterger, K. (2000). Lowermost Amazon River: evidence of late Quaternary sea-level fluctuations in a complex hydrodynamic system. *Quaternary Internat.*, 72, 53-60.
- Visher, G.S. (1969). Grain size distributions and depositional processes, *Jour. Sedi. Petro.*, 39, 1074-1106.
- Vredenburg, E.W. (1908). Considerations regarding the age of the Cuddalore series. *Record of the Geological Survey of India*, 36, 321-323
- Warth, H. (1895). *The Cretaceous Formation of Pondicherry*. *Records of the Geological Survey of India.*, 28, 15-21.
- Wadia, D.N. (1953). *Geology of India*. Macmillan and Company Ltd. St.Martin's streets, London.
- Watsan, J. S. (1996). Fast, simple method of pellet preparation for X-Ray Fluorescence. *X-Ray Spectrometry*, 25, 173-174.
- Yadagiri, K. and Govindan, A., (2000). Cretaceous carbonate platforms in Cauvery basin: Sedimentology, depositional setting and subsurface signatures. *In: Govindhan, A. (ed.), Cretaceous stratigraphy - An update*. *Memoirs of the Geological Society of India*, 46, 323-344.

Potentiality of Uranium Mineralisation in the Environs of Chhattisgarh Basin, India: a new occurrence in Chhibra

Mithilesh Sharma¹, Ashim Jana^{1*}, Ajay Kumar¹, Pramod Kumar¹, A. K. Rai²

Atomic Minerals Directorate for Exploration and Research, Department of Atomic Energy,

Jamshedpur¹- 831 002, Hyderabad²- 500 016, India

*corresponding author- ashimjana.amd@gov.in

Abstract

The Mesoproterozoic intracratonic basins are known for hosting medium to high grade, large tonnage unconformity-type uranium deposits in the world. Besides Cuddapah basin, Chhattisgarh basin is also identified as one of the major favourable targets for uranium mineralisation in India based on its geological evolution, structural and tectonic framework. Extensive uranium exploration carried out along the northeastern and southeastern margins of Chhattisgarh basin and basement Sambalpur Granitoids has brought out significant uranium occurrences hosted by both the basement rocks as well as cover sediments. Unconformity related, fracture bound, significant epigenetic uranium mineralisation is manifested in the newly located uranium occurrence at Chhibra, Mahasamund district, Chhattisgarh which is intermittently exposed over a strike length of 800m and width of 5m to 50m in the pyritiferous feldspathic arenite of Rehatikhol Formation of Singhara Group proximal to the Mesoproterozoic unconformity. Grab samples (n=43) physically assayed 0.010% to 0.120% U₃O₈ and <0.005% ThO₂. Uraninite and pitchblende have been identified as uranium minerals. Uraninite occurs as vein in association with pyrite and at places with galena. The U/Th ratio of Sambalpur Granitoids and trachyte are respectively 1:1.8 and 3.3:1 indicating fertile nature of basement which has great importance in search of unconformity related uranium mineralisation in the southeastern part of Chhattisgarh basin. The favourable factors like geological, geochemical, geophysical, sedimentological, tectonic framework and presence of fertile granitic rocks with <5-26 ppm U (n=36) in the provenance indicate its potentiality for uranium mineralisation. The exploration so far, has been mostly confined around the shallow basin margins leaving deeper part unexplored. The recent discovery of high-grade uranium mineralisation in the cover sediments near Chhibra has opened up new possibilities for further exploration in the deeper part of the basin around suitable litho-structural settings, especially along the N-S, NNW-SSE, NE-SW and ENE-WSW trending shear/fault zones and their intersections.

Keywords: Uranium, Chhattisgarh, Chhibra, Unconformity

Introduction

Globally, the Mesoproterozoic intracratonic basins are highly potential for hosting unconformity-type uranium deposit as it was the first time when uranium from all the sources came to solution after the great oxidation event (GOE) and precipitated along the unconformity surface to produce medium to high grade, large tonnage uranium deposits, e.g. Athabasca basin, Saskatchewan, Canada (Fogwill, 1981; Sibbald, 1986, 1988) and Pine Creek geosyncline, Northern Territory, Australia (Needham and Roarty, 1980; Needham et al., 1988). In India, unconformity-related small uranium deposits have been identified at Lambapur-Yellapur-Chitral in the northern part of the Cuddapah basin (Sinha, et al., 1995, 1996; Sharma, et al., 1995). Based on the geological setting, age and fertile basement provenance, the other Proterozoic basins such as the Chhattisgarh basin has been one of the major exploration targets for uranium mineralisation. The Mesoproterozoic Chhattisgarh basin has evolved on the

northern fringe of Bastar craton and occupies an area of about 33,000 sq. km. with 2500 m thick sediments (Murti, 1987; Das et al., 1992) in the central part of Chhattisgarh and western part of Odisha state. The geological evolution, structural and tectonic framework of the Chhattisgarh basin favours its potentiality for hosting uranium mineralisation in association with base metals and other polymetallic mineralisation (Patnaik, 1989; Sinha and Hansoti, 1995; Sinha et al., 1998; Yadava et al., 2007). Uranium investigations in the eastern part of Chhattisgarh basin commenced in early eighties to look for sandstone-type uranium mineralisation and during mid-nineties the exploration switched for basement hosted fracture/shear-controlled vein-type uranium mineralisation. More than forty uranium occurrences having sizeable dimensions has been located mostly along the northeastern and southeastern margins of Chhattisgarh basin and basement Sambalpur Granitoids hosted by both the basement rocks as well as cover sediments of

Chhattisgarh basin. But it covers only 4-5% area of the basin (mostly along the eastern margin) leaving the internal part of the basin unexplored.

The present paper deals with the potentiality of uranium mineralisation in Chhattisgarh basin with emphasis on recently located significant occurrence of uranium mineralisation near Chhibra in Rehatikhol Formation of Singhora Group along the southeastern margin of Chhattisgarh basin and attempts to select new prospecting targets by evolving conceptual models and exploration strategies.

Geological and Tectonic Setting

The Mesoproterozoic intracratonic Chhattisgarh basin is third largest Proterozoic basin in Central India. The near crescent-shaped Chhattisgarh basin is situated within the Central Indian craton which is surrounded by Sambalpur granitoids in the east (2380

± 44 Ma; Choudhary et al., 1996), Khairagarh volcano-sedimentary rocks in the west (2120 ± 35 Ma; Sinha, 1993), Nandgaon volcano-plutonics in the southwest (2462 ± 25 to 2039 ± 79 Ma; Pandey et al., 1995), Bilaspur-Raigarh-Surguja belt of Sausar Group in the north (1541 ± 26 to 1100 ± 20 Ma; Pandey et al., 1995) and metasediments and granitoids of Bastar craton in the south (3610 ± 336 to 2110 ± 41Ma; Pandey et al., 1995). Sonakhan volcano-sediments and volcano-plutonics (2347 ± 16 Ma; Pandey et al., 1995) trending in the NNW-SSE direction divides Chhattisgarh basin into two sub-basins, namely, Baradwar sub-basin in the east and Hirri sub-basin in the west. Baradwar sub-basin is geologically more important for hosting uranium mineralisation than Hirri sub-basin as this part hosts all the three groups of the Chhattisgarh Supergroup namely Singhora (arenites, shales and limestones), Chandrapur (predominantly sandstones/

Table-1: Stratigraphic succession of Chhattisgarh basin (after Das et al., 1992)

HIRRI SUB-BASIN			BARADWAR SUB-BASIN	
NORTHERN PART		SOUTHERN PART		
R A I P U R G R O U P	Maniari Shale	Maniari Shale with gypsum	Saradih dolomite, limestone and black shale	
	Hirri dolomite	Hirri dolomite		
	Pandaria purple calc-argillite with grey bedded limestone, stromatolitic limestone and dolomite as lenses and pockets	Tarenga argillite, arenite and cherty-clay	Bamandihi purple calc-argillite with stromatolitic limestone as lenses and pockets	
		Chandi stromatolitic limestone with argillite and arenite member		
C H A G N R D O R U A P P U R	Kansapathar glauconite arenite	Gunderdehi argillite with arenite band	Kansapathar glauconite arenite	
	----Disconformity----	Chamuria bedded limestone		
	----Disconformity----	Chaporadih argillite and arenite		
Lohardih conglomerate and arkose	Lohardih conglomerate and arkose	Lohardih conglomerate and arkose		
-----Unconformity-----			-----Disconformity-----	
Bilaspur-Raigarh-Surguja Metamorphic belt and Chilpi Group		Granite and gneisses of Bastar craton and Sonakhan Group	S I G N R G O H U O P R A	Chhuipali purple argillite and stromatolitic carbonate
				Bhalukona arenite
				Saraipali purple argillite with porcellanite
				Rehatikhol arkose and conglomerate
				-----Unconformity-----
				Sambalpur Granite of Bastar craton and Sonakhan Group

quartzites) and Raipur (shales/limestones) groups (Das et al., 1992) (Table-1). The oldest Singhora Group is exposed only along the two embryonic basins, namely the Singhora and Barapahar, situated along the southeastern and eastern portions of the Chhattisgarh basin (Fig. 1a). Singhora Group is divided into four formations namely Rehatikhol, Saraipali, Bhalukona and Chhuipali which are exposed in the southern part, overlying the basement rocks of Sambalpur granitoids (Fig. 1b). It was evolved during Paleo to Mesoproterozoic period (1600-1800 Ma) whereas, sedimentation in main Chhattisgarh basin was initiated around 1300 Ma (Das et al., 2001). The siliciclastic detritus contributed from the surrounding fertile provenance and deposited on a stable shelf environment in fluvial fan deposit. The detritus deposited in the basal part of the basin contains high uranium content which is mainly derived from the fertile granitic basement ($n=36$, $<5-26$ ppm U).

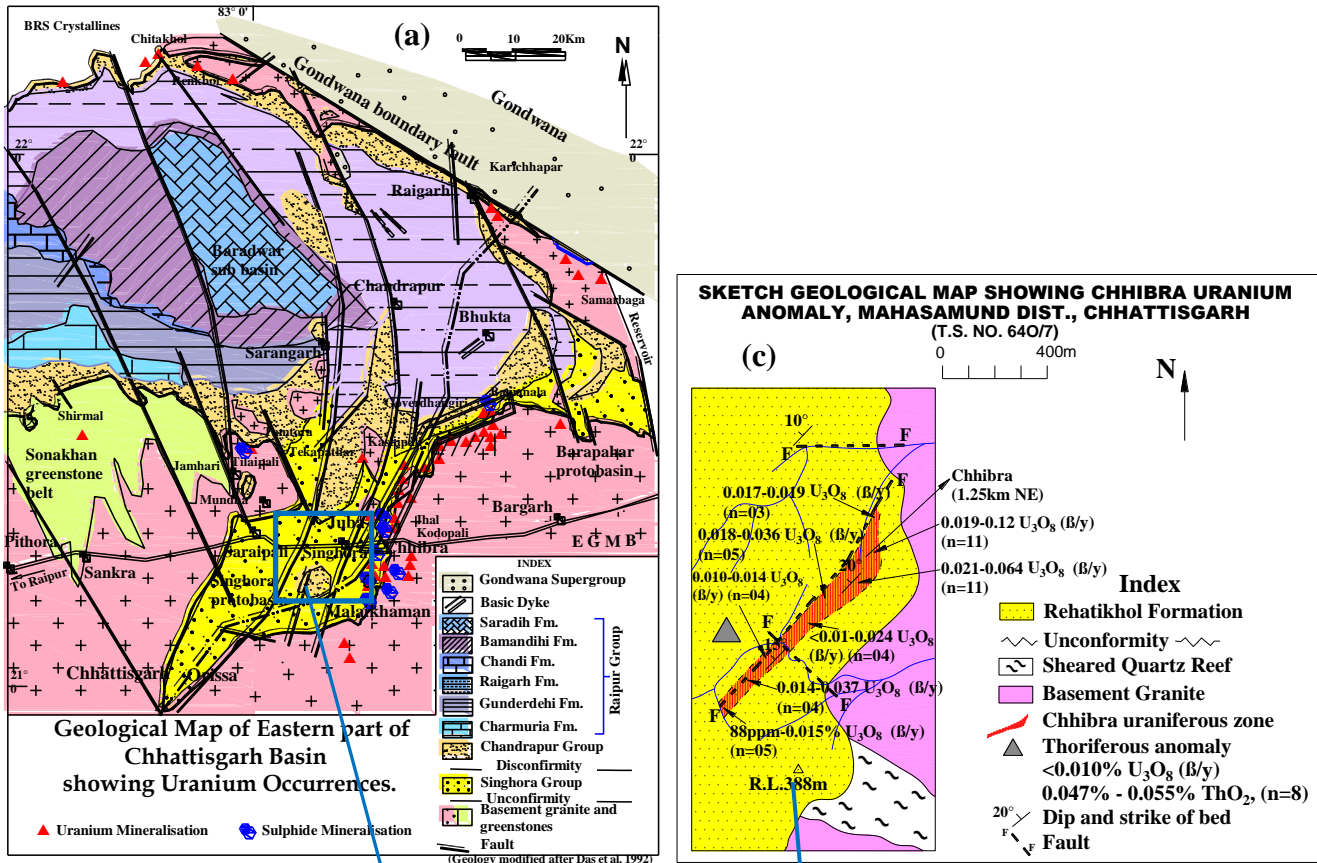
Uranium Mineralisation

Exploration for uranium in Chhattisgarh basin commenced in early 1960s by Atomic Minerals Directorate (AMD) for exploration and research and till 1990s, thoriferous anomalies associated with the basal conglomerates of Singhora and Chandrapur groups were reported. Uranium mineralisation of 0.032% $eU_3O_8 \times 0.80m$ (eU_3O_8 is equivalent uranium oxide)

was reported for the first time in greenish black shale in the borehole drilled by Bhilai Steel Plant (BSP) near Stadium at Durg in the western part of the basin in 1980. Subsequent exploration shows that the uranium mineralisation occurs in two distinct geological settings in the vicinity of the unconformity i.e., (1) cataclasites in shears/fracture zones within basement granites/migmatites and metabasic/basic rocks, and (2) arenites of Singhora and Chandrapur groups. A number of uranium occurrences were also reported from Chhattisgarh basin associated with both cover sediments e.g., Juba-Banjhapali, Govardhangiri-Bagia nala, Sapnai nala, Chitakhhol, etc. and basement granite e.g., Kashipali, Karichhapar, Dulapali, Damdama, Malaikhaman, Makarmunda, Jhal, Dumarपालि, Jharmunda, Amlipali, Samarbaga, Telan, Borjha, etc. (Sinha and Hansoti, 1995; Sinha, et al., 1998; Bhattacharjee, et al., 2005; Gupta, et al., 2008; Tiwary, et al., 2004; Kumar, et al., 2000; Mukundan, et al., 2000; Bhairam, et al., 1998; Mukundan, et al., 2000; Pant, et al., 2001; Sharma et al., 2014) (Fig. 1a, Table-2). Though reconnaissance drilling has been carried out in few areas but sizeable persistency and grade of uranium mineralisation could not be established. These uranium mineralisations invariably occur in association with polymetallic sulphides (Sinha and Hansoti, 1995; Sinha, et al., 1998; Patnaik, 1989; Yadava, et al., 2007).

Table-2: Uranium occurrences in basement and cover sediments of Chhattisgarh basin

Locality	District, State	Host Rock	% U_3O_8
Juba-Banjhapali	Mahasamund district, Chhattisgarh	cover sediments	0.010-0.078
Govardhangiri-Bagia Nala	Bargarh district, Odisha		<0.010-0.80
Kalangpali	Bargarh district, Odisha		up to 0.017
Sapnai Nala	Raigarh district, Chhattisgarh		<0.010-0.044
Chitakhhol-Renkhol-Bokarda	Korba and Janjgir-Champa district, Chhattisgarh		<0.012-0.39
Kashipali-Jaipur	Raigarh district, Chhattisgarh	basement granitoids	0.010-0.96
Karichhapar	Raigarh district, Chhattisgarh		0.011-0.41
Dulapali, Dongaripali, Paraskol-Sonabela, Damdama	Raigarh district, Chhattisgarh		0.026-0.43
Malaikhaman	Bargarh district, Odisha		0.026-0.11
Makarumunda	Bargarh district, Odisha		0.013-3.3
Ghoghara	Bargarh district, Odisha		0.086-0.30
Kanhari	Rajnandgaon district, Chhattisgarh		<0.010-0.045
Jhal- Dumarपालि	Bargarh district, Odisha		0.010-0.87
Jharmunda	Bargarh district, Odisha		0.010-0.62
Amlipali	Bargarh district, Odisha		0.032-0.33
Negimunda	Bargarh district, Odisha		0.011-0.040
Bidhanpali	Bargarh district, Odisha		0.017-0.052
Samarbaga-Telan-Borjha	Jharsuguda district, Odisha		0.011-0.63



GEOLOGICAL MAP SHOWING RADIOACTIVE ANOMALY AROUND CHHIBRA - MALAIKHAMAN - BRAHMANIDUAR AREA, BARGARH DISTT., ODISHA AND MAHASAMUND DISTT., CHHATTISGARH (T.S. No. 640/3, 4, 7 & 8)

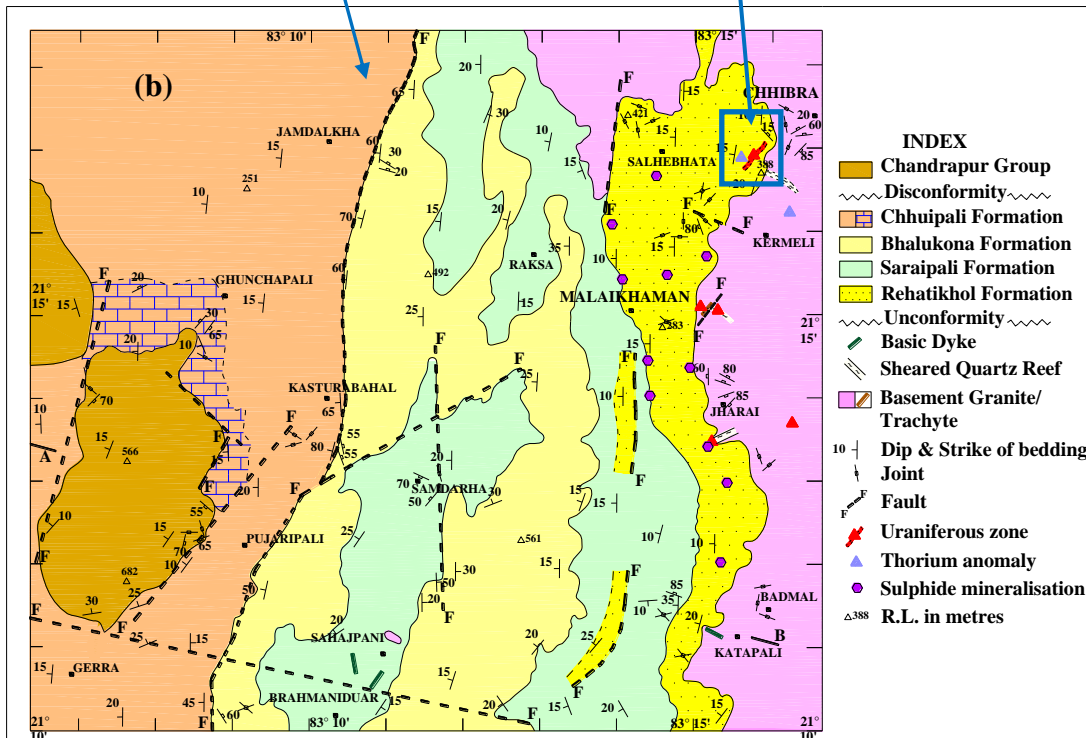


Figure 1. Geological map of (a) Eastern part of Chhattisgarh basin showing uranium occurrences, (b) Chhibra-Malaikhman-Brahmaniduar tract and (c) Chhibra uranium occurrence in details

Recently located occurrence of uranium mineralisation of Chhibra (lat. 21°16.904'N: 21°17.250'N and long. 83°15.648'E: 83°15.921'E), Mahasamund district, Chhattisgarh (Fig. 1b & c) has enhanced the potentiality of uranium along the southeastern margin of Chhattisgarh basin. The uranium mineralisation here occurs in pyritiferous feldspathic arenite of Rehatikhol Formation along a shear zone trending N60°E-S60°W direction nearly 40m above the Mesoproterozoic unconformity between Singhora Group and Sambalpur Granitoids intermittently over 800m strike length with width from 5m to 50m and thickness from 1m to 4m. The physical assay of the mineralized rock samples (n=43) indicated 0.014 to 0.140% eU₃O₈, 0.010 to 0.120% U₃O₈ (β/γ) and <0.005% ThO₂ (Table-3). Rehatikhol Formation consists of basal conglomerate which directly rests over the Sambalpur Granitoids and the conglomerate followed by pebbly feldspathic to sub-feldspathic arenite and cross bedded medium to coarse grained arenite with thin layers of pebbly arenite horizon at places.

The petrographic and mineralogical studies indicate that the host rock for uranium mineralisation is poorly to moderately sorted feldspathic arenite. It is medium to coarse grained, pale greenish to light grey coloured and mainly consists of angular to sub-angular

grains of quartz, microcline, minor plagioclase feldspar and numerous opaque minerals with approximately 10-15% matrix (visual estimation) composed of clay, chlorite and sericite (Fig. 2a). Pyrite also occurs in the matrix along grain contact of quartz and feldspar (Fig. 2b). Feldspars are commonly altered into clay and sericite (Fig. 4b). The Cellulose Nitrate (CN) film autoradiographic study indicates medium to high density alpha tracks over CN-film due to the presence of radioactive phase which has been identified as pitchblende. It occurs as vein in association with pyrite and at places with galena along grain boundary of quartz and feldspar (Fig. 3a, 3b). The XRD study shows presence of traces of uraninite along with quartz, pyrite, chalcopyrite, microcline, jarosite and titanite (Table-4). Patches of secondary uranyl mineral (Fig. 4a) as well as adsorbed uranium are also observed over clays, hydrated iron oxides and altered feldspar (Fig. 4b, 4c). Pyrite is the main sulphide ore mineral identified occurring as vein material filling the space between the grain contact of quartz and feldspar in the matrix of feldspathic arenite. The pyrites generally occur as cubic to anhedral in shape. Other ore minerals identified are galena, chalcocite, covellite and chalcopyrite occurring as vein along grain boundaries or fracture-filling in quartz.

Table-3: Physical assay result of the radioactive feldspathic arenite samples of Chhibra

Sample No.	% eU ₃ O ₈	% U ₃ O ₈ (β/γ)	% ThO ₂	% K	Sample No.	% eU ₃ O ₈	% U ₃ O ₈ (β/γ)	% ThO ₂	% K
CHB-1	0.140	0.078	<0.005	---	CHB-25	0.028	0.025	<0.005	---
CHB-2	0.089	0.062	<0.005	---	CHB-26	0.033	0.037	<0.005	---
CHB-3	0.090	0.050	<0.005	---	CHB-27	0.023	0.030	<0.005	---
CHB-4	0.066	0.050	<0.005	---	CHB-28	0.015	0.014	<0.005	1.4
CHB-5	0.076	0.041	<0.005	---	CHB-30	0.016	0.014	<0.005	1.4
CHB-6	0.056	0.038	<0.005	---	CHB-31	0.014	0.013	<0.005	2.3
CHB-7	0.058	0.035	<0.005	---	CHB-32	0.014	0.013	<0.005	1.7
CHB-8	0.043	0.043	<0.005	---	CHB-33	0.015	0.010	<0.005	1.9
CHB-9	0.036	0.034	<0.005	---	CHB-34	0.017	0.015	<0.005	<0.5
CHB-10	0.040	0.036	<0.005	---	CHB-35	0.017	0.015	<0.005	<0.5
CHB-11	0.034	0.036	<0.005	---	CHB-36	0.014	0.013	<0.005	1.6
CHB-12	0.031	0.027	<0.005	---	CHB-37	0.048	0.043	<0.005	---
CHB-13	0.023	0.018	<0.005	---	CHB-38	0.032	0.030	<0.005	---
CHB-14	0.024	0.024	<0.005	---	CHB-39	0.029	0.025	<0.005	---
CHB-15	0.021	0.024	<0.005	---	CHB-40	0.018	0.019	<0.005	---
CHB-16	0.021	0.019	<0.005	---	CHB-41	0.020	0.023	<0.005	---
CHB-17	0.017	0.019	<0.005	2.5	CHB-42	0.022	0.025	<0.005	---
CHB-18	0.018	0.017	<0.005	---	CHB-43	0.022	0.024	<0.005	---
CHB-19	0.019	0.023	<0.005	---	CHB-44	0.024	0.026	<0.005	---
CHB-22	0.120	0.120	<0.005	---	CHB-45	0.025	0.028	<0.005	---
CHB-23	0.088	0.078	<0.005	---	CHB-46	0.024	0.028	<0.005	---
CHB-24	0.074	0.064	<0.005	---					

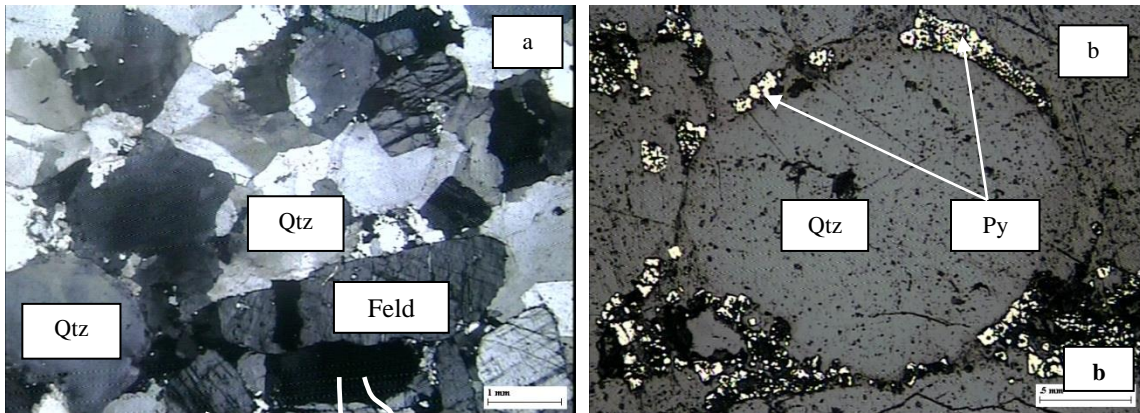


Figure 2. (a) General view of feldspathic arenite, Chhibra area, Chhattisgarh, TL, air, 2N., (b) Pyrite (Py) as matrix along grain boundary of quartz grains (Qtz) in feldspathic arenite, Chhibra area, Chhattisgarh, RL, air, 1N.

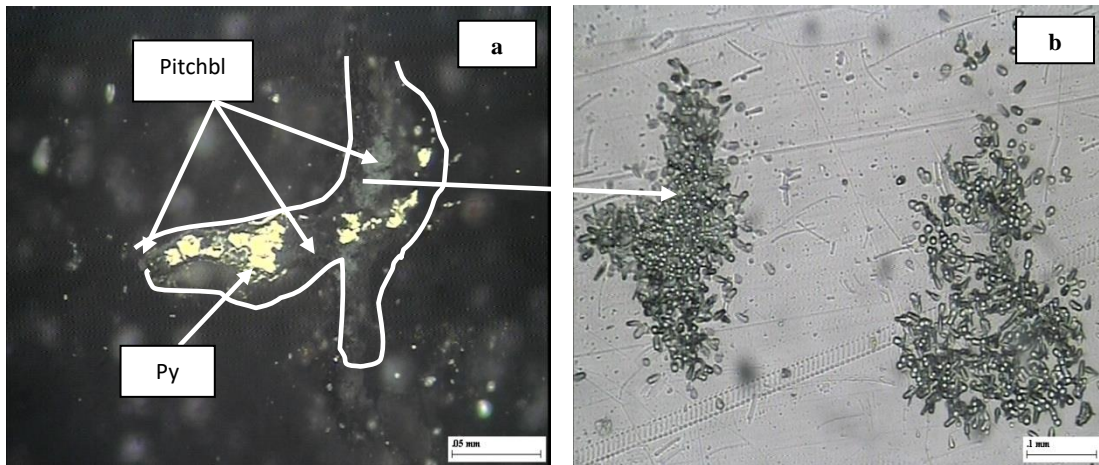


Figure 3. (a) Pitchblende (Pitchbl) as vein material in association with pyrite (Py) in quartz in feldspathic arenite, (b) Corresponding high density alpha tracks over CN films due to pitchblende in feldspathic arenite, in Figure 6a, Chhibra area, Mahasamund district, Chhattisgarh, TL, air, 1N.

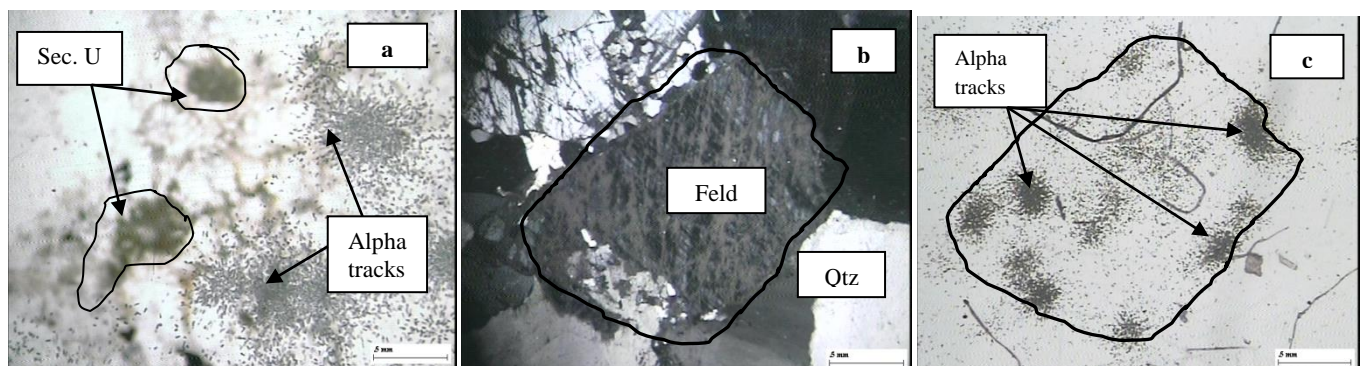


Figure 4. (a) High density alpha tracks due to patches of secondary uranyl minerals in feldspathic arenite, TL, air, 1N, (b) altered feldspar with perthitic texture in feldspathic arenite, TL, air, 2N, (c) moderate to high density alpha tracks over altered feldspar g TL- Transmitted Light; RL- Reflected Light; 1N- Under Plane Polarised Light; 2N- Under Crossed Nicols; Air- Viewed under air rain in figure 4b in feldspathic arenite, TL, air, 1N, Chhibra area, Mahasamund district, Chhattisgarh.

Table-4: XRD analysis result of feldspathic arenite

Sample no.	Atomic Minerals	Other minerals
CHB-1	None	Pyrite, quartz, traces of anatase, chalcopyrite, microcline and titanite
CHB-2	Traces of Uraninite	Jarosite, microcline, pyrite, quartz and traces of titanite

Genesis of Chhibra Uranium Mineralisation

Chhibra uranium mineralisation is significant as it occurs continuously along a shear zone forming a linear ridge in N60°E-S60°W direction showing silicification, sulphidisation, kaolinisation and ferruginisation. It is primarily structurally controlled and mineralized fluid source could be the basement pink potassic granite with felsic volcanic rock (trachyte) located nearly 40m below the unconformity between Singhora Group and the Sambalpur Granitoids. Besides, the high potassic granites, the felsic volcanic rocks especially rhyolites and trachytes have been considered to be good source of uranium world over where uranium and thorium abundances in volcanic rocks have been reported to range from 3-26 ppm and 20-32 ppm respectively (Dahlkamp, 1993). Uranium mineralisation associated with felsic volcanic rocks viz., rhyolite, trachyte, etc. have also been reported in different parts of India (Maithani and Srinivasan, 2010;

Sinha and Jain, 2008). In the present area, the U/Th ratio of Sambalpur Granitoids and intrusive trachyte are 1:1.8 (n=36; XRF data) and 3.3:1 (n=6; Chemical data) respectively showing fertile nature of the basement source rock (Table-5 & 6).

The sedimentary succession of Singhora basin is thought to be deposited by fault-controlled sedimentation under a shallow-crustal brittle deformational regime (Chaudhuri et al., 2002; Dhang and Patranbis-Deb, 2011; Patranbis-Deb, 2004; Patranbis-Deb and Chaudhuri, 2007, 2008) where the basin margins are mostly affected by several N-S, NNW-SSE, NE-SW and ENE-WSW faults cross-cutting the basement and cover sediments and their subsequent reactivation through multiple tectonic events. The uranium bearing fertile basement granites coupled with tectonic and igneous activities provided thermal gradient and channels through these fault/shear

Table-5: XRF result showing U & Th values of Sambalpur Granitoids

Sample no.	U (ppm)	Th (ppm)	U/Th	Sample no.	U (ppm)	Th (ppm)	U/Th
B13A6	<5	26	0.10	B14A9	<5	31	0.08
B13A7	8	41	0.20	B13A9	<5	36	0.07
B13A8	<5	35	0.07	B13A10	12	13	0.92
B14A5	<5	22	0.11	B13A11	<5	12	0.21
B19A0	<5	<5	1.00	B13A12	<5	<5	1.00
B19A2	<5	<5	1.00	B13A13	<5	27	0.09
B18A3	5	8	0.63	B19A1	13	11	1.18
B18A5	<5	<5	1.00	B16A4'	<5	7	0.36
B17A3'	<5	<5	1.00	B16A4	16	24	0.67
B17A2'	<5	10	0.25	B16A5	<5	24	0.10
B17A3	5	32	0.16	B15A6'	18	10	1.80
B17A4	<5	10	0.25	B15A5'	<5	19	0.13
B17A5	<5	<5	1.00	B15A4'	8	9	0.89
B12A14	<5	21	0.12	B15A4	<5	10	0.25
B11A15	<5	11	0.23	B15A5	<5	<5	1.00
B10A16	<5	14	0.18	B15A7	26	19	1.37
B16A3	8	19	0.42	B14A7	6	9	0.67
B14A6	<5	<5	1.00	B14A8	<5	12	0.21

Table-6: XRF result showing U & Th values of Trachyte

Sample no.	U (ppm)	Th (ppm)	U/Th
XG-4032	47	20	2.35
XG-4033	24	4	6.00
XG-4034	8	3	2.67
XG-4035	6	3	2.00
XG-4036	10	3	3.33
XG-4037	10	3	3.33

zones (here ENE-WSW fault) across the Mesoproterozoic unconformity for uranium migration and enrichment in pyritiferous feldspathic arenite of Chhibra. Occurrences of silica veins cutting across quartz and feldspar grains in feldspathic arenite also indicate post depositional tectonic activity near the basin margin. The discrete uranium in the basement granites and secondary uranium minerals along fractures, fissures, pore spaces might have contributed in the enrichment of uranium in the cover sediments of Singhora Group. The silicification, argillisation, kaolinisation and hematitisation accompanied the uranium mineralisation due to subsequent alteration processes. The late stage hydrothermal solutions might have caused the breakdown of feldspars by losing sodium, potassium and partially silica and subsequently formation of argillitic alteration products, iron oxy-hydroxides and uranyl oxide hydrates. The temperature ranging from meteoric water to hydrothermal solutions appears to be instrumental in near surface mineralogical alteration. This may have shifted the pH to alkaline nature causing uranium precipitation in the fractures and as adsorption on the clay minerals and iron oxy-hydroxides.

Discussion and Conclusions

Chhattisgarh basin has been one of the favourable targets for uranium exploration among the Proterozoic basins in Central India. It has been correlated with the other Proterozoic basins of Central India viz., Khariar, Ampani, Indravati and Sabari based on their litho-characters similar to siliciclastic-carbonate unit of the Singhora Group and their evolution close to Eastern Ghats mobile belt (EGMB) around 1600-1800 Ma (Ramakrishnan, M., 1990; Das et al., 2001). Based on the synthesis and analysis of data on uranium investigations carried out so far in Chhattisgarh basin, four main facts have emerged. They are: (a) uranium investigations have been carried out mainly along the basin margins which constitutes about 4-5% of the total area leaving internal part of the basin unexplored, (b) applications of required exploration techniques viz., deep borehole drilling, geophysical and geochemical techniques are negligible in the inner part, (c) lack of data on the general distribution of the radioelement concentrations in different litho-units and (d) confinement of all the major uranium occurrences (more than forty) located so far, in the eastern part of the Chhattisgarh basin. In the light of the above facts, the potentiality of uranium mineralisation in the Chhattisgarh basin, and the newly located Chhibra uranium anomaly assumes importance.

The uranium mineralisation generally occurring as fracture filled veins, stringers and around grain boundaries are the signatures of typical epigenetic hydrothermal mineralization. It has been postulated that availability of uranium bearing solutions and pyrite along with other sulphides are the main factors which

control mineralisation (Sinha et al., 1998) whereas, in the oxidized zone, iron rich hydrothermal solution might have played a key role in uranium mineralisation (Gupta et al., 2008). The occurrences of uranium, polymetallic sulphides (Pb, Zn, Cu, As±Ag), oxides of Ti and Fe in association with chert±fluorite veins in the basement of Sambalpur granitoids (Yadava et al., 2007) as well as in the arenites of Singhora and Chandrapur groups (Sinha and Hansoti, 1995; Sinha et al., 1998) along the eastern part of Chhattisgarh basin show epigenetic hydrothermal mineralisation. The large number of uranium occurrences in association with polymetallic sulphide mineralisation along the unconformity surface of Singhora Group and basement Sambalpur granitoids all along the basin margin of the eastern part of the Chhattisgarh indicate hydrothermal activity on regional scale, thus makes a favourable target for hosting shear/fracture controlled vein-type as well as unconformity-related uranium mineralisation.

The limitations of deep penetrating geophysical techniques so far, and limited exposures of the basal sequence have been the major constraints in exploration of deeper part and therefore, the exploration was confined mainly to the basin margins. The advancement in the geophysical techniques like airborne magnetic, radiometric and electromagnetic surveys in uranium exploration, the strategy needs to be revised to look into the deeper part of the basin especially along the N-S, NNW-SSE, NE-SW and ENE-WSW trending shear/fault zones and their intersections for better prospect. Along with geophysical techniques, geochemical exploration, especially litho-geochemistry, can be applied to study the alteration features like illitisation, kaolinisation and chloritisation which could prove to be a useful tool in defining the target areas for unconformity-related uranium mineralisation (Sopuck et al., 1983). This technique has become a useful exploration method and become more valuable to examine areas of conductor trends as exploration moves towards deeper areas (Mathews et al., 1997).

In view of the earlier known uranium occurrences in the cover sediments as well as in the basement rocks and the newly located epigenetic uranium mineralisation near Chhibra over a significant dimension in the form of disseminations in the matrix, inclusions in altered feldspar grains, veins and stringers along fractures and adsorbed on clay and hydrated iron oxy-hydroxides in pyritiferous feldspathic arenite of Rehatikhol Formation in the vicinity of Mesoproterozoic unconformity having fertile source rock of Sambalpur granitoids and intrusive trachyte dykes in the basement with U/Th ratio of 1:1.8 and 3.3:1 respectively bears a great significance for exploration of unconformity-related uranium mineralisation in this part of Chhattisgarh basin.

Acknowledgement

We are highly grateful to Director, AMD, Hyderabad for giving permission to publish this paper. We are also thankful to the reviewers of AMD for helping to enhance the quality of paper and related data of uranium mineralization in Chhattisgarh basin. We thank the scientists of Physics, XRD & XRF laboratories of AMD for analytical supports.

References

- Bhairam, C.L., Raju, B.V.S.N., Rao, M.K. and Dattanarayan, T.A. (1998), Delineation of uraniferous horizon in cataclastic zones using integrated technique in Precambrian basement in the environ of Chhattisgarh basin. Seminar on Precambrian Crust. (Abs.), p. 155-158.
- Bhattacharjee, I., Mukundhan, A.R., Sachan, A.S., Tiwary, K.N., Sinha, R.M., and Gupta, R.K. (2005), Proterozoic unconformity related uranium mineralization around Chitakhola area, Korba district, Chhattisgarh. India. Jour. Geol. Soc. India, 65: 619-623.
- Chaudhuri, A.K., Saha, D., Deb, G.K., Patranabis-Deb, S., Mukherjee, M.K. and Ghosh, G., (2002), The purana basins of southern cratonic province of India- a case for mesoproterozoic fossil rifts. Gondwana Research 5, 23-33.
- Choudhary, A.K., Naik, A., Mukhopadhyay, D. and Gopalan, K. (1996), Rb-Sr dating of Sambalpur Granodiorite, Western Orissa. Jour. Geol. Soc. India, 47(4): 503-506.
- Dahlkamp, F.J. (1993), Uranium Ore Deposits. Publ. Springer, Verlag, Berlin Heidelberg New York, p. 57-68.
- Das, D.P., Kundu, A., Das, N., Dutta, D.R., Kumaran, K., Ramanamurthy, S., Thanavelu, C. and Rajaiya, V. (1992), Lithostratigraphy and Sedimentation of Chhattisgarh Basin. Ind. Min., 46 (3& 4): p. 271-288.
- Das, D.P., Dutta, N.K., Dutta, D.R., Thanavellu, C. and Baburao, K. (2003), Singhora Group -The Oldest Proterozoic Lithopackage of Eastern Bastar Craton and its Significance. Ind. Min., 57(3 & 4): 127-138.
- Das, Nitish., Dutta, D.R. and Das, D.P. (2001), Proterozoic Cover Rocks of South-Eastern Chhattisgarh State and Adjoining Part of Odisha. Spl. Pub. Geol. Surv. India, No. 55, p. 237-262.
- Dhang, P.C. and Patranabis-Deb, S. (2011), Lithostratigraphy of the basal part of the Chhattisgarh Supergroup around Singhora-Saraipali area and its tectonic implication. In: Tiwari, R. P. (Ed.), Cenozoic Tectonics, Seismology and Paleobiology of the Eastern Himalayas and Indo-Myanmar Range. Geological Society of India Memoir, Bangalore, p. 77.
- Fogwill, W.D. (1981), Canadian and Saskatchewan uranium deposits: compilation, metallogeny, models, exploration, In: T.I.I. Sibbald and W. Petruk (Editors.) Geology of Uranium deposits, C.I.M. special volume, v. 34, p. 3-19.
- Gupta, P.K., Rajeeva Ranjan, Mukundan, A.R., Deshpande, M.S.M., Shrivastava, V.K. and Yadava, R.S. (2008), Uranium Mineralisation along the Northeastern Margin of Proterozoic Chhattisgarh basin around Chitakhola, Central India: A Petrological Study. Expl. and Res. for Atomic Minerals, v. 18, p. 33-53.
- Kumar, K., Mukundhan, A.R., Shivkumar, K., Tiwary, A., and Bhattacharya, A.K. (2000), A note on basement fracture controlled uranium mineralisation in Raigarh district. Proc. seminar on mineral potential of Central India: challenges in next millennium, Abstract volume, Dr. Harisingh Gaur University, Sagar.
- Maithani, P.B. and Srinivasan, S. (2010), Felsic Volcanic Rocks, a Potential Source of Uranium - An Indian Overview. (2010), Energy Proceed, Asian Nuclear Prospects.
- Mathews, R., Koch, R. and Leppin, M. (1997), Advances in Integrated Exploration for Unconformity Uranium Deposits in Western Canada. Proc. of Expl. 97. Fourth Decennial International Conference on Mineral Exploration. Edited by A.G. Gubbins. p. 993-1024.
- Mukundhan, A.R., Shrivastava, V.K., Bhattacharya, A.K., Veerbhaskar, D. (2000), Uranium mineralization from the eastern margin of the Chhattisgarh basin-A new find. Indian Jour. Geology, 72(2): 157-159.
- Murti, K.S. (1987), Stratigraphy and Sedimentation in Chhattisgarh Basin. In: Purana Basins of Peninsular India. Mem. Geol. Surv. India, 6: 239-260.
- Needham, R.S. and Roarty, M.J. (1980), An overview of metallic mineralisation in the Pine Creek Geosyncline. In: John Ferguson, and A. B. Goleby (Editors). Uranium in the Pine Creek Geosyncline, Internatl. At. Energy Agency (IAEA), p. 157-173.
- Needham, R.S., Ewers, G.R., and Ferguson, J. (1988), Pine Creek Geosyncline. In: Recognition of Uranium Provinces, Internatl. At. Energy Agency (IAEA), p. 235-261.
- Pandey, B.K., Chabria, T. and Gupta, J.N. (1995), Geochronological characterization of the Proterozoic terrains of Peninsular India: Relevance to the first order target selection for uranium exploration. Expl. and Res. for Atomic Minerals. v. 8, p. 187.
- Pant, P.C., Chaturvedi, A.K., Vidyasagar, D., Majumdar, A., Anjan Chaki and Bagchi, A.K. (2001), Uranium mineralisation in the granite protocataclastic and sheared basic rock of the Makrumunda and Ghoghara area, Bargarh district, Orissa. Journal of Atomic Mineral Science, v. 7, p. 13-22.
- Patnaik, S.K. (1989), Regional prospecting for base-metal mineralisation in parts of Chhattisgarh Supergroup, Raipur district, Madhya Pradesh (now Chhattisgarh). Rec. Geol. Surv. India, 122(6): 87.
- Patranabis-Deb, S. (2004), Lithostratigraphy of the Neoproterozoic Chhattisgarh Sequence, its bearing on the tectonics and palaeogeography. Gondwana Research 7, 323-337.
- Patranabis-Deb, S. and Chaudhuri, A.K. (2007), A retreating fan delta system in the Neoproterozoic Chhattisgarh rift basin, central India: major controls on its evolution. AAPG Bulletin 91, 785-808.
- Patranabis-Deb, S. and Chaudhuri, A.K. (2008), Stratigraphic and tectonic evolution of the Mesoproterozoic Chhattisgarh basin in central India. In: Geodynamic Regimes, Global Tectonics and Evolution of Precambrian Cratonic Basins in India, Indian Journal of Geology, 80, 1-4, (published in 2010) p.139-155.
- Ramakrishnan, M. (1990), Crustal Development in Southern Bastar, Central Indian Craton. In: Precambrian of Central India. Spec. Publ. Geol. Surv. Ind., v. 28, p. 46.
- Sharma, Mithilesh., Rai, A. K., Nagabhushana, J. C., Sinha, R. M. and Vasudeva Rao, M. (1995), Cuddapah basin and its environs as first-order uranium target in the Proterozoics of India. Expl. and Res. for Atomic Minerals, v. 8, p. 127-139.

- Sharma, U.P., Shukla, S., Sinha, P.K., Purohit, R.K., Majumdar, A. and Rai, A.K. (2014), Uranium occurrence in Proterozoic Chilpi Group, near Kanhari, Kawardha district, Chhattisgarh. *Current Science*, v. 107, 3: p. 364-367.
- Sibbald, T.I.I. (1986), Overview of Pre-cambrian geology, and aspects of metallogenesis of Northern Saskatchewan. In: G.F. Gilboy, and L.W. Vigrass (Editors). *Economic Minerals of Saskatchewan*. Special Publication. Saskatchewan Geol. Soc., Canada, p. 1-16.
- Sibbald, T.I.I. (1988), Geology and genesis of the Athabasca Basin Uranium deposits. In: *Recognition of Uranium Province*, Internatl. At. Energy Agency (IAEA), p. 61-105.
- Sinha, D.K. (1993), Stratigraphy of the Khairagarh Group of rocks, Central India: A reappraisal. *Proc. 80th Ind. Sci. Cong., Goa. Pt. IV*, p. 89.
- Sinha, D.K. and Hansoti, S.K. (1995), Uranium and polymetallic sulphides bearing Juba Member of Singhora Protobasin of Chhattisgarh Supergroup, Raipur district, Madhya Pradesh: A new horizon. *Jour. Atomic Minerals Science*, v. 3, p. 1-10.
- Sinha, D.K., Tiwary, A., Verma, S.C. and Singh, R. (1998), Geology, Sedimentary Environment and Geochemistry of Uraniferous Arenite of Singhora Group, Chhattisgarh Basin, Raipur District, Central India. *Proc. Nat. Symp.: Recent Researches in Sedimentary Basin*, p. 150-171.
- Sinha, D.K. and Jain, S.K. (2008), Uraniferous Rhyolite Vein in the basement fractures of Singhora Protobasin, Near Juba Village, Raipur District, Chhattisgarh. *Expl. and Res. for Atomic Minerals*, v. 18, p. 119-124.
- Sinha, R.M., Parthasarathy, T.N. and Dwivedy, K.K. (1996), On the possibility of low-cost, medium grade uranium deposits close to the Proterozoic unconformity in Cuddapah basin, Andhra Pradesh, India, *International Atomic Energy Agency- TECDOC- 868*, p. 35-55.
- Sinha, R.M., Shrivastava, V.K., Sharma, G.V.G. and Parthasarathy, T.N. (1995), Geological favourability for unconformity related uranium deposits in the northern parts of Cuddapah basin: evidence from Lambapur uranium occurrence, Andhra Pradesh, India, *Expl. Res. At. Min.*, v.8, p. 111-126.
- Sopuck, V.J., de Carle, A., Wray, E.M. and Cooper, B. (1983), Application of litho-geochemistry to the search for unconformity-type uranium deposits in the Athabasca Basin, in Cameron, E.M., ed., *Uranium Exploration in Athabasca Basin, Saskatchewan, Canada: Geological Survey of Canada*, p. 192-205.
- Tiwary, K.N., Sachan, A.S., Allipeera, P., and Mukundhan, A.R. (2004), Geophysical strategy to decipher the basement configuration to establish unconformity related uranium mineralization around the Chitakhola area, Korba and districts, Chhattisgarh. *Expl. and Res. for Atomic Minerals*, v. 15, p. 33-39.
- Yadava, R.S. and Rajeeva Ranjan, Shrivastava, V.K., Sachan, A.S. and Rangnath, N. (2007), Occurrences of Polymetallic Mineralisation in Sambalpur Granitoids, Bastar Craton, Central India. *Gondwana Geological Magazine*, v. 10, p. 235-242.

Impact of Elevation, Glaciations, Tectonics on landscape characteristics of the watersheds in Bhagirathi valley, Garhwal Himalaya

Dr Sarfaraz Ahmad, Khatib Khan

Department of Geology, Aligarh Muslim University, Aligarh
Sarf71@gmail.com

Abstract

Terrain attributes of the watersheds were determined in the Bhagirathi basin, Uttarakhand Garhwal Himalaya, India. Spatial distribution of terrain attributes have been used to determine the impact of elevation, glaciations and tectonic processes on terrain characteristics of the watersheds. The results indicated that permanent snowline altitude bear direct relationship with numbers of watersheds. Degree of glaciation influences the area, slope, variation of elevation, profile and plan curvature surfaces and relief of the watersheds in the Himalaya. Hypsometric Integral of few glaciated watersheds indicated the active tectonism due to high bedrock excavation in the glaciated regions of Himalaya.

Keywords; ASTER DEM, Geomorphometry, Watershed character, Landscape, Bhagirathi Basin, Garhwal Himalaya

Introduction

The continuous Himalayan arc covered by the varied geological, geographical and climatological

conditions. It lead to the enormous diversity in geomorphological processes and provide a unique natural laboratory. Therefore, numerous field based

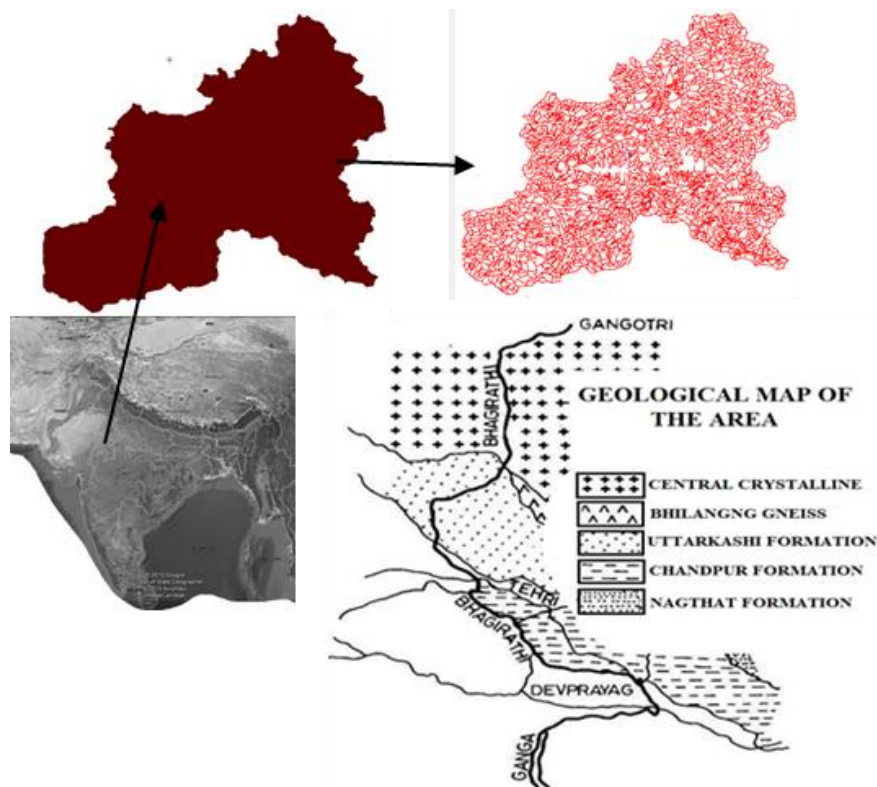


Fig. 1. Location and geological map of Bhagirathi river basin (after Pandey et al., 1999)

studies have been completed to envisage the relationship between the tectonics and weathering interaction in the Himalaya by conventional methods

such as river terrace study in river bank cross section, drilling, trenching, seismic profiling, sedimentological studies, radiometric dating, glaciological studies, etc.

Parameter	Formulas
Slope	0-90 in degree
Standard deviation of elevation (STDE)	$\sqrt{\sum(x-x')/n}$
Relief	$H_{max} - H_{min}$
Hypsometric Integral	$H_{mean} - H_{min}/H_{max} - H_{min}$
Circularity Ratio	$Re = 4\pi A/P^2$
Plan curvature surface index	Second order polynomial (Zevenbergen & Thorn (1987))
Profile curvature surface index	Second order polynomial(Zevenbergen & thorn (1987))

(Thakur, 1995; Burbank & Anderson, 2001; Philip & Sah, 1999; Malik et al., 2003). In comparison to size and length of the Himalaya, the field based geological studies are very limited and isolated. These small scale studies cannot be generalized on Himalayan scale because of high geological diversity. In such scenarios the remote sensing images and geographical information studies (GIS) techniques provide better insight of earth processes. Altitude information is the first prerequisite to reveal any geological processes in a

sensing satellites supported by NASA, ISRO and JSA provide opportunities to visualize the landscape and compute geomorphometric parameters by various software (Tobias, B., 2004; Wang & Liao 2005; Burbank & Anderson 2001; Oguchi et al., 2003; Szykaruk et al., 2004 ; Grohmann et al., 2007; Biswas & Grasemann, 2005 ; Robl et al., 2008; Goswami et al., 2012; Romshoo et al., 2012; Dortch et al., 2011; Amerson et al., 2008; Bali et al., 2012; Malik & Mohanty, 2007; Jordan, 2003). These studies used

Vaikrita Group	Undifferentiated Vaikrita/Mandhall-Chandpur-Naghat formation	Purple Grey quartzite, grit and conglomerate, thin bedded limestone – phyllite/slate laminated greenish grey phyllite /slate with lenticular greywacke, purple green quartzite, grit conglomerate
Garhwal Group	Granite	
	Bering Formation	Quartzite with mafic volcanics
	-----Disconformity-----	
	Deoban Formation	Limestone-dolomite shale
	Rautgara Formation	Quartzite with mafic volcanics
Central Crystalline	Uttarkashi Formation	Quartzite, mafic volcanic, dolomite - limestone, shale
	Badrinath Formation	Garnet, Sillimanite, Muscovite and kyanite, migmatites, pegmatite and garnet amphibolite.
	Pandukeshwar Formation	Banded quartzite gneiss and interbedded quartz mica-schist, para-amphibolite
	Joshimath Formation	Garnet mica-gneiss, staurolite and Kyanite-gneisses, garnet amphibolite.
	Bhimgora Formation	White quartzite with gneiss and schist
	Ragsi Formation	Kyanite -mica-schist, gneiss, para-amphiboles.

given landscape. The altitude information was made available through scanned topographic maps and GIS software for different parts of earth. But the restricted availability of the topographic maps of the Indian Himalayan region was a problem to the scientific community till the release of the Shuttle Radar Topographic mapping, Digital Elevation Model (SRTM DEM) in 2003 was made available. Hence, the altitude based studies in the Indian Himalaya were few in numbers (Agarwal, 1998; Asthana, 2012; Mishra, 1988; Singh and Singh, 1997). Now the free availability of DEM from ASTER, CARTOSAT, PALSAR remote

DEM information to support envisage the earth processes at small basins in specific areas of the mountains. Geomorphological processes and their mutual relationships on large scale can be revealed through analyzing the large area covering varied geological and climate conditions. In present study, the spatial distribution of the morphometric parameters of the watersheds have been analyzed to reveal the comprehensive interaction of earth processes shaping mountain system in the Himalaya.

Methodology

Morphometric analysis (Terrain Analysis) or geomorphometry is the practice of terrain modeling

and ground surface quantification, through applications of earth sciences, mathematics, engineering, and computer science. Geographic infor-

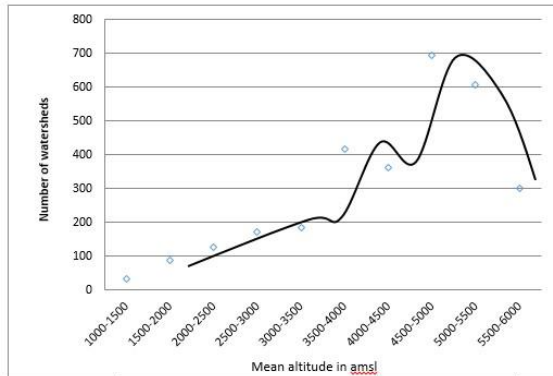


Fig. 2. Number of watersheds generation in different altitude zones.

mation Systems (GIS) and Digital Elevation Models (DEMs) allow speed, precision and reproducibility of calculation for morphometric parameters. The ASTER DEM brought regional geomorphometric analysis in a fast and inexpensive mode in the present study. In this study, we have used raster format ASTER DEM-30 meter resolution data set for determining the terrain characteristics of watersheds in the Bhagirathi basin. ASTER DEM data have been assessed from USGS explorer and imported to PCI – Geomatica V.9.1.0 and watershed boundaries were created. The images for

Geology of the Area

Bhagirathi basin is one of the largest and most important parts of the Ganga System. It forms the mountainous catchment of the river Ganga. The Bhagirathi basin covers the Chaukhamba peak in the northeast of the basin. Geographically the catchment is bounded by latitudes $30^{\circ} 10'$ to $30^{\circ} 30'$ N and longitudes $78^{\circ} 10'$ to $79^{\circ} 15'$ E. The total catchment area of the basin is around 7811 km², out of which 2328 km² is snowbound. Geologically upper catchment of the Bhagirathi is mainly composed of rocks of Central Crystallines primarily consisting of schists, micaceous quartzite, calc-silicates, amphibolites, gneisses, granites, slates, and phyllites. In the middle and lower reaches, the Bhagirathi flow through limestone and dolomite bearing Uttarkashi Formation and before the confluence with Alaknanda river, it passes through phyllites and micaceous graywacke bearing Chandpur Formation (Table 2). The average rainfall varies between 1000 to 2500 mm/year of which 50–80% falls during the monsoon period between June and September. The Bhagirathi basin experiences strong seasonal variations, which is also clearly reflected in the monthly variation in stream flows. Maximum flow takes place during June-September when both rainfall and rate of snowmelt are at maximum (Bruijnzeel and Bremmer, 1989).

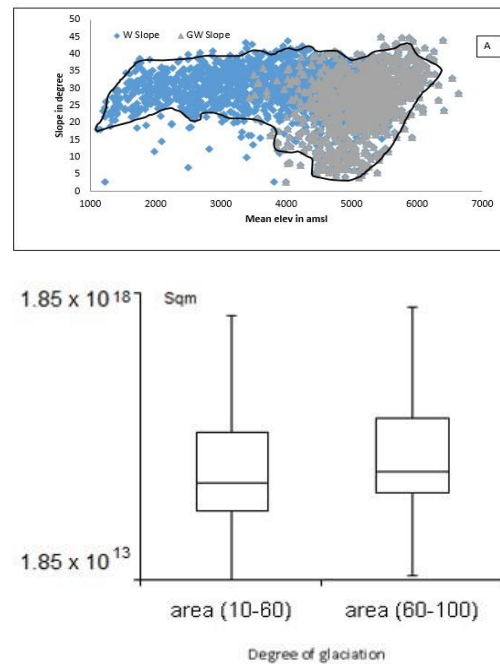


Fig. 3. Impact of glaciation on watershed area

primary and secondary terrain attribute were prepared using Terrain Analysis System 2.9.0 and extracted on watershed basis using The PCI – Geomatica V.9.1.0 (Table 1).

Results and Discussion

The land surface characteristics are the result of long term interaction of internal and external geological agencies and reflect in the landscape of a region. Changes in terrain characteristics due to earth processes may not reflect on average characteristics of the big basins. Therefore, morphometric parameters at watershed level have been studied across the Himalaya to observe the impact of various earth processes operative in various zones of Himalaya. These revelations has been unwrap using scatter diagram between watersheds morphometric parameters and mean altitudes of the watersheds across the Bhagirathi basin. A comparative analysis has also been conducted to determine the impact of elevation, glaciations and tectonic on morphometric parameters of the watersheds and their relationships. Watershed formation is the results of geological heterogeneity in an area. Therefore, distribution and size of watershed can be used to relate the environmental variability. The rate of watershed generation continuously increases from lower altitude range up to 2500 amsl and become stable from 2500 to 3500 amsl (Fig.2). A sharp increasing in numbers of watersheds has been observed from 3500 - 4000 amsl and 4500-5000 amsl. This increase is due to freezing/thawing processes operated during LGM (Last Glacial Maxima and pre-

sent time respectively at respective altitudes. Number of researches have reflected the lowering of snowline in Bhagirathi valley during LGM and shifted to 4500 - 5000 amsl in present time (Sharma et al., 1996). At the lower altitude the fluvial processes are the main contributor and resulted in lower rate of watershed generation due to fluvial erosion and low relief. The increase in average area of watersheds with altitude has been correlated with degree of freezing in glaciations at higher altitudes. It is clearly reflected in box whisker diagram (Fig. 3) indicating that the mean area of watershed of fully glaciated regions is much more than that of the moderately glaciated watersheds due to high excavation power of the glacier's ice (Amerson et al., 2008).

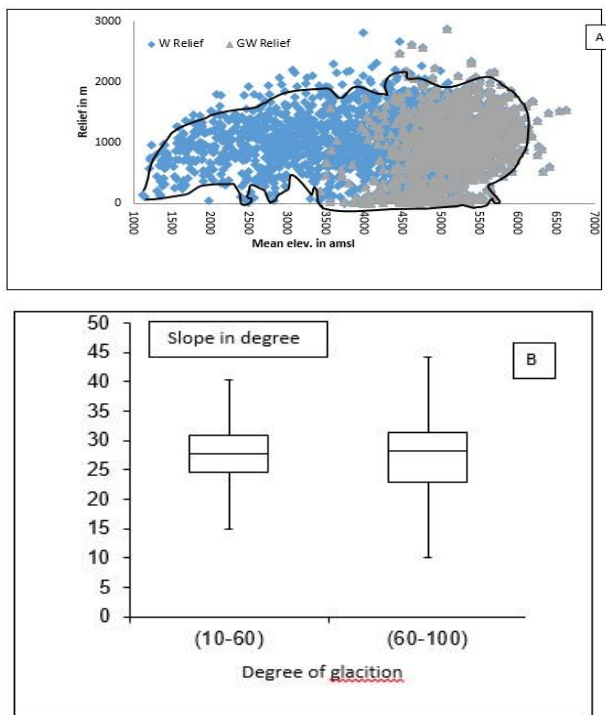


Fig. 4. Relationship between watershed slope and elevation (A), Impact of glaciation on watershed slope, (B) (*W slope for the non glaciated watersheds and GW slope for the glaciated watersheds*).

The scatter diagram (Fig. 4a) shows that the mean slope of watersheds increases with altitude from 1000 to 3000amsl and remains constant for the 3000-4000 amsl. High variation in mean slope of the watersheds at high altitude is resulting due to erosion from cirque and formation of arêtes and steep headwalls in glaciated region. Snowline in accumulation zone helps in bed rock excavation and result to the high slopes at high altitude. These high slopes are unstable and easily erodible and showing high variation in slopes than the lower altitude (Burbank et al., 1996). The box whisker diagram (Fig.4b) indicated that the lower slope values for fluvio-glaciated watersheds than that of fully glaciated watersheds. Fully ice covered glaciated valley is related to active bedrock excavation at snowline

altitude that help to maintain the high slope near permanent snowline. It is also observed that lowest slopes are also related to high glaciations than the partially glaciated valley. This lowering of slope at high altitude range can be correlated with high glaciations (Bishop et al., 2003).

Watershed relief increases with altitude up to 4500 amsl and limited in higher altitude regions (Fig. 5a). The limitation of the relief of the watersheds is attributed to continuous crowing of snowline from LGM to present day (Brozovic et al., 1997) and result

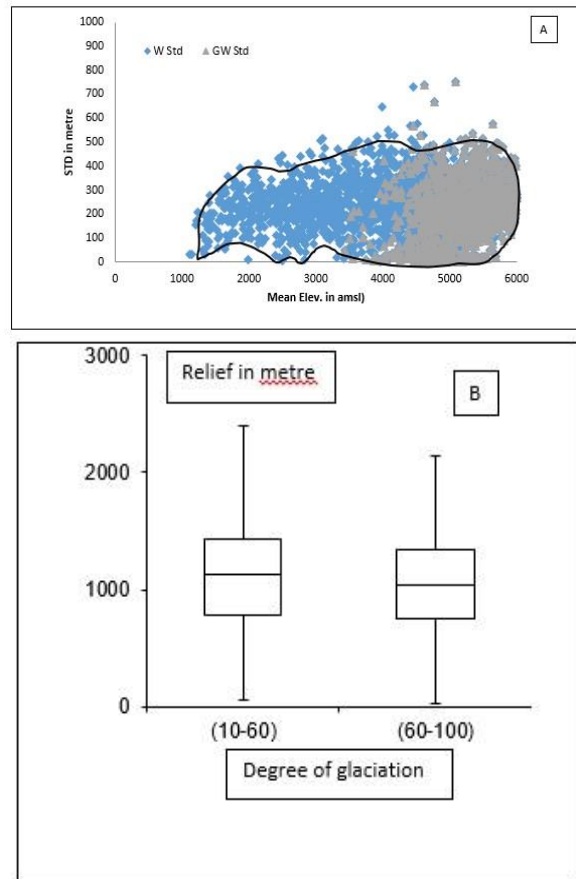


Fig. 5. Relationship between watershed relief and elevation(A), Impact of glaciation on watershed slope (B). (*W relief for non glaciated watersheds and GW relief for the glaciated watersheds*)

in limited relief in areas of present and past glaciations at high altitude (Castillo and Salinas, 2013). In fully glaciated watersheds the thick ice acts an agent for leveling the terrain. The continuous erosion of rock material at snowline results in continuous rising of mountain to adjust rock mass and limit the relief in high mountains. A comparative analysis of partial glacial watersheds (glacio-fluvial) and fully glaciated watersheds suggests that the high deposition and removal rate of earth material flux assisted by melt water in partially glaciated watersheds is responsible for high relief. While, the only erosion and transportation in fully glaciated watersheds results in

the limited relief in glaciated region at high altitude (Fig. 5b).

The scatter diagram between standard deviation of elevation in watershed and mean altitude

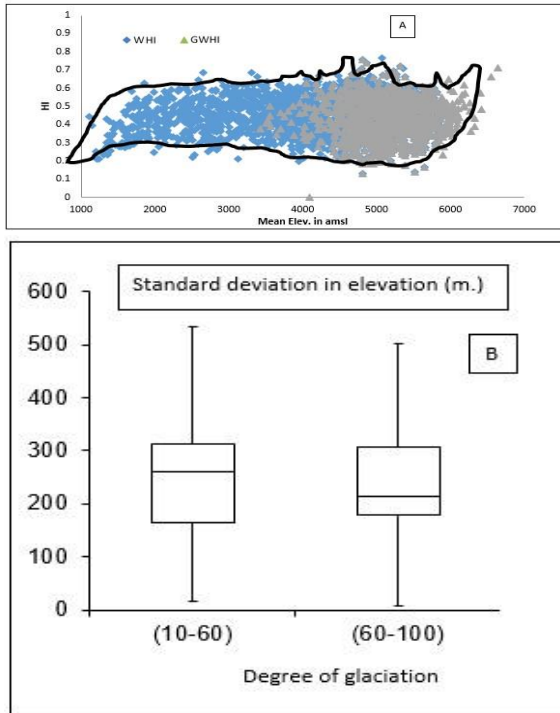


Fig. 6. Relationship between watershed elevation standard deviation of elevation (A), Impact of glaciation on watershed standard deviation in elevation (B). (*W std for the non glaciated watersheds and GW std is for the glaciated watersheds*)

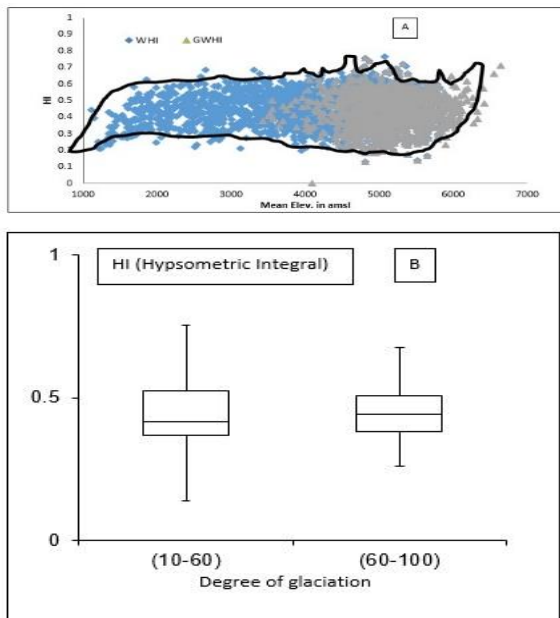


Fig. 7. Relationship between watershed elevation and Hypsometric Integral(A), Impact of glaciation on Hypsometric Integral (B). (*W HI for the non glaciated watersheds and GW HI is for the glaciated watersheds*)

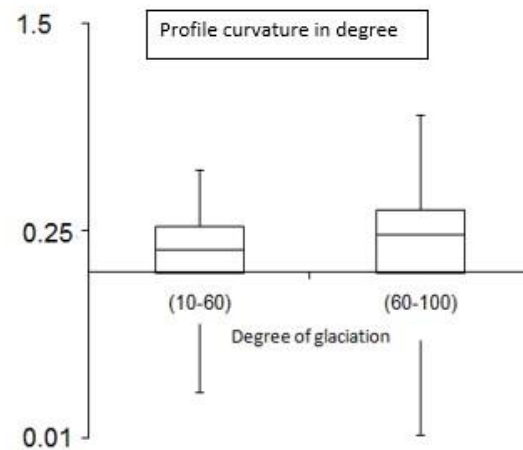


Fig. 8. Impact of glaciation on Profile curvature in Bhagirathi valley

(Fig.6a) very similar to the watershed relief distribution (Fig. 5a). It shows that watersheds with mean altitude are ranging from 4000amsl and above exhibit subdued topography indicating the maturity of the landscapes presented in the terrain due to active glacier excavation and transportation. However, higher STD of elevation in watersheds at lower altitude areas reflecting the rugged topography as a result of high degree of fluvial dissection processes associated with erosion and deposition in glacio-fluvial part of the watersheds. It is observed from box whisker (Fig.6b) that the watersheds of fully glaciated terrain are showing less mean standard deviation of elevation as compared to moderate or non- glaciated watersheds.

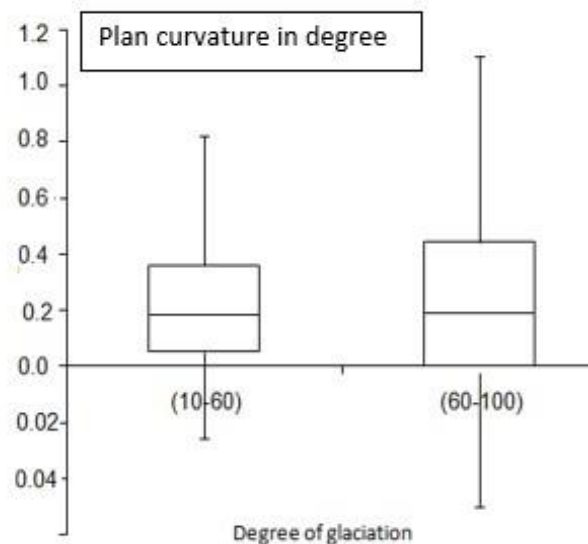


Fig. 9. Impact of glaciation on Plan curvature of watersheds in Bhagirathi valley.

Hypsometry Integral (HI) is an important tool in revealing the tectonic activities using digital topographic data of a region. Brozovic et al. (1997) used the hypsometry of glaciated landscapes in the Nanga Parbat region to examine their response to varying tectonic uplift rates, and Montgomery et al., (2001) used hypsometry of watersheds to discuss the relative importance of fluvial, glacial, and tectonic processes along the Andes Mountain. The variation of HI values of watersheds with altitude indicates the sudden high variability at 4500-5000 amsl (Fig.7a). A sudden peaking of the HI values is related to tectonic activity near snowlines altitude due to imbalance in intense excavation of earth material in this zone in glacier areas. From box whisker (fig.7b) it is clear that low mean HI with high variations can be seen in the watersheds of moderated glaciations. These are the zones of maximum thawing and freezing processes that leads erosion and finally modification of watersheds. However, fully glaciated ice and snow covered watersheds have high mean HI with least variability. The most possible factor is that the extreme coldness in this zone prevents the modification of the watersheds and tectonic forces play important role in the formation of watersheds at high altitude.

Profile curvature surfaces control the water flow acceleration and deceleration and therefore, erosion potential in the area (Calogero Schillaci et al., 2015). In the Bhagirathi valley, the scatter relationship with profile curvature surfaces values and mean altitude of the watersheds does not shows any definite trend. However, the box whisker diagram reveals the impact of glaciations on the profile curvature surfaces of watersheds (Fig. 8). It shows that the spread of profile curvature surfaces indices and median index are much lower for partially glaciated watersheds than that of the fully glaciated watersheds. This suggests that glaciation favours the formation of concave profile surfaces in the watersheds.

Plan curvatures are horizontal surfaces which control over flow convergence and negative and positive values coincide with concave features and vice versa. The box whisker diagram (Fig.9) reveals that the watersheds with moderate glaciation possess more positive median value with less standard deviation than the fully glaciated watersheds. The fully glaciated watersheds encompass the complete ice surface i.e., these areas are the snow accumulation zones of the watersheds where convergent flow is somewhat dominant.

Conclusions

An assessment of terrain characteristics of the watersheds in the Bhagirathi basin, Central Himalaya suggests that formations of the watersheds are controlled by the snowline altitude in mountain regions. The relative average size of glaciated watershed is more than that of less glaciated watersheds due to high excavating power of the

glaciated ice. Higher erosion power of glaciation is reflected in the lesser variation in standard deviation of elevation and in subdued topography in landscape of the region in glacier area. The relief is limited in higher altitude regions due to thawing and freezing processes accompanied by active transportation and deposition by active glaciations. Active erosion and deposition of rock material in the partially glaciated watersheds are responsible in higher variation in relief and standard deviation of the elevation. The tectonic imbalance produced by active glacier erosion near snowline altitude is reflected in high HI of some glaciated watersheds.

Profile and plan curvature surfaces of waterbeds do not show any systematic relationship with altitude. However, the relative contribution of fluvial and glacial processes can be distinguished by characteristics of the profile/plan curvature surfaces in high altitude Himalayan terrain.

Acknowledgements

The authors would like to express thanks to Chairman, Department of Geology, Aligarh Muslim University for providing the laboratory and library facilities. The authors would like to appreciate the financial assistance provided under DRS –II (SAP –I) program, UGC, Ministry of HRD, Govt. of India to conduct the present research work.

References

- Agarwal, C. S., (1998). Study of drainage pattern through aerial data. *Indian Journal of Remote Sensing* 26, 4, 169 – 175.
- Ahmad, S. and Islam, Z., (2011). Control of terrain on deglaciation pattern in Himalayas: a case study of glacier shrinkage in Himachal Himalayas, *Asian Journal of Water, Environment and Pollution*. 8 (1), 81- 85.
- Amerson, B. E., Montgomery, D. R. and Meyer, G., (2008). Relative size of fluvial and glaciated valleys in central Idaho. *Geomorphology*, 93, 537–547.
- Asthana, A. K. A., (2012). Landform evolution of the nayar basin Garhwal Himalaya, Uttarakhand. *Himalayan Geology*, 33, 1, 71-82.
- Bali, R., Agarwal, K., Nawaz Ali S., Rastogi, S. and Krishna, K., (2012). Drainage morphometry of Himalayan glacio-fluvial basin, India:Hydrologic and Neotectonic implications. *Environ Earth Sci* ., 66, 4, 1163-1174.
- Bishop, M.P., Shroder Jr., J.F., and Colby, J.D. (2003). Remote sensing and geomorphometry for studying relief production in high mountains. *Geomorphology*, 55, 345-361.
- Biswas, S. and Grasemann, B., (2005). Quantitative morphotectonics of the Southern Shillong Plateau (Bangladesh/India). *Austrian journal of earth sciences*, 97, 82 – 93.
- Brozovic N., Burbank D.W. and Meigs A.J.,(1997). Climatic limits on landscape development in the northwestern Himalaya. *Science*, 276, 571– 574.
- Bruijnzeel, L.A. and Bremmer, C.N. (1989). Highland-Lowland Interactions in the Ganges-Brahmaputra River Basin: A Review of Published Literature. ICIMOD Occasional Paper no. 11, International Centre for

- Integrated Mountain Development, Kathmandu, Nepal, 136pp.
- Burbank, D. J. Leland, E. Fielding, R.S. Anderson, N. Brozovik, M.R. Reid and Duncan C., (1996). Bedrock incision, rock uplift and threshold hill slopes in the northwestern Himalaya. *Nature*, 379, 505–510.
- Burbank, D.W. and Anderson, R.S., (2001). *Tectonic geomorphology*. Blackwell, Science, 274-278.
- Calogero, S., Andreas, B. and Kropáček, J., (2015). *Terrain analysis and landform recognition*. British Society For Geomorphology. ISSN, 2047-0371. London.
- Castillo M and Salinas, E.M.(2013). Assessing the impact of Quaternary glaciations on the topography of Sierra de Gredos (central Spain). *Revista mexicana de ciencias geológicas*, 30, 2, 312-323.
- Dortch, J. M., Owen, L. A., Schoenbohm, L.M. and Caffee, M. W., (2011) Catchment-wide erosion rates, glaciation, and topography of the Central Ladakh Range. *India, Journal Of Himalayan Earth Sciences*. 44,1- 14.
- Goswami, C., Mukhopadhyay, D. and Poddar, B. C., 2012.tectonic control on the drainage system in a piedmont region in tectonically active eastern Himalayas. *Front. earth sci.* 6, 1, 29–38.
- Grohmann, C.H., Riccomini, C., and Alves, F.M., (2007). Srtm-based morphotectonic analysis of the poc-os de caldas alkaline massif, southeastern Brazil. *Computers & Geosciences*, 33, 10–19.
- Günther, P., Otto, J., Montgomery, D. R. and Lothar, S., (2014). Multiscale curvature for automated identification of glaciated mountain landscapes. *Geomorphology (Amst)*. 15, 209 (100): 53–65.
- Jordan, G., (2003). Morphometric analysis and tectonic interpretation of digital terrain data: a case study. *Earth Surface Processes and Landforms*, 28, 8, 807–822.
- Kumar, G., (2005). *Geology of Uttar Pradesh and Uttaranchal*: Geological Society of India publication, Bangalore, India, 383pages.
- Malik, J. N. and Mohanty, C., (2007). Active tectonic influence on the evolution of drainage and landscape: geomorphic signatures from frontal and hinterland areas along the northwestern Himalaya, India. *Journal Of Asian Earth Sciences*, 29, 604–618.
- Malik, J.N., Nakata. T., Philip.G.,and Virdi, N.S., (2003). Preliminary observations from a trench near Chandigarh, NW, Himalaya and their bearing on active faulting. *Current Science*, 85, 12, 1793- 798.
- Mishra, N., (1988). Hypsometric integral-a basis for determining the erosion status and priority number of ungauged watershed. *J. Soil and Water cons. India*, 32, 38-45.
- Montgomery, D. R., Balco, G. and Willett, S. D. Climate, tectonics, and the morphology of the Andes (2001). *Geology* 27, 579–582.
- Oguchi, T., Aoki, T., and Matsuta, N., (2003). Identification of an active fault in the Japanese alps from dem-based hill shading. *Computers & Geosciences*, 29, 7, 885–891.
- Philip, G., and Sah, M.P., (1999) Geomorphic signatures for active tectonics in the trans-yamuna segment of the western doon valley, NW Himalaya. *International journal of applied earth observation and geoinformation*, 1, 1, 54-63.
- Robl, J., Stuwe, K., Hergarten, S. and Evans, L., (2008). Extension during continental convergence in the eastern alps: the influence of orogen-scale strike-slip faults. *Journal of Geology*, 36, 12, 963-966.
- Romshoo, S. A., Ahmad, S. and Rashid, I., (2012). Geoinformatics for assessing the morphometric control on hydrological response at watershed scale in the upper Indus Basin. *J. Earth Syst. Sci.* 121, 3, 659–686.
- Sharma, M.C. and Owen, L.A. (1996). Quaternary glacial history of NW Garhwal, Central Himalayas. *Quaternary Science Reviews*, 335-365.
- Singh, S. and Singh M.C., (1997). Morphometric analysis of kanhar river basin, National Geographical Jour. of India, 43, 1, 31-43.
- Szynkaruk, E., Graduno-Monroy, V.H., and Bocco, G., (2004). Active fault systems and tectono-topographic configuration of the central Trans-Mexican volcanic belt. *Geomorphology*, 61, 1–2, 111–126.
- Thakur, V.C., (1995). *Geology of dun valley, Gharwal Himalaya: neotectonics and coeval deposition with fault-propagation folds*. *Journal of Himalayan Geology*, 6, 1-8.
- Tobias, B., (2004). Using aster and srtm dems for studying glaciers and rock glaciers in northern tien shan proceedings part i of the conference” theoretical and applied problems of geography on a boundary of centuries”, Almaty/Kazakhstan, 8-9 june 2004, p. 254-265.
- Wang, Y. and Liao, M., (2005). Analysis of the water volume, length, total area and inundated area of the three gorges reservoir, china using the srtm dem data, *International Journal of Remote Sensing*. 26, 18, 4001–4012.
- Zevenbergen, L.W. and Thorne, C.R., (1987). Quantitative analysis of land surface topography. *Earth Surface Processes and Landforms*, 12, 1, 47 – 56.
-

OBITUARY



**Prof. V. C. Chavadi
(1942-2020)**

A popular teacher, dedicated researcher, and devoted academician of the Department of Studies in Geology, Karnatak University, Dharwad, Dr. Veerappa Channappa Chavadi passed away on 16th October 2020 morning due to a massive heart attack at his residence. Dr. Chavadi was born on 12th March 1942 in Hansi Village of Navalgund and was a native of Kotumachigi village in Gadag. Dr. Chavadi, after attaining his schooling in G.A. High-School, Belgaum, completed his graduation in Karnatak Science College; post-graduation, and Ph.D. degrees in Karnatak University, Dharwad. He has worked extensively on Vajrat Gabbro Formations of Sindhudurg, Maharashtra under the guidance of Prof. N. W. Gokhale.

Dr. Chavadi has worked as a Research scholar in Karnatak University during 1967-72; later worked as a demonstrator from 1972; served as Lecturer from 1975-78 and retired in 2001 as Professor of Geology. He was a pioneer in starting and establishing the Academic Staff College at Karnatak University Dharwad during 1987-1992 and got recognition as the best Academic staff college. He has served as - Chairman, Department of Studies in Geology twice; Dean for faculty of science; Coordinator for Western Ghat Research Projects; Academic Council member; Senate (two terms), Syndicate member (two terms) and member Finance Committee; Coordinator for NRDMS, KSCEST Karnataka for Dharwad centre, Coordinator for M. Tech. in Mineral Processing and many such coveted positions in the University.

He was very popular among students. His area of specialization was Sedimentary Petrology, Marine Geology, and Environmental Geology. He has initiated

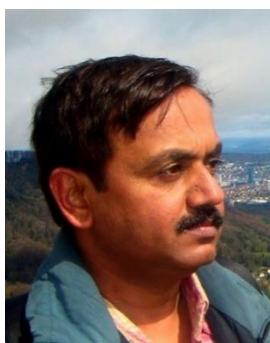
studies on beaches and coasts along North Karnataka coast through the Ph.D. program of his students and one of the first to publish scientific papers on beach morphology, sediment texture, and presence of heavy minerals and their variations with seasons along this coast. He has guided over 12 Ph.D.'s and 5 M.Phil.'s, published more than 60 research papers in national, international journals, proceedings, and books. He was a reviewer too for several journals. He has completed 5 major projects funded by central government agencies. He has actively participated in national and international seminars/symposiums/workshops and also organized several national level seminars and conferences. He has delivered several invited talks on Geology and allied subjects at various Colleges, and Universities. He was a Fellow and life member of 6 professional organizations such as the Geological Society of India (GSI), Indian Association of Sedimentologists (IAS), Mineralogical Society of India (MSI) to name a few.

Dr. Chavadi is survived by his son, daughter in law and two grandsons. With the sad demise of Dr. Chavadi, the geology fraternity and the students of Geology of this part of the country have lost a very good teacher and above all a very good human being. All his research students, (to name a few – Dr. Virupax Banakar, Retd. Scientist, NIO, Goa; Prof. G. N. Nayak, CSIR Emeritus Scientist, (Retd. Professor), Goa University, Goa; Prof. V S Hegde, Retd. Professor, S.D.M. Engg. College; and Dr. P. T. Hanamgond, Associate Professor and Head, Dept of Geology, GSS College, Belgaum), humbly convey their sincere heartfelt condolences to the bereaved family.

Dr. P. T. Hanamgond
Associate Professor & Head,
Department of Geology,
G.S. Science Degree College,
Belgaum, Karnataka
Email: hanamgondpt@gmail.com

Prof. G. N. Nayak
CSIR Emeritus Scientist
Marine Sciences
School of Earth, Ocean and
Atmospheric Sciences
Goa University, Goa, gnnayak57@gmail.com

OBITUARY



Prof. N. P. Bhatt
(18.10.1966 – 08.10.2020)

Professor Nilesh P. Bhatt whom I knew since 1987 as a student and later as a colleague. He was working as a teaching faculty in the Department of Geology, M. S. University of Baroda, Vadodara since 1996. He was a dedicated and promising researcher, committed academician and an excellent teacher. During his tenure in the department, he was actively involved with the students and was a guiding force and a source of inspiration for many young minds. His contributions in the field of Quaternary sedimentology and geomorphology are known in the geological fraternity at national and international levels which bears testimony to his academic credentials. He was a Life Member / Fellow of various organisations, an active council member of Indian Association of Sedimentologists and Gujarat Science Academy. Along with the academic contributions he had good administrative qualities. He represented the department in various academic activities at state, national and international levels.

Prof. Bhatt was an excellent human being and a kind hearted dependable person with focussed approach, independent thinking ability and inquisitive mind. His untimely and sad demise has been a great loss and has created a lacunae in the department in particular and amongst the geoscientists in general.

He leaves behind his wife Mrs. Darshana Bhatt, son Mr. Kavya Bhatt, friends and well wishers to mourn his death.

On behalf of the institution and my personal behalf, we pray the almighty to rest his soul in eternal piece and provide enough strength to his bereaved family to bear this loss.

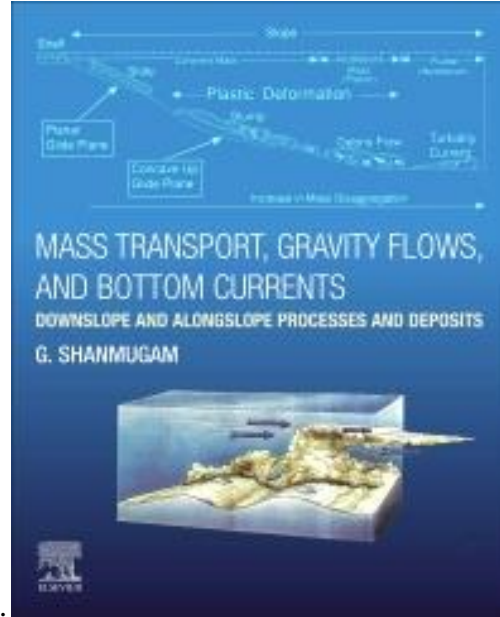
(Prof. A. V. Joshi)
Department of Geology,
M. S. University of Baroda
Vadodara.

HONOURS AND AWARDS

We congratulate our esteemed fellows of Indian Association of Sedimentologists and Sedimentologists of India for their commendable achievements in their academic endeavours.

Congratulations to:

Dr. G. Shanmugam, for his Book “Mass transport, gravity flows, and bottom currents: Downslope and alongslope processes and deposits” published by Elsevier. This the first time an Indian author has broken the tradition of publishing on the topic by European and American Colleagues over the past 6 decades.



Journal of Palaeogeography (JoP) announced its awards for excellent papers published during 2012-2020 period.

1. Single top award won by **Dr. G. Shanmugam**
2. **Professor Santanu Banerjee** won one of three First prizes
3. **S. Sarkar and his colleagues** won one of 15 second prizes

These awards are for sedimentological papers published in JOP and are based on the Science Citation Index (SCI).

On Behalf of the IAS
Managing Editors

I congratulate Professor G. M. Bhat, Vice-President of IAS and Managing Editor of Journal Indian Association of Sedimentologists for his appointment as a “**Member of the Scientific Board**” on Geohazards Theme of IGCP of UNESCO and IUGS for a term of four years (2020-24).

G. N. Nayak
President, IAS